Regional Geophysical Study of the Athabasca Region, Northeastern Alberta: Implications for Geothermal Development

by

Elahe Poureslami Ardakani

A thesis submitted in partial fulfillment of the requirements for the degree of

Doctor of Philosophy
in

GEOPHYSICS

Department of Physics
University of Alberta

Abstract

The Athabasca region located in Northeast Alberta, Canada, hosts many ongoing projects of bitumen extraction from Cretaceous oil sand and Devonian carbonate reservoirs. Despite the importance of the Athabasca region as one of the largest bitumen reserves in the world, the geology and geophysics of the area remains to a large degree poorly understood. In addition, the exploitation and production of these bitumen resources is environmentally and economically expensive and challenging. The main objective of this study is to reduce the knowledge gap of the sedimentary basin and crystalline basement by assembling multidisciplinary geophysical data to assist in investigation of the area, and provide solution for the environmental impact caused by bitumen production by assessing the potential of geothermal energy within the sedimentary formations. Interpretation of the integrated seismic-well data allows for a detailed mapping of the Grosmont topographic variations related to karst-driven erosion and some key structural maps above and below the SubMannville Unconformity. Below this unconformity, we demonstrate via 3D stratigraphy and property modeling, that wide distribution of heat values is available within five Paleozoic aquifers of Keg River, Waterways, Cooking Lake, Leduc, and Grosmont. These low enthalpy geothermal reservoirs could reduce the environmental impact of oil sand production if heat-pump technologies are used. A study of magnetic lineaments in the sedimentary basin reveals the existence of a dyke swarm referred to as the Buffalo Creek dyke field. These dykes may be related to the Farallon plate subduction under the west coast of the North American Plate. Furthermore, the tectonic boundary of Taltson Magmatic Zone and Buffalo Head Terrane is located using the Euler deconvolution of the aeromagnetic data.

ii

Preface

This thesis contains three papers that are either published or submitted for review in peer reviewed journals. I conducted all the research for the papers presented in chapter 3 and 4, and prepared each manuscript.

Chapter 2 is a published paper on research of both Todd D. Bown and I. I contributed in the research by processing and interpreting the data. I was responsible for the manuscript formation, composition, and submission for this paper.

Douglas R. Schmitt was involved with concept formation and manuscript editing in all of the publications.

Dedicated to the memory of my parents

Acknowledgements

I would like to express my sincere appreciation to my supervisor, Douglas R. Schmitt for his continuous support throughout the years of PhD study, for his patience, motivation, and immense knowledge. I could not have imagined having a better advisor for my graduate study and mentor for my life. He was always there for me when I needed someone to lean on. I always admired his dedication and keen interest for education, scientific discoveries, and geophysics in general, and I hope I caught a small amount of the passion he brings into geophysics world.

I am also using this opportunity to express my gratitude to everyone who supported me during my PhD study. Yoones Vaezi, Neda Naseri, Mostafa Naghizadeh, Ted Urbancic, Adam Baig, Brandon Reid, Soushyant Kiarasi, Reza Nourafkan, Tom Chacko, Mojtaba Rajabi, I am sincerely grateful to you for your scientific and moral support, aspiring guidance, and invaluably constructive advices during the course work, project work, and thesis preparation. Thanks for sharing your friendly, truthful, and illuminating views related to my study.

Table of Content

List of Tables

List of Figures

Chapter 1: Introduction

1.1. Athabasca region: the bitumen hot spot

The Athabasca region in Northeast of Alberta, Canada is primarily known for its significant Cretaceous oil sand deposits but less so for its substantial Devonian carbonate-hosted bitumen resources (**Figure 1.1**). The oil sand reservoirs are hosted within the Cretaceous Wabiskaw-McMurray succession, of which only a fraction can be exploited by surface mining and the bulk of these resources must be produced *in situ* (Alberta Energy and Utilities Board, 2005). The carbonate-hosted ultra-heavy oil reservoir is largely hosted by Devonian Grosmont Formation, which is projected to hold upwards of 64.5×10^9 m^3 of bitumen according to the recently updated reserves estimates of the Energy Resources Conservation Board (2010). Grosmont oil production is strongly leaning on a combination of advanced oil production technologies such as steam-assisted gravity drainage (SAGD) (Butler et al., 1981) with cyclic steam stimulation (CSS) (Batycky et al., 1997).

The oil sand deposits and the carbonate bitumen reservoir are situated within two distinct successions of Western Canada Sedimentary Basin (WCSB) that reflects contrasting geological conditions;

i)   a lower succession of Cambrian to Jurassic age, which is composed largely of carbonate rocks, with an important component of evaporite minerals and was formed during the passive margin sedimentation before the major uplift of the Canadian Cordillera. This Paleozoic carbonate and evaporite package lies above the Proterozoic metamorphic cratonic rocks of the Canadian Shield.

ii)   an upper succession of mid-Jurassic to Tertiary age, which consists mainly of shale and sandstone, was deposited following major mountain building (Columbian and Laramide Orogenies) and uplift in the Cordillera that bent the lithosphere to produce the foreland basin (Barss et al., 1964; Parsons, 1973; Porter et al., 1982; Mossop and Shetsen, 1994).
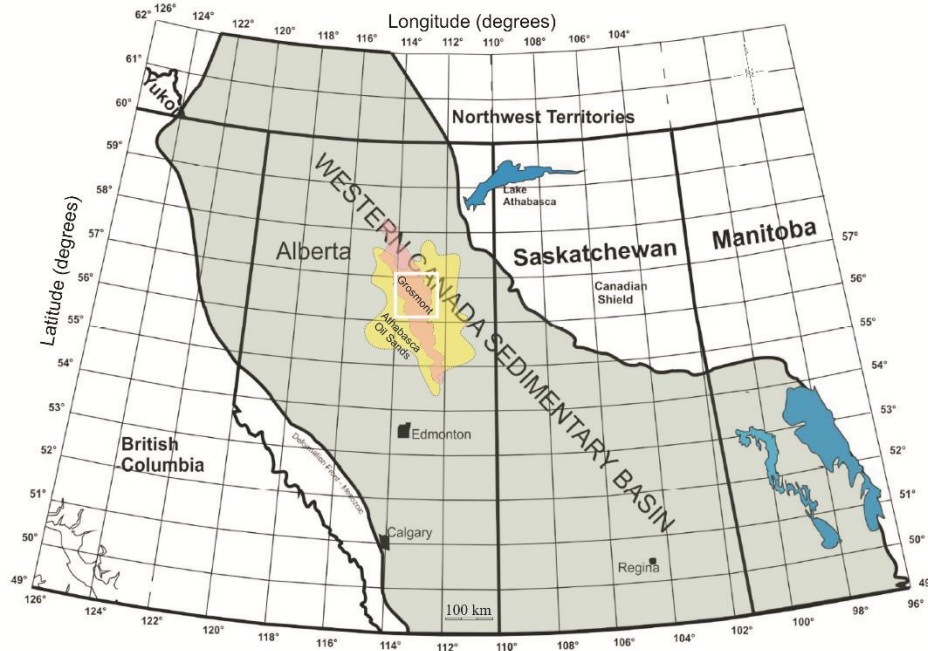
Figure 1.1. Areal coverage of the Western Canada Sedimentary Basin (modified after Grasby et al. (2011)). The Athabasca oil sand deposits and Grosmont reservoir is illustrated in yellow and pink, respectively. The study area outlined by a white box.

The boundaries between two sedimentary successions and between the WCSB and Precambrian crystalline rocks here are referred to as the SubMannville (SMU) and Precambrian (PCU) unconformities, respectively.

The SMU is the key to the development of the Grosmont resource that abuts the unconformity. The unconformity surface was modified by a combination of erosion and karsting; and this raises numerous complexities to

2

the development of the resource as it remains difficult to delineate smaller karst features. The PCU holds clues as to the potential for large scale tectonic motions that could directly or indirectly influence the subsequent sedimentary formations deposition (**Figure 1.2**).
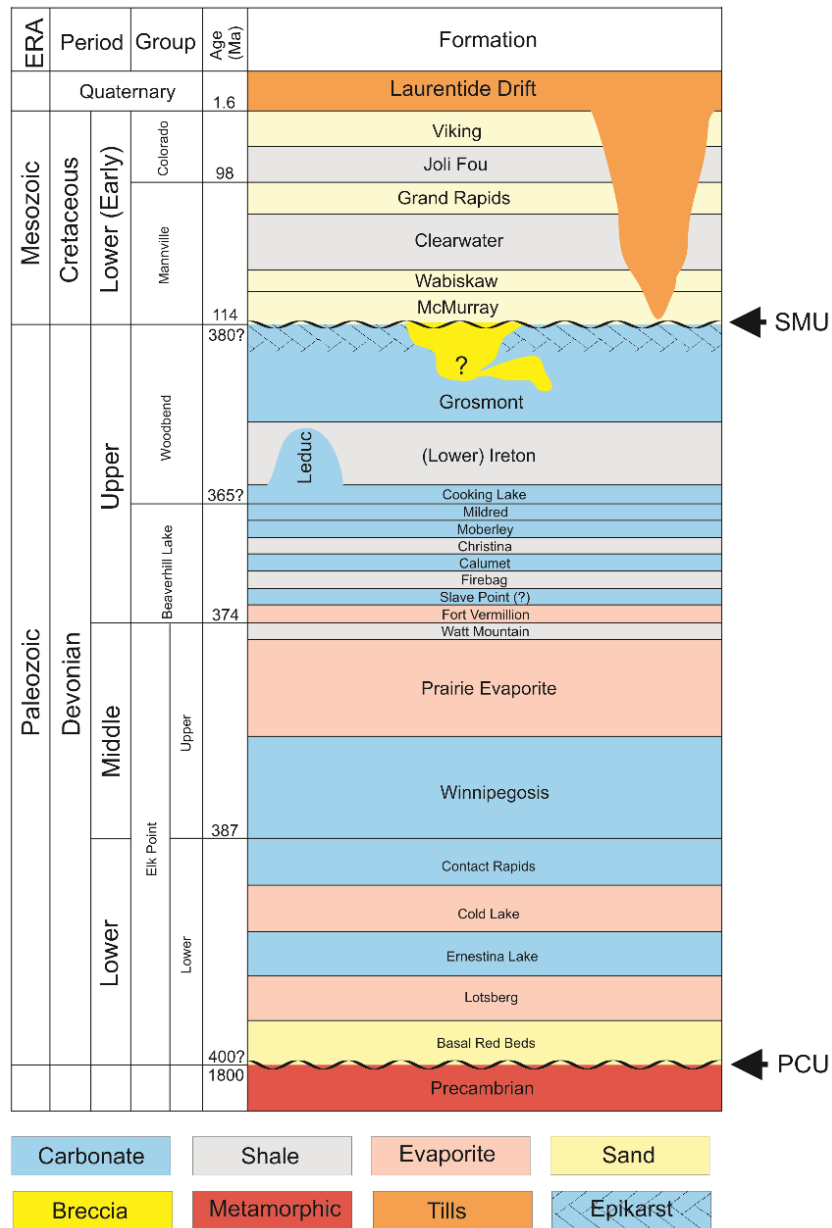
Figure 1.2. Generalized regional stratigraphy after ERCB (2009) highlighting the SMU and the PCU as wavy lines on the stratigraphy chart.

1.2. Statement of problems and objectives

Despite the importance of the Athabasca region as one of the largest bitumen reserves in the world, the geology and geophysics of the area remains to a large degree poorly understood. To our knowledge, there are not many public studies that characterize the region and its oil-bearing formations, neither from a physical property framework nor regional geophysical studies. In addition to poor geophysical knowledge of this region, the exploitation and production of its bitumen resources is challenging and expensive. Currently this process requires the burning volumes of natural gas in excess of 95.1 million m^3 per day (3.4 Bcf/day) (National Energy Board, 2015). Industry faces both economic and societal risks in continuing this practice. The economic risk is that once the means to export natural gas from North America at a large scale are put in place the cost will inevitably rise and the supply may even become restricted or prohibitively expensive. Further, the risk to the social license is that continued burning of such large volumes of natural gas invariably produces CO_2 at a rate of about 0.18 megatonnes per day for which there is strengthening societal and regulatory pressure to reduce.

The main objectives of this thesis is to find solutions for addressed issues in the Athabasca region by;

> i. Reducing the geologic and geophysical knowledge gap of the sedimentary basin and crystalline basement by assembling multidisciplinary geophysical data (many of which are proprietary) to assist in investigation of the area and present novel interpretations. Despite these efforts, the data available remain sparse and as such

recommendations for future exploration and characterization of the area are included.

ii.   Providing solution for the environmental impact caused by bitumen production by assessing the potential of clean, renewable geothermal energy within the sedimentary formations.

1.3. Methodology

The general methodology for this research can be grouped into three phases of multidisciplinary data compilation, processing-integration, and modeling-interpretation. A combination of different techniques is utilized in processing and analysis of desperate geophysical data sets with an eye to eventual integration of them. Three main types of data are employed in the research are seismic reflection, well logs, and High Resolution Aeromagnetic (HRAM) surveys. In addition, other complementary data sets are incorporated in different parts of the research as they are required for advanced interpretation. The detailed processing steps for each geophysical data type is presented in the corresponding chapters. However, a brief description of the somewhat unique compilation of differing data sets used is provided below;

1.3.1.   Seismic reflection

Seismic reflection is one of the most helpful methods that can be used for subsurface imaging particularly in detection and monitoring reservoirs within sedimentary basins. In this technique the structure of the subsurface is imaged by recording the artificially generated sound waves reflected from underground contrast surfaces (Telford et al., 1990; Sheriff, 2002; Louie et al., 2011). The seismic reflection data set here consists of about 800 km of 2D profiles within the study area (**Figure 1.3**). The seismic data-collection was primarily conducted

through donations and discounted purchase from a number of petroleum exploration companies, some of whom have expressed interest in the possibility of supplementing their thermal energy needs with geothermal heat in the Athabasca region. The vintages of the data vary from the mid-1980's to the present day. Based on the acquisition date, quality and availability of the raw data, the seismic data are divided into two parts:

i.   Recent 2D profiles with good quality in terms of having common midpoint (CMP) fold greater than 12, with mostly unavailable raw shot gathers (referred to as series A, B, C, D, E, F, G, and H),

ii. Some of the older profiles acquired in the mid-1980s with CMP fold as low as six with available raw shot gathers for reprocessing. These seismic profiles are reprocessed to enhance the quality of final processed sections. These profiles include four separate legacy seismic surveys (referred to as series K, L, M and N) and two regional seismic lines (referred to as series J). These legacy surveys at the time of acquisition in the early to mid-80s were unique, because of closely spaced receivers and sources. The series K, L, M and N are primarily reprocessed and interpreted for a detail study on topography of the Devonian Grosmont Formation surface presented in chapter 2. The detail of the reprocessing workflow and its integration with well logs is discussed in that chapter. It is worth noting that reprocessing of the data is necessitated assigning an appropriate reference datum from which all of the seismic interpretations are carried out.
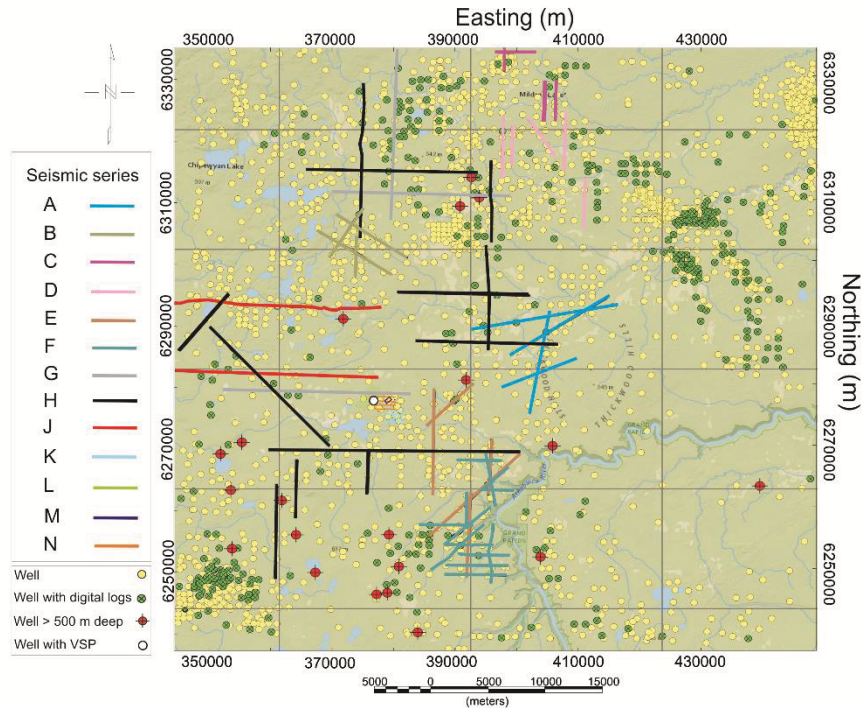
Figure 1.3. Map of the study area showing the locations of the wellbores and seismic profiles. The white circle highlights the location of the available Vertical Seismic Profile (VSP). Boreholes deeper than 500 m and with available digital logs are shown in red and green, respectively.

1.3.2. High Resolution Aeromagnetic (HRAM)

Airborne magnetic survey consists of measuring the strength of the earth's magnetic field near the ground surface (Telford et al., 1990). Such surveys look for small variations on the order of a few nanoTeslas (nT) upon the gross field strength that, in the Athabasca region, is near 58,000 nT. These small variations to the overall field are produced by magnetic susceptibility contrasts within the rocks. HRAM - largely used in regional reconnaissance - is a great tool for locating structural lineaments such as intrusive bodies, faults, and terrane boundaries within sedimentary basin and crystalline basement rock.

7

The purchased HRAM data cover the study area, which is an area of about 6000 km² (**Figure 1.4**). The survey was flown over the study area in 1998 and it represents a compilation of two diurnal corrected airborne magnetic surveys obtained by diamond exploration interests with a total line km of 79934 (**Table 1.1**). The original data have distinct leveling (bias) and therefore they show discontinuities in the primary gridded data. To resolve the leveling problem, as there are not enough overlapping flight lines, both datasets are re-leveled and interpolated using Minimum Curvature routine (Briggs, 1974) to a smaller 250 m square grid independently and knitted together and re-gridded again with grid spacing of 150 m, approximately one-eighth of the minimum line spacing of the surveys. The processing steps of this data set is presented in chapter 4 and 5.
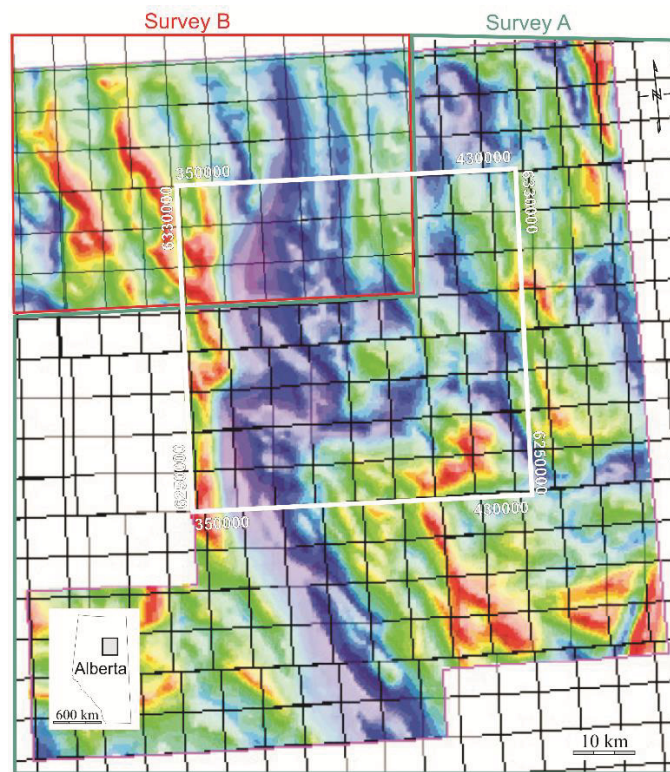
Figure 1.4. The location of the original HRAM surveys. The HRAM data within the study area (white box) is provided under purchased license from Stornoway Diamonds as assisted by B. Charters and J. Peirce at GEDCO (now Chad Data).

Table 1.1. Specification of the original HRAM surveys.

Survey	Acquisition date	Acquisition altitude (m)	Total line (km)	Tie line spacing (m)	Traverse line spacing (m)	Total area (km²)
A	1998	120	49071	2000 E/W	400 N/S	16116
B	1998	100	30863	1250 E/W	250 N/S	6392

1.3.3.   Well logs

Geophysical well logs are the record of *in situ* physical properties of the rock. Well logs also provide information about the depths to different geological features. The digital logs within the study area are obtained with vintages beginning in the 1970's from 670 boreholes through access to an industrial database. From these wells, over 7000 geological tops are obtained (**Figure 1.3**). Unfortunately, the largest portion of these boreholes was drilled for shallow gas and bitumen recovery and these provide at best only the depth to the SMU. Among these shallow boreholes less than 100 of them have digital sonic (DT) and density (RHOB) logs which are necessary for calculating synthetic seismograms and well tie process. Geophysical logs such as caliper, gamma ray, litho-density, sonic, resistivity, density porosity, and neutron porosity are some of the main logs used in chapter 2 to 5.

1.3.4.   Complementary data sets

In addition to the main three data types, complementary data sets are used in different chapters where needed for processing and final interpretations. The complementary data consist of temperature measurements, Vertical Seismic Profile, and permeability measurements.

1.3.4.1. Temperature measurements

The main goal of temperature measurements is determination of Thermal Gradient (TG) which defined as changes of temperature with depth. Having known TG and heat conductivity of rocks in a given formation, the conductive heat flow and total available heat can be calculated. Under the Helmholtz-Alberta Initiative (HAI) collaboration agreement, the temperature measurement data have been obtained for the study presented in chapter 2. The data set contains Horner extrapolated data derived from Bottom Hole Temperature (BHT) and Drill Stem Tests (DST) measurements.

1.3.4.2. Vertical Seismic Profile (VSP)

VSP (zero-offset and walkaway) is a measurement in which the seismic source is generated at the surface and seismic signal is recorded by geophones clamped at various depths to the borehole. VSP provides *in situ* measurements of rock velocity, acoustic impedance, attenuation, and anisotropy (Hardage, 2000; Stewart, 2001). An older VSP is digitized from a pilot project report (mid-80s). **Figure 1.3** shows the location of the well, which in the VSP was recorded. Unfortunately, the original digital VSP data remain lost and could not be further processed to provide additional information on the reflectivity and multiple reflections. Only the time-to-depth time picks and an image of the raw VSP data are still available. This imaged VSP data provided constraints on seismic traveltimes that were important both in assisting with the processing of the seismic data and in the interpretation of the profiles.

1.3.4.3. Permeability measurements

Permeability, which is a measure of the ability of a porous rock to allow fluids to pass through it, can be measured directly in lab (i.e. core-plug test) and

in situ (i.e. Drill Stem Test) or can be estimated from geophysical logs. As permeability estimation from logs have relatively high uncertainty, the permeability data required for analysis in chapter 3 are extracted from a previous study by Bachu et al. (1996) on core-plug and DST. The lack of these kind of data are one significant source of uncertainty as to the viability of geothermal projects in this area.

1.4. Outline

The results of this research are published in peer reviewed journals (Ardakani et al., 2014c, Ardakani and Schmitt, 2016a) and conference proceedings (Ardakani and Schmitt, 2011a, 2012a, 2013a, 2014a-b, 2015; Ardakani et al., 2011b, 2012b, 2013b), and submitted to peer reviewed journals (Ardakani and Schmitt, 2016b). Additionally, the results were presented in the form of poster and oral presentations at the Helmholtz-Alberta-Initiative (HAI) annual meetings and HAI Science forums. This thesis is outlined as follow;

Chapter 2 presents a detailed case study of the Grosmont bitumen reservoir surface within a mid-80s pilot project area. This is an eroded surface modified by karstification known as SubMannville Unconformity (SMU) within the study area. Four sets of legacy seismic profiles (K, L, M, and N) originally acquired in mid-80s are reprocessed and integrated with well logs for this study. Interpretation of the integrated seismic data allow for a relatively detailed mapping of the Grosmont surface topographic variations related to karst-driven erosion and some key structural maps above and below the SMU. A version of this chapter is published in a peer reviewed journal (Ardakani et al., 2014c) and has been presented in conferences (Ardakani and Schmitt, 2014b; Ardakani et al., 2013b).

In chapter 3 the sedimentary formations within the study area is investigated closely with the purpose of assessing low enthalpy geothermal aquifers to provide heat for oil sand and bitumen production and processing. A 3D structural geology model of the study area is developed using calibrated well tops and over 800 km of 2D seismic profiles. The model is later used as a structural framework for petrophysical property modeling. Based upon the modeling results a number of target aquifers are chosen as potential geothermal reservoirs. The volume and heat content of these geothermal reservoirs are estimated at the km^2 scale that is a typical scale for existing heat-pump geothermal projects. This chapter seeks to arrive only at estimates of the heat energy available and is an early-stage reconnaissance for future work. A version of this chapter is published in a peer reviewed journal (Ardakani et al., 2016a) and the work has been presented in numerous conferences (Ardakani and Schmitt, 2011a, 2012a, 2013a, 2014a; Ardakani et al., 2011b, 2012b).

In chapter 4 a study of structural lineaments in the sedimentary basin is presented. In this study the integrated processing and interpretation of the High Resolution Aeromagnetic and 2D seismic reflection data in the Athabasca region, near Buffalo Creek reveals the existence of a set of buried southwest-northeast striking structural elements. These lineaments are interpreted as igneous dykes that may bisect the entire sedimentary column, but remain blanketed beneath the thick glacial deposits in the area. This interpretation is supported by magnetic forward modeling. Correlation of the magnetic anomalies to irregularities in crossing 2D seismic profiles provides additional supporting evidence. We conclude with some speculations as to the provenance of these features. This chapter is a version of an under-review paper for publication in the Geological

Society of America bulletin (2016b) and an expanded abstract (Ardakani and Schmitt, 2015).

Chapter 5 focuses on the Precambrian basement and the application of HRAM and 2D seismic data to drive observation and interpretation on topography and structural elements within the Precambrian basement. Somewhat by chance, the study area covers an interpreted contact between two Proterozoic (1.8 Ga to 2.4 Ga) basement domains of the Taltson Magmatic Zone (TMZ) and the Buffalo Head Terrane (BHT). There is some discussion as to whether this contact represents a tectonic collisional plate boundary with associated subduction or if, in contrast, is more akin to intraplate displacements similar to those producing the mountain belts of Central Asia radiating from the Asian-Indian plate indentation. The Phanerozoic structure, too, is compelling here. The Leduc-Rimbey reef trend, which developed in the Devonian follows very closely the BHT-TMZ contact. Consequently, given that we have data covering both of these features, it is interesting to address questions as to the nature of the BHT-TMZ contact and whether or not this contact may also have served as a zone of weakness with vertical fault displacements perhaps being responsible for the formation of the Leduc reef trend. To address these problems, we further explore in detail the magnetic data set looking at potential structures deeper in the crust. The seismic data that do cross the boundary also show some interesting changes in character across the boundary. Regrettably, the data sets here cannot unambiguously answer the above questions, but we provide this work as motivation for future focused exploration.

Chapter 6 summarizes the general interpretations and conclusions of the results obtained in the research and provide suggestions for future work.

References

Alberta Energy and Utilities Board, 2005, Alberta's reserves 2004 and supply demand outlook 2005-2014: Statistical Series, ST98-2005.

Ardakani, E. P., and D. R. Schmitt, 2011a, Developing Engineered Geothermal Systems (EGS) in Alberta, Canada: Proceeding of the 1st EAGE Sustainable Earth Sciences (SES) Conference and Exhibition, doi: 10.3997/2214-4609.20144204, Valencia, Spain.

Ardakani, E. P., and D. R. Schmitt, 2012a, Adding to the geophysical tool box for geothermal exploration; use of seismic and magnetic surveys in a regional geophysical study for geothermal exploration in NE Alberta, Canada: Proceeding of Geothermal Research Council Transactions, 36, 985-988, Reno, USA.

Ardakani, E. P., and D. R. Schmitt, 2013a, Regional geophysical study for geothermal exploration in NE Alberta: Proceeding of the Canadian Society of Exploration Geophysics Geoconvention, Calgary, Canada.

Ardakani, E. P., and D. R. Schmitt, 2014a, Athabasca regional geophysical study - implications for geothermal development in northeastern Alberta, Canada: Proceeding of the 76th European Association of Geoscientists and Engineers Conference and Exhibition, Amsterdam, NL.

Ardakani, E. P., and D. R. Schmitt, 2014b, Investigation of Devonian Unconformity Surface Using Legacy Seismic Profiles, NE Alberta: Canadian Society of Exploration Geophysics Geoconvention, Extended abstract, Calgary, Canada.

Ardakani, E. P., D. R. Schmitt, 2016a, Geothermal energy potential of sedimentary formations in the Athabasca region, Northeast Alberta, Canada: Interpretation, 4, SR19-SR33, doi: 10.1190/INT-2016-0031.1.

Ardakani, E. P., D. R. Schmitt, 2016b, Geophysical evidence for an igneous dyke swarm, Buffalo Creek, Northeast Alberta under review for publication in Geological Society of America bulletin.

Ardakani, E. P., and D. R. Schmitt, 2015, Detecting lineaments of Athabasca region by integrated geophysical data interpretation: Canadian Society of Exploration Geophysics Geoconvention, Extended abstract, Calgary, Canada.

Ardakani, E. P., D. R. Schmitt, and T. D. Bown, 2014c, Detailed topography of the Devonian Grosmont Formation surface from legacy high resolution seismic profiles, Northeast Alberta: Geophysics, 79, B135-B149, doi: 10.1190/geo2013-0268.1.

Ardakani, E. P., D. R. Schmitt, and I. Moeck, 2012b, Use of seismic and magnetic surveys in a regional geophysical study for geothermal exploration in NE Alberta, Canada: American Geophysical Union, Fall Meeting, abstract #V13C-2863, San Francisco, USA.

Ardakani, E. P., D. R. Schmitt, and T. D. Bown, 2013b, Devonian Grosmont Formation surface investigation using legacy high resolution seismic profiles, NE Alberta, Canada: Proceeding of the 75th European Association of Geoscientists and Engineers Conference and Exhibition, London, UK.

Ardakani, E. P., D. R. Schmitt, T. Bown, J. Chan, S Idowu, J. A. Majorowicz, M. Unsworth, M. van der Baan, K. Bauer, I. Moeck, M. Pussak, and S. Weides, 2011b, Regional geophysical reconnaissance for low enthalpy geothermal resources in NE Alberta, Canada: American Geophysical Union, Fall Meeting, Abstract #H21E-1160, San Francisco, USA.

Bachu, S., J. R. Underschultz, B. Hitchon, 1996, Regional subsurface hydrogeology in Northeast Alberta: Alberta Geological Survey, open file report 1996-14.

Batycky, J. P., R. P. Leaute, and B. A. Dawe, 1997, A mechanistic model of cyclic steam stimulation: Proceedings of the International Thermal Operations and Heavy Oil Symposium, Bakersfield, CA, USA, February 10-12, SPE 37550.

Barss, D. L., E. W. Best, and N. Mayers, 1964, Triassic, in R. G. McCrossan, and R. P. Glaister, eds., Geological history of Western Canada: Alberta Society of Petroleum Geologists, chapter 9, 113-136.

Butler, R. M., G. S. McNab, and H. Y. Lo, 1981, Theoretical studies on the gravity drainage of heavy oil during in-situ steam heating: Canadian Journal of Chemical Engineering, 59, 455-460.

Energy Resources Conservation Board, 2009, Table of formations, http://www.ercb.ca/docs/products/catalog/TOF.pdf, accessed 27 July 2012.

Energy Resources Conservation Board, 2010, Alberta's energy reserves 2009 and supply/demand outlook 2010-2019, Open file report ST98-2010.

Grasby, S. E., D. M. Allen, Z. Chen, G. Ferguson, A. Jessop, M. Kelman, J. Majorowicz, M. Moore, J. Raymond, and R. Therrien, 2011, Geothermal energy resource potential of Canada: Geological Survey of Canada, open file report.

Hardage, B. A., 2000, Vertical Seismic Profiling: Principles, third edition: Pergamon, Amsterdam.

Louie, J. N., S. K. Pullammanappallil, and W. Honjas, 2011, Advanced seismic imaging for geothermal development: Proceeding of New Zealand Geothermal Workshop, Auckland.

Mossop, G., and I. Shetsen, 1994, Geological atlas of the Western Canada Sedimentary Basin: Canadian Society of Petroleum Geologists and Alberta Research Council.

National Energy Board, 2015, Energy futures supplement-demand sensitivities, https://www.neb-one.gc.ca/nrg/ntgrtd/ftr/2015/index-eng.html, retrieved January 23, 2016.

Parsons, W. H., 1973, Alberta, in R. G. McCrossan, eds., The Future Petroleum Provinces of Canada - Their Geology and Potential: Canadian Society of Petroleum Geologists, Memoir 1, 73-120.

Porter, J., R. Price, and R. McCrossan, 1982, The Western Canada Sedimentary Basin: Philosophical Transactions of the Royal Society of London, Series A, Mathematical and Physical Sciences, 305, 169-192, doi:10.1098/rsta.1982.0032.

Sheriff, R. E., 2002, Encyclopedic Dictionary of Applied Geophysics, 4th edition: Society of Exploration Geophysicists, Tulsa, Oklahoma.

Stewart, R. R., 2001, VSP: An in-depth seismic understanding: Canadian Society of Exploration Geophysics Recorder, 79-83.

Telford, W. M., L. P. Geldart, and R. E. Sheriff, 1990, Applied Geophysics, 2nd edition: Cambridge University Press, Cambridge, UK.

Grosmont Formation surface from legacy high resolution seismic profiles, Northeast Alberta

The Devonian Grosmont Formation in Northeastern Alberta, Canada is the world's largest accumulation of heavy oil in carbonate rock with estimated bitumen in place of 64.5×10^9 m³. Much of the reservoir unconformably subcrops beneath Cretaceous sediments. This is an eroded surface modified by karstification known as SubMannville Unconformity (SMU). This study describes the reanalysis and integration of legacy seismic data sets obtained in the mid-80's to investigate the structure of this surface. Standard data processing is carried out supplemented by some more modern approaches to noise reduction. The interpretation of these reprocessed data results in some key structural maps above and below the SMU. These seismic maps reveal substantially more detail than those constructed solely on the basis of well log data; in fact the use of only well log information would likely result in erroneous interpretations. Although features smaller than about 40 m in radius cannot be easily discerned at the SMU due to wave-field and data sampling limits, the data reveal the existence of a roughly east-west trending ridge-valley feature. A more minor northeast-southwest trending linear valley also is apparent. These observations are all consistent with the model of a karsted/eroded carbonate surface. Comparison of the maps for the differing horizons further suggests that deeper horizons may influence both the structure of the SMU and even the overlying Mesozoic formations. This suggests that some displacements due to karst cavity collapse or minor faulting within the Grosmont occurred during or after deposition of the younger Mesozoic sediments on top of the Grosmont surface.

2.1. Introduction

The Devonian Grosmont Formation of the Northeastern Alberta plains is a carbonate platform encompassing an area of 85000 km^2 of which about 20800 km^2 is prospective for bitumen (**Figure 2.1a**). Many authors have indicated that the area of the Grosmont platform is comparable to that of the modern day Bahama Banks (**Figure 2.1b**). Even though much of the Bahama Banks is currently submerged, during recent glacial maxima it was a dry land subject to karsting.

The Grosmont Formation is projected to hold upwards of 64.5×10^9 m^3 of bitumen according to the recently updated reserves estimates of the Energy Resources Conservation Board (ERCB, 2010). In the last decade there has been a great deal of interest in exploiting this resource. However, this is only the second round of investigation of the Grosmont reservoir. In the early to mid-80's the reservoir was first tested in a government/industry project supported through the Alberta Oil Sands Technology and Research Authority (AOSTRA). This consortium acquired geophysical and well log data and initiated a few pilot project tests. Much of the geological information, primarily from well log and cores, has already been published from various sources and entered into the public record (Belyea, 1956; Dembicki and Machel, 1996; Buschkuehle et al., 2007; Borrero and Machel, 2010; Machel, 2010; Wo et al., 2010; Barrett and Hopkins, 2010; Machel et al., 2012), however the abrupt termination of the research project related to the decline of heavy hydrocarbon prices in the late 1980's together with the general lack of now ubiquitous computer assisted interpretation programs did not allow for proper integration of all of the seismic data obtained in the research.

The primary purpose of this contribution is to illustrate using seismic data the complexities of the eroded and karsted Grosmont surface. Such detailed investigation cannot be achieved from the sparse sampling available from direct borehole measurements. Secondarily, the contribution seeks to preserve a unique and perhaps historic geophysical data set. The 2D seismic data obtained here cannot hope to compete against modern 3D seismic imaging. However, the researchers attempted to push the limits in terms of improving the ability to resolve the shallow Grosmont surface and the "high spatial resolution" sampling they finally adopted was unique for the time period and hints towards more modern data acquisition strategies. The data obtained clearly illustrate the evolution of technique over this time period as the researchers were forced to concede that standard practices could not work well in imaging the relatively shallow unconformity surface. The contribution begins with information on the current state of knowledge as to the regional and more local geological structure. The legacy data are then presented in detail and the reprocessing and integrated strategies described. Interpretation of the integrated seismic data allows for a relatively detailed mapping of the Grosmont surface over the study area that displays substantial topographic variations likely related to karst-driven erosion.

2.2. Regional geology

The gross geological structure of Alberta, east of the disturbed belt and Rocky Mountains consists of a wedge of sediments, overlying the Archean and early Proterozoic metamorphic rocks of the Canadian Shield. The sedimentary basin is about five or more kilometers thick at its western edge and thins progressively north-eastward. This veneer of sediments disappears entirely in the extreme northeastern corner of Alberta where the Canadian Shield is exposed. To

first order this sediment wedge consists of two major parts. Indurated older sediments with ages ranging from the latest Proterozoic through the Paleozoic with some limited early Mesozoic sediments immediately overlie the Canadian Shield. In large part, these were marine carbonates and shale deposits laid down on a passive continental margin. The topmost wedge, in contrast, consists of Mesozoic siliciclastic sands and shales deposited in shallow seas and estuarine and fluvial environments.

The geological unconformity separating the primarily Paleozoic and Mesozoic sediments is a major basin-wide feature and plays an important role in this study because the bulk of the bitumen resides at and immediately beneath this interface. The cross section A-B crossing the Grosmont platform (outlined in white) from **Figure 2.1a** is shown in **Figure 2.2** that represents the large scale geological structure representative of the study area. The predominant lithologies within the various sedimentary layers overlying the Canadian Shield begin with the lower Devonian Elk Point group containing significant evaporates and carbonates, the mid to Upper Devonian Beaverhill Lake group, the Upper Devonian Woodbend-Winterburn group, and the Upper Devonian and Mississippian Wabamum and other formations. These are all blanketed by the Lower Cretaceous Mannville Group which is in turn covered by Upper Cretaceous and, in some locales, Tertiary sediments (**Figure 2.2**).
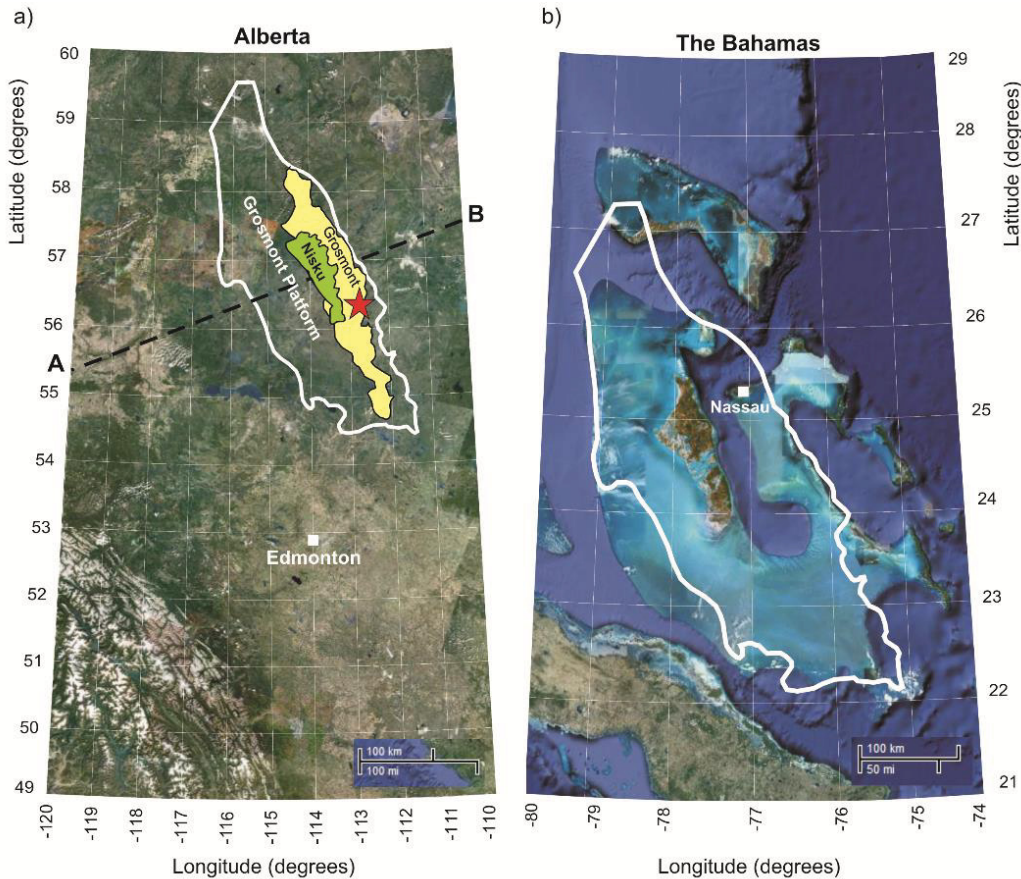
Figure 2.1. (a) Satellite image of Alberta showing the extent of the Grosmont platform in white. Outlines of the areas of the Grosmont and Nisku carbonate bitumen deposits in yellow and green, respectively. The area of study is shown with the red star. (b) Satellite image of the Bahama Banks illustrating the size of a modern-day shallow-water carbonate platform. Outline of the Grosmont platform from **Figure 2.1a** superimposed in white (images are from NASA).

Two unconformities are seen here. The first is the unconformity between the Lower Devonian Elk Point and the Precambrian metamorphic Canadian Shield (PCU). This unconformity represents an about 1.5 Ga time gap, separating rocks that formed at about 2.0 Ga and 0.5 Ga. While this unconformity will not play a major role in this study, it is important not to forget it as the unconformity may hold clues as to the potential for large scale tectonic motions that could

22

directly via faulting or indirectly via deformation of deeper sedimentary formations eventually influence the Upper Devonian formations being studied here (Cotterill and Hamilton, 1995). The second shallower SubMannville unconformity (SMU) separates the Mesozoic Lower Cretaceous siliciclastic rocks from the Upper Devonian carbonates. This unconformity goes by many different names in the literature (e.g., SubCretaceous, Paleozoic) but here we employ SubMannville because in the study area the Lower Cretaceous Mannville Group covers the subcropping Upper Devonian rocks. This unconformity is the key to the development of the Grosmont resource that abuts the unconformity. The unconformity surface was modified by a combination of erosion and karsting; and this raises numerous complexities to the development of the resource as it remains difficult to delineate smaller karst features.
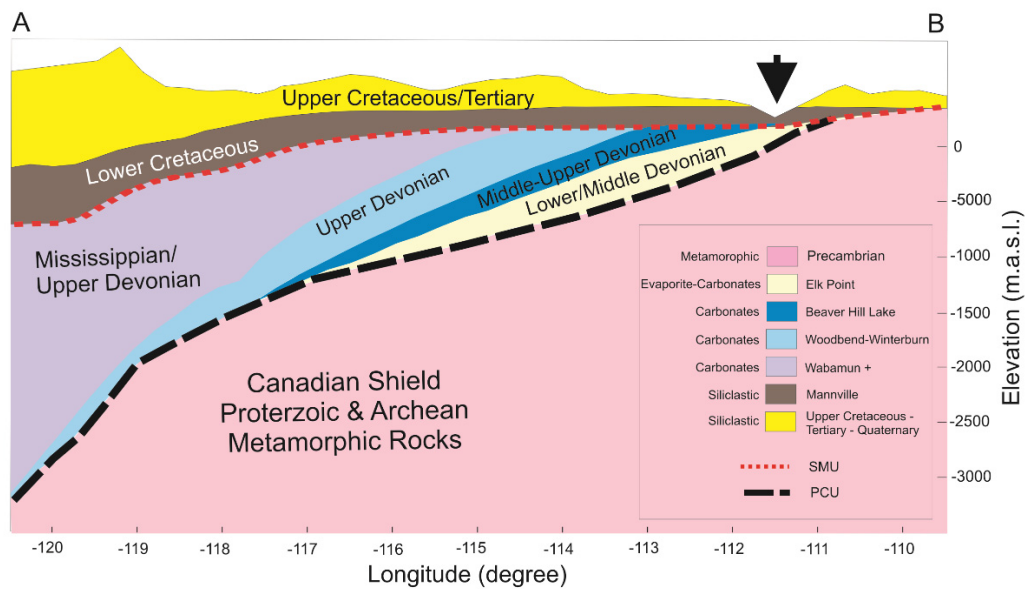
Figure 2.2. Synoptic cross section A-B (outlined in **Figure 2.1a** with the dashed line) shows the general geologic structure around the study area (black arrow) developed from digital geologic formation tops (Mossop and Shetsen, 1994).

2.3. Local stratigraphy

In the study area all of the SMU rocks are of Devonian age beginning with various Upper Devonian Nisku, Upper Ireton, and Grosmont Formation subcropping. The Ireton and Grosmont formations belong to the Upper Devonian Woodbend Group and the Nisku to the Winterburn Group (Switzer et al., 1994). At the scale of the Western Canada Sedimentary Basin (and even beyond) the Woodbend holds important siliciclastic sources (Duvernay and Muskwa formations) and reservoir rocks, particularly the large (up to 275 m high) Leduc reef complexes and the generic Grosmont subcropping bitumen reservoirs of interest here. The Woodbend-Winterburn Groups represent rapid deposition of substantial amounts of carbonates and basin filling shales that exceeds 850 m thickness in some places: a substantial fraction of the basin itself. This occurred over a short period of about only 7 Ma from the early Famennian (372 Ma to 359 Ma) through the latest Frasnian (383 Ma to 372 Ma). **Figure 2.3** illustrates the generalized regional stratigraphy (ERCB, 2009).
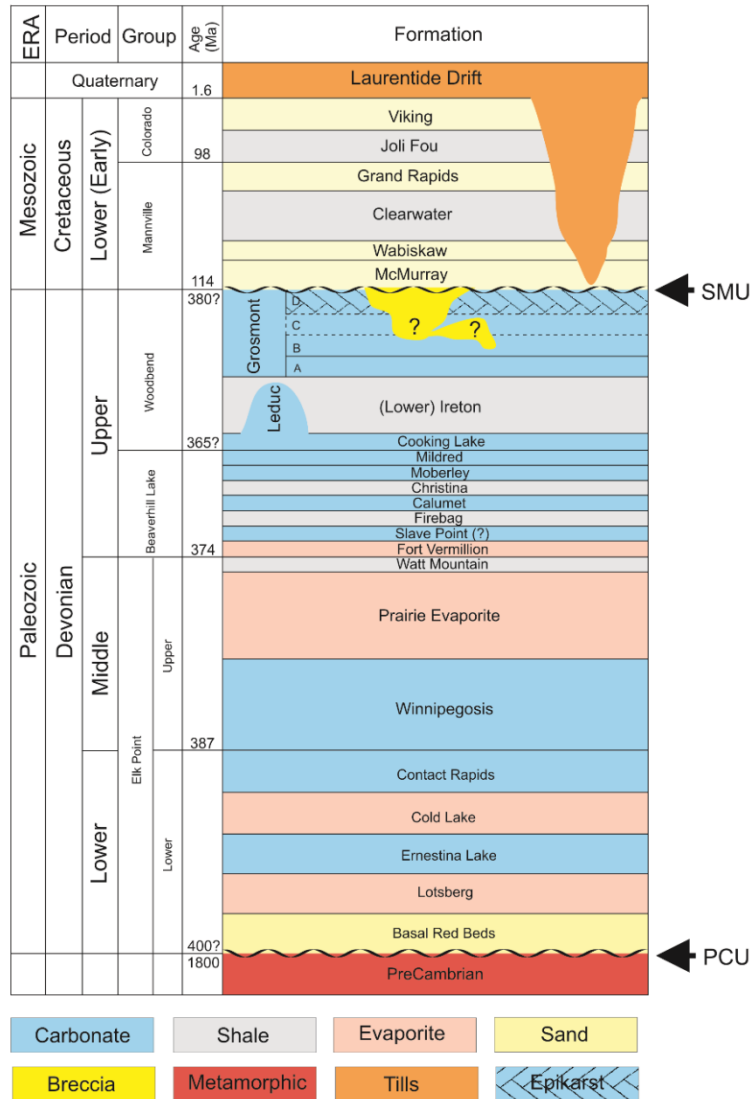
Figure 2.3. Generalized regional stratigraphy after ERCB (2009). The SMU and PCU are represented as wavy lines on the stratigraphy chart.

2.4. Grosmont Formation and karstification

The Grosmont was first described by Belyea (1952) and, despite its size, only received scant attention (Law, 1955; Norris, 1963; Belyea, 1964) until the late 1970's and early 1980's when high hydrocarbon prices motivated exploration of nonconventional reservoirs. This spurred a flurry of work by both Government at the Alberta Research Council (ARC) and Alberta Energy and Natural Resources

25

(AENR) (Harrison and McIntyre, 1981; Harrison, 1982; Harrison, 1984; Harrison, 1986; Walker, 1986; Yoon, 1986) and University scientists (Cutler, 1982; Bélanger-Davis, 1985; Hutcheon and Oldershaw, 1985; Hoffmann and Strausz, 1986; Theriault and Hutcheon, 1987; Theriault, 1988). Studies continued into the 1990's (Cotterill and Hamilton, 1995) some sponsored by Alberta Oil Sands Technology and Research Authority (AOSTRA) (Luo et al., 1994; Machel and Hunter, 1994; Luo and Machel, 1995; Dembicki and Machel, 1996; Huebscher and Machel, 1997) with a number of corresponding related thesis available (Dembicki, 1994; Huebscher, 1996). The increased value for oil beginning in the last decade motivated re-examination of the resource with public domain presentations regarding the Grosmont (Hein 2006; Buschkuehle et al., 2007; Hein et al., 2008; Wo et al., 2010) with academic contributions (Zhao, 2009; Borrero and Machel, 2010).

According to Borrero and Machel (2010) the Grosmont Formation is a complex of carbonate layers divided by three shale breaks representing Upper Devonian rapid deposition of substantial amounts of carbonates and basin filling shale. Currently, the Grosmont Formation is further divided into four distinctive units on the basis of signatures in the natural gamma ray log; Lower Grosmont, and the Upper Grosmont 1, 2, and 3 (Cutler, 1982; Harrison, 1982) but will here be called the A, B, C, and D, respectively, in accordance with ERCB nomenclature (2009). **Figure 2.4** shows how these four units are distinguishable on the well logs from a borehole (Well-02) in the study area (see well location in **Figure 2.5**). These units are composed primarily of limestone and dolostone. Units A and B are generally of low porosity (Hopkins and Jones, 2009; Barrett and Hopkins, 2010) than the uppermost C and D. This difference in porosity derived from extensive karstification. According to Huebscher (1996) karstification

occurred during the Upper Jurassic and Lower Cretaceous due to the exposure and dissolution by meteoric water. These karst features can be recognized at many scales from core samples, well logs and high resolution seismic data.
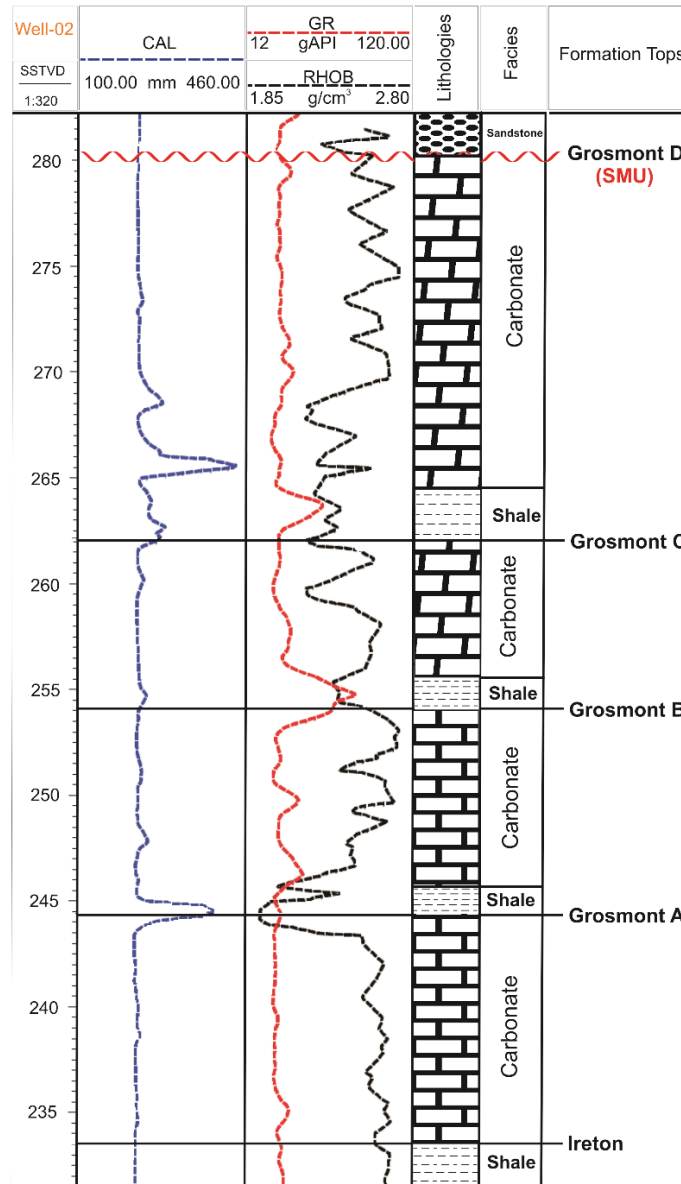
Figure 2.4. Well section from well-02 located southeast of the study area. Density (RHOB) and gamma ray (GR) log signatures are used for identifying units of the Grosmont.

2.5. Data available and methods

The data sets employed for this study consist of well logs and geological formation tops, high resolution seismic surveys, and the reported results from a Vertical Seismic Profile (VSP). The relative location of seismic profiles, wellbores, and the VSP location is given in **Figure 2.5**. Absolute locations cannot be provided and as such the final interpretations should be considered as illustration of the complex geometries of the SMU. Additional details are available in Bown (2011).
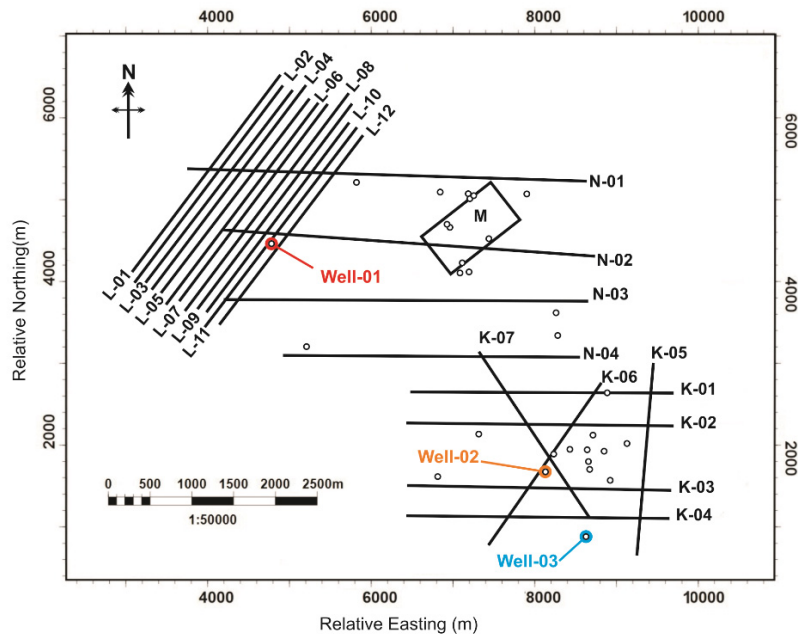
Figure 2.5. Map from the study area showing the approximate locations of the wellbores and seismic profiles. Exact locations cannot be provided.

2.5.1. Well logs and formation tops data

The database accessible to us provided 99 logs and 136 geological formation tops from 31 wells in the study area. Among the well logs, caliper, density, gamma ray and sonic logs are the most important wireline logs for detecting karst features (Dembicki, 1994; Dembicki and Machel, 1996; Huebscher

28

and Machel, 1997; Machel et al., 2012). Also, sonic and density logs are required for calculation of synthetic seismograms used in well-tie procedure. Unfortunately most of the wells in the area just touch the SMU as they were drilled for shallow gas production; this reduced the number of logs available to reveal deeper structure within the Grosmont Formation.

Well-03 is drilled into a karst feature and its logs provide an example of the expected responses (**Figure 2.6**). All the logs in **Figure 2.6** are imaged in Sub-Sea True Vertical Depth (SSTVD). The Resistivity logs in the first panel consist of Invaded Formation Resistivity filtered at 8 inches (RXO8) and True Formation Resistivity (RT). RXO8 is the measurement of the flushed zone resistivity while RT is related to the resistivity of undisturbed formation (i.e. several meter into the formation from the borehole). In the second panel Caliper (CAL) and Environmentally Corrected Gamma Ray (ECGR) logs are shown. CAL represents the internal diameter of the borehole and ECGR shows the intensity of natural gamma ray radiation emitted from the formation. The High Resolution Formation Density (RHO8) and High Resolution Enhanced Thermal Neutron Porosity of Limestone (HNPO-LIM) logs are illustrated in the last panel. RHO8 represents the density of bulk material and HNPO is a measure of porosity of the formation in a selected lithology. Looking at the Grosmont D from bottom to the top of the unit, all the presented logs are imaging different characteristics by getting closer to the SMU. RXO8 shows significant reduction of resistivity in the invaded zone (i.e. presence of porous material saturated by brine) although the RT is measuring the same resistivity as it is in the lower part of the unit. The CAL presents enlargement of the wellbore diameter and boost of ECGR represents the existence of fine grain material (such as shale, limestone contaminated with shale or breccia) in the upper section of the unit comparing with the lower section

which consists of coarse grain limestone without showing any wellbore washout in CAL. The decrease of RHO8 means less dense material in the upper section of the unit and HNPO-LIM growth is a complementary reference depicting high porosity zone. The Grosmont D composed of limestone and dolostone but as it is shown in this well section, the named logs are imaging different characteristics from the bottom of the unit to the top (SMU). These changes are all related to the karsting of the upper part of Grosmont unit D.
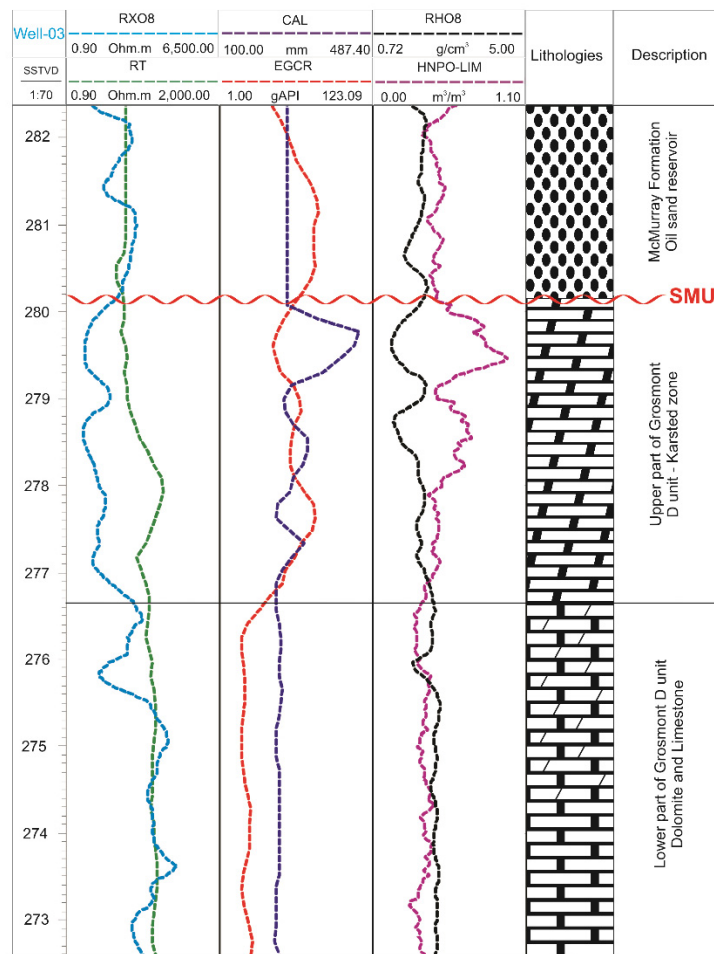
Figure 2.6. A well section from well-03 located southeast of the study area (see the well location in **Figure 2.5**) showing karstification events on top of Grosmont D. All the logs in this figure are imaged in SSTVD.

2.5.2. High resolution seismic surveys

Four separate high resolution seismic surveys of series here called K, L, M and N were obtained for this study (**Figure 2.5**). These high resolution surveys at the time of acquisition in the early to mid-80s were unique, because of closely spaced receivers and sources in the later surveys. **Table 2.1** provides a brief description of all the series acquisition parameters. Here we review the various high resolution seismic surveys obtained for the study;

Survey Series K: Seven short three to four km long profiles with closer shot and receiver spacing than would have been employed in standard industry practice at the time were acquired in order to better image the unconformity.

Survey Series L: 12 parallel profiles spaced only 110 m apart was carried out in the area in advance of potential development. This somewhat unique survey appears to have attempted pseudo 3D coverage by having the 2D profiles in close proximity to one another.

Survey Series M: A small full 3D seismic survey obtained over an area approximately 400 × 1000 m was an interesting experiment in seismic acquisition. The measurements were doubly unique because at the time 3D seismic surveying was still in its infancy and had not been accepted as the primary method it is today, but also because the short source and receiver spacing employed would still be rare in industrial practice. The short spacing between the sources and receivers as well as the small offsets show that its authors attempted to enhance the imaging of the unconformity surface. This was the only full survey to employ a surface seismic source; all others had previously used buried dynamite. This source was called a "pea shooter" (Omnes and Robert, 1982) that is

classified as a type of weight drop system in which seismic waves are generated by accelerating a mass onto a plate on the surface. Such sources have certain cost advantages in that they do not require that holes be drilled as is needed for dynamite and that they are easily moved and operated. A disadvantage of such sources, however, is that the quality of the seismic pulse put into the ground is much degraded (lower frequency and bandwidth) relative to a buried dynamite explosion. This is particularly true in marshy areas that exist at the site of the 3D survey.

Survey Series N: Four high resolution 2D profiles of series N were acquired to tie all of the earlier seismic lines together and fill in some of the unshot areas between them (see the profile locations in **Figure 2.5**). The acquisition parameters were developed with the results of prior experience and testing. Triple shots each of only 100 g of dynamite buried at 5 m depth provided high-bandwidth seismic energy. Nine geophones were clumped at each receiver station to increase the signal to noise, and the stations were spaced only 10 m apart. This seismic data allow discrimination of the Grosmont C from the Grosmont D.

Table 2.1. Acquisition parameters deployed by the vintage seismic surveys.

Survey Series	Acquisition Year	Total Distance (km)	Survey Type	Source	Source Configuration	Source Depth (m)	Source Interval (m)	Geophone	Geophone Group Configuration	Group Interval (m)	Max Offset (m)	Fold	Recording Parameters	Recording Filters
K	1981	19.93	2D	Dynamite	1×1 kg	18	45	L-15 14 Hz	6 clumped	22.5	540	12	48 traces @ 1 ms for 2 s	Low-Out High -256
L	1984	35.99	2D	Dynamite	1×0.5 kg	20	40	Mark L-28 14 Hz	12 inline over 1.8 m	10	480	12	96 traces @ 2 ms for 2 s	Low-12 High -180
M	1985	3.21	3D	P-shooter	20 drops	surface	40	L-280 14 Hz	9 inline over 20 m	20	220	10	120 traces @ 2 ms for 2 s	Low-12.5 High -125
N	1986	17.14	2D	Dynamite	3×0.1 kg	5	20	Mark OYO 14 Hz	12 inline over 10 m	10	250	12	48 traces @ 1 ms for 2 s	Low-Out High 256

2.6. Seismic data processing workflows

The bulk of the efforts towards the reanalysis of these data focussed first on the reprocessing of the profiles from the disparate data sets to a common elevation datum of 518 m above sea level (a.s.l.). Substantial efforts were expended in data preparation such as re-formatting, organizing, editing, and merging of field geometry before the application of processing workflows. This work was also all done with an eye to the eventual integration of the disparate data sets and necessitated assigning an appropriate reference datum from which all of the reprocessing was carried out. The seismic data processing package VISTA™ provided for research purposes courtesy of GEDCO was used for all of the data quality control and processing. The processing stream followed noise reduction strategies used in Ogunsuyi and Schmitt (2010) employed for the 2D and 3D data sets are given in **Table 2.2**. Although many of conventional processing steps are applied there are still specific aspects just related to the data and geological nature of the study region as follow;

The near surface conditions in this area, and indeed of much of Northern Alberta, are problematic to geophysical investigations due to the near surface lateral composition and structural variability. The near surface overburden is the result of a variety of glacial and periglacial structures combined with modern day sphagnum-moss muskeg. Glacial features can include sediment thrust faulting, creation of sub-ice tunnel valleys that can cut as deep as the SMU, and compacted tills. Compacted tills are generally high velocity while lacustrine and fluvial sediments (often coarse sands and gravels) are lower. Muskeg is problematic as it can be both very low velocity (less than 600 m/s) as well as highly attenuating to the input seismic energy. This requires that careful static corrections be carried out to account for lateral varying elevations and seismic velocities. First break

picks were used to generate the velocity structure of the near-surface for refraction static corrections. Elevation static corrections accounted for the variations in the source and receiver elevations along the profile by positioning the data onto a common datum. Refraction static corrections (Cox, 1999) was performed to correct the distortions associated with the variable thickness and velocity of the weathered layer.

Table 2.2. The general sequence of 2D and 3D seismic data processing.

2D Seismic Data Processing Sequence	3D Seismic Data Processing Sequence
- Pre-processing steps - Geometry – Load headers - Trace editing – Kill bad traces - First break picking - CMP Binning - Elevation/Refraction static corrections - Fixed datum: 518 m a.s.l. - Refraction replacement velocity: 2255 m/s - Weathering velocity: 900 m/s - Scaling - Exponential gain - Surface consistent scaling - Band-pass filtering *f-k* filtering (to suppress ground roll) - Top mute - Surface consistent predictive deconvolution (160 ms operator length) - Radial processing - Time variant spectrum balancing - Iterative velocity analyses - Iterative residual static corrections - Final velocity analyses - Residual static corrections - NMO corrections and CMP stacking - Band-pass filtering - Automatic gain control - Finite difference migration	- Pre-processing steps - Geometry – Load headers - Trace editing – Kill bad traces - First break picking - CMP Binning - Elevation/Refraction static corrections - Fixed datum: 518 m a.s.l. - Refraction replacement velocity: 2500 m/s - Weathering velocity: 800 m/s - Scaling - Exponential gain - Surface consistent scaling - Time variant band-pass filtering - Surface consistent spiking deconvolution - Time variant spectrum balancing - Iterative velocity analyses - Iterative residual static corrections - Flex binning - Mute - NMO corrections and CMP stacking - Band-pass filtering - Automatic gain control - Finite difference migration

Surface consistent amplitude scaling was carried out to correct for the spherical divergence of the source wavefield and other attenuation effects. A top mute was carried out for the removal of the direct, refracted, and guided waves.

This is essentially a brute force removal of these strong offending arrivals from the raw shot gathers. An *f-k* filter was designed and applied to suppress ground roll. This worked well for survey series L and N but it was not a suitable approach for survey series K and M because of spatially aliasing of the ground roll due to spacing. Therefore, a band-pass filter designed to reject frequencies below 20 Hz to suppress ground roll energy from series K and M. The initial band-pass filters were applied to the individual seismic surveys as outlined in **Table 2.3**.

Table 2.3. List of initial band-pass filters applied to the seismic data.

Survey Series	Band-pass filter (Hz) (low truncation / low corner - high corner / high truncation)	Comments
K	17-20-190-250	Low frequencies are removed for the suppression of ground roll.
L	8-12-150-175	
M	17-20-125-150	Low frequencies are removed for the suppression of ground roll.
N	8-12-190-250	

Predictive deconvolution was used to suppress multiples. Residual static corrections were iteratively applied with velocity analyses. The VSP traveltimes provided reference stacking velocity trends in seismic velocity picking. The residual static corrections are required to account for the short wavelength variations in the shallow velocity underneath each source and receiver. The surface consistent residual static corrections were estimated by a stack power maximization algorithm.

Migration was applied to the seismic data to overcome positioning errors, collapse diffractions and improve the vertical and lateral resolution of the images.

Two migration algorithms were employed: finite-difference migration (Berkhout, 1979) and Kirchhoff migration (Schneider, 1978). One example of the processed 2D profile is given for N-01 that contrasts the unmigrated stack (**Figure 2.7a**) with that corrected using Kirchhoff (**Figure 2.7b**) and finite-difference (**Figure 2.7c**) time migration. The top of the SMU is outlined in these figures just above 250 ms of two-way traveltime. Close examination of the unmigrated profile reveals numerous small diffractions or related (bowtie?) seismic arrival features. Such features are produced by geological structures of spatial dimensions similar to the seismic wavelengths used to illuminate the subsurface. Such structures scatter seismic energy in all directions producing localized convex, hyperbolic seismic events, the apex of which mark the location of the scatterer.

The complicated texture of the seismic events immediately beneath the SMU in **Figure 2.7a** is consistent with a series of small diffractions. This character differs significantly from the flatter and more continuous Mesozoic sediments above the SMU that do not display diffractions. The diffractions beneath the SMU are consistent with, but not conclusive of, a rough karsted topography with features too small to be properly imaged but which could still scatter the seismic energy. The migrated profiles in **Figure 2.7b** and **c** show better latterly continuity of the events immediately beneath the SMU, this is completely expected as one main purpose of migration is to collapse the diffraction back to their original scattered location. This comparison reinforces the need for the best practice of using both the unmigrated and the migrated data in interpretation. In the case studied here, the unmigrated data may actually provide more information on the location of scattering geological structures.

36
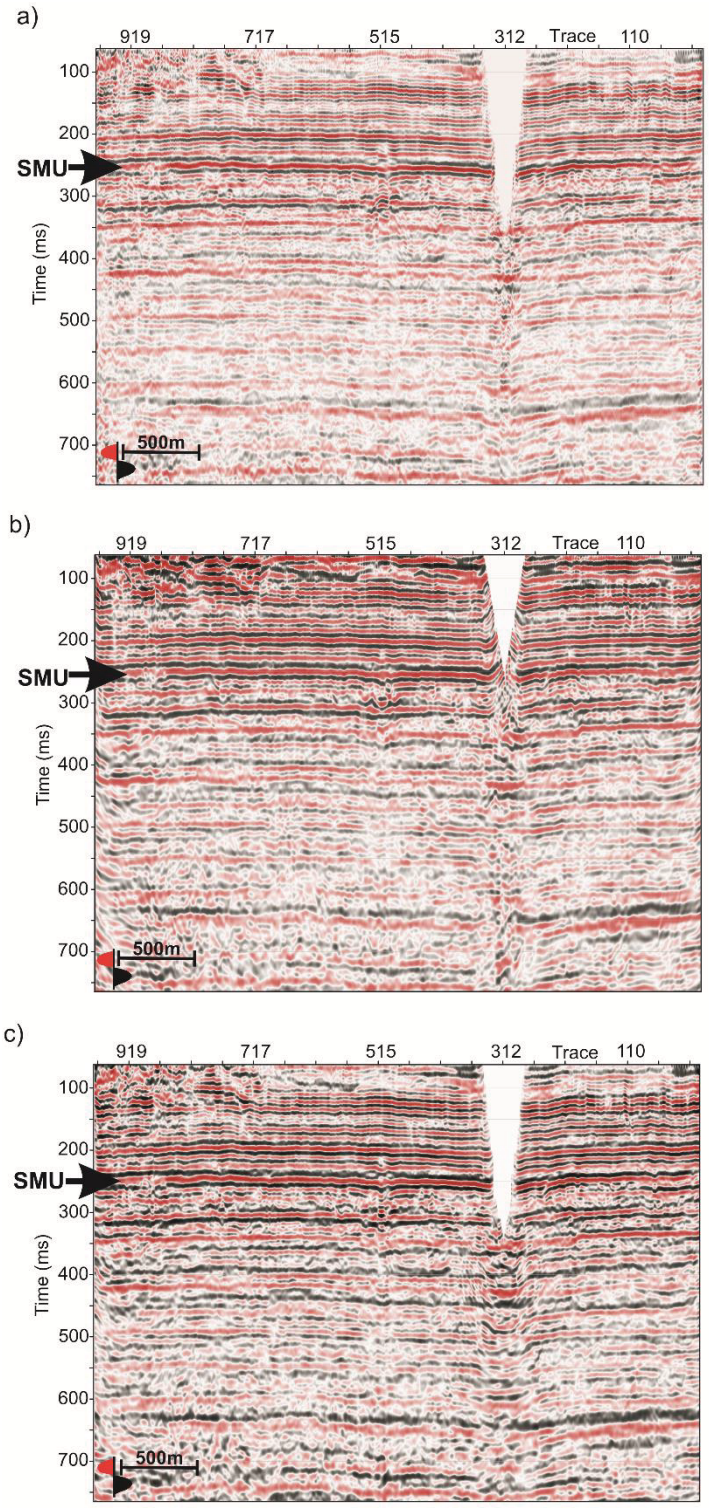
Figure 2.7. Examples of the final processed seismic profile 01 from the N series, (a) final stack, (b) Kirchhoff-migrated profile, and (c) finite-difference migrated profile.

Naturally, the processing of the 3D data differed from that for the 2D profiles but was further complicated by the low energy weight-drop seismic source employed. Such sources allow for multiple shots at each source location, but the source signature is of lower quality relative to dynamite. The processing followed procedures much like that employed for the 2D data although additional care was given to deconvolution of the data due to the poorer signal quality. Some examples of processed seismic lines from different series are shown in **Figure 2.8**. Comparison of these profiles in **Figure 2.8a, b, c** and **d** reveals the lower data quality of the 3D profiles relative to the 2D dynamite lines. This is in part due to the low 3D bin folds, the effects of static corrections in the area, and the type of source employed. Regardless, **Figure 2.8** illustrates the progression of data quality as experience was gained during the different surveys.
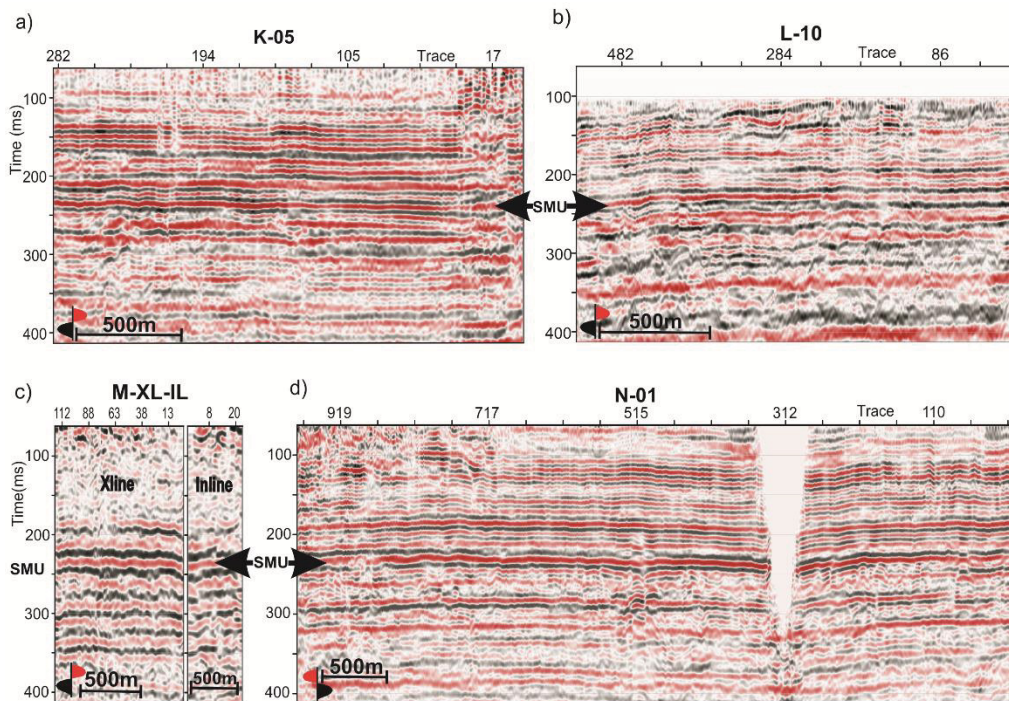
Figure 2.8. Some examples of processed seismic profiles from different seismic series showing data quality evolution from the first survey to the latest. Upon (a) profile 05 from the K series, (b) profile 10 from the L series, (c) crossline and inline profiles from the M series, and (d) profile 01 from the N-series.

2.7. Integration of the data sets and interpretation

A high resolution VSP and an extensive series of well logs were obtained in Well-01. The combination of this data allowed for the geology to be tied to the seismic images. Unfortunately, the original digital VSP data remain lost and could not be further processed to provide additional information on the reflectivity and multiple reflections. Only the time-to-depth picks and an image of the raw VSP data are still available (**Figure 2.9**). This imaged VSP data provided constraints on seismic traveltimes that were important both in assisting with the processing of the seismic data and in the interpretation of the profiles. The one-way traveltime of the VSP (blue diamonds) is plotted with the gamma ray log (green line) of the well for the interpretation of the individual Grosmont members.
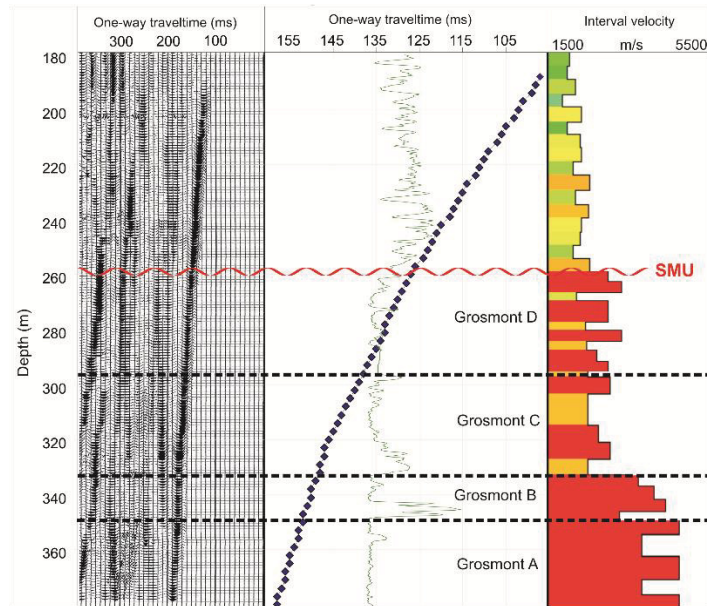
Figure 2.9. The left panel shows the image of the VSP from a confidential pilot project report for well location W-01. The middle panel shows the one-way traveltime of the VSP data (blue diamonds) superimposed on the unscaled gamma log. The interval velocity calculated using VSP data is illustrated in the right panel. The hot colors indicate higher interval velocities.

According to this comparison, the SMU resides at a True Vertical Depth (TVD) of 250 m that corresponds to a two-way seismic traveltime of about 240 ms. Sonic and density logs were acquired over a limited depth range from 180 to 400 m and used to generate a synthetic trace (**Figure 2.10**) based on a wavelet extracted from the nearby seismic traces. In this synthetic, the strong positive peak at 242 ms is associated with the SMU.
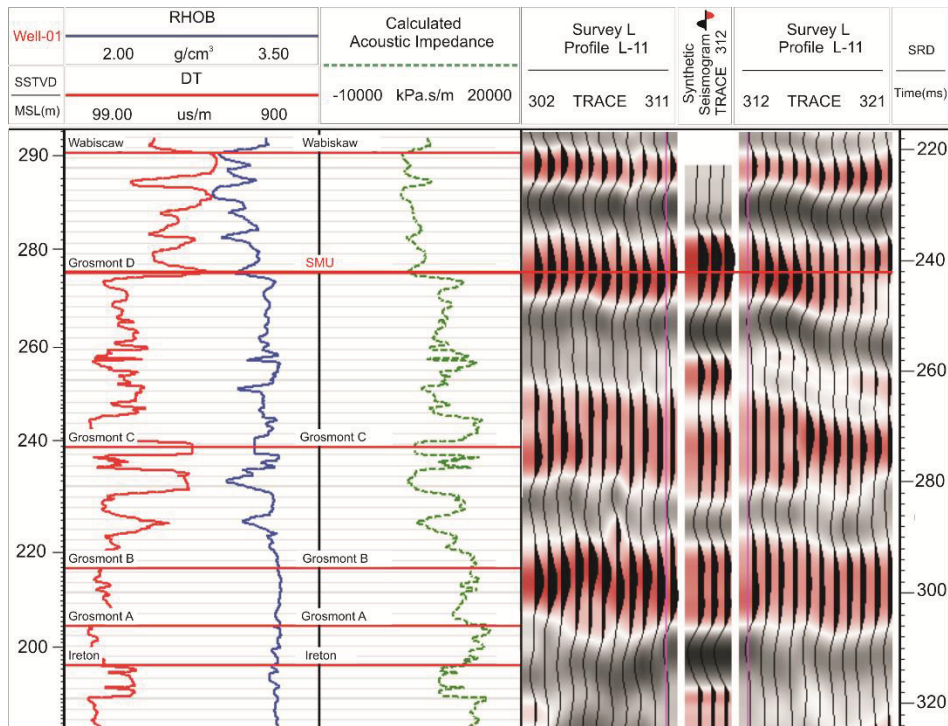
Figure 2.10. The correlation of a portion of seismic profile L-11 and constructed synthetic seismogram with the well logs used to generate a synthetic trace at the location of well-01. The calculated acoustic impedance is illustrated in the middle panels.

Despite the limitations of the VSP and well log data, the four different seismic surveys of K, L, M and N could be integrated by the prominent SMU horizon since in all of these data sets, the most prominent event is related to the SMU. It should be noted that the polarity of the N series profiles was reversed probably during the original acquisition of the data but it was apparent at tie

points and easily corrected. The strong event at the SMU is not unexpected given the large impedance contrasts between the Devonian carbonates and the Cretaceous siliciclastic rocks.

The VSP data was also used to develop an appropriate time to depth velocity model that allowed for conversion of the observed traveltimes into true elevations. The model is summarized in **Table 2.4** with **Figure 2.11** showing how the model varies in space over the Grosmont surface. Although this model is variant over the Wabiskaw-SMU and SMU-Ireton zones, the constant velocity has been used for rest of the zones due to the lack of geological tops deeper than Ireton for obtaining velocity surfaces. These constant velocities were computed using VSP for each individual zone.

Table 2.4. Summary of the velocity model used to convert two-way traveltimes to elevations.

Top Surface	Bottom Surface	Velocity Model	Comments
Seismic Reference Datum: 518 m.a.s.l.	Ground Surface	Constant interval velocity: 1720 m/s	Replacement velocity
Ground Surface	ClearWater	Constant interval velocity: 2200 m/s	Determined from VSP
ClearWater	Wabiskaw	Time to depth relation	Velocity surface made from checkshots
Wabiskaw	Grosmont D (SMU)	Time to depth relation	Velocity surface made from checkshots
Grosmont D (SMU)	Ireton	Time to depth relation	Velocity surface made from checkshots
Ireton	Prairie Evaporite	Constant interval velocity: 4900 m/s	Determined from VSP
Prairie Evaporite	Precambrian Basement	Constant interval velocity: 5400 m/s	No data - reasonable estimate
Precambrian Basement (PCU)		Constant interval velocity: 6000 m/s	No data - reasonable estimate
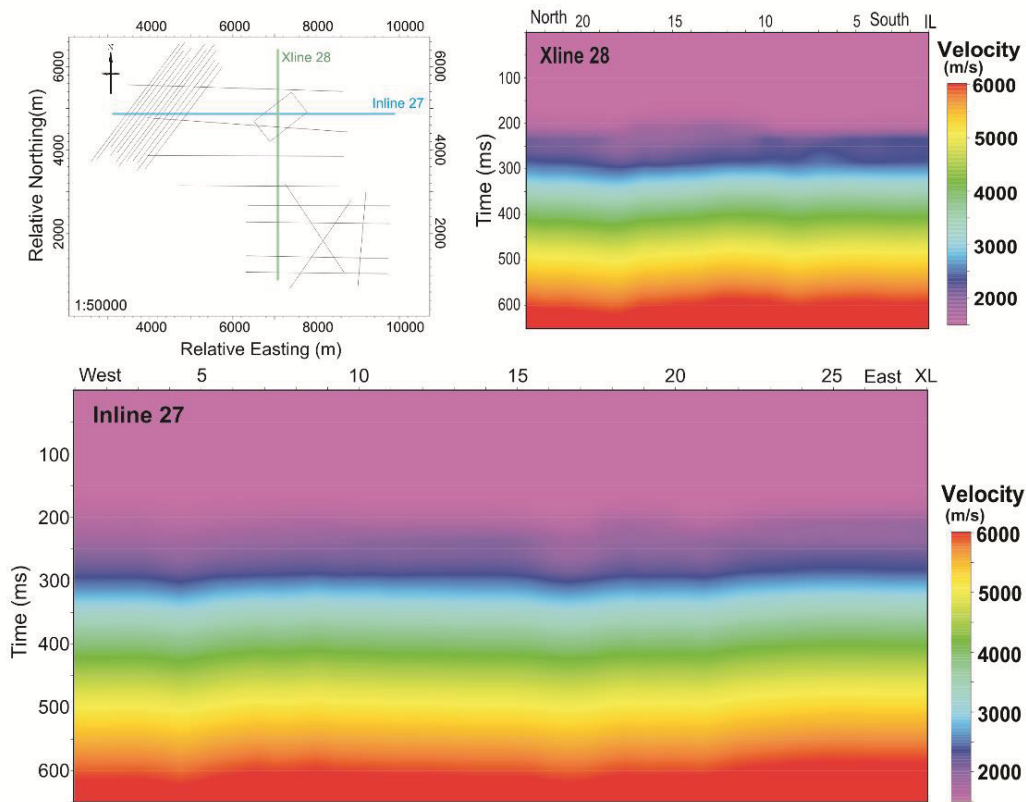
Figure 2.11. Displaying inline and crossline profiles of the generated velocity model used for depth conversion.

A few prominent seismic reflection horizons have been selected for interpretation and these are assigned to the various geological tops on the seismic profiles. However, the general lack of appropriate logs as well as the paucity of boreholes penetrating deeper than the Grosmont complicates this interpretation. The VSP was critical to obtain approximate lithological ties above the SMU horizon while lithologies deeper in the seismic section were confirmed by comparison to the interpreted regional geology knowledge. **Figure 2.12** shows these events on the profile L-11 with the synthetic seismogram used for well tie. The seismic events used for mapping and further interpretation are associated with the geological formations of the Clearwater, Wabiskaw, Grosmont (SMU), Lower Ireton, Prairie Evaporate, and finally, the Precambrian crystalline

42

Basement (PCU). Once the traveltimes to these various horizons are picked; they may be turned into maps of the surfaces in terms of seismic time, depth surfaces calculated using an appropriate velocity model, and isopach surfaces that reveal the variations in thicknesses of the intervals between two reference layers.
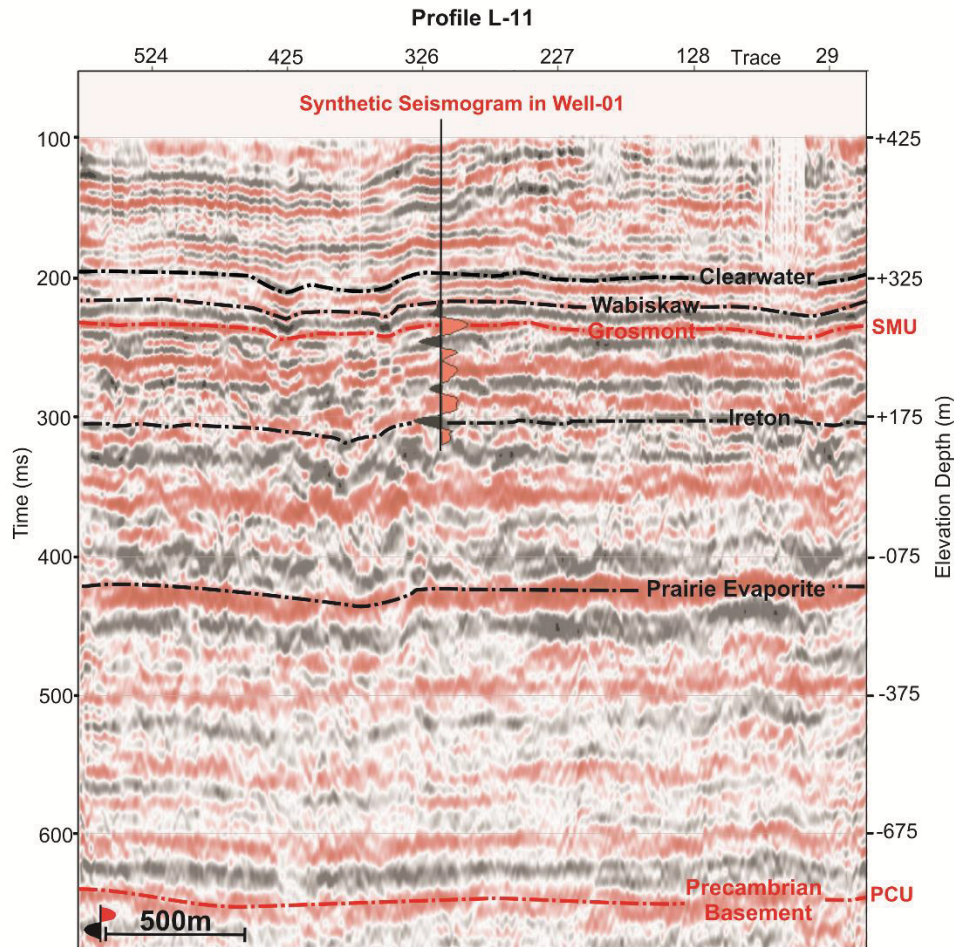
Figure 2.12. The synthetic seismogram plotted on the seismic profile L-11 at well-01. Example time picks for the seismic horizons selected for mapping are shown by the dotted-dashed line.

Figure 2.13 shows three different views of the SMU (top Grosmont D) surface elevation as determined solely from the sparse stratigraphic tops from well logs (**Figure 2.13a**), the reflection times directly picked from the integrated seismic profiles (**Figure 2.13b**), and the time-to-depth converted SMU elevation

depth (**Figure 2.13c**). In these plots, the surfaces were interpolated using the convergent gridding method. This algorithm uses a coarse grid which is initially assigned to the data, and then refined many times until the surface converges to a specified smoothness. The convergent gridding is a fast and general purpose extrapolation algorithm for randomly distributed scatter data points. It adapts to sparse or dense distribution through converging iterations at successively finer grid resolutions.

The well elevation map (**Figure 2.13a**) has 17 wells that reach the SMU but their positions were highly biased to the actual pilot project sites. In comparison, the seismic data show substantially more detail. Chiefly, the SMU varies on a smaller scale than the overall spatial sampling of well data, thus the well elevation map fails to adequately capture the topography of the SMU. Further, the validity of some of the well tops could not be confirmed because the original logs were not available for quality control purposes in some of the boreholes. Therefore, the final interpretation was conducted only on time elevation surfaces. Looking at **Figure 2.13b** the time difference from the highest to the lowest point of the map is 32 ms in two-way traveltime. This suggests a topographic variation on the order of 35 m. Whether the actual variations are that large could be questioned, but the seismic data and the resulting map provide strong evidence for rapidly varying topographic features.
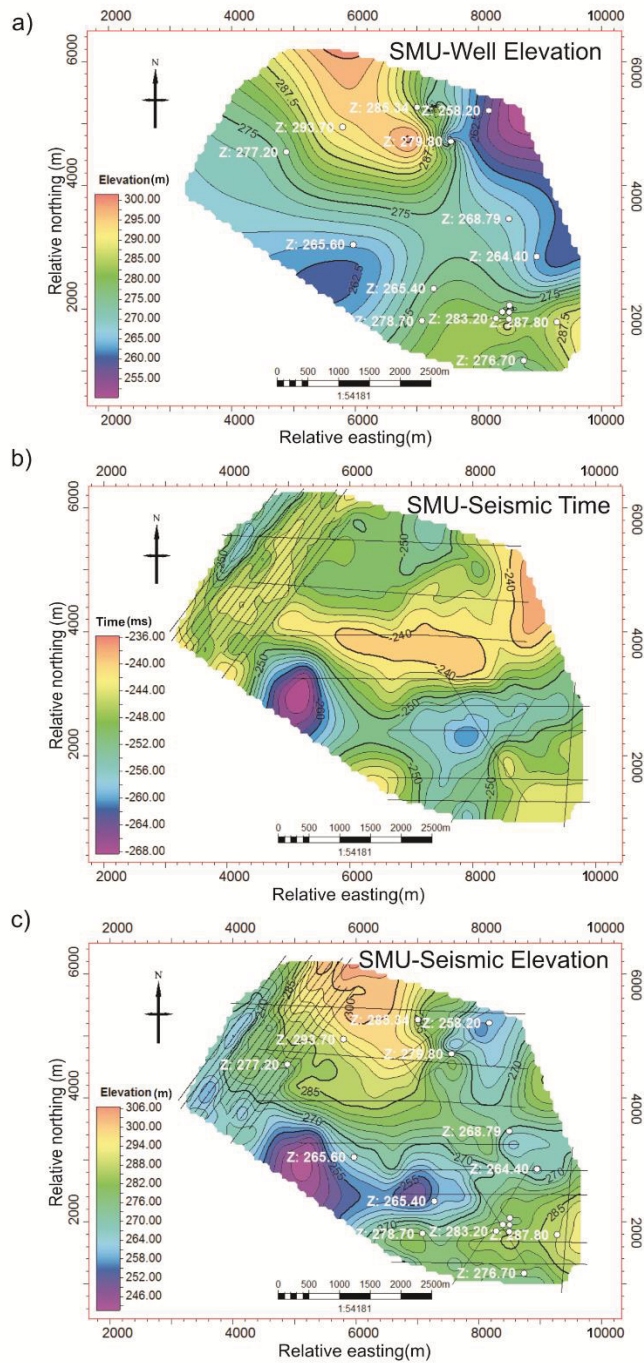
Figure 2.13. Comparison of the surface maps for the SMU as determined from interpolation of (a) well log top information, (b) the picked seismic times from the legacy seismic data processed in this study, and (c) the seismic elevations as estimated from (b) using the velocity model. The location of the wells and seismic lines and well markers elevation depth is posted on these maps.

45

At this point it is important to question the resolving power of the seismic data. One rule of thumb for the resolving capability is given by the Rayleigh ¼ wavelength, or the first Fresnel zone, criterion with radius R given by

$$R = \frac{V}{2}\sqrt{\frac{t}{f}} = \sqrt{\frac{Z\lambda}{2}} \qquad (1)$$

where V is the seismic velocity overlying the structure, t is the two-way traveltime, f is the frequency, Z is the depth and λ is the wavelength. Using representative numbers of V (2500 m/s), t (250 ms), and f (50 Hz) suggests the radius of the Fresnel zone is more than 80 m. Migration of the seismic data may halve that number, but this still means that resolving features less than 40 m is difficult with these legacy profiles. As such, the current data set can only confidently image the larger topography of the SMU. It cannot detect rapid variations in the topography that might be caused at the edge of a sinkhole nor could it adequately resolve a sharp cliff.

The SMU time surface of **Figure 2.14** is reproduced at a larger scale. There are two primary east-west trends observed in this image, ridge "A" and a valley "B". Both the valley and ridge were measured up to a kilometer width. Feature "C" appears to be a small linear valley running in a northeast-southwest alignment. Strong evidence of this narrow valley was observed in line N-01 running nearly perpendicularly to this structure.
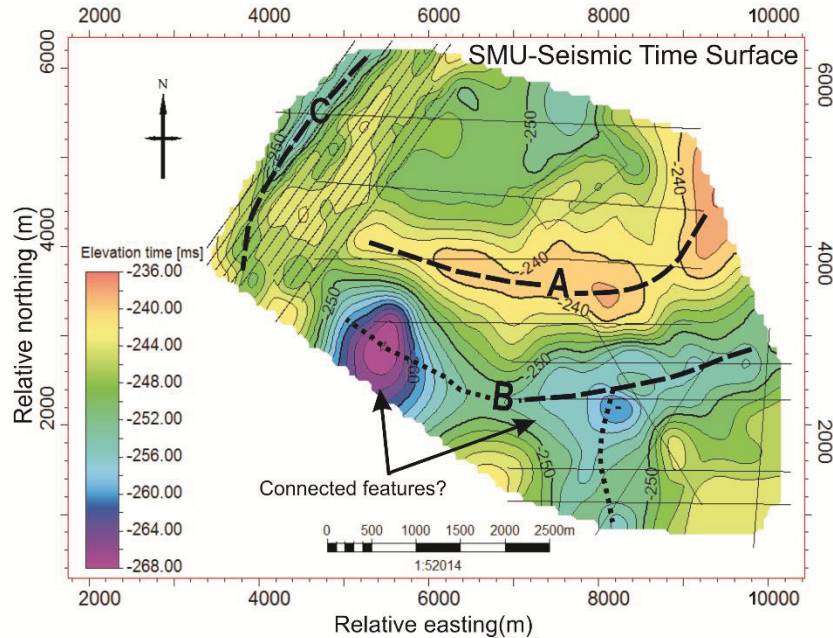
Figure 2.14. Expanded scale of **Figure 2.13b** for the picked seismic time surface for the SMU. Curved lines A and B highlight the axes of a detected ridge and a valley running roughly east-west across the study area. Axis C highlights the location of a smaller, less certain, valley running in a northeast-southwest direction.

The response of this narrow karst valley is clearly seen on the seismic section displayed **Figure 2.15** by a shift later in two-way traveltime of the SMU. The valley was estimated to be about 330 m wide (270 m if normal to strike of valley). Further analyzing the valley, one can observe a secondary feature of what appears to be about 50 m wide channel equivalent to 35 m normal to strike of valley (**Figure 2.15**) possibly cut into the bottom of the valley. Moreover, this northeast-southwest orientation of feature C may be subparallel to the expected joint trends in the Grosmont Formation (Jones, 2010). Evidence for this feature was support on the ties between the series L and series N data sets.
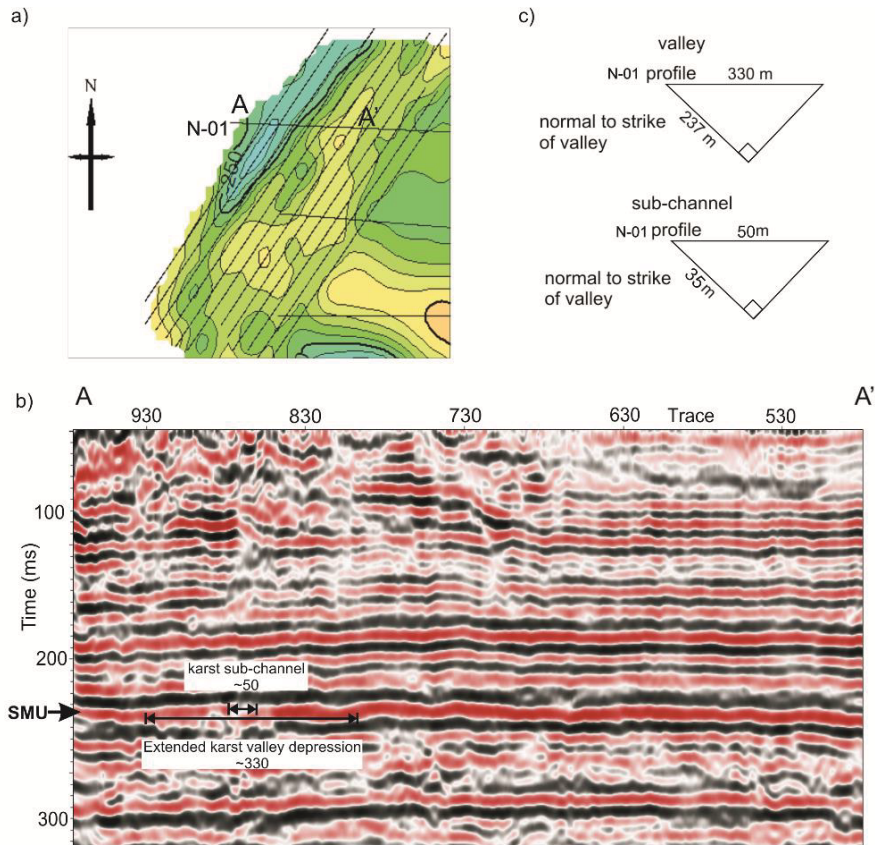
Figure 2.15. Feature C, an imaged karst valley in the seismic data of (a) the time map of the SMU, (b) a portion of seismic line N-01 profiling A-A′, and (c) the geometry of the apparent width and the true width of karst valley and subchannel.

A comparison of surface structure of SMU against other five interpreted time surfaces is shown in **Figure 2.16** in sequential order from shallow to deep. Both the Mesozoic Clearwater (**Figure 2.16a**) and the Wabiskaw (**Figure 2.16b**) surfaces correlate with the SMU (**Figure 2.16c**). This suggests that the sedimentation above the SMU was influenced by its topography. The reasons for this are not known but could be indicative of collapse of the karsted SMU, differential compaction of the Mesozoic sediments, or even fault motions.

Despite the poor imaging of our seismic data at later times of the profiles, lateral disturbances in the continuity of the seismic reflectors can be observed.

These features are particularly obvious in the profiles trending southeast-northwest and southwest-northeast.
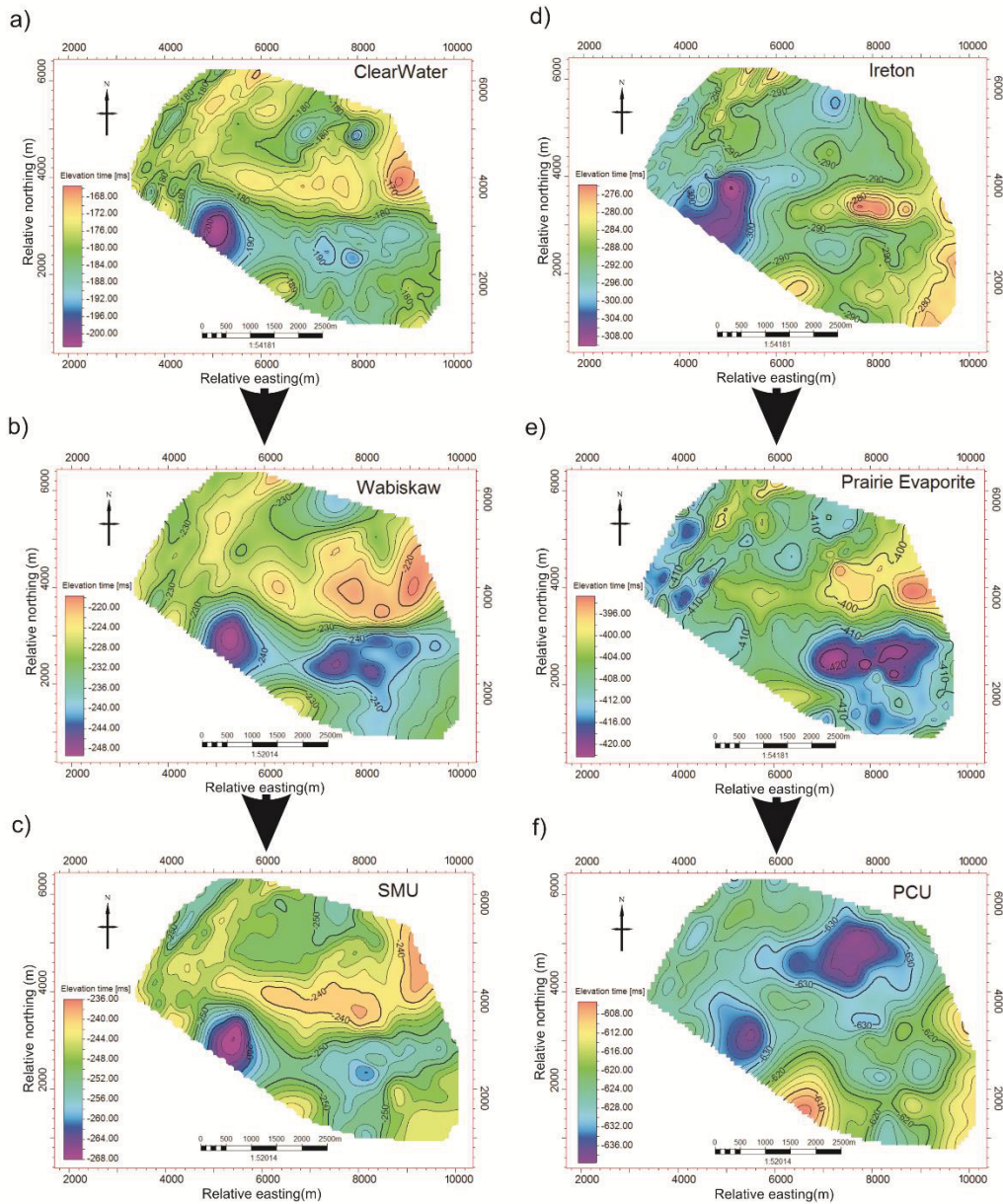
Figure 2.16. Comparison of the surface maps in time domain for the (a) Mesozoic Clearwater, (b) Mesozoic Wabiskaw, (c) SMU, (d) Paleozoic Ireton, (e) Paleozoic Prairie Evaporite, and (f) PCU. Arrows denote the progression of the panels with subsequently increasing depth.

Seismic profile K-7 (**Figure 2.17a**) shows such a disturbance zone. According to Kellett et al. (1994, 2005), the presence of strong diffractions extending to depth, cone shape disturbances and apparent pull-up and pull-down in different parts of the seismic section may be indicative of igneous intrusives. Evidence for the existence of such features in the study area comes from the filtered High Resolution Aeromagnetic (HRAM) data that show magnetic lineaments (**Figure 2.17b**) that are possibly interpreted as igneous dykes. We cannot as yet confirm these as dykes due to a lack of appropriate geological information. Best et al. (1998) and Airo and Wennerstrom (2010) in the region immediately to the northeast of the study area, see similar features that they interpreted to be faults both in the sediments and within the metamorphic basement.

The observed lineaments, regardless of their interpretation as either igneous dykes or faults, can have a significant role in the karstification of Grosmont Formation. When dykes propagate vertically upwards through the sediment overburden hot volatiles and gases would escape above the dyke tip (Wall et al., 2010). The escaped fluids may induce fractures, depression and dissolution of the overlaid Upper Elk point, Beaverhill Lake and Woodbend sedimentary groups. Faults also can act as preferential zones of enhanced fluid (surface or underground water) flow. That said, we must be always cautious about seismic processing artifacts. Vertical and sub-vertical artifacts can be produces by the existence of the low seismic velocity region, surrounded with higher seismic velocity strata. Reprocessing and examination of the near and far seismic data would result in a better understanding of these kinds of features.
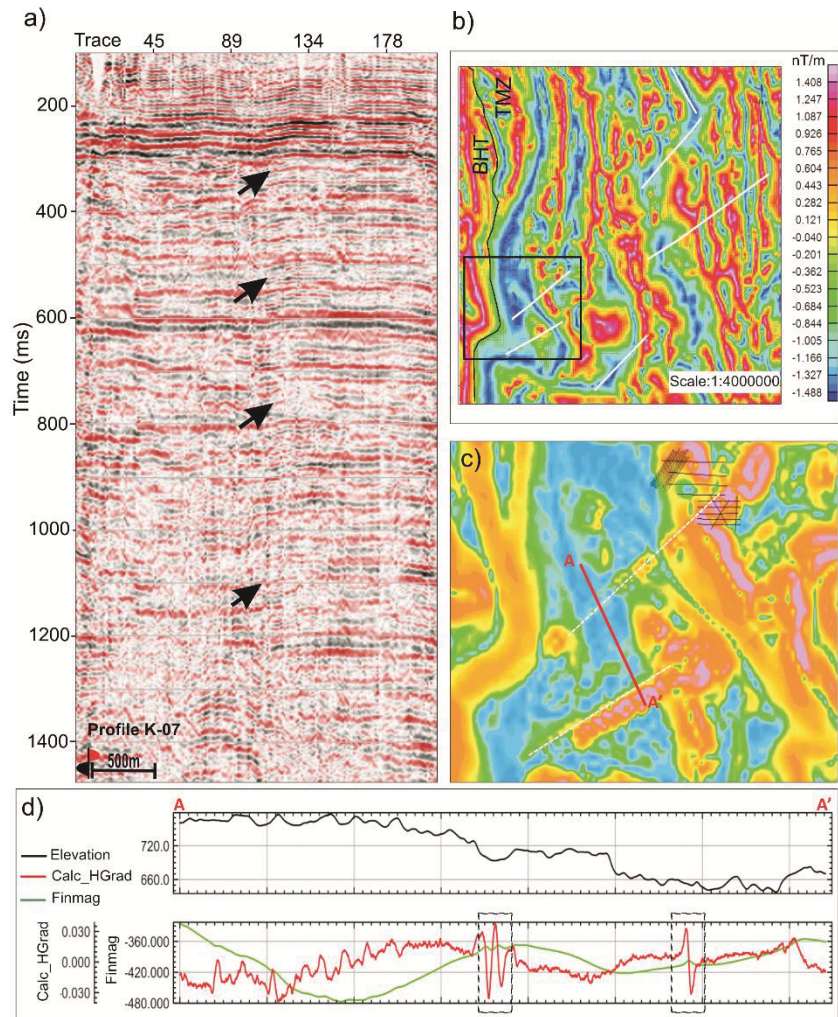
Figure 2.17. Illustration of the possible structures in the study area: (a) seismic disturbance zone on seismic profile K-07, (b) tilt derivative of magnetic anomaly map with the suggested lineaments and boundary of the Taltson Magmatic Zone (TMZ) and Buffalo Head Terrane (BHT), (c) the magnified filtered magnetic image over the seismic surveys showing the lineament crossing the area (seen on the seismic profile K-01), (d) profile A-A′ perpendicular to the lineaments of interest; black, green, and red graphs, respectively, represent elevation, reduced to pole residual magnetic (Finmag), and calculated horizontal derivative of the residual magnetic (Calc_HGrad). The black rectangles highlight magnetic lineaments in the area of interest.

2.8. Conclusion

The interpreted time structure maps of the Grosmont (SMU) and the overlying and underlying formation tops show substantially more detail than those constructed on the basis of well log information only; in fact the use of only well log information would likely result in erroneous interpretations. Although features smaller than about 40 m in radius could not be easily discerned at the SMU due to wave-field and data sampling limits, the data does reveal the existence of a ridge-valley pattern. The model like we describe here may occur in any basin that has a deep, relatively thick section of Paleozoic carbonates that underlie major unconformities. Comparison of the structural maps from surfaces below the SMU suggests that deeper features (intrusion bodies/faults) may also influence the structure of the SMU. HRAM data in the study area confirm the existence of such deeper features. Meanwhile the overlying Mesozoic formations represent almost the same structural topography as SMU surface. This may be due to collapse of karst features within the Grosmont after Mesozoic deposition, differential compaction of the Mesozoic sediments or even small fault motions. The current re-examination and integration of the legacy project data sets demonstrates the necessity for geophysical studies of this resource. Additional work would assist in adding value to any modern seismic data obtained in the production of this resource.

References

Airo, M. L., and M. Wennerström, 2010, Application of regional aeromagnetic data in targeting detailed fracture zones: Journal of Applied Geophysics, 71, 62-70, doi:10.1016/j.jappgeo.2010.03.003.

Barrett, K. R., and J. C. Hopkins, 2010, Stratiform carbonate breccias of the Grosmont Formation, Alberta: Presented at AAPG 2010 International Conference & Exhibition.

Bélanger-Davis, C. E., 1985, Mineralogical and petrophysical changes after steam testing in carbonate rocks of the Grosmont Formation, Alberta: M.S. thesis, University of Calgary.

Belyea, H. R., 1952, Notes on the Devonian system for the north-central plains of Alberta: Geological Survey of Canada.

Belyea, H. R., 1956, Grosmont Formation in the Loon Lake area: Petroleum Geology, 4, 66-69.

Belyea, H. R., 1964, Upper Devonian, Part II - Woodbend, Winterburn and Wabamun Groups, in R. G. McCrossan, and R. P. Glaister, eds., Geological History of Western Canada: Alberta Society of Petroleum Geologists, 66-68.

Berkhout, A. J., 1979, Steep dip finite-difference migration: Geophysical Prospecting, 27, 196-213, doi: 10.1111/j.1365-2478.1979.tb00965.x.

Best, M. G., 1988, Early Miocene change in direction of least principal stress, Southwestern United States; Conflicting inferences from dikes and metamorphic core-detachment fault terranes: Tectonics, 7, 249-259, doi: 10.1029/TC007i002p00249.

Borrero, M. L., and H. G. Machel, 2010, Sedimentology and diagenesis of Hondo Evaporites within the Grosmont giant heavy oil carbonate reservoir, Alberta, Canada: Presented at AAPG 2010 International Conference & Exhibition.

Bown, T. D., 2011, Legacy seismic investigations of karst surfaces; implications for heavy oil extraction from the Devonian Grosmont Formation, Northeastern Alberta, Canada: M.S. thesis, University of Alberta.

Buschkuehle, B. E., F. J. Hein, and M. Grobe, 2007, An overview of the geology of the Upper Devonian Grosmont carbonate bitumen deposit, Northern Alberta, Canada: Natural Resources Research, 1, 3-15.

Cotterill, D., and W. N. Hamilton, 1995, Geology of Devonian limestones in Northeast Alberta: Alberta Geology Survey open file report 1995-07.

Cox, M. J. G., 1999, Static corrections for seismic reflection surveys: SEG.

Cutler, W., 1982, Stratigraphy and sedimentology of the Upper Devonian Grosmont Formation, Alberta, Canada: M.S. thesis, University of Calgary.

Dembicki, E. A., 1994, The Upper Devonian Grosmont Formation; well log evaluation and regional mapping of a heavy oil carbonate reservoir in Northeastern Alberta: M.S. thesis, University of Alberta.

Dembicki, E. A., and H. G. Machel, 1996, Recognition and delineation of paleokarst zones by the use of wireline logs in the bitumen-saturated Upper Devonian Grosmont Formation of Northeastern Alberta, Canada: AAPG Bulletin, 80, 695-712.

Energy Resources Conservation Board, 2009, Table of formations, http://www.ercb.ca/docs/products/catalog/TOF.pdf, accessed 27 July 2012.

Energy Resources Conservation Board, 2010, Alberta's energy reserves 2009 and supply/demand outlook 2010-2019, Open file report ST98-2010.

Harrison, R., 1982, Geology and production history of the Grosmont carbonates pilot project, Alberta, Canada: Presented at Second United Nations Institute for Training And Research Conference on Future of Heavy Crude and Tar Sands.

Harrison, R., 1984, The bitumen-bearing Paleozoic carbonate trends of Northern Alberta: Presented at AAPG 1984 Research Conference.

Harrison, R., 1986, Regional geology and resource characterization of the Upper Devonian Grosmont Formation, Northern Alberta: Alberta Resarch Council.

Harrison, R., and B. McIntyre, 1981, The geologic setting of the Grosmont thermal recovery project, Northeastern Alberta: Presented at the Alberta Oil Sands Technology and Research Authority (AOSTRA) seminar on Advances in Petroleum Upgrading and Recovery Technology.

Hein, F. J., 2006, Heavy oil and oil (tar) sands in North America: an overview and summary of contributions: Natural Resources Research, 15, 67-84, doi: 10.1007/s11053-006-9016-3.

Hein, F. J., R. Marsh, and M. Boddy, 2008, Overview of the oil sands and carbonate bitumen of Alberta; regional geologic framework and influence of salt-dissolution effects: Presented at AAPG Hedberg Conference.

Hoffmann, C. F., and O. P. Strausz, 1986, Bitumen accumulation in Grosmont platform complex, Upper Devonian, Alberta, Canada: AAPG Bulletin, no. 70, 1113-1128.

Hopkins, J., and B. Jones, 2009, Reservoir units in the Grosmont Formation; stratigraphy, paleotopography and reservoir geology of the Grosmont Formation Twp 80-90 Rge 12-21W4: Alberta Research Concil & Carbonate Research Program Geology report no. 0708-1.

Huebscher, H., 1996, Regional controls on stratigraphic and diagenetic evolution of the Woodbend group carbonates, north-central Alberta, Canada: M.S. thesis, University of Alberta.

Huebscher, H., and H. G. Machel, 1997, Paleokarst in the Grosmont Formation, Northeastern Alberta in J. Wood, and B. Martindale, eds., Canadian Society of Petroleum Geologists for Sedimentary Geology Joint Convention: Core Conference, 129-151.

Hutcheon, I., and A. Oldershaw, 1985, The effect of hydrothermal reactions on the petrophysical properties of carbonate rocks: Bulletin of Canadian Petroleum Geology, no. 33, 359-377.

Jones, B., 2010, Fracture systems in the Grosmont Formation: Alberta Reseach Council & Carbonate Research Program Geology Report no. 0910-8a.

Kellett, R. L., A. E. Barnes, and M. Rive, 1994, The deep structure of the Grenville Front; a new perspective from western Quebec: Canadian Journal of Earth Sciences, 31, 282–292, doi: 10.1139/e94-027.

Kellett, R. L., G. J. Steensma, and R. M. Zahynacz, 2005, Geophysical signature of the Mountain Lake intrusion; a study to support future kimberlite exploration in Alberta: Alberta Geological Survey & Alberta Energy and Utilities Board.

Law, J., 1955, Geology of Northwestern Alberta and adjacent areas: AAPG Bulletin, no. 39, 1927-1978, doi: 10.1306/5CEAE29E-16BB-11D7-8645000102C1865D.

Luo, P., and H. G. Machel, 1995, Pore-size and pore throat types in a heterogeneous dolostone reservoir, Devonian Grosmont Formation, Western Canada Sedimentary Basin: AAPG Bulletin, 79, 1698-1720.

Luo, P., H. G. Machel, and J. Shaw, 1994, Petrophysical properties of matrix blocks of a heterogeneous dolostone reservoir - the Upper Devonian Grosmont Formation, Alberta, Canada: Bulletin of Canadian Petroleum Geology, 42, 465-481.

Machel, H. G., 2010, The Devonian petroleum system of the Western Canada Sedimentary Basin with implications for heavy oil reservoir geology, in S. Chopra, L. R. Lines, D. R. Schmitt and M. L. Batzle, eds., Heavy oils; Reservoir characterization and production monitoring: SEG Geophysical Developments Series, no. 13, 131-154.

Machel, H. G., M. L. Borrero, E. Dembicki, H. Huebscher, P. Luo, and Y. Zhao, 2012, The Grosmont: The world's largest unconventional oil reservoir hosted in carbonate rocks in J. Garland, J. E. Neilson, S. E. Laubach, and K. J. Whidden, eds., Advances in Carbonate Exploration and Reservoir Analysis: Geological Society of London, Special Publication, 370, 49-81, doi: 10.1144/SP370.11.

Machel, H. G., and I. Hunter, 1994, Facies models for middle to late Devonian shallow marine carbonates, with comparisons to modern reefs; a guide for facies analysis: Facies no. 30, 155-176.

MODIS, National Aeronautics and Space Administration, available from http://modis.gsfc.nasa.gov, accessed 10 July 2012.

Mossop, G., and I. Shetsen, 1994, Geological atlas of the Western Canada Sedimentary Basin: Canadian Society of Petroleum Geologists & Alberta Research Council.

Norris, A., 1963, Devonian stratigraphy of Northeastern Alberta and Northwestern Saskatchewan: Geological Survey of Canada, Memoir 313.

Ogunsuyi, F., and D. R. Schmitt, 2010, Integrating seismic velocity tomograms and seismic imaging; application to the study of a buried valley, in R. D. Miller, J. D. Bradford, and K. Holliger, eds., Near surface seismology and ground penetrating radar: SEG 361-378.

Omnes, G., and P. Robert., 1982, The P-Shooter; a fast seismic source for shallow exploration: Geophysics: AAPG Bulletin, 66, 1697-1697.

Schneider, W. A., 1978, Integral formulation for migration in two and three dimensions: Geophysics, 43, 49-76, doi: 10.1190/1.1440828.

Switzer, S. B., W. G. Holland, D. S. Christie, G. C. Graf, A. S. Hedinger, R. J. McAuley, R. A. Wierzbicki, and J. J. Packard, 1994, Devonian Woodbend-Winterburn stata of the western Canada sedimentary basin, in G. D. Mossop, and I. Shetsen, Geological Atlas of the Western Canadian Sedimentary Basin: Canadian Society of Petroleum Geologists and Alberta Research Council.

Theriault, F., 1988, Lithofacies, diagenesis, and related reservoir properties of the Upper Devonian Grosmont Formation, Northern Alberta: Bulletin of Canadian Petroleum Geology, 36, no. 1, 52-69.

Theriault, F., and I. Hutcheon, 1987, Dolomitization and calcitization of the Devonian Grosmont Formation, Northern Alberta: Journal of Sedimentary Petrology, 57, 955-966, doi: 10.1306/212F8CB5-2B24-11D7-8648000102C1865D.

Walker, D., 1986, Regional stratigraphy of the Upper Devonian Grosmont Formation, Northern Alberta: Alberta Geological Survey open file report 1986-02.

Wall, M., J. Cartwright, R. Davies, and A. McGrandle, 2010, 3D seismic imaging of a Tertiary Dyke Swarm in the southern North Sea, UK: Basin Research, 22, 181-194, doi: 10.1111/j.1365-2117.2009.00416.x.

Wo, E., L. Song, T. Hurst, and N. Sitek, 2010, Geological review and bitumen resource appraisal of the Grosmont Formation within the Athabasca oil sands area: Presented at AAPG 2010 International Conferenve & Exhibition.

Yoon, T., 1986, Bitumen resources of the Upper Devonian Grosmont Formation: Twp 88 to 98, Northern Alberta: Alberta Geologycal Survey open file report 1986-01.

Zhao, Y., 2009, Petrophysical properties of bitumen from the Upper Devonian Grosmont reservoir, Alberta, Canada: M.S. thesis, University of Alberta.

Chapter 3: Geothermal energy potential of sedimentary formations in the Athabasca region, Northeast Alberta, Canada

The Athabasca region located in Northeast of Alberta, Canada, hosts many ongoing projects of bitumen extraction from oil sand and Devonian carbonate and siliciclastic reservoirs which requires a vast amount of thermal energy. Geothermal energy as a green renewable source of heat can help to reduce the amount of fossil fuels used to provide the required thermal energy for these projects and consequently decrease the greenhouse gas emission. In order to assess the geothermal development potential in this region, an integrated regional-scale 3D model is constructed with geologic and geophysical data (~7000 formation tops and ~800 km seismic 2D profiles). Incorporation of 2D seismic profiles that fill in the gaps between sparse geological tops particularly for deeper formations adds to structural details of the modeled formations. The temperature and porosity fields are simulated using the Sequential Gaussian Simulation approach within the modeled sedimentary formations. Based on spatial distribution, thickness, formation porosity and permeability analysis five Paleozoic formations of the Keg River, Waterways, Cooking Lake, Leduc, and Grosmont, are identified as potential aquifers for geothermal development. These aquifers have enough coverage and thickness in the area and show high amount of thermal energy content. Since the sedimentary basin in the Athabasca region is quite shallow (less than 1400 m), these aquifers are all recognized as low enthalpy geothermal reservoirs with maximum temperature of 40 °C and hence direct heating applications are not feasible. Utilization of industrial-scale heat-pump technologies that have long been employed in Northern Europe with high coefficients of performance would be recommended for heat extraction from these reservoirs.

3.1. Introduction

The Athabasca region in Northeast of Alberta, Canada is primarily known for its significant Cretaceous oil sand deposits but less so for its substantial Devonian carbonate-hosted bitumen resources. Only a fraction of the oil sands and carbonate resource can be exploited by surface mining and the bulk of these resources must be produced *in situ*. Such production primarily consists of injecting pressurized mixtures of steam and water at temperatures that can exceed 250 °C. To do this currently requires the burning volumes of natural gas in excess of 95.1 million m^3 per day (3.4 Bcf/day) (NEB, 2015) which converted to units of energy is about 3.5 petajoules (3.5 x 10^{15} J).

Industry faces both economic and societal risks in continuing this practice. The economic risk is that once the means to export natural gas from North America at a large scale are put in place the cost will inevitably rise and the supply may even become restricted or prohibitively expensive. Further, the risk to the social license is that continued burning of such large volumes of natural gas invariably produces CO2 at a rate of about 0.18 megatonnes per day for which there is strengthening societal and regulatory pressure to reduce. Therefore any alternative way to provide heat could be beneficial.

In addition to these industrial needs, there are also many isolated communities in this area where energy must be imported at great cost. Utilization of geothermal energy for heating and cooling could be part of an economic solution to improve life in these communities. It is likely that a number of differing strategies will be used to reduce these risks. Geothermal heat may be able to contribute to an overall solution.

Previous studies of geothermal energy potential in the Western Canadian Sedimentary Basin (WCSB) (Anglin and Beck, 1965; Majorowicz and Jessop, 1981a, 1981b; Lam and Jones, 1984; Jones et al., 1985; Lam et al., 1985; Majorowicz et al., 1999; Majorowicz and Moore, 2008; Bell and Weis, 2009; Majorowicz and Grasby, 2010; Grasby et al., 2011; Gray et al., 2012; Pathak, 2014; Weides and Majorowicz, 2014c; Weides et al., 2014a, 2014b; Hofmann, 2015; Nieuwenhuis, 2015; Liddell et al., 2016) indicate an average geothermal temperature gradients of 22 to 35 °C/km and a heat flow of 50 to 70 mW/m². Recent thermal measurements in a 2.4 km deep borehole approximately 100 km to the east of the study area show a modest thermal gradient of about 20 °C/km (Majorowicz et al., 2014). These values are not comparable to existing higher temperature geothermal fields located in areas such as Iceland, Nevada, and New Zealand which produce electricity. Consequently, the geothermal potential in the study area would be classified as a low enthalpy resource (Majorowicz and Grasby, 2010; Grasby et al., 2011) that mainly can be used for heat production (Rybach and Mongillo, 2006). In similar geothermal environments, industrial-scale heat-pumps have been successfully used to efficiently extract heat energy in Northern Europe for many years. The study here focuses on developing the preliminary geological model that is necessary for future investigations of the feasibility of heat-pump technologies.

Traditionally, geophysical exploration of geothermal resources has relied heavily on electrical and electromagnetic methods that delineate the subsurface electrical conductivity (Hersir and Björnsson, 1991; Georgsson, 2009). The logic of this is that we expect the hot fluids and hydrothermal alternation products to have anomalous electrical resistivities and to be localized along faults and vents; conductive anomalies will direct the drilling for groundwater heated sufficiently

to drive electrical power generation. In the low enthalpy situation studied here, however, localized anomalous conductive features are not expected. Consequently, the exploration of geothermal systems in Northeastern Alberta will involve a larger combination of complementary exploration techniques from which a good understanding of the geological structures in a region will be paramount. The approach taken is essentially the same as used in the evaluation of potential hydrocarbon reservoirs. Fortunately, accelerated exploration and exploitation of oil and gas reservoirs in this region in recent years has produced some geophysical and well log data which can be used for an initial assessment of the geothermal potential. However, the available data still remais sparse particularly through the Devonian targets which influence the interpretation of the results presented here.

Ungemach (1985) and Moeck (2014) define a geothermal play as a system comprising of four components of a heat source rock, a porous and permeable reservoir, a heat carrier fluid and a cap rock which of these four components our focus is on investigation of the reservoir (aquifer). We first set out the 3D geological model of the study region using calibrated well tops which we then improve by analysis of over 800 km of 2D seismic profiles. The model is later is used as a structural framework for petrophysical property modeling. We select a number of target aquifers and make estimates of their volume and heat content at the km^2 scale that is a typical scale for existing heat-pump geothermal projects. This study seeks to arrive only at estimates of the heat energy available and is very much an early-stage reconnaissance for future work.

3.2. Geological setting

The study zone encompasses an area of 6000 km^2 in the Athabasca region located between ~350000 to ~410000 Easting (~$56°$ $17'$ N to ~$57°$ $07'$ N Latitude) and ~6240000 to ~6330000 Northing (~$113°$ $33'$ W to ~$112°$ $27'$ W Longitude) of Alberta (NAD 27 Zone 12) lying in the northeast part of the WCSB (**Figure 3.1**). This area was selected for study because it has potential for industrial development but it still remains somewhat inaccessible. As such, it may make sense to assess the viability of alternative energy technologies in this area before significant development begins.

The WCSB strata can be referred to two broad divisions that reflect contrasting geological conditions:

i)   a lower succession of Cambrian to Jurassic age, which is composed largely of carbonate rocks, with an important component of evaporite minerals and was formed during the passive margin sedimentation before the major uplift of the Canadian Cordillera;

ii)   an upper succession of mid-Jurassic to Tertiary age, which consists mainly of shale and sandstone, was deposited following major mountain building (Columbian and Laramide Orogenies) and uplift in the Cordillera in foreland basin (Barss et al., 1964; Parsons, 1973; Porter et al., 1982; Mossop and Shetsen, 1994).
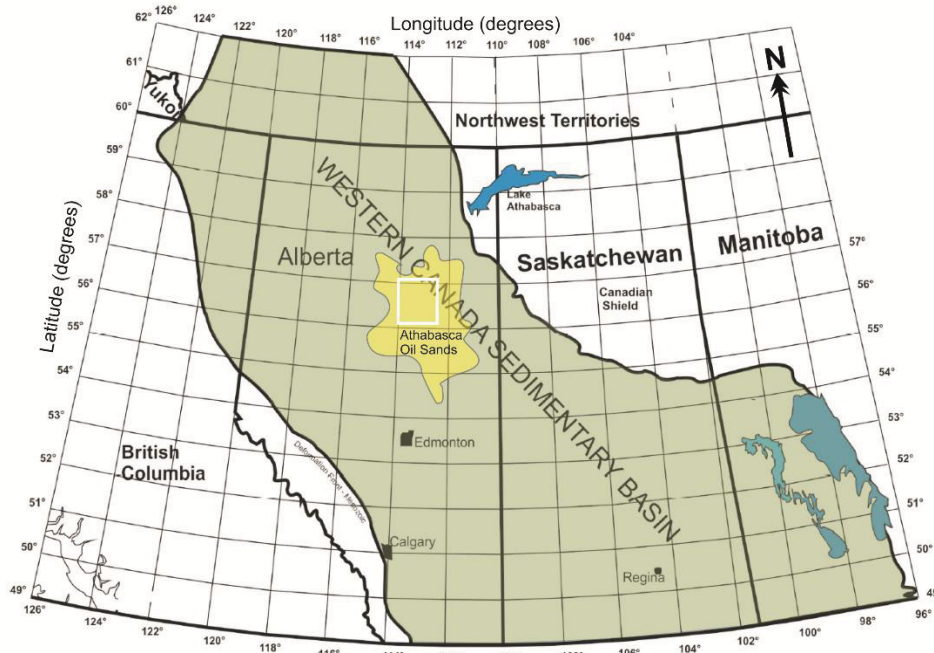
Figure 3.1. Areal coverage of the Western Canada Sedimentary Basin (modified after Grasby et al., 2011). The study area shown by the white box is located within the Athabasca oil sand deposits illustrated in yellow.

Within the study area the strata making up the passive margin basin consists of a wedge tapering sedimentary formation package with depth of ~1400 m in the southwest to ~800 m in the northeast. This Paleozoic carbonate and evaporite package lies above the Proterozoic metamorphic cratonic rocks of the Canadian Shield and below the primarily siliclastic Cretaceous sediments. These boundaries are two major unconformities that we here refer to as the Precambrian unconformity (PCU) and the SubMannville unconformity (SMU), respectively. The SMU goes by many different names in the literature (e.g., Sub-Cretaceous, Paleozoic, Devonian), but in the study area the unconformity is the lower bound everywhere to the Lower Cretaceous Mannville Group (Ardakani et al., 2014), blanketed the Devonian carbonates that were formally at the earth's surface. At the SMU, Devonian strata subcrop with increasing age to the

northeast of study area (**Figure 3.2**). Since the target formations for this study belong to the Paleozoic strata, more detailed stratigraphic information is presented in the following paragraph.
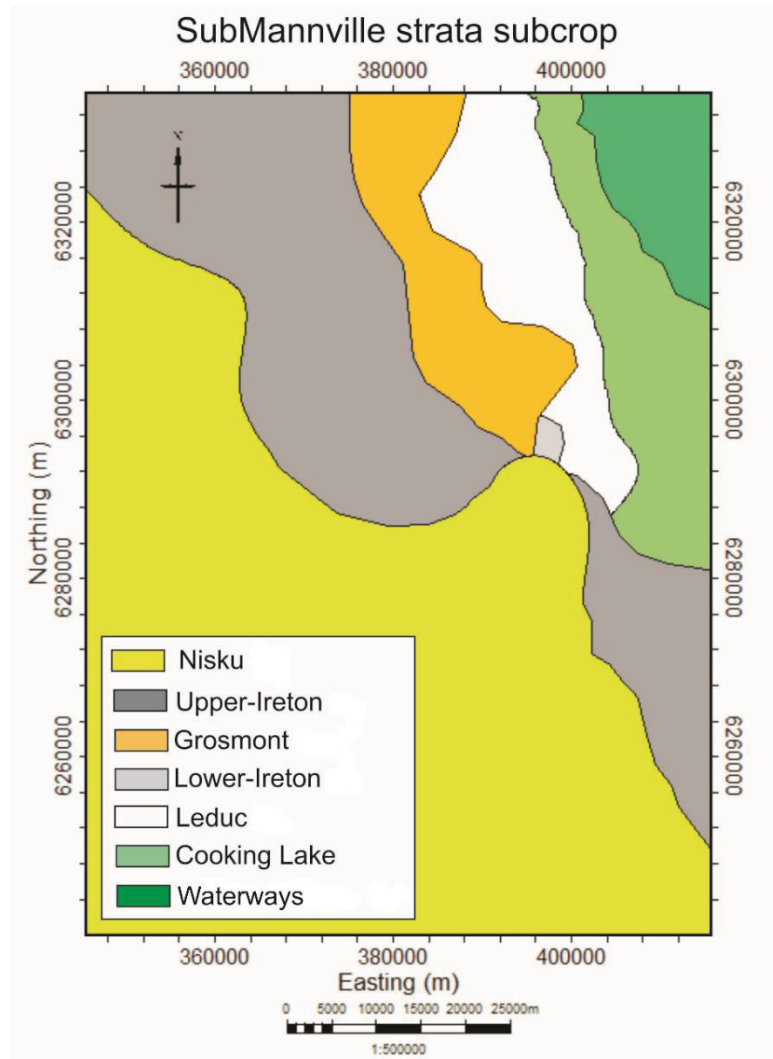
Figure 3.2. Subcrop boundaries of Devonian formations at the SubMannville Unconformity (SMU) in the study area.

The Paleozoic succession begins with Elk Point Group which is divided into Lower and Upper Elk Point by itself. The Lower Elk Point consists of Basal Red Beds, Ernestina Lake, Cold Lake and Contact Rapids. The Upper Elk Point includes Keg River, Prairie Evaporite and Watt Mountain formations (**Table**

3.1). The Basal Red Beds which belongs to the Lotsberg complex consisting of evaporite and coarser grained clastics (Sproule, 1951; Norris, 1973). These basal sands have been considered as potential target for geothermal development in central Alberta (Grasby et al., 2011; Weides et al., 2013) where they lie at significantly greater depths. The Ernestina Lake Formation is a mixture of dolomitic shale and evaporate layers that pinch out against Basal Red Beds. In the eastern portions of the study area, the Cold Lake and Contact Rapids formations overlie the Ernestina Lake. The Contact Rapids Formation consists of interbedded argillaceous dolostone and shale and plays a platform role for Keg River reefs (Law, 1955). The Cold Lake and Contact Rapids formations are too thin in the region to be resolved on seismic profiles and are negligible in comparison with the Keg River Formation. Therefore they are grouped into Keg River Formation and are not incorporated individually in the 3D model. The Keg River Formation is the lower most formation in the Upper Elk Point Group (Law, 1955; Belyea and Norris, 1962). This formation thins out closer to the exposed Canadian Shield. The Prairie Evaporite consists of a mixture of anhydrite and halite and it covers the Keg River Formation in the study area. The dolomitic shale of the Watt Mountain Formation overlies the Prairie Evaporite partially and lacks thickness, therefore it is grouped with the Prairie Evaporite into one stratigraphic unit in the 3D model.

The Beaverhill Lake Group as an inter-platform basin deposit starts with the Fort Vermillion and Slave Point formations which are relatively thin units and are combined to one unit in our model. The Waterways Formation consists of layers of calcareous shales and carbonates and is divided into five members (**Table 3.1**).

Table 3.1. Generalized stratigraphic column of Northeastern Alberta (modified after ERCB, 2009). The lithological color codes are: grey–shales, blue–carbonates (limestone, dolomite), green–evaporites (anhydrite, halite), yellow–clastics (sandstones, siltstones, and conglomerates) and pink-granitoid (igneous and metamorphic). The number of formation tops in the study area is also presented in this table. The formations of interest are in bold font.

EON	ERA	Period		Group	Formation		Tops	Hydrostratigraphy
Phanerozoic	Cenozoic	Quaternary		Preglacial and glacial drift				
		Tertiary						
	Mesozoic	Cretaceous	U	Colorado	Second White Specks		0	Colorado aquitard system
					Base of Fish Scales		116	
					Viking		392	
					Joli Fou		412	
			L	Mannville	Grand Rapids		521	Upper Mannville aquifer
					Clearwater		1340	Clearwater aquitard
					Wabiskaw		1672	Lower Mannville aquifer
					McMurray		1774	
		Jurassic						
		Triassic						
	Paleozoic	Permian						
		Carboniferous						
		Devonian	U	Wabamun	?			Upper Devonian aquifer
				Winterburn	Nisku		245	
				Woodbend	Upper Ireton		73	Upper Woodbend aquitard system
					Grosmont		625	Upper Devonian aquifer
					Lower Ireton		145	Lower Woodbend aquitard system
					Leduc		67	Middle-upper Devonian aquifer system
					Cooking Lake		15	
				Beaverhill Lake	Waternays	Mildred	3	
						Moberly	38	
						Christina	36	
						Calmut	34	
						Firebag	33	
					Slave Point		33	
					Fort Vermilion		23	
			M	Elk Point	U	Watt Mountain	22	Prairie aquiclude-aquitard system
						Prairie Evaporite	15	
						Keg River	19	Keg River aquifer
						Contact Rapids	16	Contact Rapids aquifer
			L		L	Cold Lake	8	Elk Point aquiclude system
						Ernestina Lake	2	
						Basal Red Beds	6	
		Silurian						
		Ordovician						
		Cambrian						
	Precambrian			Precambrian basement			16	Basement aquiclude

The Beaverhill Lake Group is overlain by the Woodbend Group which is made of carbonate platforms and inter-reef basin (Bachu et al., 1996). The oldest formation is a carbonate formation of Cooking Lake which plays a platform role for Leduc reefs. Although both of these formations do not cover the entire study area, they have enough thickness to be potential candidates for geothermal development. Limy shales of the Lower Ireton Formation blanket these formations acting as a cap rock. The Grosmont Formation carbonate in turn overlies the Lower Ireton Formation and are covered by the sealing thin shale layer of upper Ireton. The Nisku Formation is the only component of Winterburn Group in the study region. This formation has an eroded surface that subcrops the SMU. The thickness of Nisku varies in the area. The formations overlying the SMU (Mannville and Colorado Groups) are only used in the 3D model to constrain the underlying Paleozoic formations with high geothermal potential.

3.3. Hydrostratigraphic units

Based on porosity and permeability, the Phanerozoic sedimentary formations in this area are divided into aquifers, aquitards and aquicludes. An aquifer consists of a formation that stores and yields water in sufficient quantities, and transmits it relatively easily. An aquitard is semipermeable (only limited seepage is possible) and an aquiclude is essentially impermeable to the flow (Subramanya, 1994). From oldest to youngest formations in the region, the Contact Rapids, Keg River, Waterways, Cooking Lake, Leduc, Grosmont, Nisku, McMurray, Wabiskaw, and Grand Rapids formations are identified as aquifers and the rest of formations are classified as aquitards and aquicludes (**Table 3.1**).

The hydrogeological regime of formation waters in the sedimentary succession of study area is complex and this complexity is related to the

variability in geometry and lithology of sedimentary formations. The previous studies about formation fluid flow regimes in this area (Hitchon, 1964; Toth, 1978; Hackbarth and Nastasa, 1979; Hackbarth and Brulotte, 1981; Bachu, 1995; Adams et al., 2004; Gupta et al., 2012, 2015) show that the regional scale flow of formation waters is generally toward the northeast. The flow systems of post-Ireton formations are in equilibrium with current day hydraulic boundary conditions. The pre-Ireton formations are generally underpressured and in a transient process of equalization with the present topography. The aquifers below the thick halite beds of the Prairie Formation exhibit regional flow characteristics with a northeast flow direction and depth related salinity trends. This high formation water salinity is associated with the proximity of Elk Point Group evaporites (Bachu et al., 1996). The flow in the Beaverhill Lake-Cooking Lake aquifer system is intermediate to local in nature. Within the subcrop area and along the outcrop, local physiographic influences are superimposed over a regional northeastward trend. The Grosmont and Winterburn aquifers which are eroded in the northeast portion of the area (SMU), act as a drain for aquifers in hydraulic continuity above and below. The flow is likely toward the northwest where they are exposed and the formations water discharge into Peace River. Since the aquifers are dipping in the WCSB, the flow of formation water is driven by both gravitational and buoyancy forces.

Previous hydrogeological studies in the region (Hitchon et al., 1989a, 1989b) show that the salinity of Cretaceous aquifers is generally low, close to freshwater, and lower than Paleozoic aquifers. The salinity of the deep aquifers or the ones adjacent to evaporitic formations is higher. The salinity of the aquifer not only plays a role in density dependent groundwater flow, but also determines its suitability for geothermal heat extraction. If salinity of the groundwater is

above the standard threshold (i.e., being polluted and corrosive), it may not be economic due to the complex, high cost, and time-consuming remediation process. The detail salinity and hydrologic analysis of the aquifers here is beyond the scope of our study and the process of selecting aquifers for further analysis is mainly based on the aquifer spatial distribution, thickness, temperature, and petrophysical properties. Based on these parameters Keg River, Waterways, Cooking Lake, Leduc, and Grosmont aquifers are our main focus in the seismic interpretation and 3D modeling process. These aquifers are confined with a impermeable layer on top (cap rock). The confinement of an aquifer leads to higher groundwater pressure which can be translated to less energy use for pumps to bring the water to the surface. In addition, in case of any reservoir enhancement via hydraulic fracturing, the cap rock has an essential role in fracture containment within the aquifer.

3.4. 3D Model

The regional 3D model is constructed through the combination of well tops, and 2D seismic profiles. We accessed the digital logs within the study area with vintages beginning in the 1970's from 670 boreholes through access to an industrial database (**Figure 3.3**). From these wells, over 7000 geological tops are obtained.
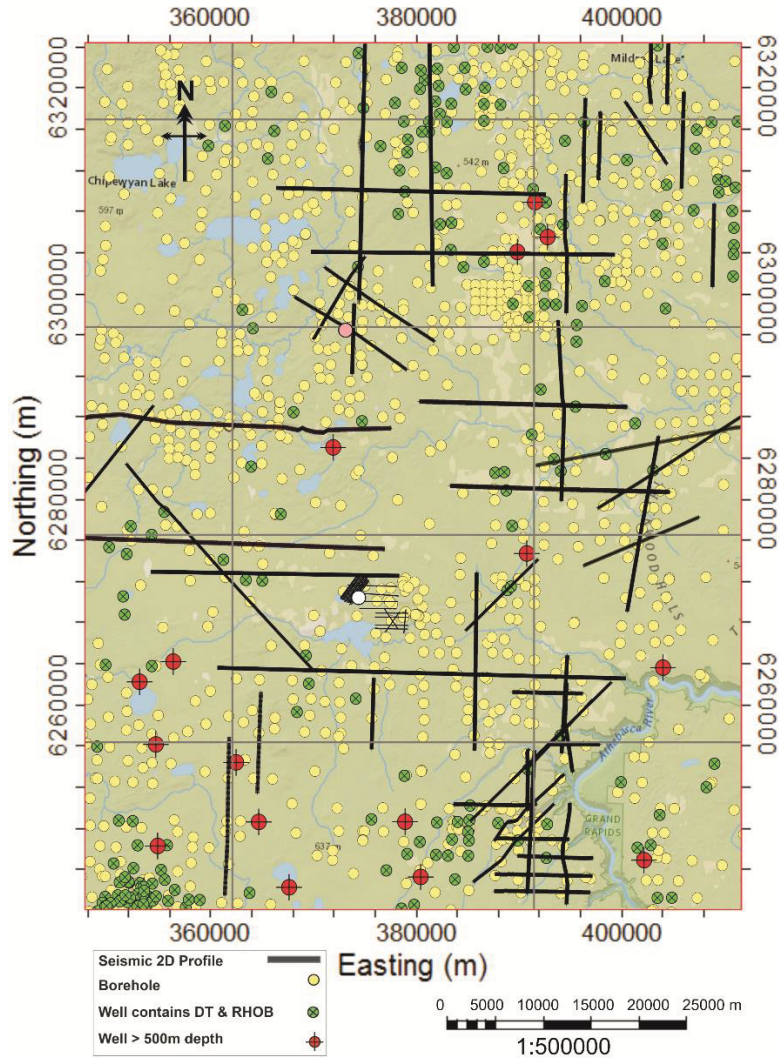
Figure 3.3. Map of the study area showing the locations of the wellbores and seismic profiles. The white and pink circle highlights the location of the Vertical Seismic Profile (VSP) acquisition and the example well tie (presented in **Figure 3.4**), respectively. Boreholes deeper than 500 m elevation depth with petrophysical logs are shown in red. Boreholes with sonic (DT) and density (RHOB) logs are colored in green.

Unfortunately, the largest portion of these boreholes was drilled for shallow gas and bitumen recovery and these provide at best only the depth to the SMU. Among these shallow boreholes less than 100 of them have digital sonic (DT) and density (RHOB) logs which are necessary for calculating synthetic

seismograms. The synthetic seismograms are used to tie the 2D seismic profiles to wells and make the depth conversion possible. In general wells deeper than 500 m (elevation depth) with petrophysical logs are rare in the area which sets a limitation on property modeling for deeper formations (**Figure 3.3**).

The nearly 800 km of 2D seismic profiles provide crucial additional information that allows for a more realistic 3D model (**Figure 3.3**). The seismic data collection was primarily conducted through donations from a number of petroleum exploration companies, some of whom have expressed interest in the possibility of supplementing their thermal energy needs with geothermal heat in this relatively isolated region. The vintages of the data vary from the mid-80's to the present day. Generally, most of the profiles are of good quality in terms of having common midpoint (CMP) folds greater than 12. Some of the older profiles acquired in the mid-1980s have folds as low as six. The processing workflow that is used to enhance the low quality profiles can be found in Ardakani et al. (2014) work.

Once reprocessed, the seismic profiles are calibrated to the synthetic seismograms (well tie process) and the formation seismic horizons are picked. An example of well tie is illustrated in **Figure 3.4**. The location of the example well-tie well is highlighted in **Figure 3.3**. One older digitized Vertical Seismic Profile (VSP) is used to assist in developing a velocity model that allows for conversion of the observed seismic traveltimes into depth (Ardakani et al., 2014). The interpreted formation horizons from depth converted seismic lines, and calibrated geological well tops provide the initial seeds for generating formation surfaces which later are used as input for 3D modeling. The formation surfaces are produced using the convergent interpolation method. This algorithm uses a

coarse grid, which is initially assigned to the data and then refined many times until the surface converges to a specified smoothness. The fine-mesh 3D gridding then is utilized to construct the model. Afterward the petrophysical properties from upscaled logs are fed into the established structural model for further property distribution analysis and generating averaged property distribution maps. In other words this model provides the essential information for the reconnaissance of potential low enthalpy geothermal reservoirs in the study area (**Figure 3.5**).
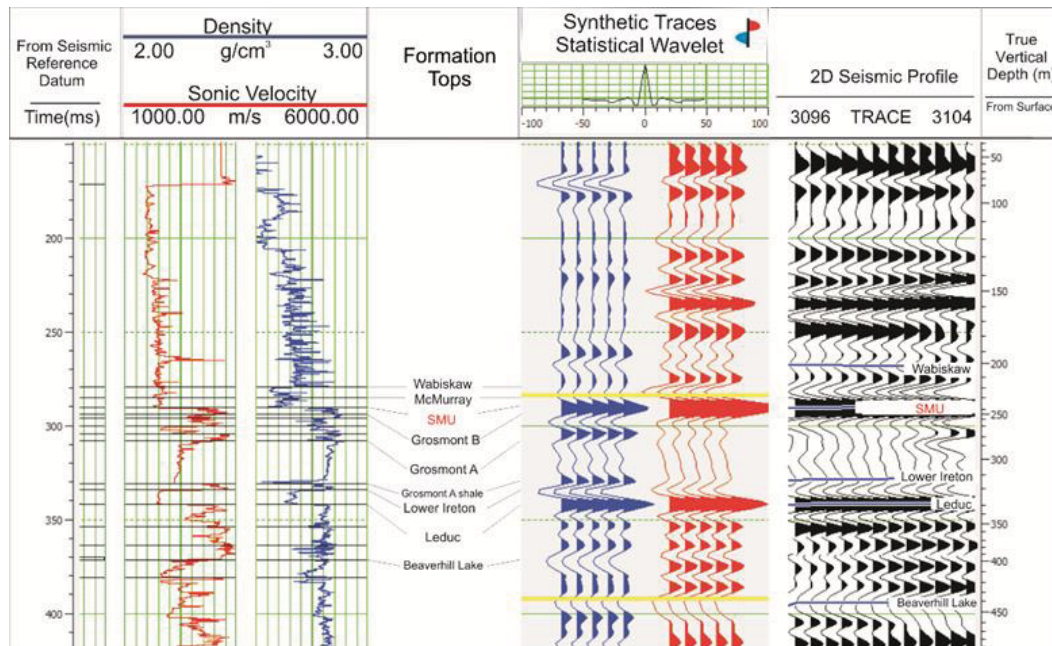
Figure 3.4. The correlation of a portion of a 2D seismic profile and constructed synthetic seismogram with the well logs used to generate a synthetic trace at the location of one of the wells within the study area. The SMU is the SubMannville Unconformity. The red seismic traces show a single composite trace plotted five times. The composite trace is a single average trace around the borehole. The blue traces are synthetic traces calculated using the sonic and density logs and the statistically extracted wavelet from seismic profile. Yellow lines in the synthetic traces track defines the well tie window length. The location of this well is shown by a pink circle in **Figure 3.3**.

In addition to spatial coverage and thickness, the properties used in this work to evaluate the potential of geothermal energy of aquifers (for thermal energy content calculation) are temperature, porosity, and permeability. Aside from a limited number of permeabilities extracted from a publicly available report by Bachu et al. (1996), the remainder of properties are modeled using the Sequential Gaussian Simulation (SGS). While we would prefer additional hard data from both core and properly conducted *in situ* testing, we are currently limited to the stochastic simulation which is a process of generating alternative, equally probable realizations of a random variable. The SGS is constrained in such a way that all realizations honor the measured data values at their locations. The generated stochastic images are called conditional. Conditional simulation is used to correct for the smoothing effect seen on the kriging maps. Essentially, we are adding back in some noise to undo the smoothing effect of kriging. The kriging estimates are weighted moving averages of the original data and they have less spatial variability than the data. A smoothed map provided by kriging is appropriate for showing global trends while conditionally simulated maps are more appropriate for studies that are sensitive to patterns of local property variability. By creating a large number of simulation maps, we try to reproduce the probability distribution at each point of the grid. From these probability distributions, we derive probabilities associated with ranges of the estimated parameter. The main steps in the SGS are: generating a random path through the grid nodes, using kriging to estimate a mean and standard deviation for the variable at that node base on surrounding data values, choosing a random value from the normal distribution and assign the variable value at that node to that number, and finally visit each successive node in the random path and repeat the process (Deutsch, 2002).
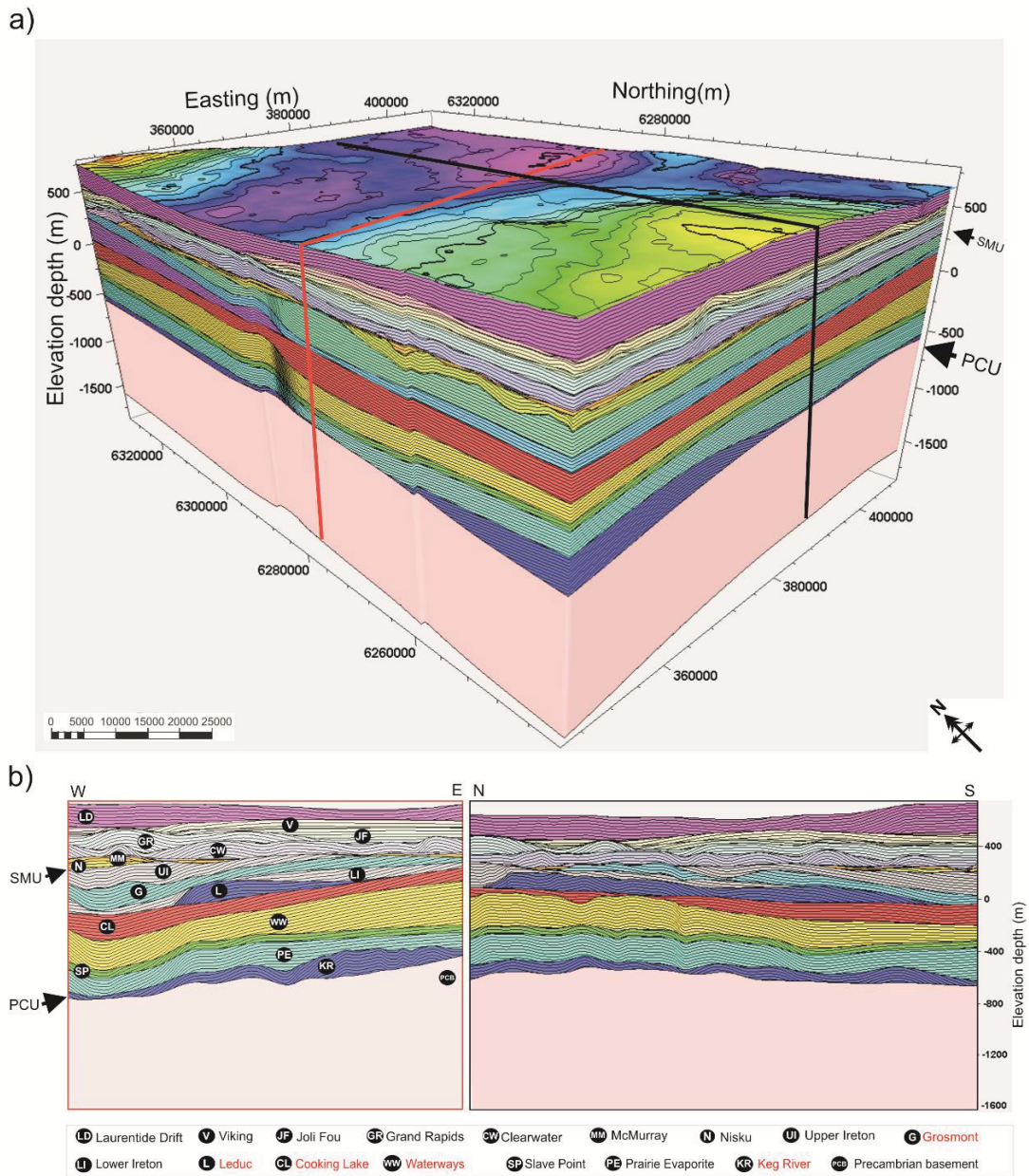
Figure 3.5. 3D model (a) in three dimension visualization with a red and black intersection planes, (b) east-west and north-south intersections within the model, with highlighted five potential Paleozoic aquifers in red letters. Stratigraphic units in model is listed from top to bottom of the basin. SMU and PCU represent the regional unconformities in the area.

3.4.1. Temperature

Recent work by Gray et al. (2012) thorough Alberta-Helmholtz collaboration has re-examined the thermal structure of a large portion of northern-central Alberta using existing well log information. The study was conducted based on measurements such as Bottom Hole Temperatures (BHT), Annual Pool Pressure Tests (APP) and Drill Stem Tests (DST) to predict geothermal gradient, heat flow and total available heat. More recently, these researchers in the Geothermal Atlas Group at the University of Alberta made the effort to complete that study with adding and cleaning up the thermal database. As our study is supported by the same initiative, we had access to the calibrated temperature measurements in our study area which are used in creating 3D temperature model and finally average temperature maps for the formations of interest. This data set contains Horner extrapolated data derived from BHT, and DST measurements. The APP data are not used in our study due to measurement inconsistency with the rest of data set. **Figure 3.6a** illustrates the temperature data points distribution in the study area.

Based on the fact that the sedimentary basin in the study area has a thickness less than 1400 m and appears to be in equilibrium with surface temperatures from the Wisconsin glaciation, the ground surface temperature correction can be set as zero (Majorowicz et al., 2012a, 2012b). With this assumption and the thermal gradient of 32 °C/km (**Figure 3.6b**) the temperature values are estimated for random points within each formation. For the purpose of comparison of selected aquifers, the average temperature map of each formation is generated in a way that the temperature of each 3D model (**Figure 3.7a** and **b**) cell has a weight corresponding to the cell thickness (**Figure 3.8**).
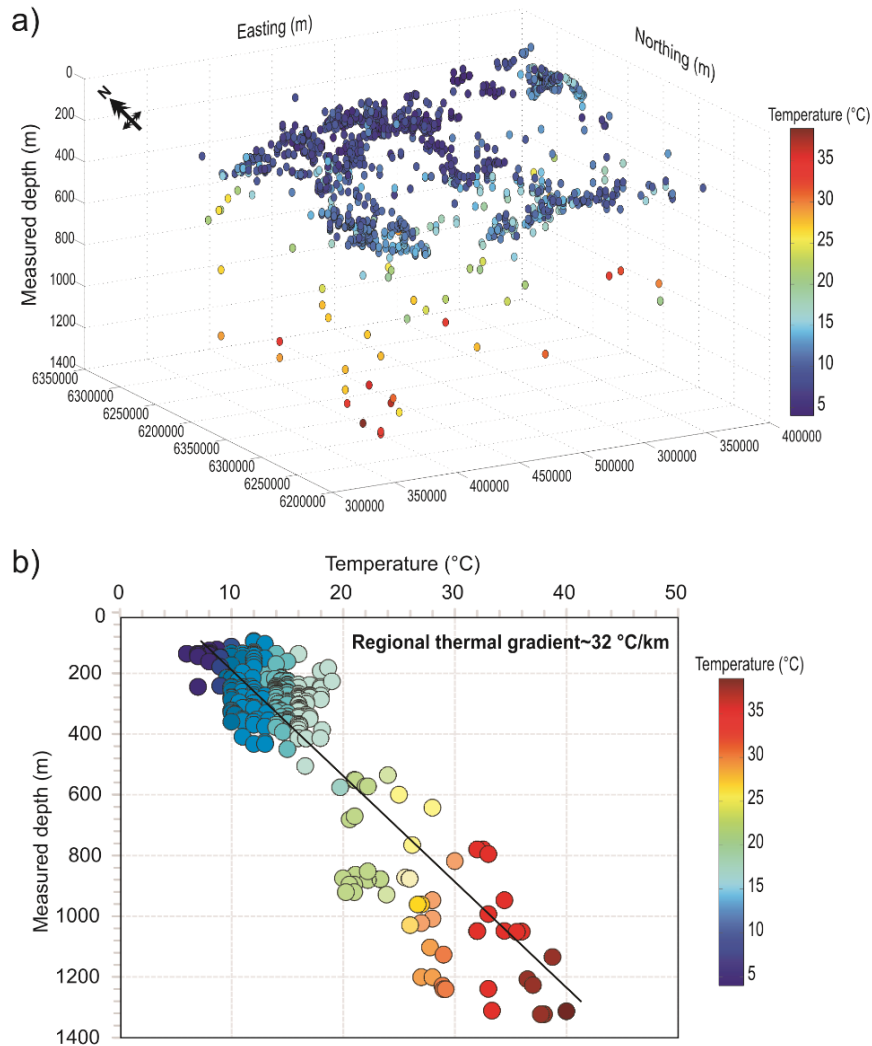
Figure 3.6. Temperature data points distribution in the study area (a) in a 3D visualization, and (b) temperature-depth cross plot.

Among the selected formations with geothermal potential the highest temperature is seen in the Keg River aquifer (**Figure 3.8b**). The temperature in this formation ranges from 21 °C in the northeast to 37 °C (with the precision of ±4 °C) in the southwest and is comparable with the temperature that can be gained at top of the crystalline basement (**Figure 3.8a**). The depth to reach the top of the Keg River Formation varies between 800 m to 1200 m. As it is expected

the temperature decreases from deeper to the shallower formations as an average of 14 °C for Grosmont Formation is anticipated (**Figure 3.8c**, **d**, **e**, and **f**).
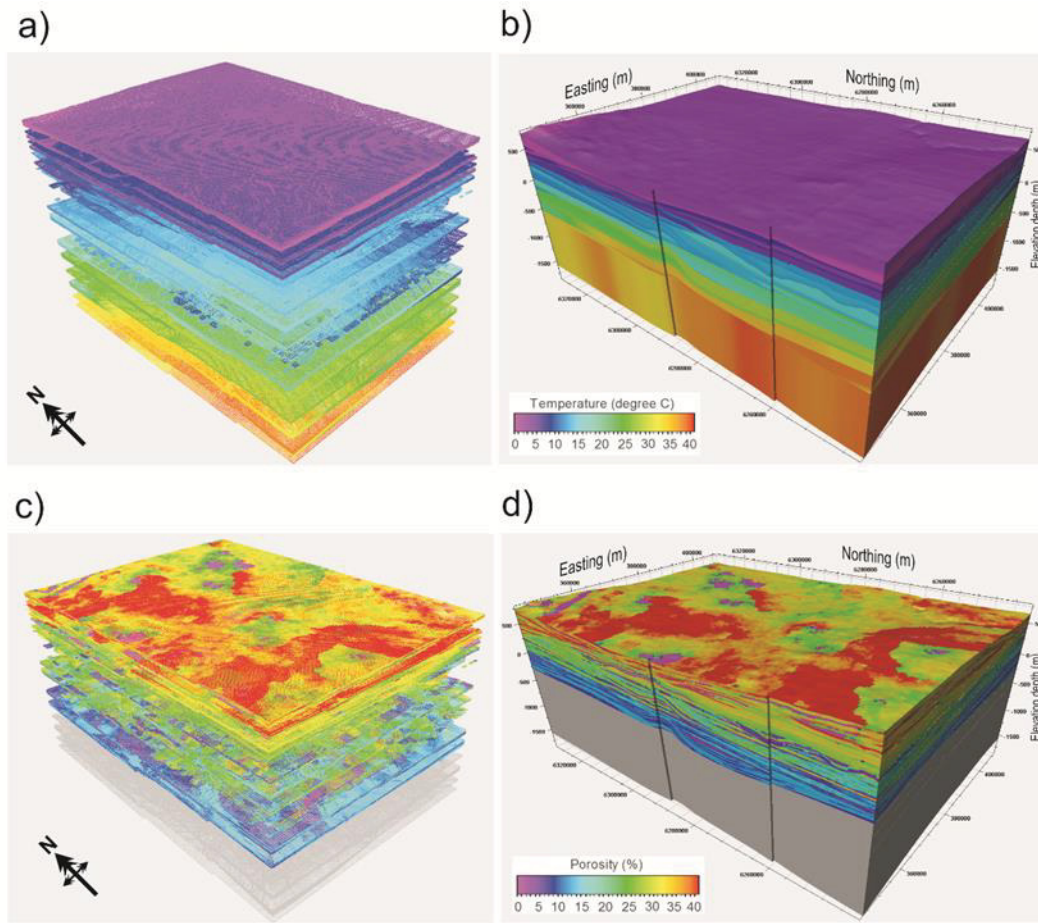
Figure 3.7. Temperature and porosity 3D models, (a) temperature model with exaggerated space between stratigraphic units, (b) the completed temperature model (the temperature varies between 0 °C at the surface and 40 °C at the top of PCU), (c) porosity model with exaggerated space between stratigraphic units (grey units represents the formations with no porosity information available), (d) the completed porosity model.
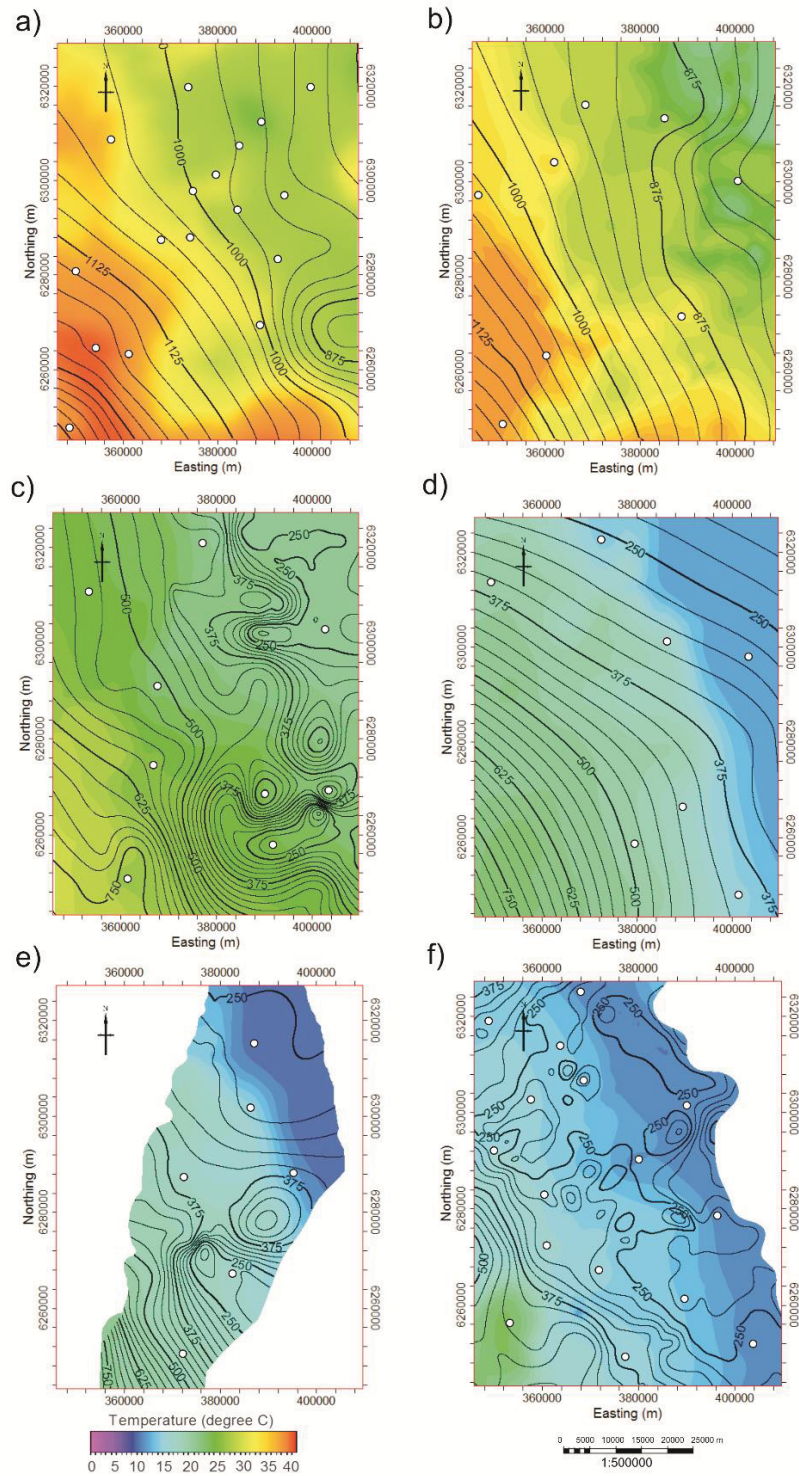
Figure 3.8. Comparison of the modeled average temperature at the (a) PCU top, and within the (b) Keg River, (c) Waterways, (d) Cooking Lake (e) Leduc, and (f) Grosmont Formation. Contour lines indicate the measured depth from surface to the formation top in meters.

3.4.2. Porosity

Porosity of the reservoir rock has a crucial role in the preliminary assessment of geothermal potential as it controls the reservoir water saturation. Accurate estimate on porosity values can be derived from several well log types, i.e., the sonic, neutron or density. The porosity input values for the property modeling here is based on neutron logs. Neutron logs measure the hydrogen content in the formation. In clean, shale-free formations, where the pore space is filled with water, the appropriately calibrated neutron log measures liquid-filled porosity; however the selected formations in the study area are partially filled with oil and gas and contain shale. Usually lower and higher neutron porosity (NPHI) is measured in the gas-filled formations and shaly zones than actual porosity, respectively. To have a better sense of whether the NPHI values are reliable they are usually compared with density derived porosity (DPHI) in a formation of interest.

Here since the main component of the selected formations are limestone, the NPHI and DPHI values are expected to overlay. Utilizing this approach the logs with outlier values are removed from the final porosity values that are upscaled for the property modeling. Although multiple simulations are conducted to achieve a porosity model which honors the input data, only the best model is shown in this paper (**Figure 3.7c** and **d**). Each formation average porosity map is presented similar to temperature maps. The isochore contours superimposed on porosity maps illustrates the vertical thickness of each formation (**Figure 3.9**). Unfortunately none of the porosity logs are deep enough to reach the Keg River Formation, therefore the porosity for this formation is obtained from a previous analysis by Bachu et al. (1996) on core samples which is estimated to be between 1 to 39 % with a geometric mean value of 9%. Due to scarce sample

points in the deeper formations (low number of well penetrations), less porosity variation is observed in the deeper formations than shallower formations (**Figure 3.10**).
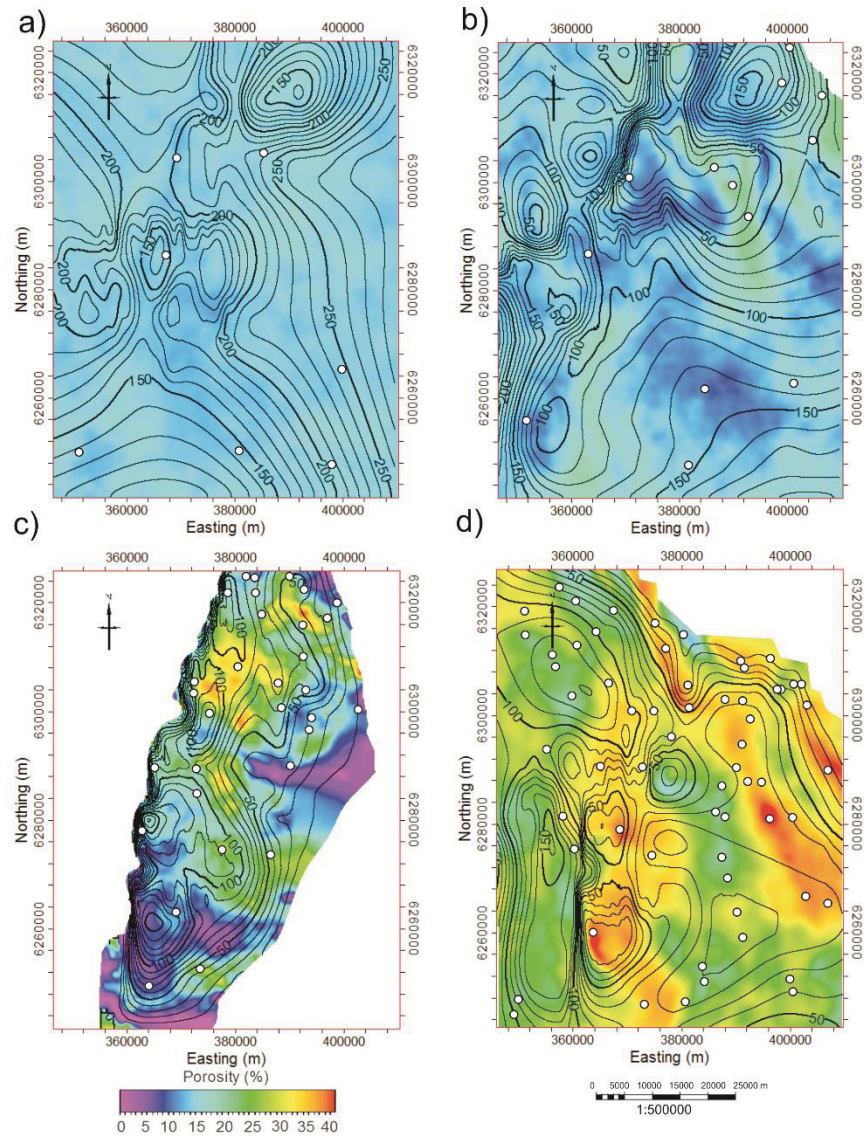
Figure 3.9. Comparison of the simulated porosity of the (a) Waterways, (b) Cooking Lake (c) Leduc, and (d) Grosmont Formation. Contour lines are isochores and indicate the area with similar thickness within the formation.
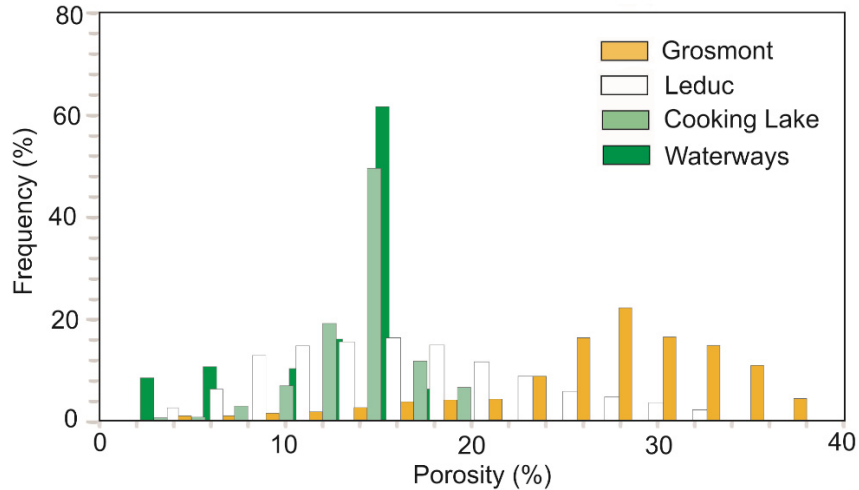
Figure 3.10. Histogram illustrating the porosity variation in the Grosmont, Leduc, Cooking Lake, and Waterways formations.

3.4.3. Permeability

Determination of permeability is not an immediate objective for this study as the uncertainty related to permeability calculation from porosity is fairly high and does not take into account fracture flow. Particularly if the porosity values themselves are derived from other parameters, the propagation error would be too high. Moreover, little measured data are available to calibrate calculated values. Based on this consideration, it is believed that performing such an exercise at this stage is not ideal. However since the knowledge of permeability is a necessity for this work, the formation permeability data are extracted from a previous study (i.e., Bachu et al., 1996) on core-plug and DST. There are specific differences between these two types of measurements. DST samples a large volume of rock, potentially reflecting features of the porous media not sampled by plug-scale measurements, such as vugs in carbonate rocks, small shale lenses or clasts or fractures. Also the DST permeability measurement is not direction dependent and generate only a single value. Assuming a uniform sedimentary rock, the geometric average of the upscaled (i.e., well-scale) permeability values is

the best estimate of the representative permeability of each hydrostratigraphic unit (Dagan, 1989). The geometric average indicates the typical value of a set of measured permeability values. The estimated average permeability values obtained from core-plugs are higher than those obtained from DST. According to Bachu et al. (1996) this could be due to the sample size, sampling procedure, depressured samples and direction dependent core-plug measurement. Also removing the bitumen from the core-plug samples for conducting the measurement could probably lead to higher permeability measurements than *in situ* DST measurements (**Figure 3.11**). Here the core-plug permeability values are used in our final integration and interpretation as the core-plug data are a better representative of formation horizontal permeability (i.e., maximum permeability).

	Grosmont	Cooking Lake	Waterways	Keg River
■ Drill-stem	0.02 —1591 mD	0.003 — 1556 mD	0.03 — 1122 mD	0.001 — 272 mD
■ Core-plug	0.02 — 6870 mD	0.25 — 96 mD	0.01 — 10200 mD	0.01 — 175 mD
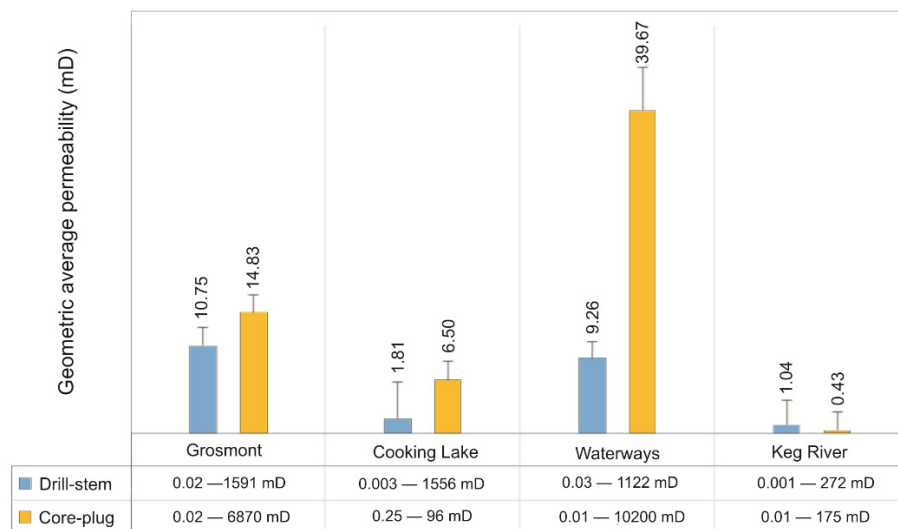
Figure 3.11. Histogram illustrating the DST and core-plug permeability analysis results for Keg River, Waterways, Cooking Lake and Grosmont aquifers.

3.5. Estimation of thermal energy quantity

Simple estimation of the quantity of the thermal energy of the rock is useful to illustrate potential amount of heat to be removed from a target

formation. This estimation is conducted using the extracted information from the 3D stratigraphic and petrophysical models and some logical assumptions. The potential heat removed from the rock thorough heat extraction can be estimated by

$$Q = Cp * \rho * V * (\delta T) \tag{1}$$

where C_p is heat capacity at constant pressure, ρ is the mass density, V is the total volume of the rock, and δT is change in the temperature resulting from the heat extraction process (Barbier, 2002). The heat capacities of the minerals dolomite and calcite (calculated from Robie et al., 1979), the primary modes in the rocks in target aquifers, and that for water (Lemmon et al., 2016) are shown as a function of temperature in **Figure 3.12a**. Note that we provide these values in the somewhat unusual form of J/m³°C of the material instead of the usual J/mol°C because in this form we can directly estimate the heat capacity for the water-saturated rock $C_p{}^R$ of porosity φ with

$$C_p^R = \varphi C_p^w + (1 - \varphi)C_p^s \tag{2}$$

where $C_p{}^w$ and $C_p{}^s$ are the temperature dependent values of the heat capacities of the water and solid mineral portion of the rock, respectively. For purposes of this study, we simply take $C_p{}^s$ to be the average for calcite and dolomite because these values do not significantly differ from one another (e.g., at a temperature of 30 °C the $C_p{}^s$ of calcite and dolomite is ~2.0 MJ/m³°C and ~2.1 MJ/m³°C, respectively). For purposes of illustration the amount of available heat in 1 m³ of a water saturated rock that can be obtained in lowering its temperature by 1°C is contoured in **Figure 3.12b**.
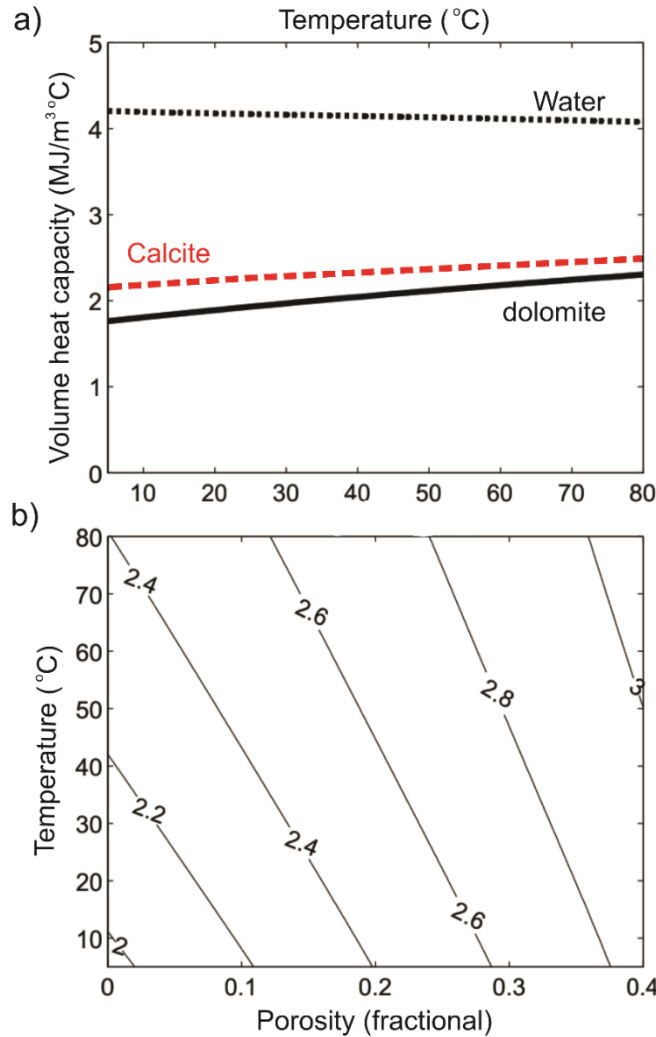
Figure 3.12. (a) Heat capacities at constant pressure as a function of temperature for pure water at 1 atm, calcite, and dolomite. Over the range of pressures expected *in situ* these values will not change appreciably. Note that units are reported in untypical units of $MJ/m^3°C$. (b) Heat content in MJ (10^6 J) per m^3 over a 1 °C change of temperature for the average carbonate rock fully saturated with water contoured as a function of rock porosity and temperature.

Using these equations, the potential quantity of thermal energy (Q) to be extracted from each Paleozoic aquifer is calculated (**Table 3.2**). In this calculation the volume and average density of each formation is obtained from the 3D model, the heat capacity is taken from the heat contents displayed in **Figure 3.12b**, and the temperature difference is set to be between rock

85

temperature median for each formation down to 5 °C. This temperature is close to the temperature of cooled water (4 °C) discharged from the heat-pump system in Lund (Bjelm and Lindeberg, 1995). According to these calculations, the ultimate total energy available from all of the reservoirs would be about 1.2 EJ (1 EJ = 10^{18} J).

More practically, however, the given unit would extract water from areas on the order of a km², and the "site" energy content of **Table 3.2** is calculated using the expected volume of each reservoir underlying a km². The energy contents in this case are a few PJ (1 PJ = 10^{15} J).

Table 3.2. The result of analysis for porosity, permeability, temperature, thickness, maximum depth to formation top, average density and thermal energy content for five selected Paleozoic aquifers.

Formation (aquifer)	Measured Depth (m) max	Thickness (m)		Volume (m³)	Temperature (°C)				Porosity (%)				Permeability (mD)	Ultimate Thermal Energy Content (EJ)	Site Thermal Energy Content (PJ)
		mean	std		min	max	mean	std	min	max	mean	std			
Grosmont	500	68.6	23.0	5.04E+11	9	22	14	2.8	5	38	28	4	14.8	11.7	1.6
Leduc	750	61.0	19.2	9.49E+10	10	20	15	3.6	4	33	15	5	NA	2.2	1.4
Cooking Lake	760	107.0	33.0	7.26E+11	11	23	17	3.7	3	20	13	2	6.5	19.5	2.9
Waterways	780	198.2	32.3	1.41E+12	20	29	24	2.3	1	15	13	0.6	39.6	60.6	8.5
Keg River	1255	69.8	21.1	4.77E+11	21	37	29	4.5	1	38	9	2	0.4	25.0	3.7

3.6. Discussion

The Keg River Formation with the mean thickness of ~70 m, average porosity of 9%, permeability of 0.43 mD, and thermal energy content of 25 EJ is the deepest aquifer in this area. Scarce drilled boreholes and petrophysical logs in this formation suggests that acquiring more geologic and geophysical information to determine its qualification for geothermal development is necessary. The water salinity of this formation can be high due to the fact that it is overlain by the Prairie Evaporite Formation and that can add to its complexity of the geothermal

exploitation. The higher temperature of the groundwater in this formation can help the dissolution of chemical components such as chloride, sodium, potassium, sulfate that if above the standard threshold will make it highly corrosive and saline and can cause damage to the heat-pump system. Further hydrologic analysis is recommended to evaluate the economic value of geothermal potential of the Keg River aquifer.

As discussed in the geology setting section, the Waterways Formation consists of five members, however since not enough information is available to us for detailed lithology modeling, it is simplified and grouped into one stratigraphic unit in the 3D model. This unit has the highest thickness (~200 m) and thermal energy content (60.6 EJ) among all investigated aquifers. The Cooking Lake, Leduc, and Grosmont aquifers have high porosity and permeability but they are shallower and cooler and this consequently reduces their thermal energy content relative to the deeper aquifers (**Table 3.2**). However, geothermal potential assessment and development is easier in these formations due to the availability of larger geophysical and geological data sets.

The analysis presented in this study demonstrates that selected five aquifers in the Athabasca region all have relatively large spatial coverage, thickness, porosity, permeability and thermal heat in place to be considered as potential targets for low enthalpy geothermal energy development. As mentioned earlier, industrial-scale heat-pump technologies may be useful for geothermal development of these aquifers. The best example for this is the geothermal heat-pump plant in Lund, Sweden (Bjelm and Lindeberg, 1995). The Lund geothermal plant pumps water (~21 °C) from a depth of 800 m in a permeable sand reservoir. Heat is transferred from the underground water to the refrigerant in the heat-

pump's evaporator cooling the water to 4°C. This cooled water is then reinjected back to the reservoir in two boreholes that are removed from the producer by over one km. The refrigerant then is pressurised in the compressor. Increase in pressure implicates higher temperature of the refrigerant. Heat is transferred from the refrigerant to the district heating water in the condenser. The water for district heating, heated by the heat-pump, reaches 77 °C and is used for the heat demand in the Lund city with an average heat production of 313 GWh (~1.13 PJ) yearly.

Energy is of course required to do all the pumping and reinjecting of water and compressing of the refrigerant. The coefficient of performance (COP) is a standard measure of efficiency of such industrial-scale processes and it is defined as the simple ratio of the heat energy output to the energy input. It is highly dependent on factors such as the temperature differences between the extracted water and the environment, the refrigerants used, the output temperature, and the energy used to pump water and compress refrigerant. Consider first the case of burning pure natural gas to heat. Ignoring the energy needed to produce, transport, and store the natural gas, the COP that can be obtained by burning natural gas to directly heat water is, by definition, one (1.0). In contrast, the COP of the Lund heat-pump is ~3.5, which indicate a high level of efficiency relative to a typical industrial COP (Alm, 1999). Consequently heat-pump technologies may be able to provide additional heat energy to assist thermal production. Detailed engineering feasibility studies to assess the energy and carbon budgets are necessary but are beyond the scope of the preliminary work here.

3.7. Conclusions

Integration of interpreted seismic profiles with well tops and utilizing both in the 3D modeling process enables us to provide a 3D model of the study area with more structural details on the geometry, coverage and thickness of formations than models only derived from well tops can provide. Also utilization of SGS method for property modeling properly captured the spatial variability of the properties generated within shallow target formations. Analysis of the information provided by the stratigraphic and property 3D models demonstrates that five Paleozoic aquifers in the Athabasca region are potentially useable for geothermal applications. Keg River, Waterways, Cooking Lake, Leduc, and Grosmont formations are identified as potential aquifers. These aquifers all have enough coverage and thickness in the area and show high amount of thermal energy content. Since the sedimentary basin in the Athabasca region is quite shallow (Less than 1400 m), these aquifers are recognized as low enthalpy geothermal reservoirs with maximum temperature of 40 °C. Therefore utilization of heat-pumps for heat generation is recommended.

This study demonstrates that wide distribution of heat values are available in Athabasca region at a depth that have already been reached in oil and gas drilling operations. The data remain sparse and evaluation of potential sites will require that workers carry out proper evaluations of *in situ* bulk permeabilities, water chemistries, and temperatures. Depending on the location of interest, the depth to these potential reservoirs are not large and they could be accessed relatively inexpensively by drilling. Regardless, our models suggest that the target aquifers may hold sufficient heat energy that could supplement potential future needs in this region if heat-pump technologies are employed.

References

Adams, J. J., B. J. Rostron, and C. A. Mendoza, 2004, Coupled fluid flow, heat, and mass transport, and erosion in the Alberta basin: Implications for the origin of the Athabasca oil sands, Canadian Journal of Earth Scienes, 41, 1077-1095.

Alm, P., 1999, Long-time study of geothermal data from a low enthalpy geothermal heat plant: Proceeding of 24th Workshop on Geothermal Reservoir Engineering, accessed 16 April 2016.

Anglin, F. M., and A. E. Beck, 1965, Regional heat flow pattern in Western Canada: Canadian Journal of Earth Science, 2, 176-182.

Ardakani, E. P., D. R. Schmitt, and T. D. Bown, 2014, Detailed topography of the Devonian Grosmont Formation surface from legacy high resolution seismic profiles, Northeast Alberta: Geophysics, 79, B135-B149, doi: 10.1190/geo2013-0268.1.

Bachu, S., 1995, Synthesis and model of formation water flow in the Alberta Basin, Canada: American Association of Petroleum Geologists Bulletin, 79, 1159-1178.

Bachu, S., J. R. Underschultz, B. Hitchon, 1996, Regional subsurface hydrogeology in Northeast Alberta: Alberta Geological Survey, open file report 1996-14.

Barbier, E., 2002, Geothermal energy technology and current status - an overview: Renewable and Sustainable Energy Reviews, 6, 3-65.

Barss, D. L., E. W. Best, and N. Mayers, 1964, Triassic, in R. G. McCrossan, and R. P. Glaister, eds., Geological history of Western Canada: Alberta Society of Petroleum Geologists, chapter 9, 113-136.

Bell, J., and T. Weis, 2009, Greening the grid - Powering Alberta's future with renewable energy: Pembina Institute, Drayton Valley, Canada.

Belyea, H. R., and A.W. Norris, 1962, Middle Devonian and older Paleozoic formations of southern district of Mackenzie and adjacent areas: Geological Survey of Canada, paper 62-15.

Bjelm, L., and L. Lindeberg, 1995, Long-term experience from a heat pump plant in Lund, Sweden, using a low-temperature geothermal aquifer, Proceedings of the World Geothermal Congress, 3, 2173-2176.

Dagan, G., 1989, Flow and transport in porous formations: Springer-Verlag, New York.

Deutsch, C. V., 2002, Geostatistical reservoir modeling: Oxford University Press.

Energy Resources Conservation Board, 2009, Table of formations, http://www.ercb.ca/docs/products/catalog/TOF.pdf, accessed 27 Dec 2015.

Georgsson, L. S., 2009, Geophysical methods used in geothermal exploration: Short Course IV on exploration for geothermal resources at Lake Naivasha, Kenya, retrieved April 16, 2016.

Grasby, S. E., D. M. Allen, Z. Chen, G. Ferguson, A. Jessop, M. Kelman, J. Majorowicz, M. Moore, J. Raymond, and R. Therrien, 2011, Geothermal energy resource potential of Canada: Geological Survey of Canada, open file report.

Gray, A., J. Majorowicz, and M. Unsworth, 2012, Investigation of the geothermal state of sedimentary basins using oil industry thermal data - Case study from Northern Alberta exhibiting the need to systematically remove biased data: Journal of Geophysics and Engineering, 9, 534-548, doi:10.1088/1742-2132/9/5/534.

Gupta, I., A. M. Wislon, and B.J. Rostron, 2012, Cl/Br compositions as indicators of the origin of brines: hydrogeologic simulations of the Alberta Basin, Canada, Geological Society of America Bulletin, 124, 200-212.

Gupta, I., A. M. Wislon, and B.J. Rostron 2015, Groundwater age, brine migration, and large-scale solute transport in the Alberta Basin, Canada: Geofluids, 15, 608-620.

Hackbarth, D., and M. Brulotte, 1981, Groundwater observation well network - Athabasca oil sands area: Alberta Research Council, Information Series 69.

Hackbarth D., and N. Nastasa, 1979, The hydrogeology of the Athabasca oil sands area, Alberta: Alberta Research Council Bulletin, 38.

Hersir, G. P., and A. Björnsson, 1991, Geophysical exploration for geothermal resources, principles and applications: United Nations University Geothermal Training Programme, report 15, retrieved April 16, 2016.

Hitchon, B., 1964, Formation fluids in R. G. McCrossan, and R. P. Glaister, eds., Geological history of western Canada: Canadian Society of Petroleum Geologists, 201-217.

Hitchon, B., C. M. Sauveplane, S. Bachu, E. H. Koster, and A. T. Lytviak, 1989a, Hydrogeology of the Swan Hills area, Alberta - Evaluation for deep waste injection: Alberta Research Council Bulletin, 58.

Hitchon, B., S. Bachu, C. M. Sauveplane, A. Ing, A. T. Lytviak, and J. R. Underschultz, 1989b, Hydrogeological and geothermal regimes in the Phanerozoic succession - Cold Lake area, Alberta and Saskatchewan: Alberta Research Council Bulletin, 59.

Hofmann, H., 2015, Development of Enhanced Geothermal Systems (EGS) in Northern Alberta, Ph.D. thesis: University of Alberta.

Jones, F. W., H. L. Lam, and J. A. Majorowicz, 1985, Temperature distributions at the Paleozoic and Precambrian surfaces and their implications for geothermal energy recovery in Alberta: Canadian Journal of Earth Science, 22, 1774-1780.

Lam, H. L., and F. W. Jones, 1984, Geothermal gradients of Alberta in western Canada: Geothermics, 13, 181-192.

Lam, H. L., F. W. Jones, and J. A. Majorowicz, 1985, A statistical analysis of bottom hole temperature data in southern Alberta, Geophysics, 50, 677-684.

Law, J., 1955, Geology of Northwestern Alberta and adjacent areas: American Association of Petroleum Geologists Bulletin, 39, 1927-1975.

Lemmon, E. W., M. O. McLinden, and D. G. Friend, Thermophysical properties of fluid systems, in P. J. Linstrom, and W. G. Mallard, eds., NIST chemistry

webbook, NIST standard reference database, 69: National Institute of Standards and Technology, http://webbook.nist.gov, retrieved February 6, 2016.

Liddell, M., M. Unsworth, and J. Pek, 2016, Magnetotelluric imaging of anisotropic crust near Fort McMurray, Alberta; implications for engineered geothermal system development: Geophysical Journal of Interpretation, published online, doi:10.1093/gji/ggw089.

Majorowicz, J. A., and S. E. Grasby, 2010, High potential regions for enhanced geothermal systems in Canada: Natural Resources Research, 19, 177-188, doi: 10.1007/s11053-010-9119-8.

Majorowicz, J. A., and A. M. Jessop, 1981a, Present heat flow and a preliminary geothermal history of the Central Prairies Basin, Canada: Geothermics, 10, 81-93.

Majorowicz, J. A., and A. Jessop, 1981b, Regional heat flow patterns in the Western Canadian Sedimentary Basin: Tectonophysics, 74, 209-238, doi: 10.1016/0040-1951(81)90191-8.

Majorowicz, J. A., G. Garven, A. M. Jessop, and C. Jessop, 1999, Present heat flow along a profile across the Western Canada Sedimentary Basin - the extent of hydrodynamic influence in A. Forster, and D. F. Merriam, eds, Geothermics in basin analysis, 61-79.

Majorowicz, J. A., and M. C. Moore, 2008, Enhanced Geothermal Systems (EGS) potential in the Alberta Basin: Institute for Sustainability, Energy, Environment and Economy.

Majorowicz, J. A., and S. E. Grasby, 2010, High potential regions for enhanced geothermal systems in Canada: Natural Resources Research, 19, 177-188, doi: 10.1007/s11053-010-9119-8.

Majorowicz, J. A., W. Gosnold, A. Gray, J. Safanda, R. Klenner, and M. Unsworth, 2012a, Implications of post-glacial warming for Northern Alberta; heat flow - correcting for the underestimate of the geothermal potential: Geothermal Resources Council Transactions, 36, 693-698.

Majorowicz, J. A., M. Unsworth, T. Chacko, A. Gray, L. Heaman, D. K. Potter, D. R. Schmitt, and T. Babadagli, 2012b, Geothermal energy as a source of heat for oil sands processing in Northern Alberta, Canada in F. J. Hein, D. Leckie, J. Suter, and S. Larter, eds., Heavy oil and oil sand petroleum systems in Alberta and beyond: American Association of Petroleum Geologists, Chapter 27, doi: 10.1306/13371602St643569.

Majorowicz, J., J. Chan, J. Crowell, W. Grosnold, L. M. Heaman, J. Kueck, G. Niewenhuis, D. R. Schmitt, M. Unsworth, N. Walsh, and S. Weides, 2014, The first deep heat flow determination in crystalline basement rocks beneath the Western Canadian Sedimentary Basin, Geophysical Journal International, 197, 731-747.

Moeck, I. S., 2014, Catalog of geothermal play types based on geologic controls: Renewable and Sustainable Energy Reviews, 37, 867-882, doi: 10.1016/j.rser.2014.05.032.

Mossop, G., and I. Shetsen, 1994, Geological atlas of the Western Canada Sedimentary Basin: Canadian Society of Petroleum Geologists and Alberta Research Council.

National Energy Board, 2015, Energy futures supplement-demand sensitivities, ISSN 2369-1476, https://www.neb-one.gc.ca/nrg/ntgrtd/ftr/2015/index-eng.html, retrieved February 1, 2016.

Nieuwenhuis, G., T. Lengyel , J. Majorowicz, M. Grobe, B. Rostron, M. Unsworth, and S. Weides, 2015, Regional-scale geothermal exploration using heterogeneous industrial temperature data; a case study from the Western Canadian Sedimentary Basin: Proceedings of the World Geothermal Congress.

Norris, A. W., 1973, Paleozoic (Devonian) geology of Northeastern Alberta and Northwestern Saskatchewan in M. A. Carrigy, and J. W. Kramers, eds., Guide to the Athabasca oil sands area: Alberta Research Council Information Series, 65, 18-76.

Parsons, W. H., 1973, Alberta, in R. G. McCrossan, eds., The Future Petroleum Provinces of Canada - Their Geology and Potential: Canadian Society of Petroleum Geologists, Memoir 1, 73-120.

Pathak, V., T. Babadagli, J. Majorowicz, and M. J. Unsworth, 2014, Evaluation of engineered geothermal systems as a heat source for oil sands production in Northern Alberta: Natural Resources Research, 23, 247-265.

Porter, J., R. Price, and R. McCrossan, 1982, The Western Canada Sedimentary Basin: Philosophical Transactions of the Royal Society of London, Series A, Mathematical and Physical Sciences, 305: 169-192. doi:10.1098/rsta.1982.0032.

Robie, R. A., B. S. Hemingway, and J. R. Fisher, 1979, Thermodyanic properties of minerals and related substantces at 298 K and 1 Bar (105 Pasacals) pressure and at higher temperatures: United State Geological Survey Bulletin, 1452.

Rybach, L., and M. Mongillo, 2006, Geothermal sustainability-A review with identified research needs, Geothermal Resources Council Transactions, 30, 1083-1090.

Sproule, D. F., 1956, Granite Wash of Northern Alberta: Journal of Alberta Society of Petroleum Geologists, 4, 197-203.

Subramanya, K. 1994, Engineering hydrology: Tata McGraw-Hill Education.

Toth, J., 1978, Gravity-induced cross-formational flow of formation fluid, Red Earth region, Alberta, Canada; Analysis, patterns, and evaluation: Water Resources Research, 14, 805-843.

Ungemach, P., 1985, An overview of the state of geothermal energy: International Journal of Energy research, 9, 223-228.

Weides, S., I. Moeck, J. Majorowicz, D. Palombi, and M. Grobe, 2013, Geothermal exploration of Paleozoic formations in central Alberta: Canadian Journal of Earth Science, 50, 519-534.

Weides, S., and J. Majorowicz, 2014c, Implications of spatial variability in heat flow for geothermal resource evaluation in large foreland basins: the case of the Western Canada Sedimentary Basin: Energies, 7, 2573-2594.

Weides, S., I. Moeck, J. Majorowicz, and M. Grobe, 2014a, The Cambrian Basal Sandstone Unit in central Alberta – an investigation of temperature distribution, petrography, and hydraulic and geomechanical properties of a deep saline aquifer: Canadian Journal of Earth Sciences, 51,783-796.

Weides, S., I. Moeck, D. R. Schmitt, J. Majorowicz, 2014b, An integrative geothermal resource assessment study for the siliciclastic Granite Wash Unit, Northwestern Alberta (Canada): Environmental Earth Sciences, 72, 4141-4154.

Chapter 4: Geophysical evidence for an igneous dyke swarm, Buffalo Creek, Northeast Alberta

A version of this chapter has been submitted for publication. Ardakani E. P. and D. R. Schmitt, 2016: Geological Society of America Bulletin.

Integrated processing and interpretation of the High Resolution Aeromagnetic and 2D seismic reflection data in the Athabasca region, near Buffalo Creek, Northeastern Alberta reveals the existence of a set of buried southwest-northeast striking structural elements. Qualitative and quantitative interpretation of the data determines that these structures lie within the Western Canada Sedimentary Basin. The anomaly signatures of these features on the aeromagnetic data appear to range between 5 to 20 nT in amplitude. Furthermore these anomalies are recognized by narrow vertical disturbance zones on the 2D seismic profiles which directly align with the linear magnetic anomalies. The forward magnetic signature modeling suggests the source of the anomalies to be dykes emplaced deeper than 200 m into Paleozoic sediments with more than 60 m thickness. We refer to these features as the Buffalo Creek dyke field. The comparison of the Buffalo Creek dykes with the present kimberlite fields and dyke swarms in Alberta implies that the interpreted dykes' emplacement occurred sometime between 70.3±1.6 to 77.6±0.8 Ma and may be related to the Farallon plate subduction under the west coast of the North American Plate.

4.1. Introduction

Today there is no known volcanic or intrusive activity in the large region east of the Canadian Cordillera encompassing the Western Canada Sedimentary Basin (WCSB) and adjacent portions of the exposed Precambrian Canadian craton. During the late Cretaceous through the Paleogene, however, igneous activity did occur sporadically in a number of locales (**Figure 4.1a**) (Heaman et al., 2003, 2004; Eccles et al., 2004, 2008). These include the Sweet Grass dykes and associated intrusive stocks of the Sweet Grass Hills (Kjarsgaard, 1994, 1997; Ross et al., 1997; Buhlmann et al., 2000; Rukhlov and Pawlowicz, 2012), the Lac de Gras kimberlites in Northwest Territories (Dufresne et al., 1994), the Fort a la Come kimberlite field in Saskatchewan (Jellicoe et al., 1998; Zonneveld et al., 2006), the Buffalo Head Hills field in North-Central Alberta (Carlson et al., 1999; Skelton and Bursey, 1998; Skelton et al., 2003; Eccles et al., 2003), the Birch Mountains field (Aravanis, 1999; Eccles et al., 2003, 2004), and the Mountain Lake intrusion in Northern Alberta (Wood and Williams, 1994; Leckie et al., 1997; Wood et al., 1998; Eccles, 2003; Kellett et al., 2005). These discoveries have demonstrated that igneous intrusion and possibly eruption had occurred into and possibly through the sediments that blanket the Precambrian crystalline basement.

In this study, we provide geophysical evidence for yet another locus of igneous activity centered at 56° 25′ N Latitude and 113° 00′ W Longitude (622600 Easting and 6252380 Northing, NAD 27-Zone 12) within the Athabasca region of Northeast Alberta (**Figure 4.1b**). Linear magnetic anomalies unexpectedly appeared within a study region selected for initial geological assessment for geothermal potential (Ardakani and Schmitt, 2016) were readily apparent in the

commercially available High Resolution Aeromagnetic (HRAM) images used as part of the development of the detailed geological model.
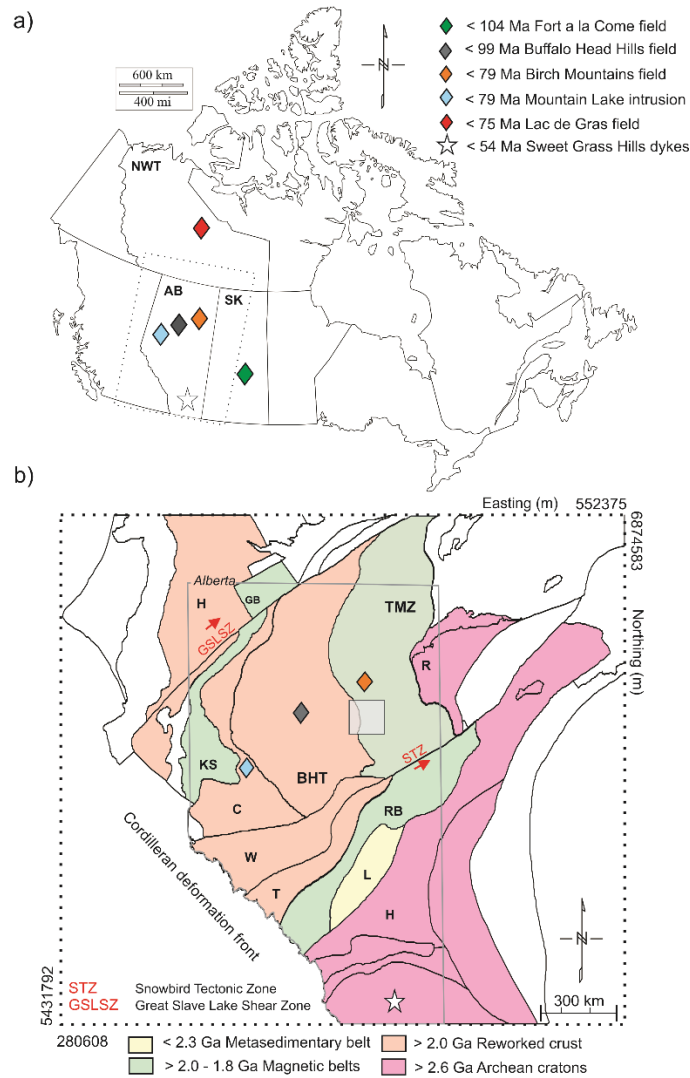
Figure 4.1. (a) Distribution of kimberlite fields and igneous intrusion complexes in WCSB, (b) The Precambrian terranes in Alberta colored by age (compiled from Hoffman, 1989; Ross et al., 1991; Kellett et al., 2005) with the study area shown by a gray box. The location of the Mountain Lake intrusion, the Buffalo Head Hills field, the Birch Mountains field, and Sweet Grass dykes are illustrated by blue, gray, and orange diamond and a star, respectively. The terranes include Buffalo Head (BHT), Taltson Magmatic Zone (TMZ), Chinchaga (C), Wabamun (W), Ksituan (KS), Great Bear (GB), Hottah (H), Rae (R), Thorsby (T), Rimby (RB), Lacombe (L), and Hearne (H).

This contribution, focuses on demonstrating that these lineaments are likely igneous dykes that may transect the entire sedimentary column, but to our knowledge remain blanketed beneath the thick glacial deposits in the area. Here, we first provide a brief overview of the geological setting followed by presentation of the magnetic anomalies that initially suggested the existence of these features. We compare these to other publicly available data from the WCSB. Finally, we support by forward modelling our interpretation that these are igneous dykes within the sedimentary column. Correlation of the magnetic anomalies to irregularities in crossing 2D seismic profiles provides additional supporting evidence. We conclude with some speculations as to the provenance of these features.

4.2. Geological setting

The study area is situated in Northeast Alberta (**Figure 4.1b**), about 30 km west of the city of Fort McMurray. The gross stratigraphy of the area can be separated into four unconformable units of Pleistocene glacial deposits, Cretaceous siliclastics, Paleozoic carbonates and evaporates, and the underlying Precambrian crystalline basement (Westgate, 1968; Beaney and Shaw, 2000).

The area has been subject to numerous advances and retreats of the Pleistocene ice sheets, with the last ice retreating from this area about 11 ka. Laurentide drift sediments blanket the area to estimated depths of 10 to 20 m (MacCormack et al., 2015), although local excursions that cut through the Mesozoic layer and into the Paleozoic are known. These recent drift sediments, combined with extensive muskeg bogs, render surface geological mapping of the underlying Lower Cretaceous siliciclastic rocks impossible.

The layer of Cretaceous sediments ranges in thickness from 80 m to 300 m in the study area. These primarily consist of weakly consolidated sands and shales. The bedrock can be from a number of Cretaceous units, the youngest of which is the Turonian age (89.8 - 93.9 Ma) Second White Specks. McMurray Formation oil sands of the Barremian to Aptian age (~125 Ma - 113 Ma) lie at the bottom. These sediments are nearly horizontal over the study area. The unconformity at their base is here referred to as the SubMannville unconformity (SMU).

The Paleozoic sediments are approximately 550 to 1000 m thick and gently dip to the southwest. Late Devonian Frasnian age (382.7 Ma - 372.2 Ma) sediments of the Nisku, Ireton, and Grosmont Formations subcrop at the SMU (see recent overview in Ardakani et al., 2014). The SMU represents a gap of more than 220 million years of missing geological record. It is important to note that some of these formations are carbonates and, as such, the topography of the SMU can be highly irregular due to extensive karsting (Machel et al, 2012; Russell-Houston and Gray, 2015). Lower Devonian Basal Red Beds lie at the bottom of the Paleozoic sediment package. The unconformity bounding the Paleozoic sediments and the underlying craton separates the rocks in time by more than 1.5 billion years and is here referred to as the Precambrian unconformity (PCU).

Figure 4.2 illustrates the topography of the basement as mapped by depth converted seismic horizons and geologic well tops. The white circles show the location of well tops and the white and black lines indicate the 2D seismic reflection profiles used. An interpreted regional seismic profile (SP-00) with more than 20 km length (**Figure 4.3**) shows the spatial distribution of the

sedimentary formations and the gross structure of the region. The SMU and PCU are highlighted in **Figure 4.3.**
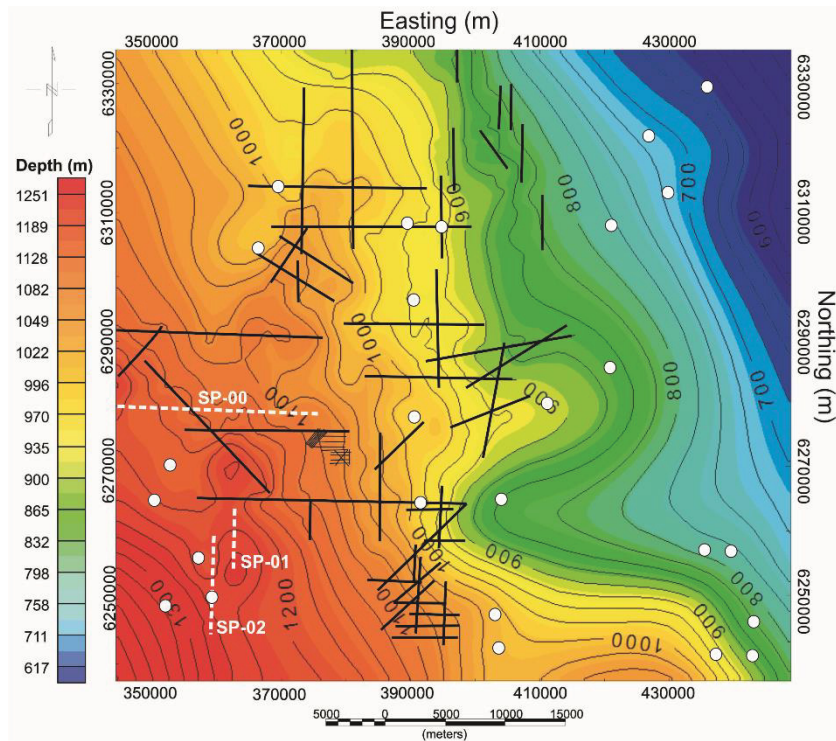
Figure 4.2. Precambrian basement (PCU top) measured depth map constructed by interpreted seismic horizons and integrated well tops. The contour interval is 25 m and is labeled every 100 m. The white circles show the location of PCU well tops. The solid black lines are 2D reflection seismic profiles over the study area. The white dashed lines highlight the seismic lines shown later in the paper in **Figure 4.3**, **4.9** and **4.10**.

The Precambrian crystalline basement in Alberta is divided into domains based on a combination of geophysical signatures of exposed geologic subdivisions of the Canadian Shield, potential field data, and age determinations of drill cores from basement intersections (Hoffman, 1989; Ross et al, 1991; Pilkington et al, 2000; Burwash et al., 2000). These terranes are illustrated in **Figure 4.1b**. The study area mostly lies within the Taltson Magmatic Zone (TMZ) and but also includes the easternmost Buffalo Head terrane (BHT). The

102

TMZ and BHT are terminated to the north by the Great Slave Lake Shear Zone (GSLSZ) and to the south by the Snowbird Tectonic Zone (STZ). The TMZ is made primarily of granitic plutons and uppermost amphibolite and granulite facies gneisses (Walsh, 2013) aged from 1.92 to 1.98 Ga. The BHT consists of felsic to intermediate metaplutonics dated 2.0 to 2.40 Ga and is older than the TMZ. The TMZ is characterized by a highly corrugated internal fabric, comprised of moderate relief, north to northwest trending sinuous magnetic anomalies. These crystalline terranes and the WCSB which overlies them have undergone periodic compressive deformation from Proterozoic into Tertiary time (O'Connell et al., 1990; Dufresne et al., 1996).
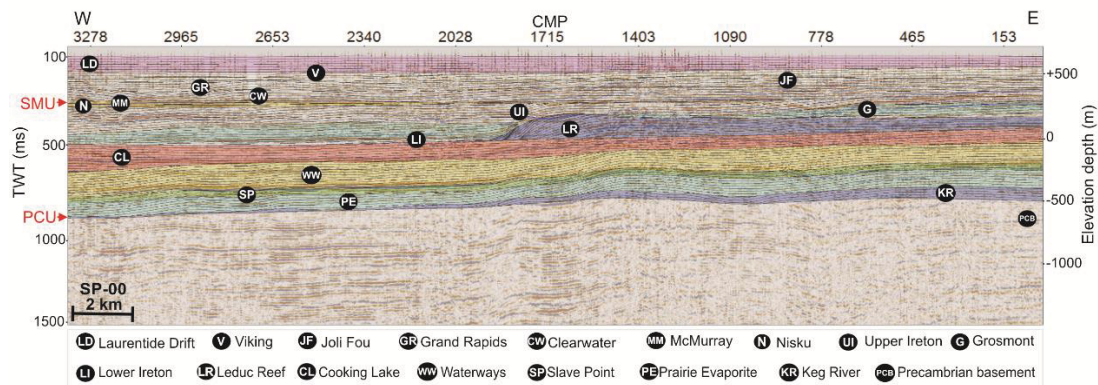
Figure 4.3. East-west trending regional interpreted seismic profile (SP-00) with highlighted regional unconformities (PCU and SMU) and sedimentary formations in the study area. Depth is presented in two forms, two-way traveltime (TWT) and elevation depth. The common midpoint (CMP) numbers are illustrated along the seismic profile.

Rocks of the sedimentary basin generally have low magnetic susceptibilities relative to the metamorphosed BHT and TMZ rocks lying beneath them. Consequently, almost all of the magnetic anomaly signatures arise from the underlying craton with the sediments essentially being magnetically transparent. This has long been exploited by researchers as noted above to map

the differing domains within the craton. As will be demonstrated, however, the magnetic anomalies found here must reach close to the surface and cannot be explained by features within the deeper craton.

4.2.1. Known igneous locales in Alberta

Little was known about igneous intrusions within the Western Canada Sedimentary Basin until the discovery late in the last century of diamondiferous kimberlite pipes nearby in the Northwest Territories. These discoveries spurred the exploration for new deposits across large regions (e.g., Dufresne et al, 1996). Much of this exploration was carried out using HRAM and remains proprietary. A number of different igneous features have since been found.

The Northern Alberta Kimberlite Province (NAKP) encompasses the majority of Northern Alberta and includes the Birch Mountains field (total number of eight kimberlite pipes), Buffalo Head Hills field (total number of 41 kimberlite pipes) and the Mountain Lake kimberlite and ultramafic intrusion field (total number of two kimberlite pipes) (Eccles et al., 2003, 2008) (**Figure 4.1b**). These serpentine to carbonate-bearing kimberlite and related alkaline bodies were discovered during the last 20 years and estimated to be emplaced during a 28 million-year period spanning the Late Cretaceous to Paleocene (~88-60 Ma) (Skelton et al., 2003; Eccles et al., 2003; Boyer, 2005; Eccles, 2011). According to Eccles et al. (2003), the Birch Mountain kimberlites are highly carbonized and are geochemically slightly different from the Buffalo Head Hills which seem to be more similar to primitive kimberlites from the Northwest Territories. Geochemical analysis of samples from these kimberlites identifies the Birch Mountain and Buffalo Head Hills kimberlites as nonmicaceous (more evolved nature) and micaceous kimberlite (primitive nature), respectively. Leckie

et al., (1997) suggest an alkaline, ultrabasic volcanic origin for the Mountain Lake kimberlites that is more similar to Sweet Grass Hills dykes composition (Kjarsgaard, 1994).

The Sweet Grass Hills dykes near Milk River in Southern Alberta (**Figure 4.1b**) (Ross et al., 1997; Leblanc and Morris, 1999; Buhlmann et al., 2000; Rukhlov and Pawlowicz, 2012) were discovered in HRAM surveys in the early 1990's (see **Figure 4.4a** for survey area). **Figure 4.4c** is an image of the first order vertical derivative showing the aeromagnetic anomaly related to these dykes. Although the existence of dykes in the vicinity of the Sweet Grass Hills on the Alberta-Montana border had long been known (Dawson, 1884), there was a great deal of skepticism in the interpretation of these magnetic anomalies as igneous dykes until they were traced to limited surface exposures in the Milk River Ridge. These dykes represent an eastern and northern continuation of the alkaline magmatism and Eocene extension that characterizes the Southeastern Canadian Cordillera and the Montana Alkalic Province (Ross et al., 1997).

Best et al., (1998) interpret a series of similar magnetic features in the Athabasca region, immediately northeast of the current study area (**Figure 4.4a**), to be caused by faulting of the basement and overlying sediments (**Figure 4.4b**). Given that now numerous igneous features have been discovered in Northern Alberta, it would be useful to re-examine their data to investigate if these anomalies can be interpreted otherwise.
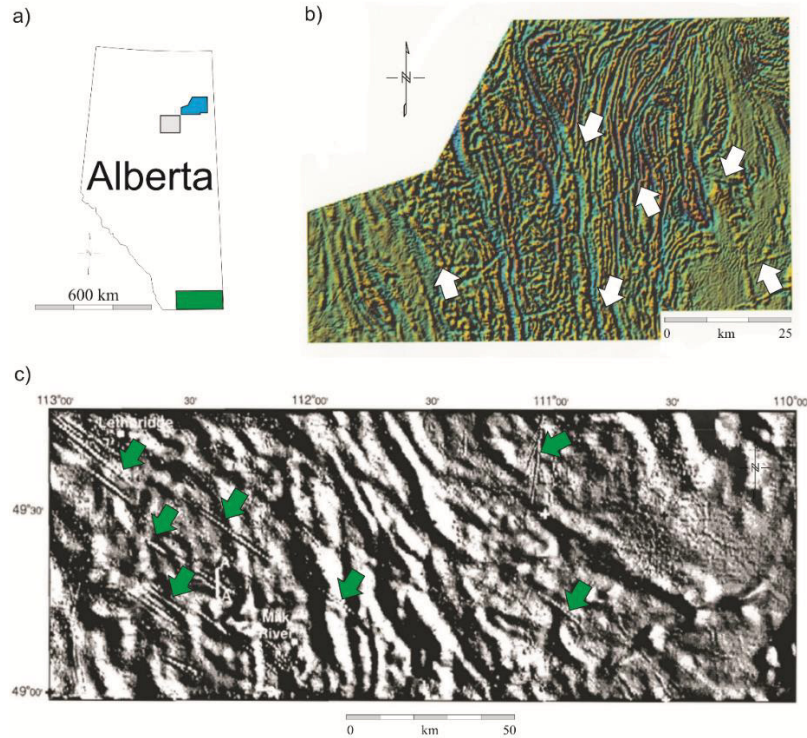
Figure 4.4. (a) The location of aeromagnetic surveys of the Sweet Grass Hills and the Athabasca faults studies in respect to our study area (gray box) are shown in green and blue, respectively. (b) Second vertical derivative with northwest shading of aeromagnetic survey from the Athabasca study by Best et al. (1998). Interpreted faults are highlighted with white arrows (modified after Best et al., 1998). (c) First vertical derivative with northeast shading of the aeromagnetic survey from the Sweet Grass Hills study by Ross et al. (1997). Interpreted faults are highlighted with green arrows (modified after Ross et al., 1997).

4.3. HRAM data processing

The HRAM grid originally comprises of two diurnal corrected proprietary airborne surveys (surveys A and B) with different line spacing (**Table 4.1**). The Geosoft Oasis Montaj software package is used for mapping and further processing of this data. These two surveys are re-elevated and interpolated using Minimum Curvature routine (Briggs, 1974) to a 250 m square grid independently. Then, the re-elevated grids are knitted together and re-gridded again with grid

spacing of 150 m, approximately one-eighth of the minimum line spacing of the surveys (**Figure 4.5a**). Using the elevations, inclinations, declinations, and coordinates of every sampling location, the International Geomagnetic Reference Field (IGRF) values are calculated and subtracted from the total magnetic field (i.e., total magnetic intensity) measurements.

Table 4.1. Specification of two HRAM surveys used in the study.

Survey	Acquisition date	Acquisition Altitude (m)	Total line (km)	Tie line spacing (m)	Traverse line spacing (m)	Total area (km²)
A	1998	120	49071	2000 E/W	400 N/S	16116
B	1998	100	30863	1250 E/W	250 N/S	6392

The data are then reduced to pole using a filter in the Fourier domain (**Figure 4.5b**). This filter migrates the observed field from the observed magnetic inclination and declination, to what the field would look like at the magnetic pole. The transfer function of reduction to the magnetic pole can be expressed in the form of

$$L(f) = \frac{1}{[Nn - Mm + j\, sgn(f)(Nm + Mn)]} \tag{1}$$

where f, is the spatial frequency, $sgn\,(f)$ is the sign of f, j is the imaginary unit. M, N, m and n are the direction cosines of the magnetization and of the earth's magnetic field, respectively (Blakely and Cox, 1972). The direction cosines can be expressed by the inclination a and declination b of the magnetization, and by the inclination I and declination D of the earth's magnetic field

$$M = \cos a \cos(A - b), \qquad N = \sin a,$$
$$m = \cos a \cos(A - D), \qquad n = \sin I \tag{2}$$

where *A* is the azimuth of the profile measured clockwise from geographic north.
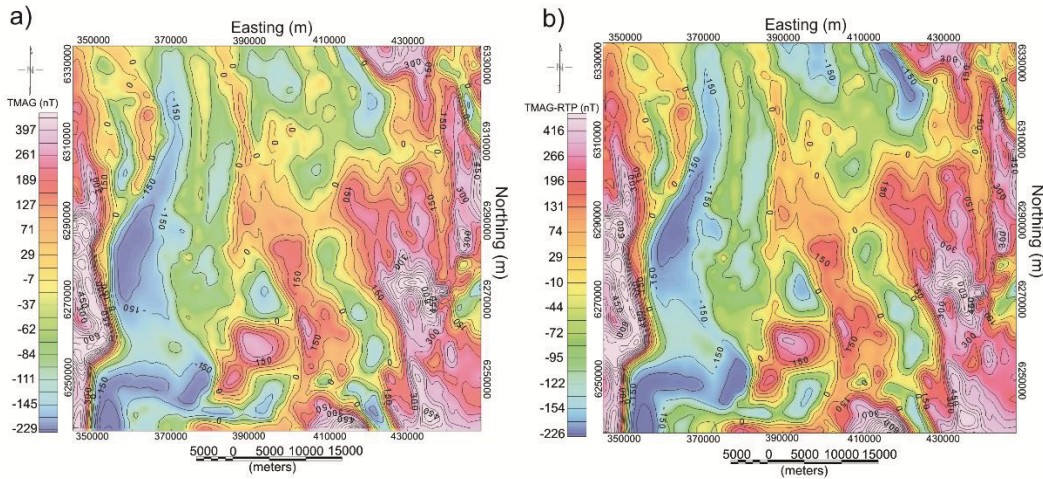
Figure 4.5. (a) Total magnetic field intensity map (TMAG), High amplitudes are colored in pink and lows in blue. The contour interval is 50 nT and is labeled every 150 nT, (b) reduced to pole total magnetic intensity map (TMAG-RTP).

The reduced to pole magnetic data, hereafter referred to as TMAG-RTP, shows the magnetic anomalies independent of the magnetic inclination of the source bodies and it is subsequently used as the base within which smaller wavelength features are further enhanced by band-pass and derivative filtering providing the data against which forward models are calculated.

The goal of band-pass filtering is to differentiate the shallow magnetic anomalies from the deeper long wavelength features. The Butterworth band-pass (BWBP) filter is among the most beneficial filters used for HRAM image processing. This filter allows passing the desired mid wavenumber range with a smooth cutoff. If k, k_0 and n is the wavenumber, central wavenumber of the filter, and degree of the Butterworth filter function, respectively, the filter is simply defined as

$$L(k) = \frac{1}{\left[1 + \left(\frac{k}{k_0}\right)^n\right]}$$
(3)

In order to determine the BWBP wavelength cutoff values, the power spectrum analysis (Spector and Grant, 1970) is used. This technique is primarily used for predicting the depth of the magnetized bodies from the relationship between the logarithmic power spectrum and frequency. The Spector and Grant (1970) equation is

$$|F(k)|^2 = 4\pi^2 C_m^2 |\theta_m|^2 |\theta_f|^2 M_0^2 e^{-2|k|z_t}(1 - e^{-|k|(z_b - z_t)})^2 S^2(a, b)$$
(4)

where F is the Fourier power spectrum, k is wavenumber in cycles km^{-1} or 2π km^{-1}, C_m is a constant related to units, θ_m is a factor related to magnetization direction, θ_f is a factor related to magnetic field direction, M_0 is magnetization, Z_t and Z_b are the depths to the top and the bottom of the ensemble of magnetic sources, and $S^2(a, b)$ is the factor related to horizontal dimensions of sources.

Figure 4.6a shows the power spectrum of the TMAG-RTP grid plotted versus wavenumber and wavelength (note that the wavenumber used in calculation of the slope is multiplied in 2π). The slope of the best linear fit of each segment (shown in different colors) corresponds to the estimated depth to the top of an ensemble of magnetic sources (Ravat et al., 2007; Rabeh et al., 2008). The lower estimated depth is related to higher wavenumbers and shorter wavelength as it is expected. Based on the wavelength components with frequency bands ranging from 0.4 to 1.4 cycle km^{-1}, and from 1.4 to 2.7 cycle km^{-1}, the wavelength band-pass of 1-3 km and 3-6 km are estimated and used through the BWBP technique to generate magnetic residual maps (**Figure 4.6b** and **4.7c**, respectively). Typically, the depth of resolution is approximately half of the

wavelength; therefore, the 1-3 km BWBP filtered map resolves mostly the anomalies of the sedimentary basin (0.5 km) to the topmost portion of the crystalline basement (1.5km) and the 3-6 km illustrates the regional features within the basement (1.5-3 km). Based on these maps the short wavelength magnetic anomalies appear to be within the sedimentary basin (**Figure 4.6b**) rather than crystalline basement (**Figure 4.6c**).
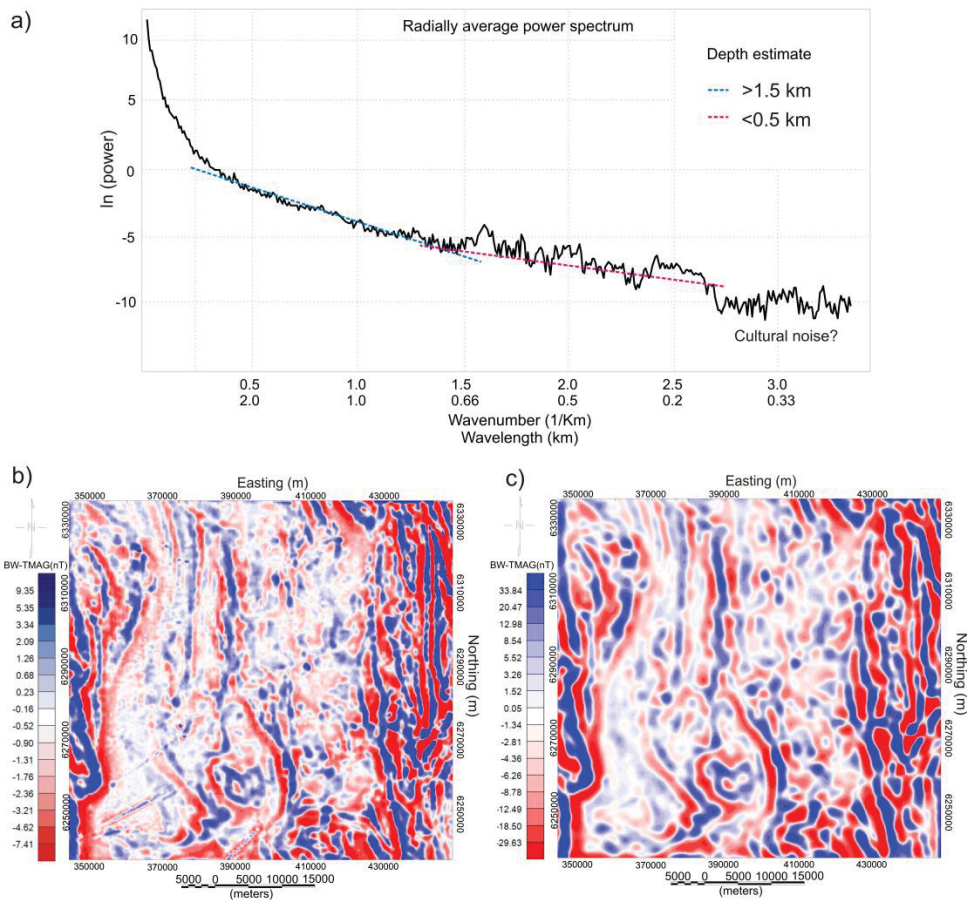
Figure 4.6. (a) The radially averaged power spectrum of the TMAG-RTP plotted versus wavenumber (km^{-1}) and wavelength (km). The best linear fits on each segment are shown in dashed line with different colors. The depth of each assemblage is calculated from the slope of each segment. (b) Butterworth bandpass filtered TMAG-RTP for wavelength of 1-3 km for shallow depth (within sedimentary basin), (c) Butterworth bandpass filtered TMAG-RTP for wavelength of 3-6 km for medium depth (within Precambrian basement).

Vertical and tilt derivative maps of the magnetic data are effective tools for focusing on shallow (short wavelength) magnetic features (Miller and Singh, 1994; Best et al., 1998; Verduzco et al., 2004). The first derivatives of the TMAG-RTP data are calculated using the 3D Hilbert transform approach proposed by Nabighian (1984). He defines the Hilbert transform as a composition of two part acting on the x component and one part on the y component and therefore the magnetic vertical and horizontal derivatives as the Hilbert transforms of each other. The generalized relationship can be presented as

$$\mathcal{H}(M) = \frac{1}{2\pi} \int_{-\infty}^{\infty} \int_{-\infty}^{\infty} M(\xi, \eta) \nabla_h \left(\frac{1}{R}\right) d\xi d\eta \tag{5}$$

where (ξ, η) is the integration point in the x, y plane, ∇_h is the horizontal gradient at the integration point, and R is the integration point residual. The detail math work of this transformation is beyond the scope of this paper and we encourage readers to refer to Nabighian's paper for more information (1984).

The first order vertical derivative (VDRV) of the magnetic field TMAG-RTP is calculated using the z component of the wavenumber and can be shown as follows

$$VDRV = \left(\frac{\partial T}{\partial z}\right) \tag{6}$$

The tilt derivative (TDRV) or tilt angle is the ratio of the vertical and total horizontal (THDRV) derivatives (Miller and Singh, 1994; Verduzco, 2004), given by

$$TDRV = \tan^{-1}\left(\frac{VDRV}{THDRV}\right) \tag{7}$$

where the THDRV is computed using the first derivatives of the magnetic field in the x and y directions, given by

$$THDRV = \sqrt{\left(\frac{\partial T}{\partial x}\right)^2 + \left(\frac{\partial T}{\partial y}\right)^2} \tag{8}$$

The tilt angle is positive over the source and passes through zero when over or near the edge, where the vertical derivative is zero. It is restricted to values between $+\pi/2$ and $-\pi/2$ regardless of the amplitudes of vertical and total horizontal gradients which makes this relationship function like an Automatic Gain Control (AGC) filter and tends to equalize the amplitude output of TMAG anomalies across the grid. Vertical and tilt gradients enhance imaging of the short wavelength anomalies (**Figure 4.7a** and **4.7b**).
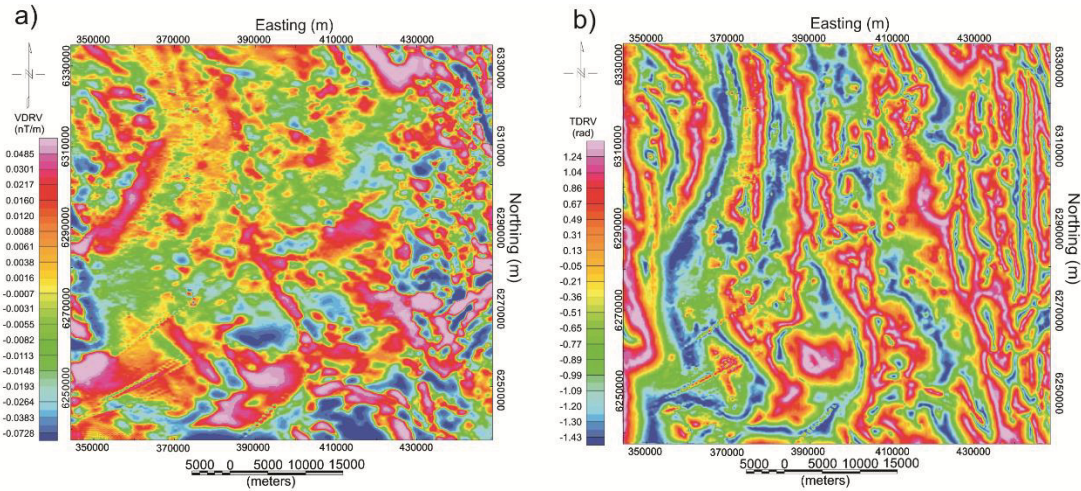
Figure 4.7. (a) Vertical derivative (VDRV), and (b) Tilt derivative (TDRV) of the TMAG-RTP.

The enhanced HRAM images clearly reveal the presence of linear short wavelength anomalies (within the sedimentary succession) that are clearly distinct from longer wavelength magnetic anomalies associated with the metamorphic basement. These anomalies, radiating from the southwest corner of

the maps, comprise a series of southwest-northeast striking linear features that attain lengths up to 15 km (**Figure 4.8a**). The red solid lines in **Figure 4.8b** highlight the location of the magnetic anomalies.

It is important to note that the study area has been under exploration and exploitation by oil industry for hydrocarbon production in the past decades and as such steel infrastructure could be misinterpreted. The location of the wellheads and the pipelines acquired from infrastructure databases are shown in **Figure 4.8a**, however, no coincidence between the HRAM anomalies and cultural structures is apparent. Follow up investigations using recent satellite imagery, also show no anthropomorphic surface disruption along the locus of the magnetic anomalies. In this regard it is useful to mention that disruption from seismic cut lines, for example, obtained in the early 1980's are still readily visible in such imagery; one would similarly expect more intrusive infrastructure such as a buried pipelines to also be readily visible. In the following sections of the paper we will use HRAM detrending and forward magnetic modeling as a tool to verify the nature of the causative bodies for these anomalies.

4.4. Detrending HRAM Data

The filtered maps are useful in demonstrating the existence of the linear anomalies, but the filtered data cannot easily be applied to more quantitative interpretations necessary to constrain the geological structure. Consequently, the magnetic lineaments are isolated by subtracting a low-order polynomial trend surface from TMAG-RTP grid. The 2D profile of this polynomial trend surface is presented in dashed line along with the TMAG and magnetic residual 2D profiles in **Figure 4.9a** and **4.10a**. After detrending, linear anomalies range between 5 to 20 nT in amplitude on the TMAG residual curves.
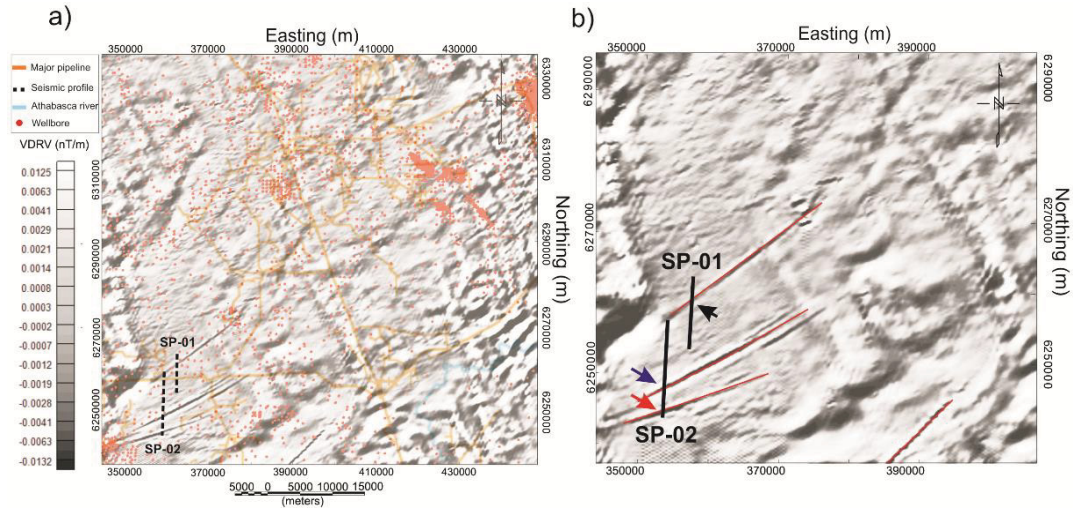
Figure 4.8. Shaded relief first vertical derivative of TMAG-RTP with illumination from the northwest, (a) Seismic profiles over the HRAM anomalies, wellheads, and major pipelines are shown by black dashed lines, red dots, and orange lines, respectively. (b) Magnified image of the magnetic anomalies highlighted by red solid lines. The intersection of the anomalies and seismic 2D profiles (SP-01 and SP-02) is pointed out by colored arrows.

To shed some light on the geometry of the anomaly within the sedimentary basin, the magnetic profiles shown in **Figure 4.9a** and **4.10a** are taken along the seismic lines of SP-01 and SP-02. Out of a large 2D reflection seismic data set (about 800 km) available to us through donations and purchase via brokerage databases (**Figure 4.2**), these two seismic profiles cross the HRAM anomalies (**Figure 4.8b**).

Some of older seismic profiles are reprocessed to enhance the quality of final stacks (Ardakani et al., 2014). The seismic profiles are eventually integrated with available formation tops and after depth conversion, are used for imaging the surface of PCU and sedimentary formations (**Figure 4.3**). We highlighted the intersections of the seismic profiles and the lineaments by colored arrows in **Figure 4.8b**, **4.9**, and **4.10**.

114
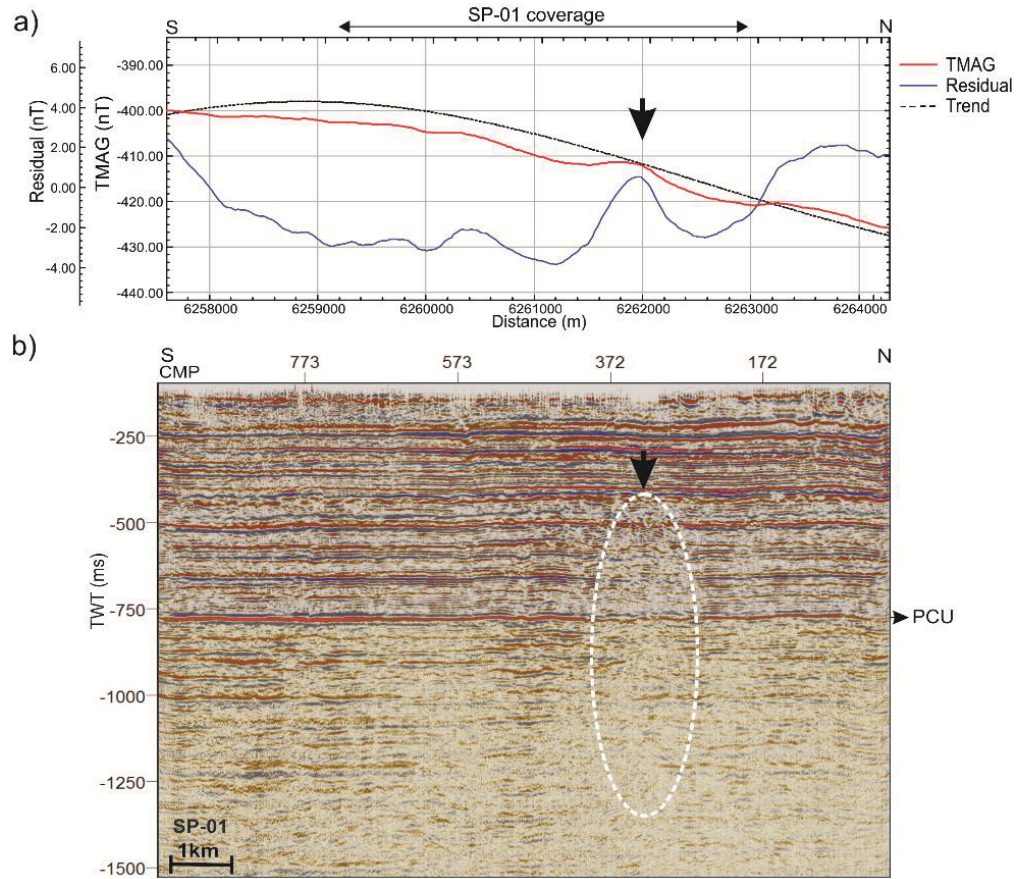
Figure 4.9. The seismic profile SP-01 and its corresponding HRAM profile (a) TMAG-RTP, residual magnetic, and removed polynomial trend profile is illustrated by red, blue and black curves, respectively. (b) Seismic profile SP-01 in two-way traveltime (TWT). The seismic disturbed zones corresponding to the magnetic anomaly are circled in white. The PCU is highlighted.

The zones highlighted in white circles on each of the seismic profiles in **Figure 4.9b** and **4.10b**) are pointed out by the same colored arrows in **Figure 4.9a** and **4.10a** that indicate where the seismic profiles cross the HRAM anomalies. In each of these highlighted vertical zones on the seismic reflection a disruption of the continuity of reflectors, subtle diffractions extending to depth, and interference patterns can be identified. The seismic reflection demonstrate

115

that the HRAM anomalies have a common upper stratigraphic limit within the Early Cretaceous sediments.
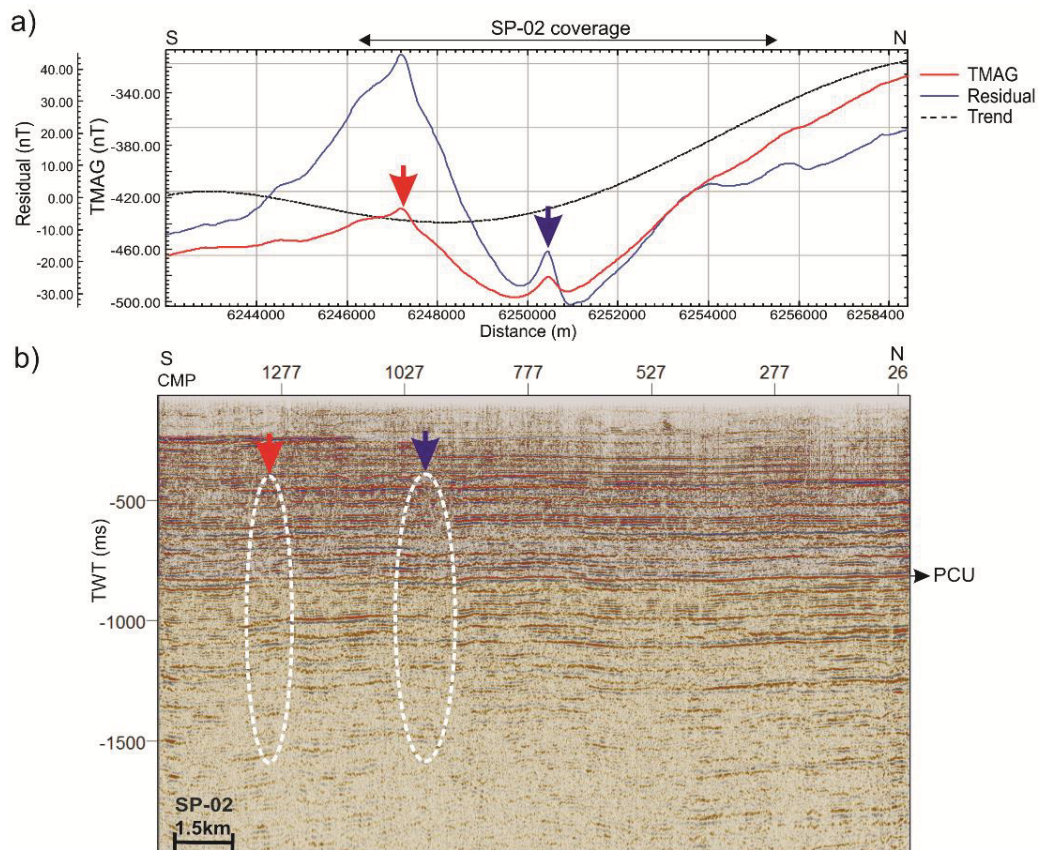
Figure 4.10. The seismic profile SP-02 and its corresponding HRAM profile (a) TMAG-RTP, residual magnetic, and removed polynomial trend profile is illustrated by red, blue and black curves, respectively. (b) Seismic profile SP-02 in two-way traveltime (TWT). The seismic disturbed zones corresponding to the magnetic anomaly are circled in white. The PCU is highlighted.

4.5. Forward Magnetic Modeling

The linear nature of the magnetic anomalies is unusual and may suggest on one hand that they arise from human constructions, such as steel borehole casings, pipelines, or power lines. On the other hand, the lineaments are also suggestive of natural faults or igneous dykes. In order to gain a better understanding of what structures actually produce the magnetic anomalies, the

116

signatures of a vertical steel borehole casing, a horizontal steel pipeline, a fault vertically offsetting two magnetic layers, and a vertical dyke are modeled (**Figure 4.11** and **4.12**). Note that in all equations used for modeling it is assumed that the body is magnetized solely by induction caused by and in the direction of earth's magnetic field. The *x*-axis in **Figure 4.11** and **4.12** show the locations of the points at which the magnetic anomalies are calculated and its direction is a principal profile. The principal profile for 2D bodies (dyke and fault) is the direction perpendicular to the strike of the magnetic anomalies (~northeast-southwest) and positive in the northern geomagnetic half-plane of the unprimed system. The strike is measured positive clockwise in the same way. The average inclination (I_0) of 77°, declination *(D)* of 15°, and total geomagnetic field (T_0) of 58000 nT are used in the modeling process when required. The schematic shapes for different causative bodies in **Figure 4.11c**, **4.11d**, **4.12c**, and **4.12d** are solely for the purpose of illustration of each modeling scenario and scales are not proportional to variable values used in the modeling process.

4.5.1. Cultural causative bodies

The vertical steel casing is modeled by a single magnetic dipole (**Figure 4.11a** and **4.11c**). Assuming the magnetic dipole is magnetized by induction in the direction of earth's field, the magnetic response along the dipole can be obtained from (Telford, 1990)

$$\Delta T(x) = \frac{2pl}{r^5}\{(3\cos^2 I_0 - 1)\,x^2 - 6xz_m\sin I_0\cos I_0 + (3\sin^2 I_0 - 1)z_m{}^2\} \qquad (9)$$

where *p, l,* and *r* is strength of each pole, half distance between poles, and distance from the middle point of dipole to the surface points at which the magnetic anomaly is calculated, respectively. Since this model is a representative

of a vertical borehole casing and most of the boreholes in the area barely reach beyond Cretaceous formations, the dipole source is assumed to be extended from the surface to 200 m, therefore z_m which is the depth of the middle point of the dipole is 100 m. p and l are set to be 5 nT and 100 m, respectively. As it was mentioned before x represents the location of the points at which the magnetic anomaly is calculated.

A horizontal cylinder simulates a pipeline (**Figure 4.12b** and **4.12d**). The pipeline is buried at 10 m and, is given an exaggerated diameter of 5 m. The model presented here is adopted from Gay (1965) and Rao et al. (1986). The horizontal cylinder is extended infinitely along the observed anomaly (y-axis) and assumed to be made of steel that has the susceptibility of 10 (SI unit) (Breiner, 1999). The normal section of the cylinder is in the x-z plane. The origin of the coordinate system is on the surface vertically above the center of the cylinder and z_m is the depth to the center of the cylinder (10 m). The expression for the magnetic anomaly on the principal profile of the magnetized cylinder is given by

$$\Delta T(x) = C \left[\frac{(z_m{}^2 - x^2) \cos \theta + 2xz_m \sin \theta}{(z_m{}^2 + x^2)^2} \right] \tag{10}$$

where C and θ are the amplitude coefficient and the index parameter, respectively. For the total magnetic anomaly due to long horizontal cylinder, C and θ are given by

$$C = \frac{2KT_0{}'S \sin I_0{}'}{\sin I_0{}'} \tag{11}$$

$$\theta = 2I_0 - 180° \tag{12}$$

where K is the magnetic susceptibility contrast, S is the cross-sectional area and T_0' and I_0' are the values of effective total intensity and inclination, and they are related to true total intensity, T_0 and real inclination, I_0 by

$$T_0' = \frac{T_0 \sin I_0}{\sin I_0'} \tag{13}$$

$$I_0' = \tan^{-1}\left(\frac{\tan I_0}{\sin \alpha}\right) \tag{14}$$

where α is the strike of the cylinder measured clockwise from magnetic north.
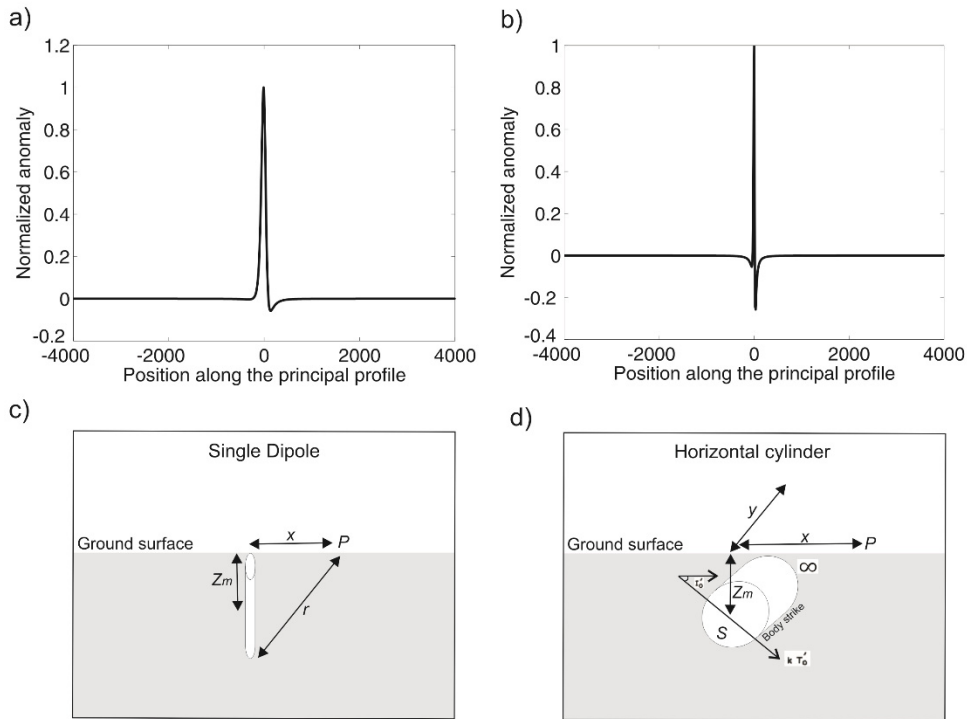
Figure 4.11. Modeled magnetic signature of (a) borehole casing simulated by a single dipole, (b) pipeline simulated by a horizontal cylinder. The schematic geometry of (c) the single dipole and (d) the horizontal cylinder presented as the causative bodies.

The magnetic responses caused by these two types of man-made structures have significantly higher amplitudes that exceed the observed detrended anomalies by tens of nT. Their shapes, too, are much narrower (i.e.,

119

composed of shorter wavelengths). As a result, these simple models further confirm that anthropogenic structures cannot explain the observed anomalies and that they must arise from natural geological structures.

4.5.2. Geologic causative bodies

The modeled geologic causative bodies consist of simulated signature of a vertical fault and a dyke. The vertical fault is simulated by two semi-infinite horizontal 2D sheets with 50 m offset (**Figure 4.12a** and **4.12c**). The strike of the fault plane assumed to be identical to the strike of the observed lineaments on the HRAM data. The semi-infinite sheets are considered here as it is crucial to traverse a considerable distance before the magnetic background is reached and often it cannot be done because there are likely to be other magnetic features in the vicinity. The vertical fault is modeled by (Telford, 1990)

$$\Delta T(x) = -2KtT_0\left[\left(\frac{1}{r_1{}^2}\right)\{Z_s \sin 2l \sin \beta - (X + Z_s \cos \varepsilon)(\cos^2 l \sin^2 \beta - \sin^2 l)\}\right.$$

$$\left. -\left(\frac{1}{r_2{}^2}\right)\{Z_d \sin 2l \sin \beta - (X + Z_d \cos \varepsilon)(\cos^2 l \sin^2 \beta - \sin^2 l)\}\right] \ (15)$$

where $K, t,$ and T_0 are magnetic susceptibility contrast, thickness of the sheets, and total geomagnetic intensity in the area, respectively, and set to be 10 (SI unit), 25 m, and 58000 nT in the modeling process . Z_d, and Z_s represent the depth to the deeper and shallower sheet (i.e., the bottom and top of the fault plane) and are 1450 and 1400 m. The reason for choosing this depth is first that no known faults with such displacements are known in the sedimentary column in this area and second that if a fault existed it must lie within the Precambrian basement rock as it has higher magnetic susceptibility. The ε and β are the angles related to the dip and strike of the fault plane. Since the model is for a vertical

fault, ε is assumed to be 90 degrees and β is estimated to be in line with the magnetic anomaly. The r_1 and r_2 are the distance from the tip of the sheets at the fault plane to the surface where the magnetic anomaly is calculated (**Figure 4.12c**). This modeled fault is a highly simplified scenario, as one would not expect to have such a simple geometry in the top of PCU given the deformation within the metamorphic rocks in WCSB.

The dyke signature is modeled by a 2D vertical prism (**Figure 4.12b** and **4.12d**) based on the assumptions that the dyke consists of a flat, horizontal top with parallel sides, extends infinitely along strike and also along its downward direction, and is magnetized uniformly. In the same way as the fault was modeled, the y-axis is along the strike of the dyke and the x-axis is along the normal profile to the anomaly strike. The general expression for such a dyke at any point on the x-axis is given by (Ram Babu et al., 1986; Hood, 1964)

$$\Delta T(x) = C \left[\cos\theta \left\{ \tan^{-1}\left(\frac{X+B}{H}\right) - \tan^{-1}\left(\frac{X-B}{H}\right) \right\} \right.$$
$$\left. + \frac{1}{2}\sin\theta \log_e \frac{(X+B)^2 + H^2}{(X-B)^2 + H^2} \right] \tag{16}$$

C and θ have been defined in the horizontal cylinder modeling section. X, B, and H are the distance of the point of observation from the origin, half-thickness, and depth to the top of the dyke from the plane of observation. For the model presented in **Figure 4.12b,** the B and H are set to be 30 m and 250 m. The magnetic susceptibility of the dyke is considered to be 2.5 (SI unit). This value is an average of magnetic susceptibility from field and laboratory measurements of the Sweet Grass Hills dykes by Kjarsgaard (1994).

The modeled vertical fault response (**Figure 4.12a**) with strong positive and negative excursions does not resemble our observation of HRAM anomalies and we can exclude them from being faults. In contrast, the observed magnetic signatures look much similar to the modeled dyke in shape (**Figure 4.12b**).
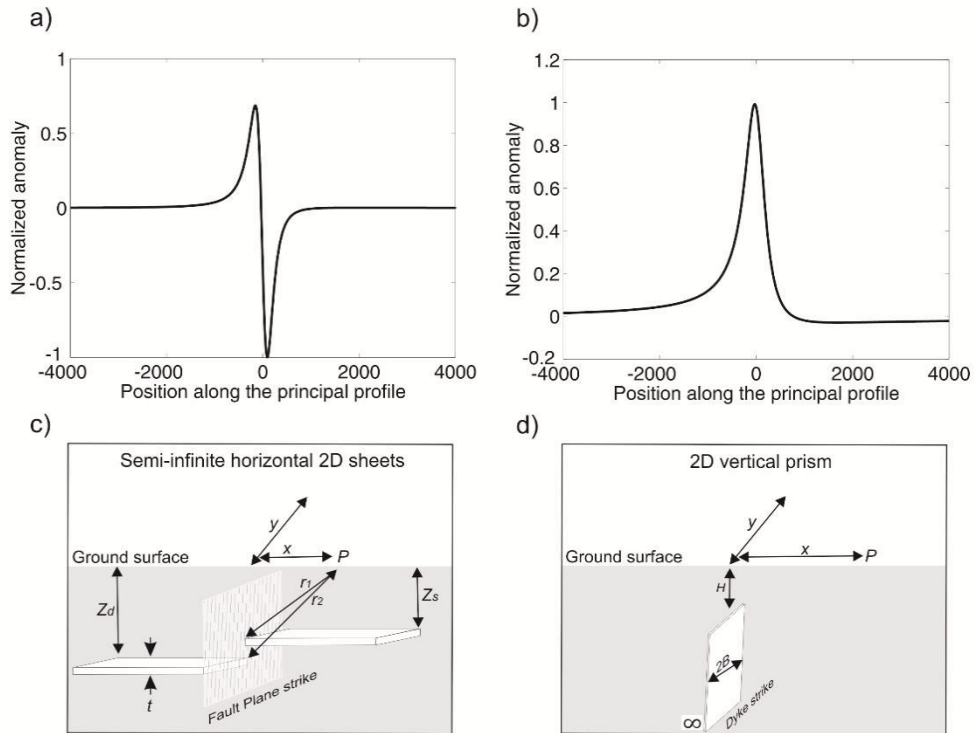
Figure 4.12. Modeled magnetic signature of (a) fault simulated by two semi-infinite horizontal sheets, (b) dyke simulated by a semi-infinite 2D vertical prism. The schematic geometry of (c) the two semi-infinite horizontal sheets and (d) the semi-infinite 2D vertical prism presented as the causative bodies.

To further clarify the resemblance of the computed and observed signatures and to determine the depth and thickness of the source, the observed residual anomaly and its vertical derivative (highlighted by the blue arrow in **Figure 4.10**) is compared with ensembles of modeled dykes in **Figure 4.13**. Note that the HRAM anomaly is appropriately picked in a principal profile to the strike of the lineament to account for the perpendicular crossing of the modeled dykes. The observed anomaly is illustrated as a blue dashed line and modeled

122

responses are shown in different colors which differ by half thickness and depth to the top of the modeled dyke. This comparison constrains the thickness and depth of the causative body to be more than 60 m and 200 m, respectively.
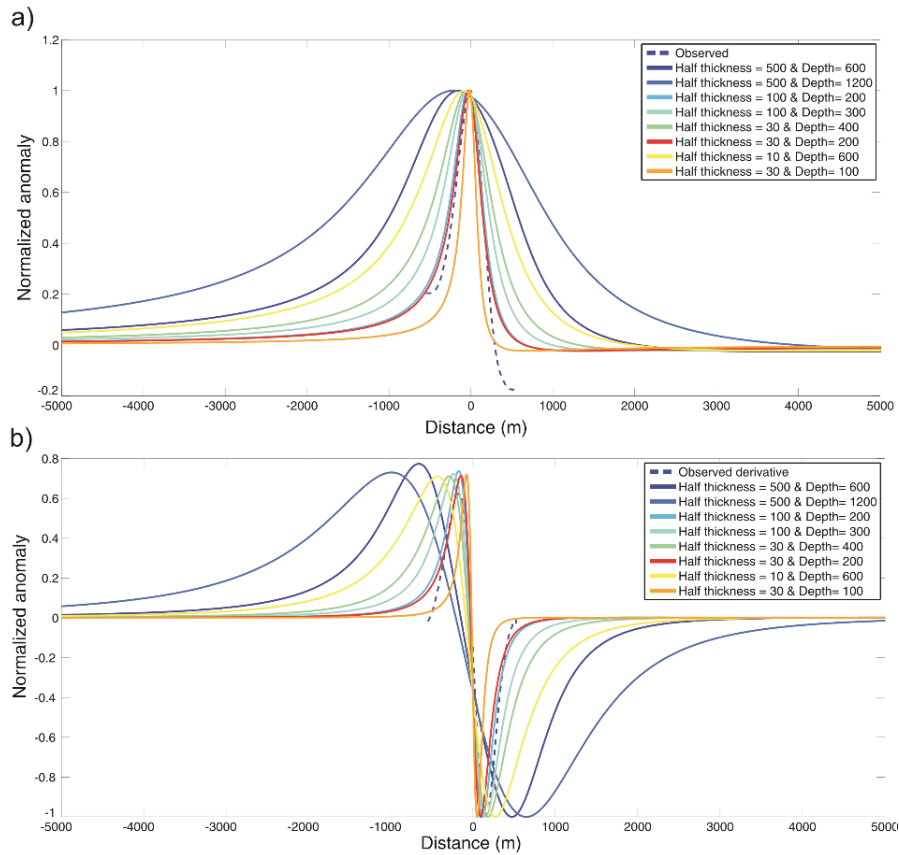
Figure 4.13. Comparison of (a) the observed residual anomaly and (b) its vertical derivative with modeled dyke responses and their vertical derivatives calculated with different source depth and half thickness. Note that anomaly curves are normalized.

4.6. Discussion

The comparison of the observed anomaly profiles with computed magnetic responses for different magnetic sources indicates the linear HRAM anomalies are generated by igneous dykes that intrude the sedimentary column. We refer to these features as the Buffalo Creek dyke field. Regrettably, there are no known outcrops that can be found to confirm this interpretation. It is also not

123

likely that any will be found as the entire area over the anomalies is blanketed with the glacial tills, preglacial sediments, and muskeg (sphagnum moss bogs) that conceal the underlying lithified Cretaceous bedrock. Definitive confirmation requires that core or cuttings be obtained from shallow drilling directly into one of these anomalies.

In magnetic anomaly maps the character of the Buffalo Creek dykes is similar to that of the Sweet Grass Hill dykes near Milk River (**Figure 4.4c**). The features observed to the northeast in the Athabasca magnetic survey described by Best et al. (1998), interpreted as faults could also benefit from a detailed forward modeling to test their hypothesis.

The coincident seismic profiles provide additional evidence to support our interpretation. Observing a disturbance of the lateral continuity of seismic reflectors, the presence of diffractions extending to depth in the section, interference patterns, and apparent pull-up and pull-down in the seismic images (**Figure 4.9b** and **4.10b**) confirm the likeliness of intrusive bodies as the source of the HRAM observations. Kellet et al. (2005) previously reported the same seismic characteristics for the Mountain Lake intrusion. When dykes propagate vertically upward through the sediment overburden, hot volatiles and gases would escape above the dyke tip (Wall et al., 2010). The escaped fluids may induce fractures, depression, and dissolution of the overlaid sedimentary formations. The dykes strike parallel to the modern southwest-northeast trending trajectories of the maximum horizontal stress (Bell and Grasby, 2012, Reiter et al., 2014) is in agreement with the preferential fluid flow theory. The fracture mechanics and fluid flow pathway studies suggest that opening faults and joints (i.e., Mode I or extensional fractures) are often parallel to the maximum *in situ*

horizontal stress direction as fracturing the rock in the direction of the least resistance (minimum horizontal stress) is much easier (Secor, 1965; Barton et al., 1995; Zoback, 2007). We believe further analysis of the reflection seismic such as processing the data with accurate tomographic velocity model over the zones of interest and employment of prestack depth migration (Ogunsuyi and Schmitt, 2010) would result in better imaging of these anomalies.

In terms of the location of the intrusive bodies' emplacement, the Buffalo Creek dykes are within the NAKP and the Birch Mountain pipes are the closest intrusions to them. The Birch Mountain pipes have ages between 70.3±1.6 to 77.6±0.8 Ma as determined by U-Pb perovsite and Rb-Sr phlogopite dating (Aravanis, 1999; Eccles et al., 2003). The presence of a common upper stratigraphic limit within the Early Cretaceous sediments on the seismic profiles suggests that the current dykes are probably older than the Birch Mountain intrusive bodies. That said, our interpretation of the Buffalo Creek intrusions emplacement is limited by the resolution of the available seismic profiles. In addition, the complex geology of the Upper Devonian and Early Cretaceous stratigraphic units adds to the difficulty of determination of the upper boundary of the dykes from the surrounding host rock. Based upon the magnetic signature modeling the top of the dykes is estimated to be at a depth of 200 m which means they intruded the Late Cretaceous stratigraphic layer and have identical emplacement age to the Birch Mountain kimberlite pipes. Since the Birch Mountain kimberlites are the most northern site that may be related to low-angle Farallon plate subduction (Currie and Beaumont, 2011) the Buffalo Creek dykes could have the same origin. Previous studies used the kimberlite corridor mechanism to relate Cretaceous kimberlites of the Western Interior of North America to Farallon plate subduction (McCandless, 1999; McCandless and

Tosdal, 2005). This mechanism invokes a relationship between kimberlite magmatism and lithospheric subduction, in which fluids released by prograde metamorphism of the subducting plate trigger partial melting of the overlying material to form kimberlite magma.

4.7. Conclusions

The integrated processing and interpretation of the HRAM and seismic reflection data reveal the existence of structural lineaments within the WCSB in the southwest of the Athabasca region. The anomaly signatures of these features on the aeromagnetic data appear to range between 5 to 20 nT in amplitude. Magnetic forward modeling of cultural and geologic causative bodies was conducted to further clarify the source of these anomalies. The modeling indicates that these lineaments are possibly related to the buried dykes/kimberlite pipes deeper than 200 m and thicker than 60 m. We refer to these features as the Buffalo Creek dyke field. Based upon the magnetic response and linearity of the Buffalo Creek dykes, they could be compared with the Sweet Grass Hills alkaline ultrabasic dykes. The emplacement age and origin of the Buffalo Creek dyke field is estimated to be correlative with the Birch Mountain kimberlite pipes in the NAKP, which is between 70.3±1.6 to 77.6±0.8 Ma determined by U-Pb perovsite and Rb-Sr phlogopite dating. This association, however, is based on the fact that the Buffalo Creek dykes are only 100 km away; obviously no definitive conclusion with regards to the age or composition of these dykes can be made without direct sampling. These Cretaceous dykes may be related to the Farallon plate subduction under the west coast of the North American Plate.

References

Ardakani, E. P. and D. R. Schmitt, 2016, Geothermal energy potential of sedimentary formations in the Athabasca region, Northeast Alberta, Canada: Interpretation, accepted for publication.

Ardakani, E. P., D. R. Schmitt, and T. D. Bown, 2014, Detailed topography of the Devonian Grosmont Formation surface from legacy high-resolution seismic profiles, Northeast Alberta: Geophysics, 79, B135-B149, doi: 10.1190/geo2013-0268.1.

Aravanis, T., 1999, Legend property assessment report, Birch Mountain area, Alberta: Alberta Energy and Utilities Board, Report 20000003.

Barton, C., M. D. Zoback, and D. Moos, 1995, Fluid-flow along potentially active faults in crystalline rock: Geology, 23(8), 683-686, doi: 10.1130/0091-7613(1995)023<0683: FFAPAF>2.3.Co;2.

Beaney, C. L., and J. Shaw, 2000, The subglacial geomorphology of southeast Alberta; evidence for subglacial meltwater erosion: Canadian Journal of Earth Sciences, 37, 51-61, doi: 10.1139/cjes-37-1-51.

Bell, J. S. and S. E. Grasby, 2012, The stress regime of the Western Canada Sedimentary Basin: Geofluids, 12, 150-165, doi: 10.1111/j.1468-8123.2011.00349.x.

Best, M. E., H. J. Abercrombie, and J. W. Peirce, 1998, Interpreted faulting patterns in Northeast Alberta using high resolution aeromagnetic data: Canadian Journal of Exploration Geophysics, 34, 49-57.

Blakely, R. J. and A. Cox, 1972, Identification of short polarity events by transforming marine magnetic profiles to the pole: Journal of Geophysical Research, 77, 4339-4349.

Boyer, L. P., 2005, Kimberlite volcanic facies and eruption in the Buffalo Head Hills, Alberta, Canada, M.Sc. thesis: University of British Columbia.

Breiner, S., 1999, Applications manual for portable magnetometers: Geometrics, San Jose, California.

Briggs, I. C., 1974, Machine contouring using Minimum Curvature: Geophysics, 39 (1), 39-48, doi: 10.1190/1.1440410.

Buhlmann, A. L., P. Cavell, R. A. Burwash, R. A. Creaser, and R. W. Luth, 2000, Minette bodies and cognate mica-clinopyroxenite xenoliths from the Milk River area, southern Alberta: records of a complex history of the northernmost part of the Archean Wyoming craton: Canadian Journal of Earth Sciences, 37, 1629–1650, doi: 10.1139/e00-058.

Burwash, R. A., T. Chacko, K. Muehlenbachs, and Y. Bouzidi, 2000, Oxygen isotope systematics of the Precambrian basement of Alberta, implications for Paleoproterozoic and Phanerozoic tectonics in Northwestern Alberta: Canadian Journal of Earth Sciences, 37, 1611-1628, doi: 10.1139/e00-090.

Carlson, S. M., W. D. Hillier, C. T. Hood, R. P. Pryde, and D. N. Skelton, 1999, The Buffalo Hills kimberlites; a newly-discovered diamondiferous kimberlite province in North-Central Alberta, Canada: Proceeding of the 7th International Kimberlite Conference, 1, 109-116.

Currie, C. A., and C. Beaumont, 2011, Are diamond-bearing Cretaceous kimberlites related to low-angle subduction beneath western North America?: Earth and Planetary Science Letters, 303, 59-70, doi:10.1016/j.epsl.2010.12.036.

Dawson, G. M., 1884, Report of progress 1882-83-84, part c: Geological Survey of Canada, 16-17 and 45-47.

Dufresne, M. B., R. A. Olson, D. R. Schmitt, B. McKinstry, D. R. Eccles, M. M. Fenton, J. G. Pawlowicz, W. A. D. Edwards, and R. J. H. Richardson, 1994, The Diamond Potential of Alberta: A regional synthesis of the structural and stratigraphic setting, and other preliminary indications of diamond potential: Alberta Research Council, open file report 1994-10.

Dufresne, M. B., D. R. Eccles, B. McKinstry, D. R. Schmitt, M. M. Fenton, J. G. Pawlowicz, and W. A. D. Edwards, 1996, The diamond potential of Alberta: Alberta Geological Survey Bulletin, 63.

Eccles, D. R., L. M. Heaman, and A. R. Sweet, 2008, Kimberlite-sourced bentonite, its paleoenvironment and implications for the Late Cretaceous K14 kimberlite cluster, Northern Alberta: Canadian Journal of Earth Sciences, 45, 531-547, doi: 10.1139/E07-065.

Eccles, D. R., L. M. Heaman, R. W. Luth, and R. A. Creaser, 2003, Petrogenesis of the Late Cretaceous Northern Alberta kimberlite province: Proceeding of the 8th International Kimberlite Conference.

Eccles, D. R., L. M. Heaman, R. W. Luth, and R. A. Creaser, 2004, Petrogenesis of the Late Cretaceous Northern Alberta kimberlite province: Lithos, 76, 435-459, doi: 10.1016/j.lithos.2004.03.046.

Eccles, D. R., 2011, Northern Alberta Kimberlite Province - The first 20 years: Energy Resources Conservations Board, ERCB/AGS Bulletin 65.

Gay, P. S., 1963, Standard curves for the interpretation of magnetic anomalies over long tabular bodies: Geophysics, 28 (2), 161-200, doi: 10.1190/1.1439164.

Heaman, L. M., B. A. Kjarsgaard, and R. A. Creaser, 2003, The timing of kimberlite magmatism in North America: implications for global kimberlite genesis and diamond exploration: Lithos, 71, 153-184 doi: 10.1016/j.lithos.2003.07.005.

Heaman, L. M., B. A. Kjarsgaard, and R. A. Creaser, 2004, The temporal evolution of North American kimberlites: Lithos, 76, 377-397.

Hoffman, P. F., 1989, Precambrian geology and tectonic history of North America, *in* A. Bally, and A. R. Palmer, eds., The geology of North America; an overview: Geological Society of America, 487-512.

Hood, P. J., 1964, The Koenigsberger ratio and the dipping dike equation: Geophysical Prospecting, 12, 440-456.

Jellicoe, B. C., P. Robertshaw, P. Williamson, and J. Murphy, 1998, Summary of exploration activities and results for the Fort à la Corne diamond project, Saskatchewan: Saskatchewan Geological Survey, Report 98-4, 144-157.

Kellett, R. L., G. J. Steensma, and R. M. Zahynacz, 2005, Geophysical signature of the Mountain Lake intrusion; a study to support future kimberlite exploration in Alberta: Alberta Geological Survey and Alberta Energy and Utilities Board, Special Report 064.

Kjarsgaard, B. A., 1994, Potassic magmatism in the Milk River area, Southern Alberta-petrology and economic potential: Geological Survey of Canada, Current Research 1994-B, 59-68.

Kjarsgaard, B. A., 1997, Diamonds in Alberta: studies of potential host rocks of deep-seated origin and applications of indicator mineral exploration techniques; *in* R. W. Macqueen, eds., Exploring for minerals in Alberta: Geological Survey of Canada, Bulletin 500, 185-207.

Leblanc, G. E., and W. A. Morris, 1999, Aeromagnetics of Southern Alberta within areas of hydrocarbon accumulation: Bulletin of Canadian Petroleum Geology, 47, 439-454.

Leckie, D. A., B. A. Kjarsgaard, J. W. Peirce, A. M.Grist, M. Collins, A. Sweet, L. Stasiuk, M. A. Tomica, R. Eccles, M. Durfresne, M. M. Fenton, J. G. Pawlawicz, S. A. Balzar, D. J. McIntyre, and D. H. McNeil, 1997, Geology of a Late Cretaceous possible kimberlite at Mountain Lake, Alberta; chemistry, petrology, indicator minerals, aeromagnetic signature, age, stratigraphic position and setting: Geological Survey of Canada, Open File Report 3441.

MacCormack, K. E., N. Atkinson, and S. Lyster, 2015, Sediment thickness of Alberta, Canada: Alberta Energy Regulator Map 603; scale 1:1,000,000.

Machel, H. G., M. L. Borrero, E. Dembicki, H. Huebscher, L. Ping, and Y. Zhao, 2012, The Grosmont: the world's largest unconventional oil reservoir hosted in carbonate rocks, *in* J. Garland, J. E. Neilson, S. E. Laubach and K. J. Whidden, eds., Advances in carbonate exploration and reservoir analysis: Geological Society, London, Special Publication 370, 49-81.

McCandless, T. E., 1999, Kimberlites: Mantle expressions of deep-seated subduction, *in* J. J. Gurney, J. L. Gurney, M. D. Pascoe, S. H. Richardson,

eds.: Proceeding of the 7th International Kimberlite Conference, 2, 545-549.

McCandless, T. E., R. M. Tosdal, 2005, Base metal porphyries and diamond-enriched kimberlites of the Laramide orogeny: products of convergent margin magmatism: Geological Society of America Abstracts with Programs, 37.

Miller, H. G., and V. J. Singh, 1994, Potential field tilt; A new concept for location of potential field sources: Applied Geophysics, 32, 213-217, doi: 10.1016/0926-9851(94)90022-1.

Nabighian, M. N., 1984, Toward a three-dimensional automatic interpretation of potential field data via generalized Hilbert transforms; Fundamental relations: Geophysics, 49, 780-786.

Ogunsuyi, F., and D. R. Schmitt, 2010, Integrating seismic velocity tomograms and seismic imaging: Application to the study of a buried valley, *in* R. D. Miller, J. D. Bradford, and K. Holliger, eds., Near surface seismology and ground penetrating radar: Society of Exploration Geophysics, 361-378, doi: 10.1190/1.9781560802259.ch22.

O'Connell, S. C., G. R. Dix, and J. E. Barclay, 1990, The origin, history and regional structural development of the Peace River Arch, Western Canada: Bulletin of Canadian Petroleum Geology, 38A, 4-24.

Pilkington, M., W. F. Miles, G. M. Ross, and W. R. Roest, 2000, Potential-field signatures of buried Precambrian basement in the Western Canada Sedimentary Basin: Canadian Journal of Earth Sciences, 37, 1453-1471, doi: 10.1139/e00-020.

Rao, T. K. S. P., M. Subrahmanyam, and A. Srikrishna Murthy, 1986, Nomogram for the direct interpretation of magnetic anomalies due to long horizontal cylinders: Geophysics, 51(11), 2156-2159, doi: 10.1190/1.1442067.

Rabeh, T., T. Abdallatif, M. Mekkawi, A. Khalil, and A. El-emam, 2008, Magnetic data interpretation and depth estimation constraints; a correlative study

on magnetometer and gradiometer data: NRIAG Journal of Astronomy and Geophysics, 185-209.

Ram Babu, H. V., V. Vijayakuma, and D. Atchuta Rao, 1986, A simple method for the analysis of magnetic anomalies over dike-like bodies: Geophysics, 51 (5), 1119-1126, doi: 10.1190/1.1442166.

Ravat, D., A. Pignatelli, I. Nicolosi, and M. Chiappini, 2007, A study of spectral methods of estimating the depth to the bottom of magnetic sources from near-surface magnetic anomaly data: Geophysical Journal International, 169, 421-434, doi: 10.1111/j.1365-246X.2007.03305.x.

Reiter, K., O. Heidbach, D. R. Schmitt, K. Haug, M. Ziegler, and I. Moeck, A revised crustal stress orientation database for Canada: Tectonophysics, 636, 111-124, doi: 10.1016/j.tecto.2014.08.006, 2014.

Ross, G. M., R. R. Parrish, M. E. Villeneuve, and S. A. Bowring, 1991, Geophysics and geochronology of the crystalline basement of the Alberta Basin, Western Canada: Canadian Journal of Earth Sciences, 28, 512-522, doi: 10.1139/e91-045.

Ross, G. M., J. Mariano, R. Dumont, B. A. Kjarsgaard, and D. Teskey, 1997, Was Eocene magmatism widespread in the subsurface of Southern Alberta? Evidence from new aeromagnetic anomaly data, i*n* R.W. Macqueen, eds., Exploring for minerals in Alberta; Geological Survey of Canada geoscience contributions, Canada-Alberta Agreement on Mineral Development (1992-1995): Geological Survey of Canada, Bulletin 500, 235-246.

Rukhlov, A. S., and J. G. Pawlowicz, 2012, Eocene potassic magmatism of the Milk River area, southern Alberta (NTS 72E) and Sweet Grass Hills, Northern Montana; overview and new data on mineralogy, geochemistry, petrology and economic potential: Energy Resources Conservation Board and Alberta Geological Survey, open file report 2012-01.

Russel-Houston, J., and K. Gray, 2014, Paleokarst in the Grosmont Formation and reservoir implications, Saleski, Alberta, Canada: Interpretation-a Journal of Subsurface Characterization, 2, SF29-SF50.

Secor, D. T., 1965, Role of fluid pressure in jointing: American Journal of Science, 263, 633-646.

Skelton, D., and T. Bursey, 1998, Buffalo Head Hill property (AL01) assessment report - Ashton Mining of Canada Inc.: Alberta Geological Survey, Report 19980015.

Skelton, D., B. Clements, T. E. McCandless, C. Hood, S. Aulbach, R. Davies, and L. P. Boyer, 2003, The BHH kimberlite province, Alberta: Proceeding of the 8th International Kimberlite Conference, Northern Alberta-Slave kimberlite field trip guide book: Geological Survey of Canada.

Spector, A., and F. S. Grant, 1970, Statistical models for interpreting aeromagnetic data, Geophysics, 35 (2), 293-302, doi: 10.1190/1.1440092.

Telford, W. M., L. P. Geldard, R. E. Sherriff, and D. A. Keys, 1990, Applied Geophysics, 2nd edition: Cambridge University Press.

Verduzco, B., J. D. Fairhead, C. M. Green, and C. MacKenzie, 2004, New insights into magnetic derivatives for structural mapping: The Leading Edge, 23 (2), 116-119, doi: 10.1190/1.1651454.

Wall, M., J. Cartwright, R. Davies, and A. McGrandle, 2010, 3D seismic imaging of a Tertiary Dyke Swarm in the southern North Sea, UK: Basin Research, 22, 181-194, doi: 10.1111/j.1365-2117.2009.00416.x.

Walsh, N. J., 2013, Geochemistry and geochronology of the Precambrian basement domains in the vicinity of Fort McMurray, Alberta; A geothermal perspective, M.Sc. thesis: University of Alberta.

Westgate, J. A., 1968, Surficial geology of the Foremost-Cypress Hills area, Alberta: Research Council of Alberta, RCA/AGS Bulletin 022, 137 p.

Wood, B. D., and A. C. Williams, 1994, Mountain Lake Prospect, Alberta: Alberta Energy and Utilities Board/Alberta Geological Survey, Assessment Report 1994000.

Wood, B. D., B. H. Scott Smith, and S. de Gasparis, 1998, The Mountain Lake kimberlitic pipes of Northwest Alberta; exploration, geology and

emplacement model: 7th International Kimberlite Conference, South Africa, Extended Abstract.

Zoback, M., 2007, Reservoir Geomechanics: Cambridge University Press.

Zonneveld, J. P., B. A. Kjarsgaard, S. E. Harvey, and D. H. McNeil, 2006, Accommodation space and kimberlite edifice preservation; implications for volcanological models of Fort à la Corne kimberlites., Saskatchewan Kimberlite Emplacement Workshop, Extended Abstract.

Chapter 5: Precambrian basement structural features in the Athabasca region, Northeast Alberta

5.1. Introduction

Although the main purpose here is to provide detailed geologic and geophysical interpretation of the sedimentary basin and evaluate the geothermal potential of the study area, the relatively large amount of seismic reflection and aeromagnetic data obtained allows for other aspects of the subsurface geology to be evaluated. For the most part, the basement rocks have been mostly ignored with focus on structure and resources within the sedimentary basin. This is, of course, because we do not expect the craton rocks in this region to contain hydrocarbon or hot water for conventional geothermal energy production or unconventional geothermal energy (engineered geothermal system) at economic depths. However, the metamorphic basement rocks of the Canadian craton do provide a record of the construction of the core of North America. By chance, the region studied here lies over the contact between two Proterozoic domains of the Buffalo Head Terrane and the Taltson Magmatic Zone. There remains a great deal of discussion in the literature with regards to the origin and tectonics of these domains, and it is worth examining the data to see if it can shed any additional light on this topic.

In this chapter, we present some findings from the seismic data and from further investigation of the magnetic data obtained. We further make suggestions, at this time preliminary and speculative, as to the geological interpretation of the contact between the two basement Taltson Magmatic Zone

and Buffalo Head Terrane domains and with respect to the possibility that this boundary may have served as the locus for later crustal motions. We make recommendations that might spur additional crustal scale work in this area.

5.2. Tectonic and geology setting

From the context of past plate tectonics, the study area is interesting for two reasons. First, the study area covers the inferred boundary between two distinct Proterozoic domains within the Canadian Shield: The Taltson Magmatic Zone (TMZ) and the Buffalo Head Terrane (BHT). Second, the study area also encompasses a zone of rapid change in the structure of the sedimentary basin with a relatively rapid drop in the elevation of the top of the metamorphic basement. The Devonian Leduc reef trend lies on or close to this change in topography and to its east lies the Grosmont Platform. There are three questions that can be asked. The first concerns the tectonic nature of the BHT-TMZ contact: is it related to direct plate collision, subduction, or something else? Second, could the changes in topography of the basement as well as the Devonian reefs and platforms be related to vertical relative fault displacements? And third, if so, could the Devonian features have resulted from tectonic motions along crustal zones of weakness associated with the Proterozoic domain boundaries? To our knowledge, outside of the Peace River Arch zone, there are very few efforts on attempting to link structures within the Proterozoic basement to those in the overlying Phanerozoic sediments.

5.2.1. Proterozoic Basement Tectonic Domains

The assembly of the Canadian Shield is the result of tectonic accretionary and collisional processes of pre-existing Proterozoic and Archean cratons during the 2.0 to 1.8 Ga time period (Hoffman, 1989; Pană, 2003). Hoffman's (1989)

and Gibb et al.'s (1983) reviews brought together a variety of studies that produced an overall picture of the craton 'Laurentia' as being constructed of a series of Early Proterozoic (2.5-1.6 Ga) orogenic belts from the collisions between previously isolated pieces of continental and oceanic crusts and island arcs of Archean (prior to 2.5 Ga) and Early Proterozoic age. These studies were crucial in that they tell us that plate tectonics were active during this phase of the earth's history much as it is today.

The differing domains and the sutures that weld them have been delineated by a variety of techniques that include direct geological mapping of structures and textures, age dating using primarily U-Pb methods, other isotopic methods (e.g., Sm-Nd) that allow differentiation of the source of the rocks between mantle or crust, and geophysical gravity and magnetic surveys. Many of the orogenic belts may have involved the closure of oceanic basins and consumption of oceanic lithosphere that produced magmatic rocks with the presence of magnetite as an accessory mineral phase (Henderson et al., 1987; Meyer et al., 1992; Ross, 2002), although one should take care that this may not be the case for all situations (e.g., Chacko et al., 2000). Reflection seismology, too, has played a role in examining the boundaries between these crustal domains. Chacko et al.'s (2000) tectonic map of Western Laurentia provides a relatively recent summary on the dates, provenance, and boundaries of the domains (**Figure 5.1**). It should be noted, however, that the boundary lines drawn represent what are often very complex geological structures that may be 3D depending on the nature of the boundary itself.
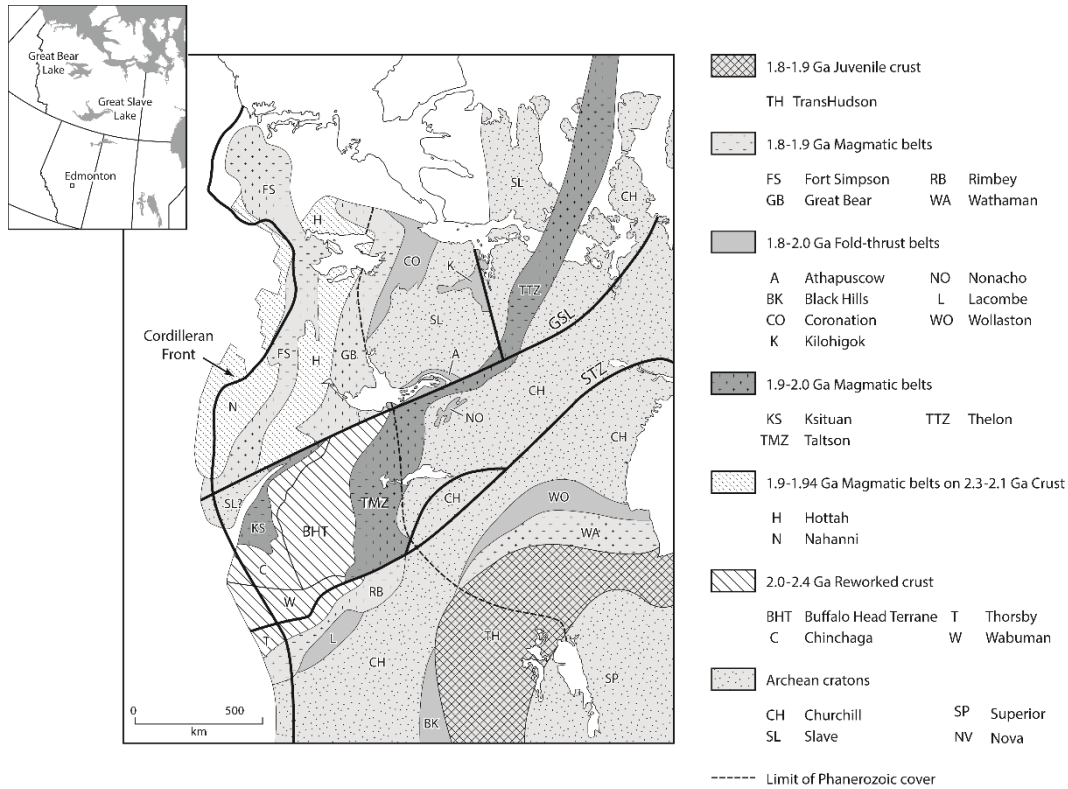
Figure 5.1. Generalized tectonic map of Western Laurentia (modified after Chacko et al., 2000; De et al., 2000). Area to the west of dashed line is blanketed by Phanerozoic cover. STZ and GSL represent the loci of the Snowbird Tectonic Zone and the Great Slave Lake shear zone, respectively.

The definition of the domain boundaries is relatively straightforward in those exposed parts of the Canadian Shield, although it is likely that this vast area still holds many surprises not yet incorporated to the summary map of **Figure 5.1**. However, a good deal of the shield remains hidden from direct access by the sediments of the Phanerozoic Western Canada Sedimentary Basin. The domain boundaries are shown in **Figure 5.2** within Alberta, only the northeast corner of Alberta is free of sediment cover. In regions where the rocks of the shield are buried, the tectonic domains have been delineated by extending domains mapped on the exposed Canadian Shield, from geophysical signatures on potential field maps (Hoffman, 1989; Pilkington et al., 2000, Villeneuve et al., 1993; Lyatsky et

138

al., 2005), and from similarities in geochemical and isotopic measurements from limited drill cores (e.g., Ross et al., 1991; Burwash et al., 1993; Chacko et al., 2000).
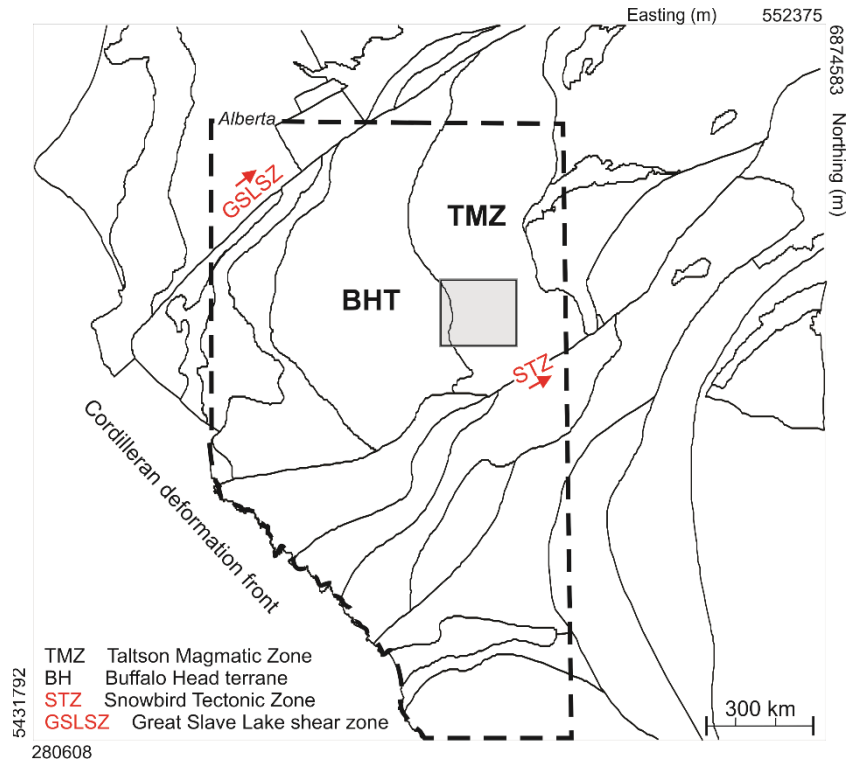
Figure 5.2. Generalized map of crustal domains of the Western Canad Shield (compiled from Hoffman, 1989 and Ross et al., 1991) within Alberta (dashed black line). The study area is outlined with a gray box.

It is interesting to note that Garland and Burwash (1959) made the first attempts to combine core and gravity data, although their pioneering interpretations are now obsolete. The crustal structure of the basement beneath Alberta has been inferred from gravity and magnetic maps with some control on rock type and age from the limited core that has been collected in the basement (**Figure 5.3**) (Ross et al., 1991). An anomaly in the geophysical field map is an indirect indication of some perturbation in the geometric distribution of a particular physical property of underlying rocks (Lyatsky and Pană, 2003).

Crustal seismic data in Alberta reveals the complex internal structural fabrics and the non-homogeneous nature of the subsurface rocks in the basement domains (Ross and Eaton, 1999, Bouzidi et al., 2002).
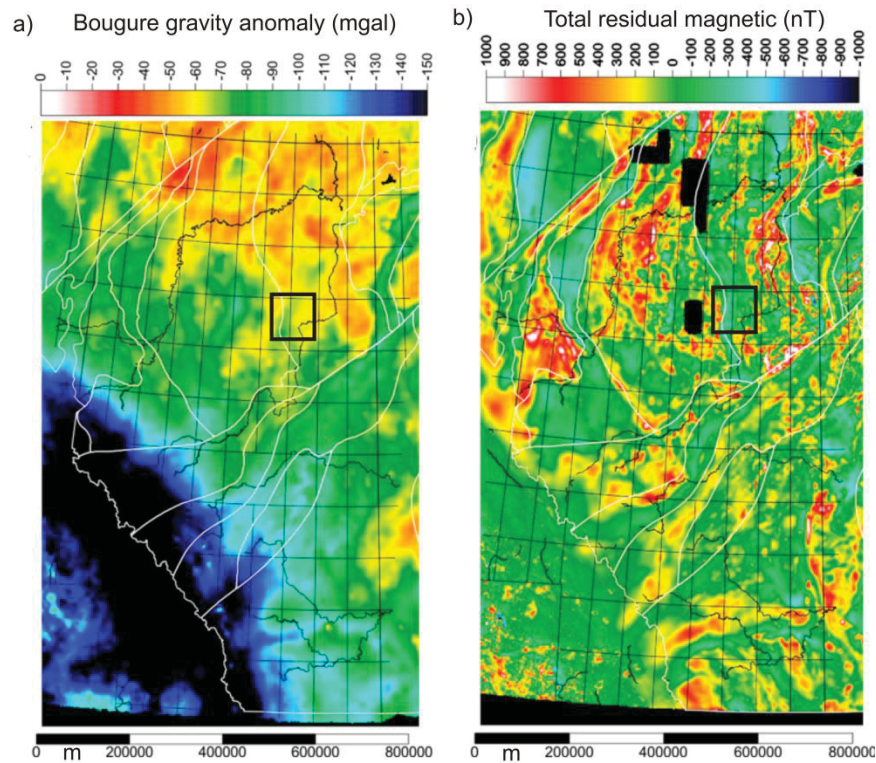
Figure 5.3. Geophysical potential field maps over Alberta with the generalized tectonic boundaries (See **Figures 5.**1 and **5.2**) superimposed as white lines (UTM-NAD27-Zone12). The study area is shown by a black box. (a) Bouguer gravity map from the 2 km gridded data (GSC 2016a). Note truncated scaling with values < 150 mgal appearing as black. (b) Total residual magnetic field map (GSC 2016b). Black areas here represent zones with no data. Data obtained from the publicly available databases maintained by the Geological Survey of Canada (GSC).

In terms of composition, the TMZ is made primarily of granitic plutons and uppermost amphibolite and granulite facies gneisses (see Chacko et al., (2000) for more information on zones with differing rock types) with Chacko et al., 2000 recognizing two granitoid intrusive phases ranging from 1963 to 1986

Ma and from 1927 to 1955 Ma. These phases intrude into a wide range of older gneisses and metasediments of ages greater than 2 Ga. There are two samples (aged from 1.92 to 1.98 Ga) available from basement rock in TMZ at our study area described in **Table 5.1** (after Walsh, 2013). The pictures of these two samples (TMZ-S1 and TMZ-S2) are presented in **Figure 5.4**. Although, the TMZ is exposed in the northeast of Alberta, it is covered by the Phanerozoic sedimentary rocks in our study area and these samples obtained from drill cores. Chan and Schmitt (2015) have studied the seismic anisotropy and mechanical strength of a sample of core from 2350 m depth in the deep AOC GRANITE 7-32-89-10 borehole near Fort McMurray.

The BHT does not outcrop and its existence and boundaries are inferred by Ross et al. (1991) based somewhat subjectively on the aeromagnetic signature and fabric particularly with comparison to neighboring domains. With regards to this interpretation, Theriault and Ross (1991) write:

> *"Buffalo Head domain: a 200-300 km wide elongate subsurface crustal domain characterized by internally complex, north trending, convex-westward, moderately positive aeromagnetic anomalies containing aeromagnetic negative septa."*

Theriault and Ross (1991) analyzed 12 core samples within this magnetically delineated region. The rock types are generally metaplutonic rocks with a wide range from gabbro to leucogranite, with some metavolcanics and paragneisses. The U-Pb ages range from 1998 to 2332 Ma but with model estimates of the time the rocks were extracted from a depleted mantle from the Sm-Nd method as old as 2.51 to 2.93 Ga. Regardless, the rocks in the BHT appear to be older than those in the adjacent TMZ. There are two core samples available

141

from the BHT in the study area (**Figure 5.4**). The samples mineral descriptions are presented in **Table 4.1**.

Table 5.1. Full description of rock samples from TMZ and BHT (after Walsh, 2013) within the study area.

ID	Rock type	Major Minerals* Model abundance (%)			Minor Minerals* Model abundance (%)					Alteration	Foliation	Age (Ga)
TMZ-S1	garnet monzogranite	qtz 31.1	kfs 44.0	plag 18.8	grt 5.5	bt 0.5	calc <0.1	zrc <0.1	mnz <0.1	minor	minor	1.92-1.94
TMZ-S2	biotite syenogranite	qtz 27.7	kfs 55.7	plag 8.6	bt 6.1			zrc <1.9		none	none	1.95-1.98
	granitic pegmatite	qtz 38.7	kfs 28.5	plag 23.1	bt 5.8	hm 2.4	p-rut 0.3	Zrc <0.6	mnz <0.6	minor	minor	2.25-2.40
BHT-S1	biotite amphibolite gneiss	qtz 41.3	kfs 21.0	plag 19.7	bt 10.4		grt 5.0	Ilm <1.3	Zrc <1.3	none	gneissosity	2.25-2.40
BHT-S2	monzogranite	qtz 28.0	kfs 33.6	plag 32.1	hm 3.4		Mt <1.5	Zrc <1.5		minor	minor	2.25-2.40

*Minerals: qtz = quartz, kfs = potassium feldspar, plag = plagioclase feldspar, bt = biotite, grt = garnet, mt = magnetite, ilm = ilmenite, hm = hematite, p-rut = pseudorutile, calc = calcite, zrc = zircon, mnz = monazite
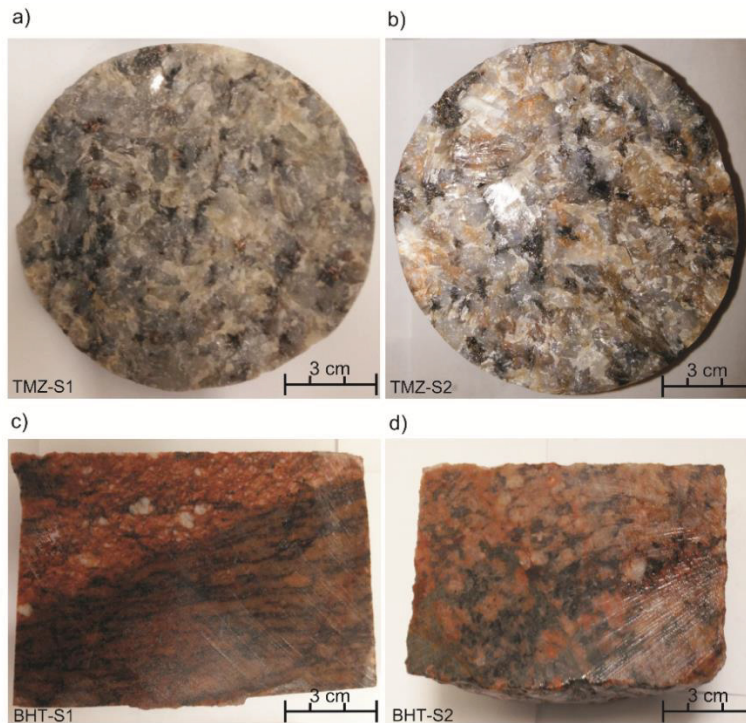
Figure 5.4. Pictures of TMZ and BHT rock samples. (a) first sample of TMZ (garnet monzogranite), (b) second sample of TMZ (biotite syenogranite), (c) first sample of BHT (biotite amphibolite gneiss), and (d) second sample of BHT (monzogranite).

There is extensive discussion as to the geological history of the contact between these two domains. One model is that the TMZ is magmatic arc material produced from either eastward-dipping continental or oceanic subduction associated with closure between the BHT and the Rae Province (e.g., Theriault and Bostock, 1989; Theriault and Ross, 1991; Ross et al., 1991; Ross and Eaton, 1999; McDonough et al., 2000). Chacko et al. (2000) tested this model by comparing the geochemical and isotopic databases available for TMZ granitoids, with similar databases for Phanerozoic granitoid suites from different tectonic environments. Their results demonstrate the TMZ rock samples lack the expected mantle signature. Instead, the geochemistry is more consistent with intracrustal magmas that usually form in the distant hinterland of a convergent plate margin. Consequently, they suggest that the BHT-TMZ is not a subduction zone at 1.97-2.0 Ga. Therefore another tectonic model was proposed which envisions formation of the TMZ in a plate-interior rather than a plate-margin setting and relate the magmatism in response to thickening of crust in the continental interior (Chacko et al., 2000; De et al., 2000).

Almost all of the evidence for these various models is derived from the interpretation of geochemical measurements on rock samples, particularly with regards to the completely blanketed BHT where the core is sparse. In terms of the locus of the domains contact, regretfully, there is no deep seismic profiling that crosses the BHT-TMZ boundary that could provide additional evidence to may help constraining these interpretations. The nearest LITHOPROBE deep seismic profile lies more than 200 km away to the southwest (Bouzidi et al, 2002). A short (~20 km long) but deep (4.5 seconds or approximately 12 km) profile, too, was collected for exploration purposes near Fort McMurray over 100 km to the east (Chan and Schmitt, 2015) and as such does not cross the boundary. More

recently, Chen et al. (2015) by P to S receiver functions and Gu and Shen (2015) with noise correlation tomography, have mapped gross structures within the craton, but these results, too, lie principally to the south of the study area. Here, we are fortunate to have a few conventional industry reflection profiles that do cross the boundary as will be described later although it must be stressed that these were not designed for deep crustal seismological studies.

5.2.2. Phanerozoic Structures

Briefly, the gross structure of the Western Canada Sedimentary Basin overlying Proterozoic/Archean basement in the study area consists of a Middle to Upper Devonian section of carbonates, shales, and evaporites deposited in a passive margin setting following a hiatus of about 250 million years by Cretaceous siliciclastic deposits in a foreland basin setting. A good deal of discussion has already been centered on the existence of the large bitumen deposits within those karstified zones of the Grosmont and Nisku formations that were at or near the earth's surface when the Cretaceous sedimentation began. We do not expect a great deal of structure within gently dipping Cretaceous section, aside from the potential igneous dykes revealed in Chapter 4. However, another large scale Devonian feature of the Leduc reefs bisect the study area (**Figure 5.5**). The 700-km long Leduc-Meadowbrook-Rimbey (LMR) reef trend in a general north-northeast direction terminates to the north of the study area (Dembicki and Podvisnky, 2012). There are a number of reef buildups within Alberta, these have held enormous reserves of hydrocarbons (see Figure 12.21 of Switzer et al., 1994). Of these, the LMR trend is not only the longest but also, because of its relatively small width to length ratio, appears the most linear.
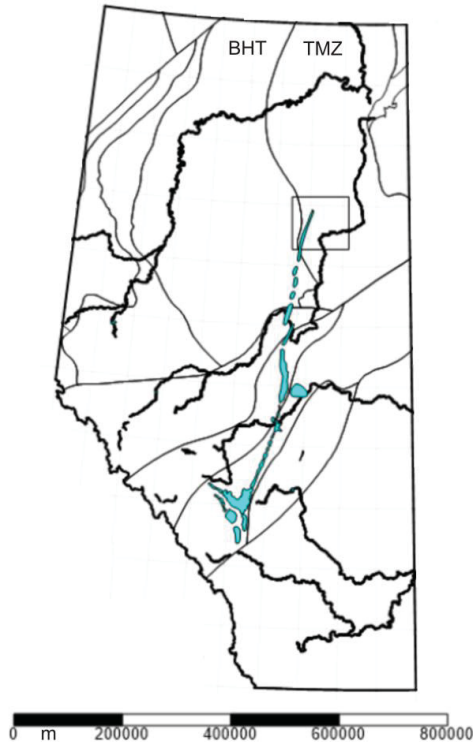
Figure 5.5. Map of Alberta showing the Leduc-Meadowbrook-Rimbey reef trend in light blue as provided from shape file data compiled by Switzer et al., (1994). Study area is shown as a rectangle. Note that the Leduc reef trend shown here extends further to the north than suggested by this generalization.

This linearity leads to suggestions that the LMR may be associated with faulting or at least some kind of disruption in the basement. Even today there has not been definitive proof of tectonic control although this was first suggested more than 60 years ago by Belyea (1955) who indicated that

> *"Differential subsidence, probably controlled by lines of weakness in the basement complex, may have been the important factor in determining reef distribution."*

However, many authors have shied away from any tectonic association. Mountjoy (1980) suggests that the growth of the reefs is primarily due to epeirogenic displacement of the basement and eustatic changes to sea level. Edwards and

Brown (1999), in an examination of 2D seismic reflection and potential field data, suggest that Devonian deposition was influenced by small irregularities in the basement topography that do not necessarily have any relationship to discrete faults. Indeed, there appears to be no resolvable basement structure beneath the Homeglen-Rimbey reef that is part of the LMR. They also find little evidence for a relationship between gravity and magnetic fields. In the same volume, Dietrich (1999) observed a number of features in the basement topography, but found no systematic links between the tectonic domains and structure in the Paleozoic. Ross and Eaton (1999) suggested that there was evidence for faulting within the Precambrian craton, but not much linkage between this and tectonic activity within the overlying Phanerozoic. These suggestions elicited a strong rebuttal from Gay (2001) who cited many studies that did link basement motion to faulting in the overlying sediments, albeit mostly in relation to the Peace River Arch. In short, this issue remains unresolved.

Figure 5.6a shows the boundary of Leduc reef as determined from seismic and geologic well tops in this study superimposed on the basement topography map. The disturbance of the topography map of the crystalline basement may indicate the structural lineament where the Leduc reef is located above the basement top of it, however the observed structure on the topography map must be interpreted with caution as that can be partly related to seismic velocity variation (pull-up/push-down) due to the reef existence. In order to have a better understanding of the relationship between the basement structure and Leduc reef location, the isochore (thickness) map of the Leduc reef is overlaid on the residual magnetic field map (**Figure 5.6b**). The greatest topographic expression of the Leduc reef is seen at the western edge, which seems to correlate with abrupt magnetic changes within the basement. In the following sections, the processing and

interpretation of this High Resolution Aeromagnetic (HRAM) data is presented with the purpose of clarifying of the tectonic boundary discussed previously and also finer lineaments.
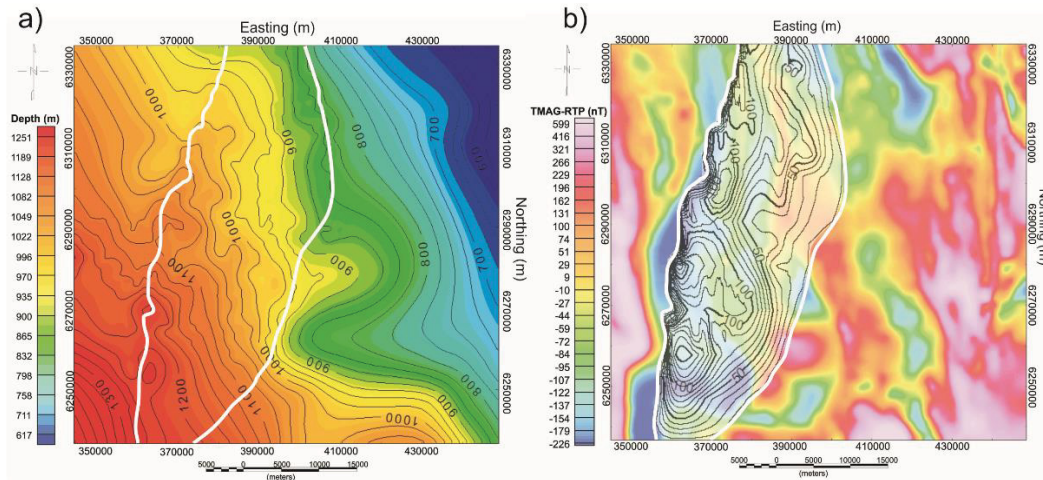
Figure 5.6. (a) The Leduc boundary polygon in white overlaid on the Precambrian basement top mapped in measured depth. (b) Isochore (thickness) of Leduc formation contoured every 10 m as determined from seismic and well log data in this study superimposed on the residual magnetic field map.

5.3. HRAM processing and interpretation techniques

HRAM data post-processing and interpretation involves applying a variety of mathematical filters to data with the purpose of highlighting anomalies (qualitative interpretation) of interest and obtaining preliminary information on source location or magnetization (quantitative interpretation) (Nabighian et al., 2005). In our study, several interpretation methods are applied, with the final goal of enhancing signature of shallow and deep lineaments and estimating their depths. We start with qualitative interpretation methods such as reduction to magnetic pole, horizontal/vertical/tilt derivatives, upward continuation, and analytic signal. Then the quantitative interpretation is carried out using Euler deconvolution for the qualitatively interpreted features.

5.3.1. Qualitative interpretation

This process consists of different anomaly-enhancement techniques to identify the individual lineaments and anomalous bodies (intrusions/faults) in the study area. We note that these types of processing may cause some artefacts in addition to enhancement of anomalies related to real geological features and the only way to distinguish them from each other is data integration. These basic HRAM data corrections of IGRF and reduction to pole have already been discussed in Chapter 4. The reduced to pole total magnetic referred to as TMAG-RTP shows the magnetic anomalies independent of the magnetic inclination of the source bodies and it is utilized in the next interpretation steps as the primary input (**Figure 5.7**).
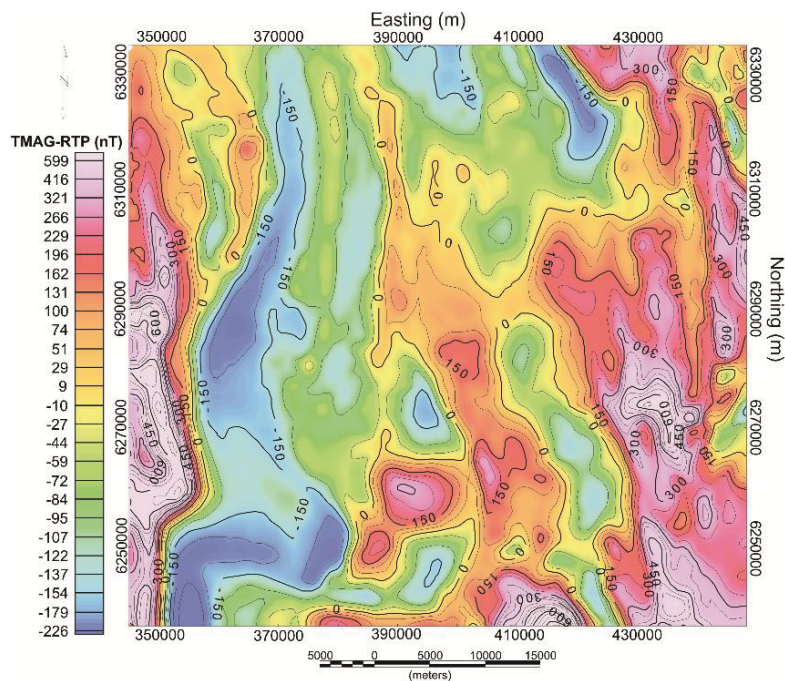
Figure 5.7. Reduced to pole total magnetic intensity map. High amplitudes are colored in pink and lows in blue. The magnetic data are provided under purchased license from Stornoway Diamonds as assisted by B. Charters and J. Peirce at GEDCO (now Chad Data).

5.3.1.1. Pseudo-gravity

A pseudo-gravity map computed from the magnetic grid shows the gravity map that would have been observed if density were proportional to magnetization or susceptibility. Comparison of gravity and pseudo-gravity maps can reveal a good deal about the local geology. Where anomalies coincide, the source of the gravity and magnetic disturbances is likely to be the same geological structure (Baranov, 1957). Our computed pseudo-gravity map (**Figure 5.8a**) of the study area is visually very similar to the real gravity map (**Figure 5.8b**) sharing a N-S running gravity low towards the western side, although there are some discrepancies in middle of the area that they can be linked to the wider spacing between the gravity stations. This map shows the steepest gradients mostly in north-south trend.
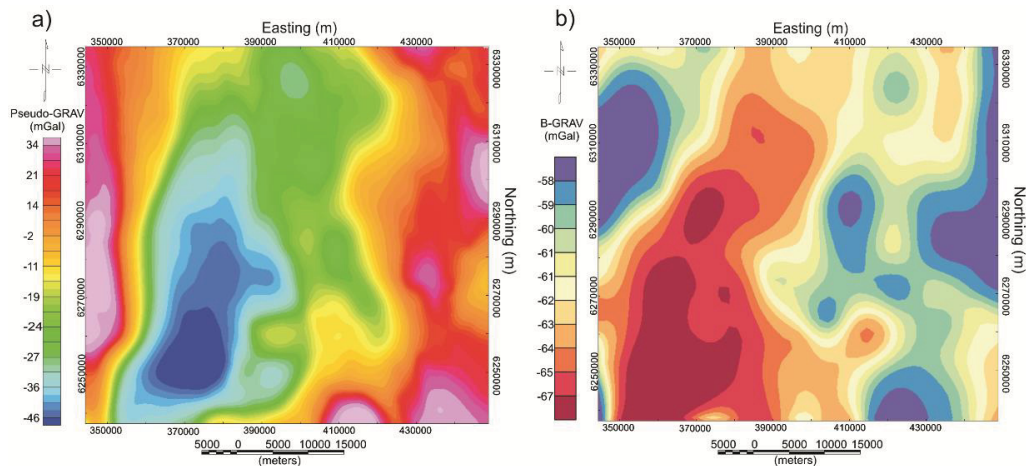
Figure 5.8. (a) Pseudo-gravity map computed from TMAG-RTP data shown in **Figure 5.7**. (b) Observed Bouguer gravity over the study area from the GSC data set as in **Figure 5.3**.

5.3.1.2. Derivative-based filtering

Total horizontal, vertical, tilt derivative, and analytic signal maps are the most powerful and simple products of HRAM data to identify the anomaly texture and pattern discontinuity. The horizontal gradient magnitude (THDRV) is

given by the square root of the sum of the squares of the horizontal derivatives of the potential field T

$$THDRV = \sqrt{\left(\frac{\partial T}{\partial x}\right)^2 + \left(\frac{\partial T}{\partial y}\right)^2} \tag{1}$$

where $\partial T/\partial x$ and $\partial T/\partial y$ are the first derivatives of the field T in the x and y directions. The vertical derivative just utilizes the field T in the z direction as follow

$$VDRV = \left(\frac{\partial T}{\partial z}\right) \tag{2}$$

Total horizontal and vertical gradients (THDRV and VDRV) enhance the short wavelength anomalies (**Figure 5.9a** and **5.9b**) in the southwest of our study area, allowing clearer imaging of the magnetic lineaments. The transformation can be noisy since it amplifies short wavelength noise, upward continuation can help to remove these short wavelength noise, albeit at a price of sacrificing some useful anomaly information (Lyatsky, 2004). Here, the noise suppression is achieved by 0.6 km upward continuation of the TMAG-RTP data and then the upward continued grid is used to drive horizontal and vertical gradients (**Figure 5.9c** and **5.9d**). The upward continuation uses wavelength filtering to simulate the appearance of magnetic maps if the HRAM is obtained at a higher altitude. The lineaments in the SW corner of the study area look smoother but still recognizable after upward continuation. Also some discontinuities and breaks with southwest-northeast trends are observed on these maps.

The tilt derivative (TDRV) map which is useful for mapping shallow basement structures (Miller, 1994; Verduzco, 2004) is shown in **Figure 5.9e**.

This grid is computed by vertical and horizontal derivatives of TMAG-RTP as inputs using the equation

$$TDRV = \tan^{-1}\left(\frac{VDRV}{THDRV}\right) \tag{3}$$

The TDRV values are restricted to values between $+\pi/2$ and $-\pi/2$ regardless of the amplitudes of VDRV or THDRV which makes this relationship function like an Automatic Gain Control (AGC) filter and tends to equalize the amplitude output of TMAG anomalies across a grid or along a profile.

The analytic signal (ASig) or total gradient shown in **Figure 5.9f** is calculated as the square root of the sum of the squares of the derivatives in the x, y and z directions (Roest et al., 1992). The absolute value of amplitude of the analytic signal at location (x, y) is derived from three orthogonal gradients of the total magnetic field using the equation

$$\sqrt{\left(\frac{\partial T}{\partial x}\right)^2 + \left(\frac{\partial T}{\partial y}\right)^2 + \left(\frac{\partial T}{\partial z}\right)^2} = |A(x,y)| \tag{4}$$

Applying this method to the HRAM data generates maximum amplitude over magnetic discrete bodies as well as their edges regardless of magnetization direction (MacLeod et al., 1993).

5.3.1.3. Bandpass filtering

The Butterworth bandpass (BWBP) filter is among the most beneficial filters used for HRAM image processing. This filter allows passing the desired mid-wavenumber range with a smooth cutoff. The power spectrum technique proposed by Spector and Grant (1970) enables us to find the right cutoffs for

BWBP filters. This technique and BWBP have been discussed in Chapter 4 previously.
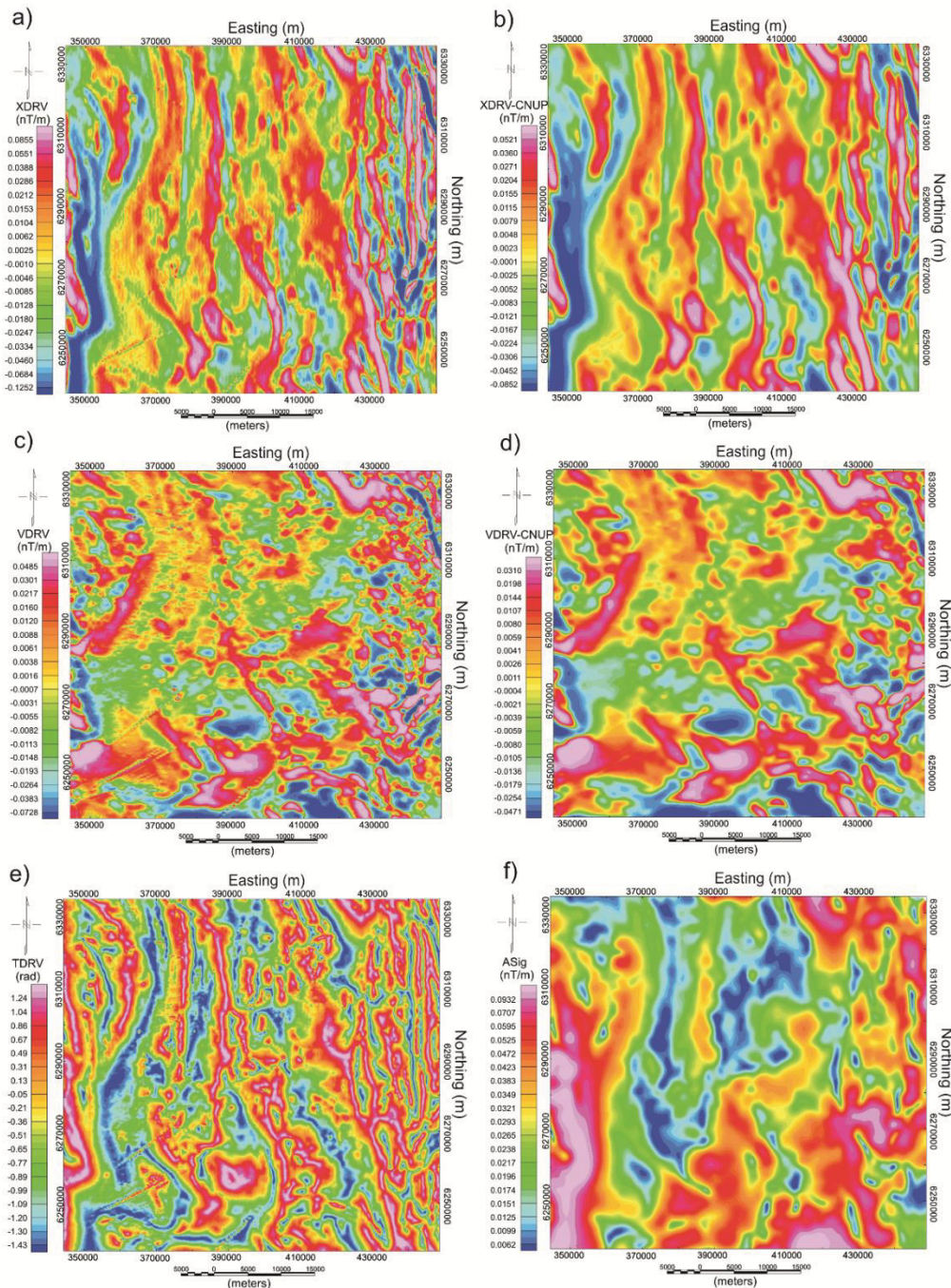
Figure 5.9. Different products of TMAG-RTP derivative, (a) horizontal gradient, (b) horizontal gradient of upward continued TMAG-RTP, (c) Vertical gradient, (d) Vertical gradient of upward continued TMAG-RTP, (e) tilt derivative, (f) analytic signal of upward continued TMAG-RTP.

Figure 5.10 shows the power spectrum of the TMAG-RTP grid plotted versus wavenumber and wavelength (note that the wavenumber used in the calculation of the slope is multiplied in 2π). The slope of best fit of each segment (shown in different colors) corresponds to the estimated depth values to the top of an ensemble of magnetic sources (Ravat et al., 2007; Rabeh et al., 2008). Higher estimated depth are related to lower wavenumbers and longer wavelength as it is expected.
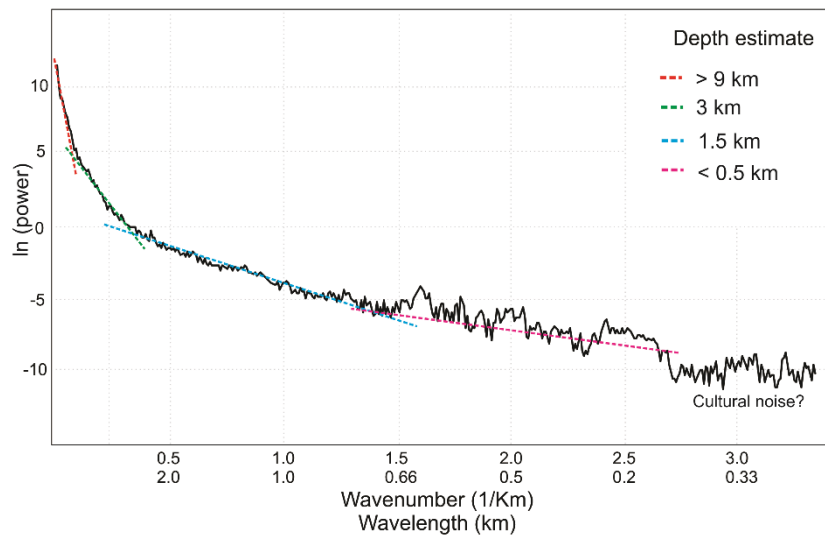
Figure 5.10. The radially averaged power spectrum of the TMAG-RTP plotted versus wavenumber (1/km) and wavelength (km). The best linear fits on each segment are shown in dashed lined with different colors. The depth of each assemblage is calculated from the slope.

The wavelength cutoff for BWBP is about two times of estimated depth of each segment of radially average power spectrum. We use BWBP (order of three) with the values of 1-3 km for shallow depth (**Figure 5.11a**), 3-6 km for medium depth (**Figure 5.11b**), 6-9 km for deep (**Figure 5.11c**), and 9-20 km for very deep features (**Figure 5.11d**). As mentioned before, the resolution depth is approximately half of wavelength. Therefore the 1-3 km BWBP filtered map

resolves mostly the anomalies of sedimentary basin (0.5 km) to the topmost portion of the crystalline basement (1.5 km).
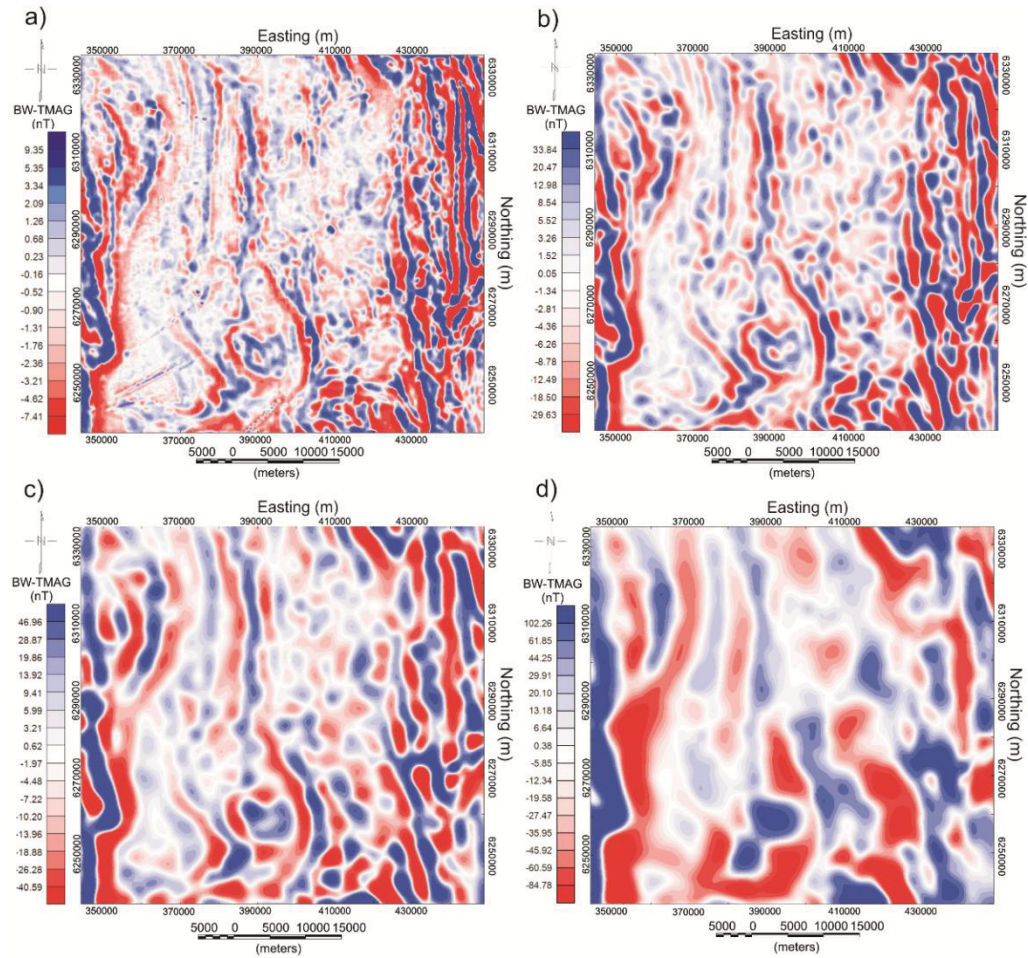
Figure 5.11. BWBP filtered TMAG-RTP, (a) 1-3 km for shallow depth, (b) 3-6 km for medium depth, (c) 6-9 km for deep, and (d) 9-20 km for very deep.

5.3.2. Quantitative interpretation

All the HRAM enhancement methods described in earlier sections lead to the location map of anomalous features and somewhat their shape on a surficial 2D plane. The quantitative process helps to refine these determined locations by depth estimation. Among various methods for depth estimation, 3D Euler

deconvolution is used to obtain quantitative estimation of depth to the top of the observed structures.

5.3.2.1. Euler 3D deconvolution

Euler 3D deconvolution (Reid et al., 1990) is applied to the TMAG-RTP to determine the source structure in the basement. Euler 3D deconvolution calculates location, depth below sensor, and the reliability of each depth solution. It requires calculation of the horizontal and vertical derivatives of the magnetic field. The primary signal that is measured in potential field data derives from the edges or contacts of geological units. In the standard Euler deconvolution process, each model contains solutions of a particular structural type, defined by the structural index (SI) parameter. Thompson (1982) called this the fall-off rate (i.e., the negative of the degree of homogeneity). The Euler's homogeneity relationship for HRAM data can be written in the form

$$(x - x_0)\frac{\partial T}{\partial x} + (y - y_0)\frac{\partial T}{\partial y} + (z - z_0)\frac{\partial T}{\partial z} = N(B - T) \tag{5}$$

where (x_0, y_0, z_0) is the position of the magnetic source whose total field (T) is detected at $(x, y, z,)$, B is the regional magnetic field and N is the measure of the SI.

The type of geological target of interest used in the Euler deconvolution procedure is defined by SI. A sill edge, dyke, or fault with a limited throw is best displayed with an index of 1.0, while a fault with large throw and geological contact is best displayed with a zero index. Irregular boundaries are exceptional in this case as irregular sill-like bodies can be well delineated by the Euler method with an index of 1.0, while irregular contacts are well shown with a zero SI (Reid et al., 1990).

The upward continued TMAG-RTP grid and its gradient components ($\partial T/\partial x$, $\partial T/\partial y$, $\partial T/\partial z$) calculated in frequency domain are the inputs to Standard Euler 3D method. The system uses a least squares method to solve Euler's equation simultaneously for each grid position within a window and then determines the anomaly position, depth, and base level for a specific magnetic source.

The method also involves the determination of two variables of SI and a window size. We have assigned the window size of 10 and SI values of zero (0.0), 0.5, and one (1.0), and then mapped out the Euler 3D solutions (**Figure 5.12**). These maps illustrate the source positions as circles over the study area. The sizes of the circles are proportional to the depth of magnetic sources. The solution maps show differing lineament trends, depths and degree of clustering. The reason behind choosing 10 by 10 window is to cover the large structural lineaments. Structural Indices of zero to one also give us the chance to identify geological contacts with three to two infinite dimensions (reasonably large dimensions), respectively. Since the created solutions for Euler deconvolution have high uncertainty and they may lead to misinterpretation, the choice of acceptance level is crucial. The acceptance level here is the maximum depth tolerance to allow and it means that all depth solutions with error estimate smaller than this tolerance is accepted.

The large-scale geological contact of BHT-TMZ boundary trending north-south shows the best clustering using SI of zero with acceptance level of 1% and the depth estimation of 1 to 3 km (**Figure 5.12a**). Although the pattern of the boundary is still distinguishable using the SI of 0.5 (**Figure 5.12b**), it does not show a solution clustering as tight as when the SI of zero is used. This pattern

starts to disappear from the solution map when the SI goes up to one (**Figure 12.5c**). As the size of the structural lineaments decrease, the higher assigned SI helps to identify them. These structural lineaments are located within the sedimentary basin and they typically have more complicated patterns.
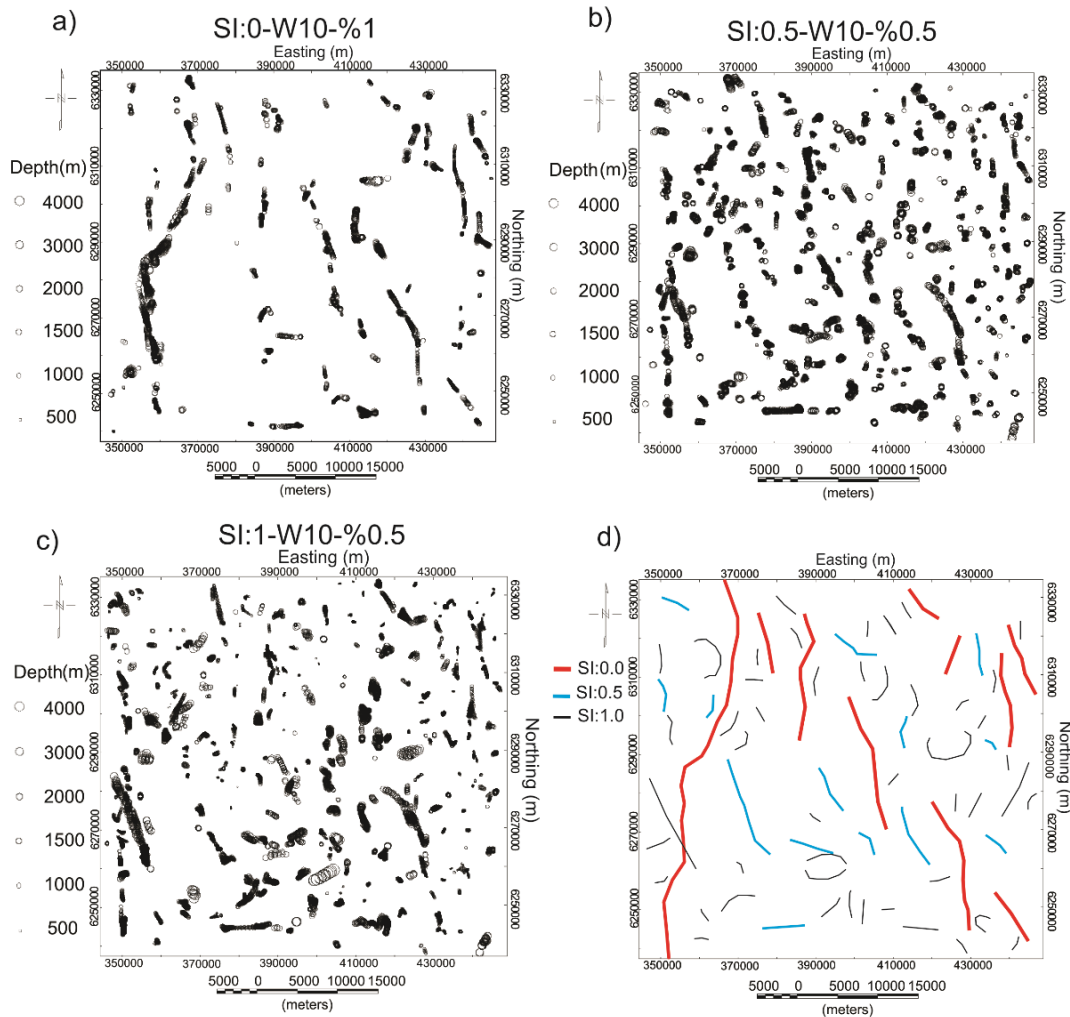
Figure 5.12. Euler 3D deconvolution of HRAM data. Source depth is indicated by circle diameter. (a) SI zero with 1% acceptance level, (b) SI 0.5 with 0.5% acceptance level, (c) SI one with 0.5% acceptance level, (d) structural lineaments interpretation of Euler trends; red, blue, and black lines represent interpreted lineaments obtained by SI zero, 0.5, and one, respectively.

In addition of depth estimation, Euler deconvolution helps to delineate the trends of geologic features in the Athabasca region. **Figure 5.12d** displays

such structural interpretation of Euler trends. The red, blue and black lines represent lineaments trends generated using SI zero, 0.5 and one, respectively. We believe the NW-SE trending red and blue lineament are more related to the metamorphic basement with deeper sources and the NE-SW trending black lineaments are more representative of intrasedimentary structures, however the wavelength overlap of magnetic signature may lead to some discrepancies in interpretation of such features.

5.4. Integrated interpretation

Based upon our magnetic texture interpretation by analysis of wavelength and anomaly amplitude, we divide the features in the Athabasca region into two categories: long wavelength and high amplitude regional anomalies, and short wavelength and high amplitude local anomalies.

As rocks of the sedimentary basin possess much lower magnetic susceptibility than the crystalline basement, the dominant fabric of the TMAG-RTP and lower frequency filtered products originate from the basement rocks in NW-SE direction. The north-south trending terrane boundary of TMZ and BHT at the west side of the TMAG-RTP grid and its products are identified by a long wavelength and high amplitude regional anomaly. As was discussed before, this boundary has been defined previously by Ross et al. (1991) using the regional aeromagnetic data acquired by the GSC (**Figure 5.3**). The sharp contrast between low and high values may suggest the existence of a fault within the metamorphic basement but this requires additional data to confirm. Ross et al. (1991) indicated domain boundaries of Western Canada crystalline basement by using the zero contour of the residual magnetic field intensity as an indicator of magnetic source body edges. Although the error in using the zero contour versus

the true body edge is ~20% of the depth to the source for vertically sided bodies, it was not producing appreciable differences at the scale of their study. Later Pilkington et al. (2000) used the same data set for locating boundaries but this time they relied on mapping source distribution within the basement rather than mapping the anomalies they generate.

Our interpretation of the BHT-TMZ boundary is based on the source distribution obtained by Euler solutions for SI of zero (**Figure 5.12d**). The depth of this contact is estimated to be more than 1.5 km and less than 3 km. **Figure 5.13** shows Ross et al.'s (1991) and our interpretation of the boundary by red and black colors, respectively.
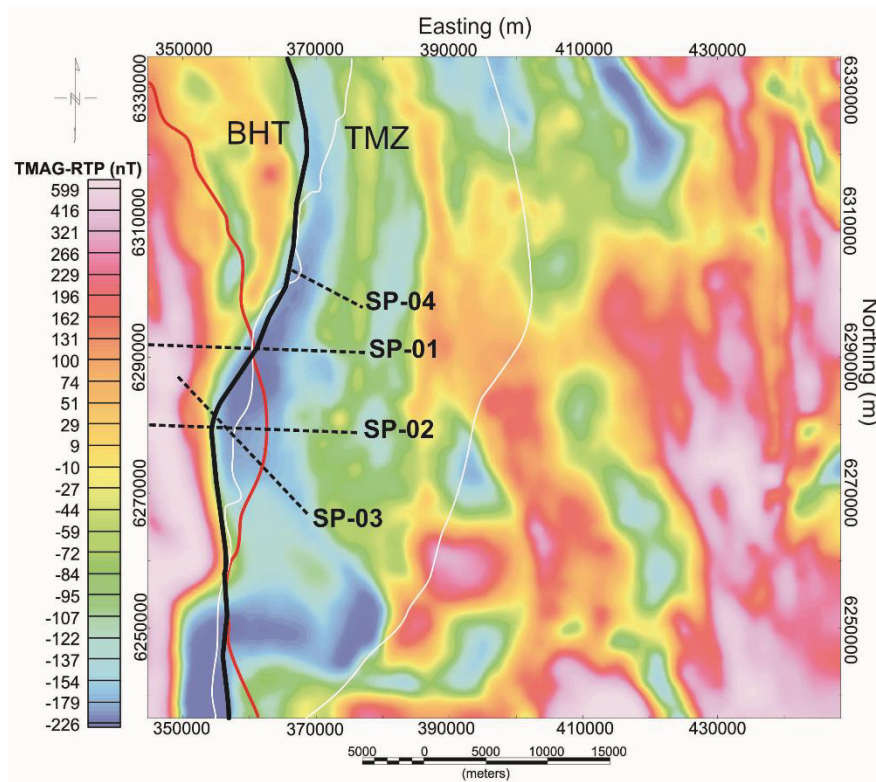
Figure 5.13. The location of the interpreted BHT-TMZ contact in this study and by Ross et al. (1991) are shown by red and black color, respectively. The dashed black lines highlight the 2D seismic reflection profiles intersecting the terrane boundary. The LMR is outlined in white.

A few of the seismic profiles in the study cross the inferred BHT-TMZ boundary. These are the only ones available to our knowledge for research purposes although they were not collected with imaging of the basement rocks in mind. The dashed black lines in this **Figure 5.13** are the location of these 2D seismic profiles (SP-01, SP-02 and SP-03). The seismic profiles with their corresponding TMAG, VDRV and Bouguer gravity profiles are illustrated in **Figure 5.14**, **5.15**, and **5.16**. In addition to the TMAG and B-GRAV curves, the profile of measured depth to the basement top (PCU-MD) is displayed. These curves are extracted from reduced to pole residual magnetic intensity (**Figure 5.7**), Bouguer gravity (**Figure 5.8b**), and basement depth (**Figure 5.6a**) maps with 10 m sampling interval. A good correlation is observed between the TMAG and B-GRAV curves (**Figure 5.14a**, **5.15a**, and **5.16a**) as it was also anticipated from the pseudo-gravity and gravity comparison.
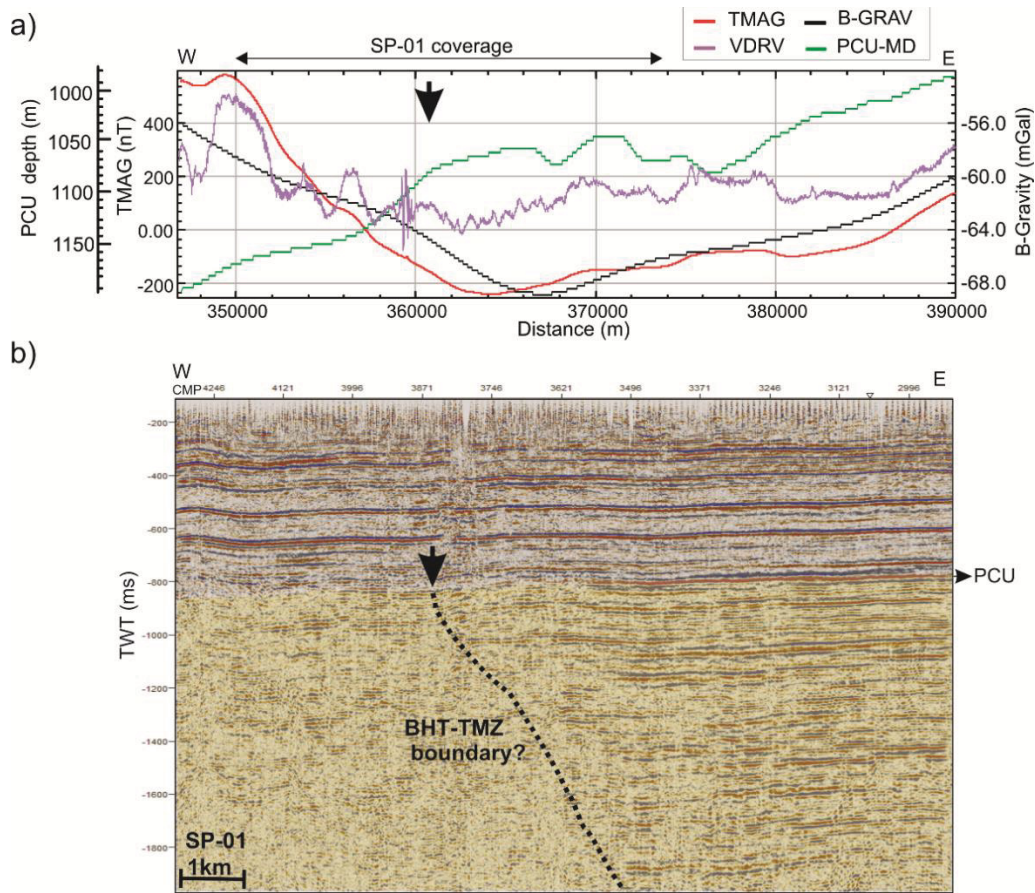
Figure 5.14. (a) Corresponding residual magnetic (TMAG) in red, vertical magnetic derivative (VDRV) in purple, Bouguer gravity (B-GRAV) in black, and measured depth to the basement (PCU-MD) in green curves along (b) the regional seismic line, SP-01.

161
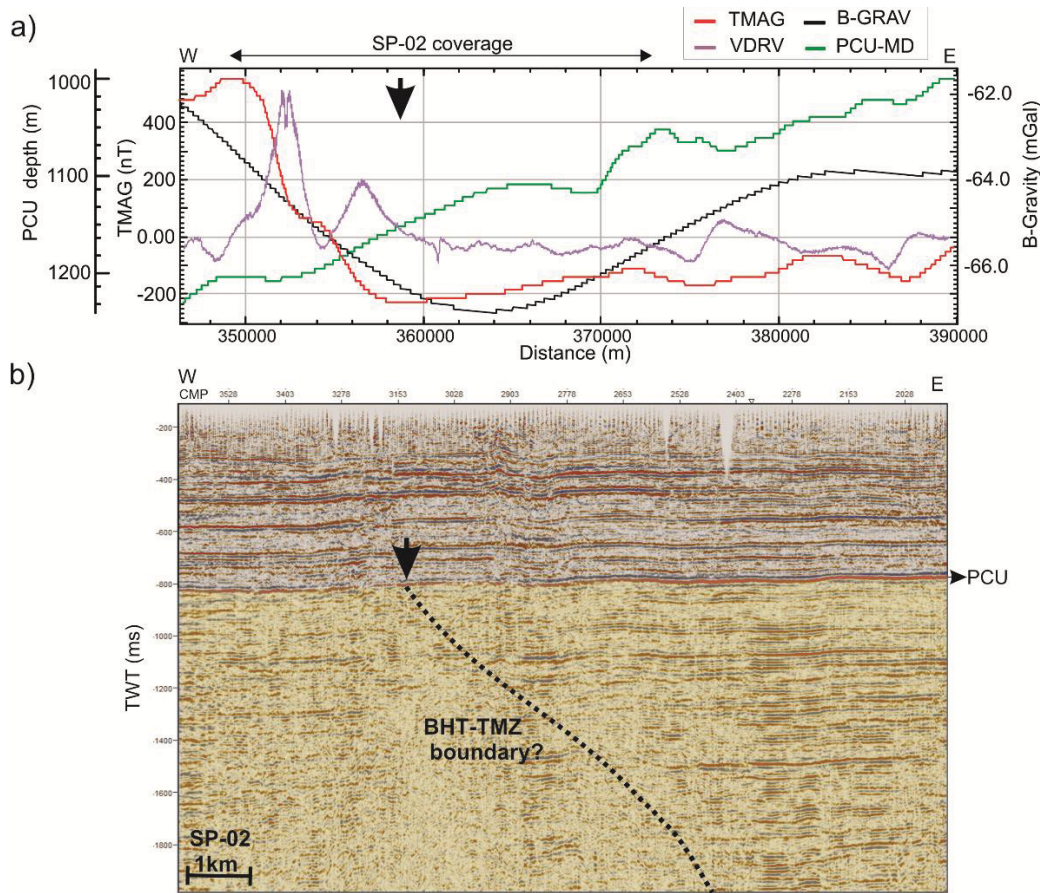
Figure 5.15. (a) Corresponding residual magnetic (TMAG) in red, vertical magnetic derivative (VDRV) in purple, Bouguer gravity (B-GRAV) in black, and measured depth to the basement (PCU-MD) in green curves along (b) the regional seismic line, SP-02.

The locus of the BHT-TMZ boundary based on our Euler source locations seems to be along local minima of TMAG and B-GRAV curves in the profiles shown in these figures. The black dashed lines on the seismic images delineate such boundary. The accuracy of this positioning is unknown at present, however it is interesting to note that the western edge of the LMR reef trend, as shown in **Figure 5.13**, in this area closely tracks this inferred BHT-TMZ boundary in the study area and seems to correlate well with the large spike on the vertical magnetic (purple curve) derivative in **Figure 5.14a**, **5.15a**, **5.16a**. As noted in earlier discussions, this does not appear to be the case in other areas of Alberta

(e.g., Dietrich, 1999; Edwards and Brown, 1999) and as such the association here may only be coincidental.
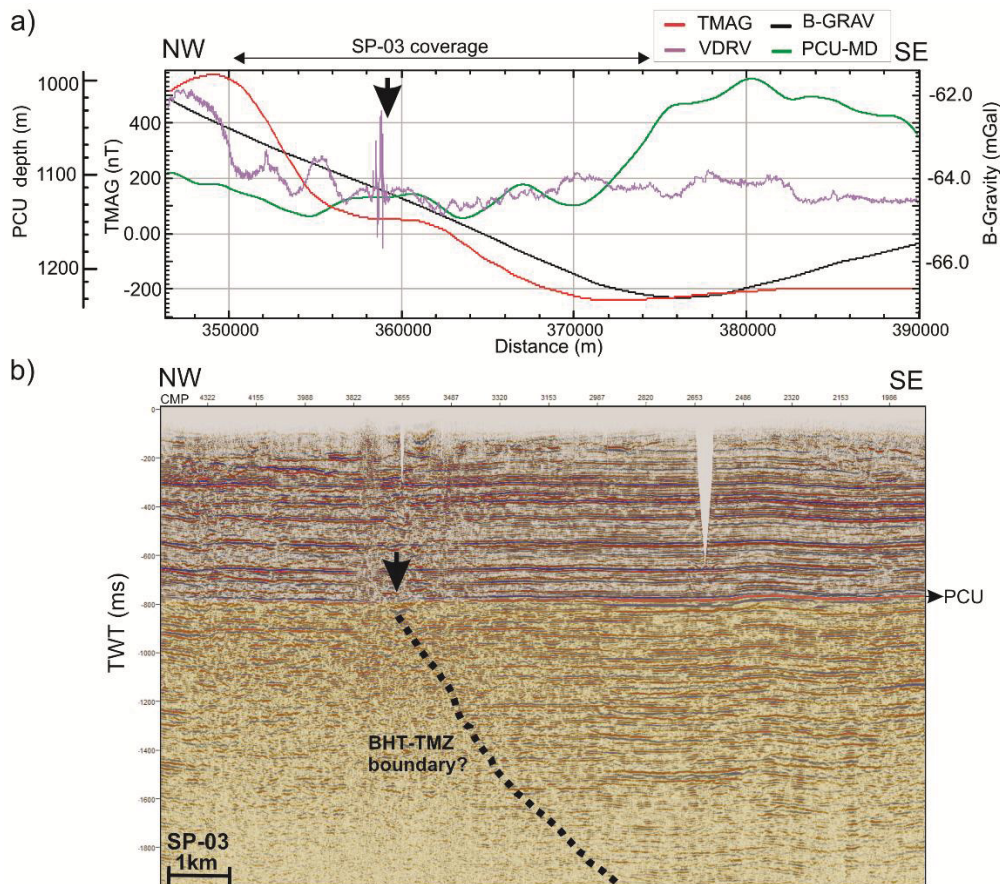
Figure 5.16. (a) Corresponding residual magnetic (TMAG) in red, vertical magnetic derivative (VDRV) in purple, Bouguer gravity (B-GRAV) in black, and measured depth to the basement (PCU-MD) in green curves along (b) the regional seismic line, SP-03.

The morphology of the basement curves exhibit increasing depth of the Precambrian basement from east to west (green curve in **Figure 5.14a**, **5.15a**, and **5.16a**). The Precambrian unconformity (PCU) is highlighted on the seismic profiles and the metamorphic basement is colored in light yellow (**Figure 5.14b**, **5.15b**, and **5.16b**). There are no noticeable differences in the seismic images as one crosses the inferred BHT-TMZ boundary, except for a change in character of

the 'apparent reflectivity' within the basement. It is interesting to note that in all three seismic profiles there are a number of flat lying events to the north and east of the boundary within the TMZ. To the south and west in the BHT, however, the events are much more muted.

One could be drawn into making a face-value interpretation that the TMZ contains essentially horizontal reflectivity. As noted earlier, many workers have assumed the TMZ was created from melts associated with collision between the BHT to the west and the Rae Province to the east. Other workers have observed strong horizontal seismic reflectivity within batholiths. In early deep crustal profiles, Lynn et al. (1981) observed horizontal reflectivity over presumed batholiths in Texas and Nevada. They tentatively suggested this reflectivity could result from the gabbroic underplating or from igneous cumulate layering. In contrast, the Boulder Batholith in Montana displays at best weak reflectivity but with a strong series of horizontal reflectors beneath it (Vejmelek and Smithson, 1995).

As already noted, a short 20 km long deep seismic profile was recently reprocessed and compared to vertical seismic profiling. No horizontal seismic events are evident in that profile, although one can see a number of eastward dipping reflectors that may be related to fracture zones (Chan and Schmitt, 2015). We cannot discount the possibility that the events within the TMZ in **Figure 5.14b**, **5.15b**, and **5.16b** truly represent changes in lithology in the metamorphic crust be they produced from the rock mass's original layering within a plutonic body or from intrusion of magma bodies into earlier crustal material. However, an alternative and perhaps more probable interpretation is that the seismic events observed below the PCU are no more than multiple reflections originating

within the sedimentary section. Such multiples are known to be problematic in the processing of deep seismic reflection profiles in areas where crystalline basement is covered with sediments (e.g., Bouzidi et al., 2002).

Close examination of the seismic lines reveals a strong and continuous reflection at the PCU to the east of the inferred BHT-TMZ contact; such a strong reflector would promote the generation of multiples. The PCU reflection is muted to the south and west of the contact and multiples would be lower correspondingly.

A number of factors could control the change in the PCU reflectivity. These include

i.   contrasts in the density and seismic waves speeds of the sediments and the metamorphic rocks across the PCU

ii.   variations in the smaller scale topography of the PCU such that the PCU reflection is not as coherent over the BHT as the TMZ

iii.   changes in sedimentary deposition patterns due to variations in the earlier erosional surface that could result in differences in the physical properties of the rocks deposited or the structure of the sedimentary column immediately above the PCU.

There is, of course, insufficient evidence to confidently demonstrate that any of these possibilities is correct.

One final common feature in these seismic lines is the zone of reduced reflectivity below the basement top; such zones are often said to be seismically transparent. This zone may dip at a high angle to the east. Interpretation of this is somewhat subjective. Again, given the lack of hard constraint this transparent

zone could be interpreted as either a real geological feature related to the BHT-TMZ contact or it could be an artefact of the seismic processing (**Figure 5.17**).

In the former, a seismically transparent zone means that one does not observe reflectivity. This state of affairs could either mean that the zone is highly uniform so that no contrasts in physical properties exist, or that the structure is highly complex at scales of about the seismic wavelength in which case the seismic waves are more randomly scattered and no coherent reflections are produced. This might be expected at a boundary between two tectonic domains but it is important to ask whether the relatively small width of at most a few kilometers is reasonable for a major tectonic boundary as suggested by the plate collision models. Such a sharp contact may not even be reasonable for the intraplate transform fault deformation model.

The alternative is that the 'transparent zone' results from issues related to the processing of the seismic data. In this context it is again important to note that the zone lies immediately below the Leduc reefs. Recall in **Figure 5.6** that there is an apparent trough in the topography at the west side edge (the thickest portions of the reef) that possibly is a velocity 'pull-down' feature due to lower seismic wave speeds within the off-reef shale strata (Ireton Formation) relative to the on-reef carbonate strata. **Figure 5.17** shows an example of a seismic line (SP-04) and possible artefacts caused by lateral velocity variation. Such lateral heterogeneity, if not properly accounted for by more advanced seismic processing techniques, would also be expected to reduce any coherent reflectivity, be it primary or multiple, arriving to the surface.
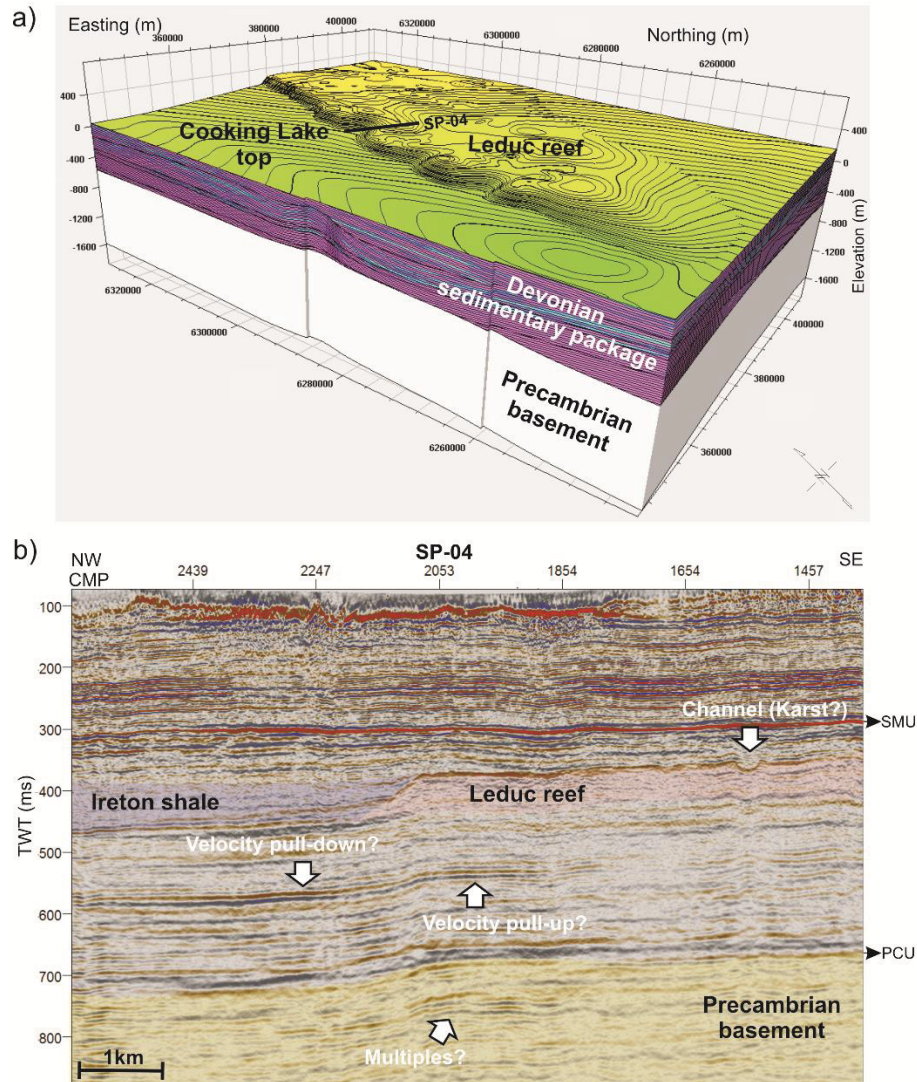
Figure 5.17. (a) The LMR in the study area sitting on top of the Cooking Lake Formation and the rest of Devonian Sedimentary formations. The solid black line is the location of seismic line SP-04. (b) Portions of the SP-04, showing the possible artefacts such as multiples and velocity pull-up/pull-down. The SubMannville and Precambrian unconformities (SMU and PCU) are highlighted.

5.5. Conclusions

The intent of this chapter is to fully exploit the extensive seismic and magnetic data sets collected as part of the study by using it to examine the metamorphic craton beneath the sediments. One motivation for this is the

coincidence that the study area, chosen for purposes of evaluation for geothermal energy because of the imminent need for energy in this region, includes the inferred contact between the Proterzoic Taltson Magmatic Zone and Buffalo Head Terrane tectonic domains.

As the overlap of wavelength distribution generated from different magnetic sources is always a common problem associated with HRAM interpretation, integrating this type of data with other geophysical data seems necessary. Based on this integrated study several conclusions can be drawn with respect to the structure of Athabasca region

i. The HRAM texture is more influenced by the Precambrian metamorphic basement than the sedimentary basin in Athabasca region since the sedimentary basin is very thin in comparison with the Canadian Shield in this area.

ii. Long wavelength anomalies generated from Precambrian basement show a trend of NW-SE; however the short wavelength intrasedimentary lineaments tend to be in both NW-SE and NE- SW directions.

iii. The TMZ-BHT boundary is recognized as a long wavelength and high amplitude feature. Euler deconvolution demonstrates that the depth of this boundary is within 1.5 and 3 km in Athabasca region. This estimation is correlative with the basement depth map constructed by reflection seismic and well tops data.

iv. Although the seismic data set here was not acquired for the deep craton study, its integration with of the HRAM data provided some interesting observations with coincidences of the LMR reefs with the BHT-TMZ boundary and the differing seismic fabric between TMZ and BHT.

References

Baranov, V., 1957, A new method for interpretation of aeromagnetic maps; pseudo-gravimetric anomalies: Geophysics, 22, 359-383, doi: 10.1190/1.1438369.

Belyea, H., 1955, Cross-sections through the Devonian system of the Alberta plains: Geological Survey of Canada, Paper 55-3.

Bouzidi, Y., D. R. Schmitt, R. A. Burwash, and E. R. Kanasewich, 2002, Variations in crustal thickness in Alberta from depth-migrated seismic reflection profiles: Canadian Journal of Earth Sciences, 39, 331-350.

Burwash, R. A., A. G. Green, A. M. Jessop, and E. R. Kanasewich, 1993, Geophysical and petrologic characteristics of the basement rocks of the Western Canada Basin in D. F. Stott, and J. D. Aitken, eds., Sedimentary cover of the craton in Canada: Geological Survey of Canada, Geology of Canada, 5, 57-77.

Chacko, T., S. K. De, R. A. Creaser, and K. Muehlenbachs, 2000, Tectonic setting of the Taltson magmatic zone at 1.9-2.0 Ga; a granitoid-based perspective: Canadian Journal of Earth Sciences, 37, 1597-1609, doi: 10.1139/e00-029.

Chan, J. and D. R. Schmitt, 2015, Examining the *in situ* metamorphic rock in Northeastern Alberta using zero-offset VSP: International Journal of Earth Sciences, 104, 1549-1562, DOI 10.1007/s00531-014-1110-x.

Chen Y. F., Y. J. Gu, R. M. H. Dokht, and M. D. Sacchi, 2015, Crustal imprints of Precambrian orogenesis in western Laurentia: Journal of Geophysical Research-Solid Earth, 120, 6993-7012.

De, S. K., T. Chacko, R. A. Creaser, and K. Muehlenbachs, 2000, Geochemical and Nd-Pb-O isotope systematics of granites from the Taltson Magmatic Zone, NE Alberta; implications for early Proterozoic tectonics in western Laurentia: Precambrian Research, 102, 221-249, doi:10.1016/S0301-9268(00)00068-1.

Dembicki, E. A., and T. J. Podvinsky, 2012, Geological and geophysical evaluation of the Leduc Formation in Northeastern Alberta, Canada: Proceeding of

the Canadian Society of Exploration Geophysicist Geoconvention, Calgary, Canada.

Dietrich, J., 1999, Seismic stratigraphy and structure of the Lower Paleozoic, Central Alberta LITHOPROBE Transect: Canadian Society of Petroleum Geologists Bulletin, 47, 362-374.

Edwards, D. J., and R. J. Brown, 1999, Understanding the influence of Precambrian crystalline basement on Upper Devonian carbonates in central Alberta from a geophysical perspective: Bulletin of Canadian Petroleum Geology, 47, 412-438.

Garland, G., and R. Burwash, 1959, Geophysical and petrological study of the Precambrian of central Alberta, Canada: American Association of Petroleum Geologists Bulletin 43, 790-806.

Gay, S. P., 2001, Basement reactivation in the Alberta Basin: Observational constraints and mechanical rationale – Comment: Bulletin of Canadian Petroleum Geology, 49, 426-428.

Geological Survey of Canada, 2016a, Canadian Geodetic Information System: Gravity and Geodetic Networks Section, Geodetic Survey Division, Geomatics Canada, Earth Sciences Sector, Natural Resources Canada, data retrieved from http://gdr.agg.nrcan.gc.ca/gdrdap/, June 2016.

Geological Survey of Canada, 2016b, Canadian Aeromagnetic Data Base: Airborne Geophysics Section, Central Canada Division, Earth Sciences Sector, Natural Resources Canada, data retrieved from http://gdr.agg.nrcan.gc.ca/gdrdap/, June 2016.

Gibb, R. A., and M. D. Thomas, 1983, Geophysics of proposed Proterozoic sutures in Canada: Precambrian Research, 19, 349-394.

Gu, Y. J., and L. Shen, 2015, Noise correlation tomography of Southwest Western Canada Sedimentary Basin: Geophysical Journal International, 202, 142-162, doi:10.1093/gji/ggv100.

Henderson, J. B., P. H. McGrath, D. T. James, and R. I. Macfie, 1987, An integrated geological, gravity and magnetic study of the Artillery Lake

area and the Thelon Tectonic Zone, District of Mackenzie: Geological Survey of Canada, Current Research, Part A, Paper 87-1A, 803-814.

Hoffman, P. F., 1989, Precambrian geology and tectonic history of North America, in A. Bally, and A.R. Palmer, eds., The Geology of North America-An Overview: Geological Society of America, 487-512.

MacLeod, I. N., K. Jones, and T. F. Dai, 1993, 3-D analytic signal in the interpretation of total magnetic field data at low magnetic latitudes: Exploration Geophysics, 24, 679-688.

McDonough, M. R., V. J. McNicoll, E. M. Schetselaar, and T. W. Grover, 2000, Geochronological and kinematic constraints on crustal shortening and escape in a two-sided oblique-slip collisional and magmatic orogen, Paleoproterozoic Taltson Magmatic Zone, Northeastern Alberta: Canadian Journal of Earth Sciences, 37, 1549-1573.

Meyer, M. T., M. F. Bickford, and J. F. Lewry, 1992, The Wathaman Batholith; an early Proterozoic arc in the Trans-Hudson orogenic belt, Canada: Geological Society of American Bulletin, 104, 1073-1085.

Miller, H. G., and V. J. Singh, 1994, Potential Field tilt-A new concept for location of potential field sources: Applied Geophysics, 32, 213-217, doi: 10.1016/0926-9851(94)90022-1.

Mountjoy, E., 1980, Some questions about the development of upper Devonian carbonate buildups (reefs), western Canada: Bulletin of Canadian Petroleum Geology, 28, 315-344.

Nabighian, M. N., V. J. S. Grauch, R. O. Hansen, T. R. LaFehr, Y. Li, J. W. Peirce, J. D. Phillips, and M. E. Ruder, 2005, The historical development of the magnetic method in exploration: Geophysics, 70, 33ND-61ND, doi: 10.1190/1.2133784.

Lyatsky, H. V., and D. I. Pana, 2003, Catalogue of selected regional gravity and magnetic maps of Northern Alberta: Alberta Energy and Utilities Board, EUB/AGS Special Report 56.

Lyatsky, H. V., D. I. Pana, and R. Olson, 2004, Detection of subtle basement faults with gravity and magnetic data in the Alberta Basin, Canada; a data-use tutorial: The Leading Edge, 23, 1282-1288, doi: 10.1190/1.1843375.

Lyatsky, H. V., D. I. Pana, and M. Grobe, 2005, Basement structure in central and Southern Alberta; Insights from gravity and magnetic maps: Alberta Geological Survey, Special publication, 72.

Lynn, H. B., L. D. Hale, and G. A. Thompson, 1981, Seismic reflections from the basal contacts of batholiths: Journal of Geophysical Research, 86, doi: 10.1029/JB080i011p10633.

Pană, D. I., 2003, Precambrian basement of the Western Canada Sedimentary Basin in Northern Alberta: Alberta Geological Survey, EUB/AGS Earth Sciences Report 2002-02.

Pilkington, M., W. F. Miles, G. M. Ross, and W. R. Roest, 2000, Potential-field signatures of buried Precambrian basement in the Western Canada Sedimentary Basin: Canadian Journal of Earth Science, 37, 1453-1471.

Rabeh, T., T. Abdallatif, M. Mekkawi, A. Khalil, and A. El-emam, 2008, Magnetic data interpretation and depth estimation constraints; a correlative study on magnetometer and gradiometer data: NRIAG Journal of Geophysics, 185-209.

Ravat, D., A. Pignatelli, I. Nicolosi, and M. Chiappini, 2007, A study of spectral methods of estimating the depth to the bottom of magnetic sources from near-surface magnetic anomaly data: Geophysical Journal International, 169, 421-434, doi: 10.1111/j.1365-246X.2007.03305.x.

Reid, A. B., J. M. Allsop, H. Granser, A. J. Millett, and I. W. Somerton, 1990, Magnetic interpretation in three dimensions using Euler deconvolution: Geophysics, 55, 80-91, doi: 10.1190/1.1442774.

Roest, W. R., J. Verhoef, and M. Pilkington, 1992, Magnetic interpretation using the 3-D analytic signal, Geophysics, 57, 116-125, doi: 10.1190/1.1443174.

Ross G. M., 2002, Evolution of Precambrian continental lithosphere in Western Canada: results from Lithoprobe studies in Alberta and beyond: Canadian Journal of Earth Sciences, 39, 413-437, doi: 10.1139/E02-012.

Ross G. M., and D. W. Eaton, 1999, Basement reactivation in the Alberta Basin; Observational constraints and mechanical rationale: Bulletin of Canadian Petroleum Geology, 47, 391-411.

Ross, G. M., R.R. Parrish, M. E. Villeneuve, and S. A. Bowring, 1991, Geophysics and geochronology of the crystalline basement of the Alberta Basin, Western Canada: Canadian Journal of Earth Sciences, 28, 512-522.

Switzer, S. B., W. G. Holland, D. S. Christie, G. C. Graf, A. S. Hedinger, R. J. McAuley, R. A. Wierzbicki, and J. J. Packard, 1994, Devonian Woodbend-Winterburn stata of the western Canada sedimentary basin, in G. D. Mossop, and I. Shetsen, Geological Atlas of the Western Canad Sedimentary Basin: Canadian Society of Petroleum Geologists and Alberta Research Council.

Theriault, R. J., and H. H. Bostock, 1989, Nd isotopic studies in the ca 1.9 Ga Taltson Magmatic Zone, Northwest Teritories: Geological Association of Canada, Program with abstracts, 14.

Theriault, R. J., and G. M. Ross, 1991, Nd isotopic evidence for crustal recycling in the ca. 2.0 Ga subsurface of western Canada: Canadian Journal of Earth Sciences, 28: 1140-1147.

Thompson, D. T., 1982, EULDPH: A new technique for making computer-assisted depth estimates from magnetic data, Geophysics, 47, 31-37.

Verduzco, B., J. D. Fairhead, C. M. Green, and C. MacKenzie, 2004, New insights into magnetic derivatives for structural mapping: The Leading Edge, 23, 116-119.

Vejmelek, L., and B. Smithson, 1995, Seismic reflection profiling in the Boulder batholith, Montana: Geology, 23, 811-814, doi: 10.1130/0091-7613(1995)023<0811: SRPITB>2.3.CO;2.

Villeneuve, M. E., G. M. Ross, R.J. Theriault, M. Miles, R. R. Parrish, and J. Broome, 1993, Tectonic subdivision and U-Pb geochronology of the crystalline basement of the Alberta Basin, Western Canada: Geological Survey of Canada Bulletin, 447.

Walsh, N. J., 2013, Geochemistry and geochronology of the Precambrian basement domains in the vicinity of Fort McMurray, Alberta; A geothermal perspective, M.Sc. thesis: University of Alberta.

Chapter 6: Conclusions

Integration of multidisciplinary data sets offered an exceptional opportunity to provide not only large-scale observations and novel interpretation of the WCSB and Precambrian crystalline basement within the Athabasca region but also a detail subsurface modeling and characterization of sedimentary formations and regional unconformities (PCU and SMU). The research work was divided into three phases of data compilation, processing-integration, and modeling-interpretation. Different techniques were used for processing and analysis of these individual geophysical data sets with the purpose of final advanced interpretation. In this chapter a summary of thesis contributions and recommendations for future work is provided.

6.1. Scientific and practical contributions

The primary purpose of the study presented in chapter 2 was to illustrate using seismic data the complexities of the eroded and karsted surface of Grosmont Formation (i.e., SMU). Secondarily, the contribution sought to preserve a unique and perhaps historic geophysical data set acquired for a pilot project in mid-80s. Comparison of the interpreted structural maps from surfaces below the SMU suggests that deeper features (intrusion bodies/faults) may also influence the structure of the SMU. Meanwhile the overlying Mesozoic formations represent almost the same structural topography as SMU surface. This may be due to collapse of karst features within the Grosmont after Mesozoic deposition, differential compaction of the Mesozoic sediments or even small fault motions.

In chapter 3, we demonstrated that wide distribution of heat values are available in the Athabasca region at a depth that have already been reached in oil and gas drilling operations. The thermal content of the formations are estimated using the information provided by 3D geology and SGS property models. As a result five Paleozoic aquifers of Keg River, Waterways, Cooking Lake, Leduc, and Grosmont were indicated to be potentially useable for geothermal applications. These aquifers were recognized as low enthalpy geothermal reservoirs with maximum of 40 °C temperature which could supplement potential future needs in this region if heat-pump technologies are used.

The integrated processing and interpretation of the HRAM and seismic reflection data presented in chapter 4, revealed the existence of short wavelength structural lineaments within the WCSB in the southwest of the Athabasca region. The forward magnetic modeling indicates that these lineaments are possibly related to the buried dykes/kimberlite pipes deeper than 200 m and thicker than 60 m. We referred to these features as the Buffalo Creek dyke field. Based upon the magnetic response and linearity of the Buffalo Creek dykes, they could be compared with the Sweet Grass Hills alkaline ultrabasic dykes in Southern Alberta. Such existence of such dykes would not necessarily be that surprizing as nearby there are already well known igneous intrusions. As such, the emplacement age and origin of the Buffalo Creek dyke field is possibly correlative with the adjacent Birch Mountains kimberlite pipes in the NAKP, which is between 70.3±1.6 to 77.6±0.8 Ma determined by U-Pb perovsite and Rb-Sr phlogopite dating. This association, however, is based on the fact that the Buffalo Creek dykes are only 100 km away; obviously no definitive conclusion with regards to the age or composition of the interpreted dykes can be made without

direct sampling by drilling. These Cretaceous dykes may be related to the Farallon plate subduction under the west coast of the North American Plate.

Chapter 5 deals with issues that are of a more fundamental scientific interest attempting to answer questions related to the nature and assembly of the craton during the Proterozoic. The TMZ-BHT contact in the Athabasca region is recognized as a long wavelength and high amplitude feature on the HRAM data. Euler deconvolution demonstrates that the depth of this boundary is within 1.5 and 3 km. This estimation is correlative with the basement depth map constructed by seismic reflection and well tops. Although the seismic data set here was not acquired for the deep craton study, we were able to tie it to our HRAM findings and provide some interesting observations with coincidences of the LMR reefs with the BHT-TMZ boundary and the differing seismic fabric between TMZ and BHT.

6.2. Suggested future work

While the presented results adds to our geophysical knowledge of sedimentary basin and Precambrian basement in the Athabasca region, and also lead to a proposal to partially replace energy generation from natural gas burning process by clean geothermal to benefit the environment and economics of bitumen production, the following suggestions for future work can enhance the results and interpretations presented in this thesis.

Despite all the efforts in terms of compiling the required data for this project, in many ways the data in the region remains sparse, particularly for evaluating the geothermal potential of WCSB and pinpointing potential geothermal sites. The study presented in chapter 3 should be seen primarily as the first step in the proper evaluation of the feasibility of geothermal

development. Much detail work remains and it is needed that workers carry out proper evaluations of *in situ* bulk permeabilities, water chemistries, and temperatures. This can only be accomplished by drilling and coring, geophysical logging including oriented image logs, fluid sampling, and transient pressure testing. In reality, the depths to many of the target formations are quite modest and the costs of carrying out such programs should not be high. Obtaining a complete set of core together with a high quality borehole data using mining industry diamond coring technologies would allow these data to be acquired at less cost than if traditional petroleum exploration methods are used.

One further issue with regards to geothermal exploitation that may build from this study is more exhaustive engineering studies with regards to the feasibility of the entire process of providing hot water using the heat-pump technology. This was not attempted here, in part, because of the large uncertainties in knowing the hydrologic regime in the target reservoirs. With improved information on proper *in situ* permeability, one will be able to properly assess the flow rates that can be achieved. This is a key parameter as significant flow permeability must be available to maintain flows as well as to provide sufficient water to allow for economic rates of heat extraction. Other key factors that will need to be considered would include the effects of the water chemistry, the electrical power requirements to operate pumps and compressors, and the influence of local climate extremes on the heat-pump operation. Proper environmental assessments, too, must be made particularly when dealing with issues related to ground water. These of course are challenges, but it is worth pointing out that the technologies to carry out this are already well developed and have been working successfully in Northern Europe for decades.

In terms of seismic reflection data, acquiring modern seismic reflection will significantly improve the reliability of the results and interpretations. Moreover more advanced seismic routines need to be considered for the processing of the seismic profiles and the suppression of artifacts for an improved final image. Borehole seismic methods, too, could be used to properly calibrate the seismic signal in this area. Again, the modest depths make carrying out such measurements relatively economic.

Finally, for speculating on how we might learn more about this 'contact' between the Buffalo Head Terrane and the Taltson Magmatic Zone, further geophysical studies of course would be of interest. It is doubtful that much more could be extracted from renewed magnetic studies as they are already at a relatively dense spacing with regards to the basement, but the gravity data set used here is one obtained from a compilation of measurements by the Geological Survey of Canada. The true number of data points used to make these gravity maps can be quite small in reality and a more intensive set of gravity measurements might show promise here. It was noted that there are no deep seismic profiles over this boundary with the closest LITHOPROBE lines being over 200 km away. As such, obtaining a new deep seismic profile over this contact using modern 2D seismic profiling technologies could provide additional useful information as to the nature of the contact. This should be supported by large offset refraction studies that would allow for tomographic inversions for velocities structure that could reveal differences between the two domains. Drilling into the basement to obtain new basement core material would also help.

Bibliography

Adams, J. J., B. J. Rostron, and C. A. Mendoza, 2004, Coupled fluid flow, heat, and mass transport, and erosion in the Alberta basin: Implications for the origin of the Athabasca oil sands, Canadian Journal of Earth Scienes, 41, 1077-1095.

Alberta Energy and Utilities Board, 2005, Alberta's reserves 2004 and supply demand outlook 2005-2014: Statistical Series, ST98-2005.

Alm, P., 1999, Long-time study of geothermal data from a low enthalpy geothermal heat plant: Proceeding of 24th Workshop on Geothermal Reservoir Engineering, accessed 16 April 2016.

Anglin, F. M., and A. E. Beck, 1965, Regional heat flow pattern in Western Canada: Canadian Journal of Earth Science, 2, 176-182.

Aravanis, T., 1999, Legend property assessment report, Birch Mountain area, Alberta: Alberta Energy and Utilities Board, Report 20000003.

Ardakani, E. P., and D. R. Schmitt, 2011a, Developing Engineered Geothermal Systems (EGS) in Alberta, Canada: Proceeding of the 1st EAGE Sustainable Earth Sciences (SES) Conference and Exhibition, doi: 10.3997/2214-4609.20144204, Valencia, Spain.

Ardakani, E. P., and D. R. Schmitt, 2012a, Adding to the geophysical tool box for geothermal exploration; use of seismic and magnetic surveys in a regional geophysical study for geothermal exploration in NE Alberta, Canada: Proceeding of Geothermal Research Council Transactions, 36, 985-988, Reno, USA.

Ardakani, E. P., and D. R. Schmitt, 2013a, Regional geophysical study for geothermal exploration in NE Alberta: Proceeding of the Canadian Society of Exploration Geophysics Geoconvention, Calgary, Canada.

Ardakani, E. P., and D. R. Schmitt, 2014a, Athabasca regional geophysical study - implications for geothermal development in northeastern Alberta, Canada: Proceeding of the 76th European Association of Geoscientists and Engineers Conference and Exhibition, Amsterdam, NL.

Ardakani, E. P., and D. R. Schmitt, 2014b, Investigation of Devonian Unconformity Surface Using Legacy Seismic Profiles, NE Alberta: Canadian Society of Exploration Geophysics Geoconvention, Extended abstract, Calgary, Canada.

Ardakani, E. P., D. R. Schmitt, 2016a, Geothermal energy potential of sedimentary formations in the Athabasca region, Northeast Alberta, Canada: Interpretation, 4, SR19-SR33, doi: 10.1190/INT-2016-0031.1.

Ardakani, E. P., D. R. Schmitt, 2016b, Geophysical evidence for an igneous dyke swarm, Buffalo Creek, Northeast Alberta under review for publication in Geological Society of America bulletin.

Ardakani, E. P., and D. R. Schmitt, 2015, Detecting lineaments of Athabasca region by integrated geophysical data interpretation: Canadian Society of Exploration Geophysics Geoconvention, Extended abstract, Calgary, Canada.

Ardakani, E. P., D. R. Schmitt, and T. D. Bown, 2014c, Detailed topography of the Devonian Grosmont Formation surface from legacy high resolution seismic profiles, Northeast Alberta: Geophysics, 79, B135-B149, doi: 10.1190/geo2013-0268.1.

Ardakani, E. P., D. R. Schmitt, and I. Moeck, 2012b, Use of seismic and magnetic surveys in a regional geophysical study for geothermal exploration in NE Alberta, Canada: American Geophysical Union, Fall Meeting, abstract #V13C-2863, San Francisco, USA.

Ardakani, E. P., D. R. Schmitt, and T. D. Bown, 2013b, Devonian Grosmont Formation surface investigation using legacy high resolution seismic profiles, NE Alberta, Canada: Proceeding of the 75th European Association of Geoscientists and Engineers Conference and Exhibition, London, UK.

Ardakani, E. P., D. R. Schmitt, T. Bown, J. Chan, S Idowu, J. A. Majorowicz, M. Unsworth, M. van der Baan, K. Bauer, I. Moeck, M. Pussak, and S. Weides, 2011b, Regional geophysical reconnaissance for low enthalpy geothermal resources in NE Alberta, Canada: American Geophysical Union, Fall Meeting, Abstract #H21E-1160, San Francisco, USA.

Bachu, S., 1995, Synthesis and model of formation water flow in the Alberta Basin, Canada: American Association of Petroleum Geologists Bulletin, 79, 1159-1178.

Bachu, S., J. R. Underschultz, B. Hitchon, 1996, Regional subsurface hydrogeology in Northeast Alberta: Alberta Geological Survey, open file report 1996-14.

Baranov, V., 1957, A new method for interpretation of aeromagnetic maps; pseudo-gravimetric anomalies: Geophysics, 22, 359-383, doi: 10.1190/1.1438369.

Barton, C., M. D. Zoback, and D. Moos, 1995, Fluid-flow along potentially active faults in crystalline rock: Geology, 23(8), 683-686, doi: 10.1130/0091-7613(1995)023<0683: FFAPAF>2.3.Co;2.

Barbier, E., 2002, Geothermal energy technology and current status - an overview: Renewable and Sustainable Energy Reviews, 6, 3-65.

Barss, D. L., E. W. Best, and N. Mayers, 1964, Triassic, in R. G. McCrossan, and R. P. Glaister, eds., Geological history of Western Canada: Alberta Society of Petroleum Geologists, chapter 9, 113-136.

Barrett, K. R., and J. C. Hopkins, 2010, Stratiform carbonate breccias of the Grosmont Formation, Alberta: Presented at AAPG 2010 International Conference & Exhibition.

Batycky, J. P., R. P. Leaute, and B. A. Dawe, 1997, A mechanistic model of cyclic steam stimulation: Proceedings of the International Thermal Operations and Heavy Oil Symposium, Bakersfield, CA, USA, February 10-12, SPE 37550.

Beaney, C. L., and J. Shaw, 2000, The subglacial geomorphology of southeast Alberta; evidence for subglacial meltwater erosion: Canadian Journal of Earth Sciences, 37, 51-61, doi: 10.1139/cjes-37-1-51.

Bell, J. S. and S. E. Grasby, 2012, The stress regime of the Western Canada Sedimentary Basin: Geofluids, 12, 150-165, doi: 10.1111/j.1468-8123.2011.00349.x.

Bélanger-Davis, C. E., 1985, Mineralogical and petrophysical changes after steam testing in carbonate rocks of the Grosmont Formation, Alberta: M.S. thesis, University of Calgary.

Bell, J., and T. Weis, 2009, Greening the grid - Powering Alberta's future with renewable energy: Pembina Institute, Drayton Valley, Canada.

Belyea, H. R., 1952, Notes on the Devonian system for the north-central plains of Alberta: Geological Survey of Canada.

Belyea, H. R., 1955, Cross-sections through the Devonian system of the Alberta plains: Geological Survey of Canada, Paper 55-3.

Belyea, H. R., 1956, Grosmont Formation in the Loon Lake area: Petroleum Geology, 4, 66-69.

Belyea, H. R., 1964, Upper Devonian, Part II - Woodbend, Winterburn and Wabamun Groups, in R. G. McCrossan, and R. P. Glaister, eds., Geological History of Western Canada: Alberta Society of Petroleum Geologists, 66-68.

Belyea, H. R., and A. W. Norris, 1962, Middle Devonian and older Paleozoic formations of southern district of Mackenzie and adjacent areas: Geological Survey of Canada, paper 62-15.

Berkhout, A. J., 1979, Steep dip finite-difference migration: Geophysical Prospecting, 27, 196-213, doi: 10.1111/j.1365-2478.1979.tb00965.x.

Best, M. G., 1988, Early Miocene change in direction of least principal stress, Southwestern United States; Conflicting inferences from dikes and metamorphic core-detachment fault terranes: Tectonics, 7, 249-259, doi: 10.1029/TC007i002p00249.

Best, M. E., H. J. Abercrombie, and J. W. Peirce, 1998, Interpreted faulting patterns in Northeast Alberta using high resolution aeromagnetic data: Canadian Journal of Exploration Geophysics, 34, 49-57.

Bjelm, L., and L. Lindeberg, 1995, Long-term experience from a heat pump plant in Lund, Sweden, using a low-temperature geothermal aquifer, Proceedings of the World Geothermal Congress, 3, 2173-2176.

Blakely, R. J. and A. Cox, 1972, Identification of short polarity events by transforming marine magnetic profiles to the pole: Journal of Geophysical Research, 77, 4339-4349.

Borrero, M. L., and H. G. Machel, 2010, Sedimentology and diagenesis of Hondo Evaporites within the Grosmont giant heavy oil carbonate reservoir, Alberta, Canada: Presented at AAPG 2010 International Conference & Exhibition.

Bouzidi, Y., D. R. Schmitt, R. A. Burwash, and E. R. Kanasewich, 2002, Variations in crustal thickness in Alberta from depth-migrated seismic reflection profiles: Canadian Journal of Earth Sciences, 39, 331-350.

Bown, T. D., 2011, Legacy seismic investigations of karst surfaces; implications for heavy oil extraction from the Devonian Grosmont Formation, Northeastern Alberta, Canada: M.S. thesis, University of Alberta.

Boyer, L. P., 2005, Kimberlite volcanic facies and eruption in the Buffalo Head Hills, Alberta, Canada, M.Sc. thesis: University of British Columbia.

Breiner, S., 1999, Applications manual for portable magnetometers: Geometrics, San Jose, California.

Briggs, I. C., 1974, Machine contouring using Minimum Curvature: Geophysics, 39 (1), 39-48, doi: 10.1190/1.1440410.

Buhlmann, A. L., P. Cavell, R. A. Burwash, R. A. Creaser, and R. W. Luth, 2000, Minette bodies and cognate mica-clinopyroxenite xenoliths from the Milk River area, southern Alberta: records of a complex history of the northernmost part of the Archean Wyoming craton: Canadian Journal of Earth Sciences, 37, 1629–1650, doi: 10.1139/e00-058.

Burwash, R. A., A. G. Green, A. M. Jessop, and E. R. Kanasewich, 1993, Geophysical and petrologic characteristics of the basement rocks of the Western Canada Basin in D. F. Stott, and J. D. Aitken, eds., Sedimentary cover of the craton in Canada: Geological Survey of Canada, Geology of Canada, 5, 57-77.

Buschkuehle, B. E., F. J. Hein, and M. Grobe, 2007, An overview of the geology of the Upper Devonian Grosmont carbonate bitumen deposit, Northern Alberta, Canada: Natural Resources Research, 1, 3-15.

Burwash, R. A., T. Chacko, K. Muehlenbachs, and Y. Bouzidi, 2000, Oxygen isotope systematics of the Precambrian basement of Alberta, implications for Paleoproterozoic and Phanerozoic tectonics in Northwestern Alberta: Canadian Journal of Earth Sciences, 37, 1611-1628, doi: 10.1139/e00-090.

Butler, R. M., G. S. McNab, and H. Y. Lo, 1981, Theoretical studies on the gravity drainage of heavy oil during in-situ steam heating: Canadian Journal of Chemical Engineering, 59, 455-460.

Carlson, S. M., W. D. Hillier, C. T. Hood, R. P. Pryde, and D. N. Skelton, 1999, The Buffalo Hills kimberlites; a newly-discovered diamondiferous kimberlite province in North-Central Alberta, Canada: Proceeding of the 7th International Kimberlite Conference, 1, 109-116.

Chacko, T., S. K. De, R. A. Creaser, and K. Muehlenbachs, 2000, Tectonic setting of the Taltson magmatic zone at 1.9-2.0 Ga; a granitoid-based perspective: Canadian Journal of Earth Sciences, 37, 1597-1609, doi: 10.1139/e00-029.

Chan, J. and D. R. Schmitt, 2015, Examining the *in situ* metamorphic rock in Northeastern Alberta using zero-offset VSP: International Journal of Earth Sciences, 104, 1549-1562, DOI 10.1007/s00531-014-1110-x.

Chen Y. F., Y. J. Gu, R. M. H. Dokht, and M. D. Sacchi, 2015, Crustal imprints of Precambrian orogenesis in western Laurentia: Journal of Geophysical Research-Solid Earth, 120, 6993-7012.

Cotterill, D., and W. N. Hamilton, 1995, Geology of Devonian limestones in Northeast Alberta: Alberta Geology Survey open file report 1995-07.

Cox, M. J. G., 1999, Static corrections for seismic reflection surveys: SEG.

Currie, C. A., and C. Beaumont, 2011, Are diamond-bearing Cretaceous kimberlites related to low-angle subduction beneath western North America?: Earth and Planetary Science Letters, 303, 59-70, doi:10.1016/j.epsl.2010.12.036.

Cutler, W., 1982, Stratigraphy and sedimentology of the Upper Devonian Grosmont Formation, Alberta, Canada: M.S. thesis, University of Calgary.

Dagan, G., 1989, Flow and transport in porous formations: Springer-Verlag, New York.

Dawson, G. M., 1884, Report of progress 1882-83-84, part c: Geological Survey of Canada, 16-17 and 45-47.

De, S. K., T. Chacko, R. A. Creaser, and K. Muehlenbachs, 2000, Geochemical and Nd-Pb-O isotope systematics of granites from the Taltson Magmatic Zone, NE Alberta; implications for early Proterozoic tectonics in western Laurentia: Precambrian Research, 102, 221-249, doi:10.1016/S0301-9268(00)00068-1.

Deutsch, C. V., 2002, Geostatistical reservoir modeling: Oxford University Press.

Dembicki, E. A., 1994, The Upper Devonian Grosmont Formation; well log evaluation and regional mapping of a heavy oil carbonate reservoir in Northeastern Alberta: M.S. thesis, University of Alberta.

Dembicki, E. A., and H. G. Machel, 1996, Recognition and delineation of paleokarst zones by the use of wireline logs in the bitumen-saturated Upper Devonian Grosmont Formation of Northeastern Alberta, Canada: AAPG Bulletin, 80, 695-712.

Dembicki, E. A., and T. J. Podvinsky, 2012, Geological and geophysical evaluation of the Leduc Formation in Northeastern Alberta, Canada: Proceeding of the Canadian Society of Exploration Geophysicist Geoconvention, Calgary, Canada.

Dietrich, J., 1999, Seismic stratigraphy and structure of the Lower Paleozoic, Central Alberta LITHOPROBE Transect: Canadian Society of Petroleum Geologists Bulletin, 47, 362-374.

Dufresne, M. B., R. A. Olson, D. R. Schmitt, B. McKinstry, D. R. Eccles, M. M. Fenton, J. G. Pawlowicz, W. A. D. Edwards, and R. J. H. Richardson, 1994, The Diamond Potential of Alberta: A regional synthesis of the structural and stratigraphic setting, and other preliminary indications of diamond potential: Alberta Research Council, open file report 1994-10.

Dufresne, M. B., D. R. Eccles, B. McKinstry, D. R. Schmitt, M. M. Fenton, J. G. Pawlowicz, and W. A. D. Edwards, 1996, The diamond potential of Alberta: Alberta Geological Survey Bulletin, 63.

Eccles, D. R., L. M. Heaman, and A. R. Sweet, 2008, Kimberlite-sourced bentonite, its paleoenvironment and implications for the Late Cretaceous K14 kimberlite cluster, Northern Alberta: Canadian Journal of Earth Sciences, 45, 531-547, doi: 10.1139/E07-065.

Eccles, D. R., L. M. Heaman, R. W. Luth, and R. A. Creaser, 2003, Petrogenesis of the Late Cretaceous Northern Alberta kimberlite province: Proceeding of the 8th International Kimberlite Conference.

Eccles, D. R., L. M. Heaman, R. W. Luth, and R. A. Creaser, 2004, Petrogenesis of the Late Cretaceous Northern Alberta kimberlite province: Lithos, 76, 435-459, doi: 10.1016/j.lithos.2004.03.046.

Eccles, D. R., 2011, Northern Alberta Kimberlite Province - The first 20 years: Energy Resources Conservations Board, ERCB/AGS Bulletin 65.

Edwards, D. J., and R. J. Brown, 1999, Understanding the influence of Precambrian crystalline basement on Upper Devonian carbonates in central Alberta from a geophysical perspective: Bulletin of Canadian Petroleum Geology, 47, 412-438.

Energy Resources Conservation Board, 2009, Table of formations, http://www.ercb.ca/docs/products/catalog/TOF.pdf, accessed 27 July 2012.

Energy Resources Conservation Board, 2010, Alberta's energy reserves 2009 and supply/demand outlook 2010-2019, Open file report ST98-2010.

Garland, G., and R. Burwash, 1959, Geophysical and petrological study of the Precambrian of central Alberta, Canada: American Association of Petroleum Geologists Bulletin 43, 790-806.

Gay, P. S., 1963, Standard curves for the interpretation of magnetic anomalies over long tabular bodies: Geophysics, 28 (2), 161-200, doi: 10.1190/1.1439164.

Gay, S. P., 2001, Basement reactivation in the Alberta Basin: Observational constraints and mechanical rationale – Comment: Bulletin of Canadian Petroleum Geology, 49, 426-428.

Geological Survey of Canada, 2016a, Canadian Geodetic Information System: Gravity and Geodetic Networks Section, Geodetic Survey Division, Geomatics Canada, Earth Sciences Sector, Natural Resources Canada, data retrieved from http://gdr.agg.nrcan.gc.ca/gdrdap/, June 2016.

Geological Survey of Canada, 2016b, Canadian Aeromagnetic Data Base: Airborne Geophysics Section, Central Canada Division, Earth Sciences Sector, Natural Resources Canada, data retrieved from http://gdr.agg.nrcan.gc.ca/gdrdap/, June 2016.

Georgsson, L. S., 2009, Geophysical methods used in geothermal exploration: Short Course IV on exploration for geothermal resources at Lake Naivasha, Kenya, retrieved April 16, 2016.

Gibb, R. A., and M. D. Thomas, 1983, Geophysics of proposed Proterozoic sutures in Canada: Precambrian Research, 19, 349-394.

Grasby, S. E., D. M. Allen, Z. Chen, G. Ferguson, A. Jessop, M. Kelman, J. Majorowicz, M. Moore, J. Raymond, and R. Therrien, 2011, Geothermal energy resource potential of Canada: Geological Survey of Canada, open file report.

Gray, A., J. Majorowicz, and M. Unsworth, 2012, Investigation of the geothermal state of sedimentary basins using oil industry thermal data - Case study from Northern Alberta exhibiting the need to systematically remove biased data: Journal of Geophysics and Engineering, 9, 534-548, doi:10.1088/1742-2132/9/5/534.

Gu, Y. J., and L. Shen, 2015, Noise correlation tomography of Southwest Western Canada Sedimentary Basin: Geophysical Journal International, 202, 142-162, doi:10.1093/gji/ggv100.

Gupta, I., A. M. Wislon, and B.J. Rostron, 2012, Cl/Br compositions as indicators of the origin of brines: hydrogeologic simulations of the Alberta Basin, Canada, Geological Society of America Bulletin, 124, 200-212.

Gupta, I., A. M. Wislon, and B.J. Rostron 2015, Groundwater age, brine migration, and large-scale solute transport in the Alberta Basin, Canada: Geofluids, 15, 608-620.

Hackbarth, D., and M. Brulotte, 1981, Groundwater observation well network - Athabasca oil sands area: Alberta Research Council, Information Series 69.

Hackbarth D., and N. Nastasa, 1979, The hydrogeology of the Athabasca oil sands area, Alberta: Alberta Research Council Bulletin, 38.

Hardage, B. A., 2000, Vertical Seismic Profiling: Principles, third edition: Pergamon, Amsterdam.

Harrison, R., 1982, Geology and production history of the Grosmont carbonates pilot project, Alberta, Canada: Presented at Second United Nations Institute for Training and Research Conference on Future of Heavy Crude and Tar Sands.

Harrison, R., 1984, The bitumen-bearing Paleozoic carbonate trends of Northern Alberta: Presented at AAPG 1984 Research Conference.

Harrison, R., 1986, Regional geology and resource characterization of the Upper Devonian Grosmont Formation, Northern Alberta: Alberta Resarch Council.

Harrison, R., and B. McIntyre, 1981, The geologic setting of the Grosmont thermal recovery project, Northeastern Alberta: Presented at the Alberta Oil Sands Technology and Research Authority (AOSTRA) seminar on Advances in Petroleum Upgrading and Recovery Technology.

Heaman, L. M., B. A. Kjarsgaard, and R. A. Creaser, 2003, The timing of kimberlite magmatism in North America: implications for global kimberlite genesis and diamond exploration: Lithos, 71, 153-184 doi: 10.1016/j.lithos.2003.07.005.

Heaman, L. M., B. A. Kjarsgaard, and R. A. Creaser, 2004, The temporal evolution of North American kimberlites: Lithos, 76, 377-397.

Hein, F. J., 2006, Heavy oil and oil (tar) sands in North America: an overview and summary of contributions: Natural Resources Research, 15, 67-84, doi: 10.1007/s11053-006-9016-3.

Hein, F. J., R. Marsh, and M. Boddy, 2008, Overview of the oil sands and carbonate bitumen of Alberta; regional geologic framework and influence of salt-dissolution effects: Presented at AAPG Hedberg Conference.

Henderson, J. B., P. H. McGrath, D. T. James, and R. I. Macfie, 1987, An integrated geological, gravity and magnetic study of the Artillery Lake area and the Thelon Tectonic Zone, District of Mackenzie: Geological Survey of Canada, Current Research, Part A, Paper 87-1A, 803-814.

Hersir, G. P., and A. Björnsson, 1991, Geophysical exploration for geothermal resources, principles and applications: United Nations University Geothermal Training Programme, report 15, retrieved April 16, 2016.

Hitchon, B., 1964, Formation fluids in R. G. McCrossan, and R. P. Glaister, eds., Geological history of western Canada: Canadian Society of Petroleum Geologists, 201-217.

Hitchon, B., C. M. Sauveplane, S. Bachu, E. H. Koster, and A. T. Lytviak, 1989a, Hydrogeology of the Swan Hills area, Alberta - Evaluation for deep waste injection: Alberta Research Council Bulletin, 58.

Hitchon, B., S. Bachu, C. M. Sauveplane, A. Ing, A. T. Lytviak, and J. R. Underschultz, 1989b, Hydrogeological and geothermal regimes in the Phanerozoic succession - Cold Lake area, Alberta and Saskatchewan: Alberta Research Council Bulletin, 59.

Hoffmann, C. F., and O. P. Strausz, 1986, Bitumen accumulation in Grosmont platform complex, Upper Devonian, Alberta, Canada: AAPG Bulletin, no. 70, 1113-1128.

Hoffman, P. F., 1989, Precambrian geology and tectonic history of North America, *in* A. Bally, and A. R. Palmer, eds., The geology of North America; an overview: Geological Society of America, 487-512.

Hofmann, H., 2015, Development of Enhanced Geothermal Systems (EGS) in Northern Alberta, Ph.D. thesis: University of Alberta.

Hood, P. J., 1964, The Koenigsberger ratio and the dipping dike equation: Geophysical Prospecting, 12, 440-456.

Hopkins, J., and B. Jones, 2009, Reservoir units in the Grosmont Formation; stratigraphy, paleotopography and reservoir geology of the Grosmont Formation Twp 80-90 Rge 12-21W4: Alberta Research Concil & Carbonate Research Program Geology report no. 0708-1.

Huebscher, H., 1996, Regional controls on stratigraphic and diagenetic evolution of the Woodbend group carbonates, north-central Alberta, Canada: M.S. thesis, University of Alberta.

Huebscher, H., and H. G. Machel, 1997, Paleokarst in the Grosmont Formation, Northeastern Alberta in J. Wood, and B. Martindale, eds., Canadian Society of Petroleum Geologists for Sedimentary Geology Joint Convention: Core Conference, 129-151.

Hutcheon, I., and A. Oldershaw, 1985, The effect of hydrothermal reactions on the petrophysical properties of carbonate rocks: Bulletin of Canadian Petroleum Geology, no. 33, 359-377.

Jellicoe, B. C., P. Robertshaw, P. Williamson, and J. Murphy, 1998, Summary of exploration activities and results for the Fort à la Corne diamond project, Saskatchewan: Saskatchewan Geological Survey, Report 98-4, 144-157.

Jones, B., 2010, Fracture systems in the Grosmont Formation: Alberta Reseach Council & Carbonate Research Program Geology Report no. 0910-8a.

Jones, F. W., H. L. Lam, and J. A. Majorowicz, 1985, Temperature distributions at the Paleozoic and Precambrian surfaces and their implications for geothermal energy recovery in Alberta: Canadian Journal of Earth Science, 22, 1774-1780.

Kellett, R. L., A. E. Barnes, and M. Rive, 1994, The deep structure of the Grenville Front; a new perspective from western Quebec: Canadian Journal of Earth Sciences, 31, 282–292, doi: 10.1139/e94-027.

Kellett, R. L., G. J. Steensma, and R. M. Zahynacz, 2005, Geophysical signature of the Mountain Lake intrusion; a study to support future kimberlite exploration in Alberta: Alberta Geological Survey & Alberta Energy and Utilities Board, Special Report 064.

Kjarsgaard, B. A., 1994, Potassic magmatism in the Milk River area, Southern Alberta-petrology and economic potential: Geological Survey of Canada, Current Research 1994-B, 59-68.

Kjarsgaard, B. A., 1997, Diamonds in Alberta: studies of potential host rocks of deep-seated origin and applications of indicator mineral exploration techniques; *in* R. W. Macqueen, eds., Exploring for minerals in Alberta: Geological Survey of Canada, Bulletin 500, 185-207.

Lam, H. L., and F. W. Jones, 1984, Geothermal gradients of Alberta in western Canada: Geothermics, 13, 181-192.

Lam, H. L., F. W. Jones, and J. A. Majorowicz, 1985, A statistical analysis of bottom hole temperature data in southern Alberta, Geophysics, 50, 677-684.

Law, J., 1955, Geology of Northwestern Alberta and adjacent areas: American Association of Petroleum Geologists Bulletin, 39, 1927-1975.

Leblanc, G. E., and W. A. Morris, 1999, Aeromagnetics of Southern Alberta within areas of hydrocarbon accumulation: Bulletin of Canadian Petroleum Geology, 47, 439-454.

Leckie, D. A., B. A. Kjarsgaard, J. W. Peirce, A. M.Grist, M. Collins, A. Sweet, L. Stasiuk, M. A. Tomica, R. Eccles, M. Durfresne, M. M. Fenton, J. G. Pawlawicz, S. A. Balzar, D. J. McIntyre, and D. H. McNeil, 1997, Geology of a Late Cretaceous possible kimberlite at Mountain Lake, Alberta; chemistry, petrology, indicator minerals, aeromagnetic signature, age, stratigraphic position and setting: Geological Survey of Canada, Open File Report 3441.

Lemmon, E. W., M. O. McLinden, and D. G. Friend, Thermophysical properties of fluid systems, in P. J. Linstrom, and W. G. Mallard, eds., NIST chemistry webbook, NIST standard reference database, 69: National Institute of Standards and Technology, http://webbook.nist.gov, retrieved February 6, 2016.

Liddell, M., M. Unsworth, and J. Pek, 2016, Magnetotelluric imaging of anisotropic crust near Fort McMurray, Alberta; implications for engineered geothermal

system development: Geophysical Journal of Interpretation, published online, doi:10.1093/gji/ggw089.

Louie, J. N., S. K. Pullammanappallil, and W. Honjas, 2011, Advanced seismic imaging for geothermal development: Proceeding of New Zealand Geothermal Workshop, Auckland.

Luo, P., and H. G. Machel, 1995, Pore-size and pore throat types in a heterogeneous dolostone reservoir, Devonian Grosmont Formation, Western Canada Sedimentary Basin: AAPG Bulletin, 79, 1698-1720.

Luo, P., H. G. Machel, and J. Shaw, 1994, Petrophysical properties of matrix blocks of a heterogeneous dolostone reservoir - the Upper Devonian Grosmont Formation, Alberta, Canada: Bulletin of Canadian Petroleum Geology, 42, 465-481.

Lyatsky, H. V., and D. I. Pana, 2003, Catalogue of selected regional gravity and magnetic maps of Northern Alberta: Alberta Energy and Utilities Board, EUB/AGS Special Report 56.

Lyatsky, H. V., D. I. Pana, and R. Olson, 2004, Detection of subtle basement faults with gravity and magnetic data in the Alberta Basin, Canada; a data-use tutorial: The Leading Edge, 23, 1282-1288, doi: 10.1190/1.1843375.

Lyatsky, H. V., D. I. Pana, and M. Grobe, 2005, Basement structure in central and Southern Alberta; Insights from gravity and magnetic maps: Alberta Geological Survey, Special publication, 72.

Lynn, H. B., L. D. Hale, and G. A. Thompson, 1981, Seismic reflections from the basal contacts of batholiths: Journal of Geophysical Research, 86, doi: 10.1029/JB080i011p10633.

MacCormack, K. E., N. Atkinson, and S. Lyster, 2015, Sediment thickness of Alberta, Canada: Alberta Energy Regulator Map 603; scale 1:1,000,000.

Machel, H. G., 2010, The Devonian petroleum system of the Western Canada Sedimentary Basin with implications for heavy oil reservoir geology, in S. Chopra, L. R. Lines, D. R. Schmitt and M. L. Batzle, eds., Heavy oils;

Reservoir characterization and production monitoring: SEG Geophysical Developments Series, no. 13, 131-154.

Machel, H. G., M. L. Borrero, E. Dembicki, H. Huebscher, P. Luo, and Y. Zhao, 2012, The Grosmont: The world's largest unconventional oil reservoir hosted in carbonate rocks in J. Garland, J. E. Neilson, S. E. Laubach, and K. J. Whidden, eds., Advances in Carbonate Exploration and Reservoir Analysis: Geological Society of London, Special Publication, 370, 49-81, doi: 10.1144/SP370.11.

Machel, H. G., and I. Hunter, 1994, Facies models for middle to late Devonian shallow marine carbonates, with comparisons to modern reefs; a guide for facies analysis: Facies no. 30, 155-176.

MacLeod, I. N., K. Jones, and T. F. Dai, 1993, 3-D analytic signal in the interpretation of total magnetic field data at low magnetic latitudes: Exploration Geophysics, 24, 679-688.

Majorowicz, J. A., and S. E. Grasby, 2010, High potential regions for enhanced geothermal systems in Canada: Natural Resources Research, 19, 177-188, doi: 10.1007/s11053-010-9119-8.

Majorowicz, J. A., and A. M. Jessop, 1981a, Present heat flow and a preliminary geothermal history of the Central Prairies Basin, Canada: Geothermics, 10, 81-93.

Majorowicz, J. A., and A. Jessop, 1981b, Regional heat flow patterns in the Western Canadian Sedimentary Basin: Tectonophysics, 74, 209-238, doi: 10.1016/0040-1951(81)90191-8.

Majorowicz, J. A., G. Garven, A. M. Jessop, and C. Jessop, 1999, Present heat flow along a profile across the Western Canada Sedimentary Basin - the extent of hydrodynamic influence in A. Forster, and D. F. Merriam, eds, Geothermics in basin analysis, 61-79.

Majorowicz, J. A., and M. C. Moore, 2008, Enhanced Geothermal Systems (EGS) potential in the Alberta Basin: Institute for Sustainability, Energy, Environment and Economy.

Majorowicz, J. A., and S. E. Grasby, 2010, High potential regions for enhanced geothermal systems in Canada: Natural Resources Research, 19, 177-188, doi: 10.1007/s11053-010-9119-8.

Majorowicz, J. A., W. Gosnold, A. Gray, J. Safanda, R. Klenner, and M. Unsworth, 2012a, Implications of post-glacial warming for Northern Alberta; heat flow - correcting for the underestimate of the geothermal potential: Geothermal Resources Council Transactions, 36, 693-698.

Majorowicz, J. A., M. Unsworth, T. Chacko, A. Gray, L. Heaman, D. K. Potter, D. R. Schmitt, and T. Babadagli, 2012b, Geothermal energy as a source of heat for oil sands processing in Northern Alberta, Canada in F. J. Hein, D. Leckie, J. Suter, and S. Larter, eds., Heavy oil and oil sand petroleum systems in Alberta and beyond: American Association of Petroleum Geologists, Chapter 27, doi: 10.1306/13371602St643569.

Majorowicz, J., J. Chan, J. Crowell, W. Grosnold, L. M. Heaman, J. Kueck, G. Niewenhuis, D. R. Schmitt, M. Unsworth, N. Walsh, and S. Weides, 2014, The first deep heat flow determination in crystalline basement rocks beneath the Western Canadian Sedimentary Basin, Geophysical Journal International, 197, 731-747.

McCandless, T. E., 1999, Kimberlites: Mantle expressions of deep-seated subduction, *in* J. J. Gurney, J. L. Gurney, M. D. Pascoe, S. H. Richardson, eds.: Proceeding of the 7th International Kimberlite Conference, 2, 545-549.

McCandless, T. E., R. M. Tosdal, 2005, Base metal porphyries and diamond-enriched kimberlites of the Laramide orogeny: products of convergent margin magmatism: Geological Society of America Abstracts with Programs, 37.

McDonough, M. R., V. J. McNicoll, E. M. Schetselaar, and T. W. Grover, 2000, Geochronological and kinematic constraints on crustal shortening and escape in a two-sided oblique-slip collisional and magmatic orogen, Paleoproterozoic Taltson Magmatic Zone, Northeastern Alberta: Canadian Journal of Earth Sciences, 37, 1549-1573.

Meyer, M. T., M. F. Bickford, and J. F. Lewry, 1992, The Wathaman Batholith; an early Proterozoic arc in the Trans-Hudson orogenic belt, Canada: Geological Society of American Bulletin, 104, 1073-1085.

Miller, H. G., and V. J. Singh, 1994, Potential field tilt; A new concept for location of potential field sources: Applied Geophysics, 32, 213-217, doi: 10.1016/0926-9851(94)90022-1.

MODIS, National Aeronautics and Space Administration, available from http://modis.gsfc.nasa.gov, accessed 10 July 2012.

Moeck, I. S., 2014, Catalog of geothermal play types based on geologic controls: Renewable and Sustainable Energy Reviews, 37, 867-882, doi: 10.1016/j.rser.2014.05.032.

Mossop, G., and I. Shetsen, 1994, Geological atlas of the Western Canada Sedimentary Basin: Canadian Society of Petroleum Geologists and Alberta Research Council.

Mountjoy, E., 1980, Some questions about the development of upper Devonian carbonate buildups (reefs), western Canada: Bulletin of Canadian Petroleum Geology, 28, 315-344.

Nabighian, M. N., 1984, Toward a three-dimensional automatic interpretation of potential field data via generalized Hilbert transforms; Fundamental relations: Geophysics, 49, 780-786.

Nabighian, M. N., V. J. S. Grauch, R. O. Hansen, T. R. LaFehr, Y. Li, J. W. Peirce, J. D. Phillips, and M. E. Ruder, 2005, The historical development of the magnetic method in exploration: Geophysics, 70, 33ND-61ND, doi: 10.1190/1.2133784.

National Energy Board, 2015, Energy futures supplement-demand sensitivities, https://www.neb-one.gc.ca/nrg/ntgrtd/ftr/2015/index-eng.html, retrieved January 23, 2016.

Nieuwenhuis, G., T. Lengyel , J. Majorowicz, M. Grobe, B. Rostron, M. Unsworth, and S. Weides, 2015, Regional-scale geothermal exploration using heterogeneous industrial temperature data; a case study from the Western

Canadian Sedimentary Basin: Proceedings of the World Geothermal Congress.

Norris, A., 1963, Devonian stratigraphy of Northeastern Alberta and Northwestern Saskatchewan: Geological Survey of Canada, Memoir 313.

Norris, A., 1973, Paleozoic (Devonian) geology of Northeastern Alberta and Northwestern Saskatchewan in M. A. Carrigy, and J. W. Kramers, eds., Guide to the Athabasca oil sands area: Alberta Research Council Information Series, 65, 18-76.

O'Connell, S. C., G. R. Dix, and J. E. Barclay, 1990, The origin, history and regional structural development of the Peace River Arch, Western Canada: Bulletin of Canadian Petroleum Geology, 38A, 4-24.

Ogunsuyi, F., and D. R. Schmitt, 2010, Integrating seismic velocity tomograms and seismic imaging: Application to the study of a buried valley, *in* R. D. Miller, J. D. Bradford, and K. Holliger, eds., Near surface seismology and ground penetrating radar: Society of Exploration Geophysics, 361-378, doi: 10.1190/1.9781560802259.ch22.

Omnes, G., and P. Robert., 1982, The P-Shooter; a fast seismic source for shallow exploration: Geophysics: AAPG Bulletin, 66, 1697-1697.

Pană, D. I., 2003, Precambrian basement of the Western Canada Sedimentary Basin in Northern Alberta: Alberta Geological Survey, EUB/AGS Earth Sciences Report 2002-02.

Parsons, W. H., 1973, Alberta, in R. G. McCrossan, eds., The Future Petroleum Provinces of Canada - Their Geology and Potential: Canadian Society of Petroleum Geologists, Memoir 1, 73-120.

Pathak, V., T. Babadagli, J. Majorowicz, and M. J. Unsworth, 2014, Evaluation of engineered geothermal systems as a heat source for oil sands production in Northern Alberta: Natural Resources Research, 23, 247-265.

Pilkington, M., W. F. Miles, G. M. Ross, and W. R. Roest, 2000, Potential-field signatures of buried Precambrian basement in the Western Canada Sedimentary Basin: Canadian Journal of Earth Sciences, 37, 1453-1471, doi: 10.1139/e00-020.

Porter, J., R. Price, and R. McCrossan, 1982, The Western Canada Sedimentary Basin: Philosophical Transactions of the Royal Society of London, Series A, Mathematical and Physical Sciences, 305, 169-192, doi:10.1098/rsta.1982.0032.

Rao, T. K. S. P., M. Subrahmanyam, and A. Srikrishna Murthy, 1986, Nomogram for the direct interpretation of magnetic anomalies due to long horizontal cylinders: Geophysics, 51(11), 2156-2159, doi: 10.1190/1.1442067.

Rabeh, T., T. Abdallatif, M. Mekkawi, A. Khalil, and A. El-emam, 2008, Magnetic data interpretation and depth estimation constraints; a correlative study on magnetometer and gradiometer data: NRIAG Journal of Astronomy and Geophysics, 185-209.

Ram Babu, H. V., V. Vijayakuma, and D. Atchuta Rao, 1986, A simple method for the analysis of magnetic anomalies over dike-like bodies: Geophysics, 51 (5), 1119-1126, doi: 10.1190/1.1442166.

Ravat, D., A. Pignatelli, I. Nicolosi, and M. Chiappini, 2007, A study of spectral methods of estimating the depth to the bottom of magnetic sources from near-surface magnetic anomaly data: Geophysical Journal International, 169, 421-434, doi: 10.1111/j.1365-246X.2007.03305.x.

Reid, A. B., J. M. Allsop, H. Granser, A. J. Millett, and I. W. Somerton, 1990, Magnetic interpretation in three dimensions using Euler deconvolution: Geophysics, 55, 80-91, doi: 10.1190/1.1442774.

Reiter, K., O. Heidbach, D. R. Schmitt, K. Haug, M. Ziegler, and I. Moeck, A revised crustal stress orientation database for Canada: Tectonophysics, 636, 111-124, doi: 10.1016/j.tecto.2014.08.006, 2014.

Robie, R. A., B. S. Hemingway, and J. R. Fisher, 1979, Thermodyanic properties of minerals and related substantces at 298 K and 1 Bar (105 Pasacals) pressure and at higher temperatures: United State Geological Survey Bulletin, 1452.

Roest, W. R., J. Verhoef, and M. Pilkington, 1992, Magnetic interpretation using the 3-D analytic signal, Geophysics, 57, 116-125, doi: 10.1190/1.1443174.

Ross G. M., 2002, Evolution of Precambrian continental lithosphere in Western Canada: results from Lithoprobe studies in Alberta and beyond: Canadian Journal of Earth Sciences, 39, 413-437, doi: 10.1139/E02-012.

Ross, G. M., R. R. Parrish, M. E. Villeneuve, and S. A. Bowring, 1991, Geophysics and geochronology of the crystalline basement of the Alberta Basin, Western Canada: Canadian Journal of Earth Sciences, 28, 512-522, doi: 10.1139/e91-045.

Ross G. M., and D. W. Eaton, 1999, Basement reactivation in the Alberta Basin; Observational constraints and mechanical rationale: Bulletin of Canadian Petroleum Geology, 47, 391-411.

Ross, G. M., R.R. Parrish, M. E. Villeneuve, and S. A. Bowring, 1991, Geophysics and geochronology of the crystalline basement of the Alberta Basin, Western Canada: Canadian Journal of Earth Sciences, 28, 512-522.

Ross, G. M., J. Mariano, R. Dumont, B. A. Kjarsgaard, and D. Teskey, 1997, Was Eocene magmatism widespread in the subsurface of Southern Alberta? Evidence from new aeromagnetic anomaly data, i*n* R.W. Macqueen, eds., Exploring for minerals in Alberta; Geological Survey of Canada geoscience contributions, Canada-Alberta Agreement on Mineral Development (1992-1995): Geological Survey of Canada, Bulletin 500, 235-246.

Rukhlov, A. S., and J. G. Pawlowicz, 2012, Eocene potassic magmatism of the Milk River area, southern Alberta (NTS 72E) and Sweet Grass Hills, Northern Montana; overview and new data on mineralogy, geochemistry, petrology and economic potential: Energy Resources Conservation Board and Alberta Geological Survey, open file report 2012-01.

Russel-Houston, J., and K. Gray, 2014, Paleokarst in the Grosmont Formation and reservoir implications, Saleski, Alberta, Canada: Interpretation-a Journal of Subsurface Characterization, 2, SF29-SF50.

Rybach, L., and M. Mongillo, 2006, Geothermal sustainability-A review with identified research needs, Geothermal Resources Council Transactions, 30, 1083-1090.

Schneider, W. A., 1978, Integral formulation for migration in two and three dimensions: Geophysics, 43, 49-76, doi: 10.1190/1.1440828.

Secor, D. T., 1965, Role of fluid pressure in jointing: American Journal of Science, 263, 633-646.

Sheriff, R. E., 2002, Encyclopedic Dictionary of Applied Geophysics, 4th edition: Society of Exploration Geophysicists, Tulsa, Oklahoma.

Skelton, D., and T. Bursey, 1998, Buffalo Head Hill property (AL01) assessment report - Ashton Mining of Canada Inc.: Alberta Geological Survey, Report 19980015.

Skelton, D., B. Clements, T. E. McCandless, C. Hood, S. Aulbach, R. Davies, and L. P. Boyer, 2003, The BHH kimberlite province, Alberta: Proceeding of the 8th International Kimberlite Conference, Northern Alberta-Slave kimberlite field trip guide book: Geological Survey of Canada.

Spector, A., and F. S. Grant, 1970, Statistical models for interpreting aeromagnetic data, Geophysics, 35 (2), 293-302, doi: 10.1190/1.1440092.

Sproule, D. F., 1956, Granite Wash of Northern Alberta: Journal of Alberta Society of Petroleum Geologists, 4, 197-203.

Stewart, R. R., 2001, VSP: An in-depth seismic understanding: Canadian Society of Exploration Geophysics Recorder, 79-83.

Subramanya, K. 1994, Engineering hydrology: Tata McGraw-Hill Education.

Switzer, S. B., W. G. Holland, D. S. Christie, G. C. Graf, A. S. Hedinger, R. J. McAuley, R. A. Wierzbicki, and J. J. Packard, 1994, Devonian Woodbend-Winterburn stata of the western Canada sedimentary basin, in G. D. Mossop, and I. Shetsen, Geological Atlas of the Western Canadian Sedimentary Basin: Canadian Society of Petroleum Geologists and Alberta Research Council.

Telford, W. M., L. P. Geldart, and R. E. Sheriff, 1990, Applied Geophysics, 2nd edition: Cambridge University Press, Cambridge, UK.

Theriault, F., 1988, Lithofacies, diagenesis, and related reservoir properties of the Upper Devonian Grosmont Formation, Northern Alberta: Bulletin of Canadian Petroleum Geology, 36, no. 1, 52-69.

Theriault, F., and I. Hutcheon, 1987, Dolomitization and calcitization of the Devonian Grosmont Formation, Northern Alberta: Journal of Sedimentary Petrology, 57, 955-966, doi: 10.1306/212F8CB5-2B24-11D7-8648000102C1865D.

Theriault, R. J., and H. H. Bostock, 1989, Nd isotopic studies in the ca 1.9 Ga Taltson Magmatic Zone, Northwest Teritories: Geological Association of Canada, Program with abstracts, 14.

Theriault, R. J., and G. M. Ross, 1991, Nd isotopic evidence for crustal recycling in the ca. 2.0 Ga subsurface of western Canada: Canadian Journal of Earth Sciences, 28: 1140-1147.

Thompson, D. T., 1982, EULDPH: A new technique for making computer-assisted depth estimates from magnetic data, Geophysics, 47, 31-37.

Toth, J., 1978, Gravity-induced cross-formational flow of formation fluid, Red Earth region, Alberta, Canada; Analysis, patterns, and evaluation: Water Resources Research, 14, 805-843.

Ungemach, P., 1985, An overview of the state of geothermal energy: International Journal of Energy research, 9, 223-228.

Verduzco, B., J. D. Fairhead, C. M. Green, and C. MacKenzie, 2004, New insights into magnetic derivatives for structural mapping: The Leading Edge, 23 (2), 116-119, doi: 10.1190/1.1651454.

Vejmelek, L., and B. Smithson, 1995, Seismic reflection profiling in the Boulder batholith, Montana: Geology, 23, 811-814, doi: 10.1130/0091-7613(1995)023<0811: SRPITB>2.3.CO;2.

Villeneuve, M. E., G. M. Ross, R.J. Theriault, M. Miles, R. R. Parrish, and J. Broome, 1993, Tectonic subdivision and U-Pb geochronology of the crystalline basement of the Alberta Basin, Western Canada: Geological Survey of Canada Bulletin, 447.

Walker, D., 1986, Regional stratigraphy of the Upper Devonian Grosmont Formation, Northern Alberta: Alberta Geological Survey open file report 1986-02.

Wall, M., J. Cartwright, R. Davies, and A. McGrandle, 2010, 3D seismic imaging of a Tertiary Dyke Swarm in the southern North Sea, UK: Basin Research, 22, 181-194, doi: 10.1111/j.1365-2117.2009.00416.x.

Walsh, N. J., 2013, Geochemistry and geochronology of the Precambrian basement domains in the vicinity of Fort McMurray, Alberta; A geothermal perspective, M.Sc. thesis: University of Alberta.

Weides, S., I. Moeck, J. Majorowicz, D. Palombi, and M. Grobe, 2013, Geothermal exploration of Paleozoic formations in central Alberta: Canadian Journal of Earth Science, 50, 519-534.

Weides, S., and J. Majorowicz, 2014c, Implications of spatial variability in heat flow for geothermal resource evaluation in large foreland basins: the case of the Western Canada Sedimentary Basin: Energies, 7, 2573-2594.

Weides, S., I. Moeck, J. Majorowicz, and M. Grobe, 2014a, The Cambrian Basal Sandstone Unit in central Alberta – an investigation of temperature distribution, petrography, and hydraulic and geomechanical properties of a deep saline aquifer: Canadian Journal of Earth Sciences, 51,783-796.

Weides, S., I. Moeck, D. R. Schmitt, J. Majorowicz, 2014b, An integrative geothermal resource assessment study for the siliciclastic Granite Wash Unit, Northwestern Alberta (Canada): Environmental Earth Sciences, 72, 4141-4154.

Westgate, J. A., 1968, Surficial geology of the Foremost-Cypress Hills area, Alberta: Research Council of Alberta, RCA/AGS Bulletin 022, 137 p.

Wo, E., L. Song, T. Hurst, and N. Sitek, 2010, Geological review and bitumen resource appraisal of the Grosmont Formation within the Athabasca oil sands area: Presented at AAPG 2010 International Conferenve & Exhibition.

Wood, B. D., and A. C. Williams, 1994, Mountain Lake Prospect, Alberta: Alberta Energy and Utilities Board/Alberta Geological Survey, Assessment Report 1994000.

Wood, B. D., B. H. Scott Smith, and S. de Gasparis, 1998, The Mountain Lake kimberlitic pipes of Northwest Alberta; exploration, geology and emplacement model: 7th International Kimberlite Conference, South Africa, Extended Abstract.

Yoon, T., 1986, Bitumen resources of the Upper Devonian Grosmont Formation: Twp 88 to 98, Northern Alberta: Alberta Geologycal Survey open file report 1986-01.

Zhao, Y., 2009, Petrophysical properties of bitumen from the Upper Devonian Grosmont reservoir, Alberta, Canada: M.S. thesis, University of Alberta.

Zoback, M., 2007, Reservoir Geomechanics: Cambridge University Press.

Zonneveld, J. P., B. A. Kjarsgaard, S. E. Harvey, and D. H. McNeil, 2006, Accommodation space and kimberlite edifice preservation; implications for volcanological models of Fort à la Corne kimberlites., Saskatchewan Kimberlite Emplacement Workshop, Extended Abstract.